KUVEMPU UNIVERSITY

Department of P.G. Studies and Research in Industrial Chemistry,
School of Chemical Sciences, Jnana Sahyadri, Kuvempu University,
Shankaraghatta-577451

"DEVELOPMENT OF NEW METAL BASED PHOTOSENSITIZERS FOR PHOTODYNAMIC ANTIMICROBIAL CHEMOTHERAPY; AN ALTERNATIVE APPROACH TO ANTIMICROBIAL DRUGS"

Thesis submitted to the Faculty of Science, Kuvempu University

for the award of the Degree of

DOCTOR OF PHILOSOPHY

in

INDUSTRIAL CHEMISTRY

Submitted by

Mrs. Teja H.B. M.Sc.,

Research Guide

Dr. H.S. Bhojya Naik M.Sc., Ph.D.
Professor
Department of P.G. Studies and Research in Industrial Chemistry
School of Chemical Sciences
Jnana Sahyadri, Kuvempu University
Shankaraghatta- 577 451

2023

Declaration

I hereby declare that the research work presented in this thesis entitled **"DEVELOPMENT OF NEW METAL BASED PHOTOSENSITIZERS FOR PHOTODYNAMIC ANTIMICROBIAL CHEMOTHERAPY; AN ALTERNATIVE APPROACH TO ANTIMICROBIAL DRUGS"** is submitted to the Department of Industrial Chemistry, Kuvempu University for the award of the degree of **Doctor of Philosophy in Industrial Chemistry** is bonafide work of the research work carried out by me under the supervision of **Dr. H.S. Bhojya Naik,** Professor, Department of P.G. Studies and Research in Industrial Chemistry, Jnana Sahyadri, Kuvempu University, Shankaraghatta, Shimoga-577451.

I further declare that the contents presented in the thesis or any part, therefore, has not been submitted elsewhere for any other degree, diploma or similar title in any other Universities.

Date: 16.01.2023

Place: Shankaraghatta

(TEJA H B)

KUVEMPU UNIVERSITY

Dr. H.S. Bhojya Naik, M.Sc., Ph.D
Professor
Dept. of P.G. Studies and Research in Industrial Chemistry
School of Chemical Sciences
Jnana Sahyadri, Kuvempu University
Shankaraghatta- 577 451,
Shivamogga Dist.,
E-mail: hsb_naik@rediffmail.com
Karnataka, INDIA.

Phone No: +91 8282-256228(O); +91 8282-257229®; Cell: +91 9448438281; Fax: +91 8282-256255

Certificate

This is to certify that the work reported in this thesis entitled "**DEVELOPMENT OF NEW METAL BASED PHOTOSENSITIZERS FOR PHOTODYNAMIC ANTIMICROBIAL CHEMOTHERAPY; AN ALTERNATIVE APPROACH TO ANTIMICROBIAL DRUGS"** submitted by **Mrs. Teja H B** to the Faculty of Science, Kuvempu University, for the award of **Doctor of Philosophy in Industrial Chemistry** is a record of the bonafide and original research work carried out by him under my guidance and direct supervision. The work reported in this thesis has formed the basis for the award of any degree or diploma or any other similar title in any other institution or university.

Date: 16-01-2023

Place: Shankaraghatta

(Prof. H.S. Bhojya Naik)
Dr. H.S. Bhojya Naik, M.Sc., Ph.D.,
Professor
Dept. of Industrial Chemistry
Kuvempu University
Jnana Sahyadri, Shankaraghatta

Dedicated To

My parents, family members, friends and all my teachers for their encouragement love and support……

Acknowledgements

Major research work like this is never the work of anyone alone. The contribution of many different people in their different ways have made this possible. It gives me immense pleasure to acknowledge all the persons who came in contact in the way with helping hands, during my research tenure. I would like to expend my appreciation especially to the following.

Foremost, I would like to express my sincere gratitude to my guide **Dr. H.S. Bhojya Naik,** Professor and Chairperson, Department of Industrial Chemistry, Kuvempu University, for the continuous support of my Ph.D., study and research, for his patience, motivation, enthusiasm, and immense knowledge. His guidance helped me in all the time of research and writing of this thesis. I could not have imagined having a better advisor and mentor for my Ph.D., study.

It is my pleasant duty to express my sincere thanks to **Dr. B.E. Kumara Swamy**, Professor and **Dr. Itte Pushpavathi,** Assistant Professor Department of Industrial Chemistry, Kuvempu University, for his kind co-operation during my research work.

I also thank **Prof. K. Vasantha Kumar Pai,** Retaired proferssor and all faculty members of the Department of Industrial Chemistry, Kuvempu University, and also non-teaching staff of the department for their encouragement.

I place on records my sincere thanks to **OBC Cell,** Kuvempu University for financial support to carry out the research.

I shall be failing in my duties if I don't express my deep sense of gratitude to **Dr. M.C. Prabhakara**, Assistant Professor, Sir M.V. Government Science College, Bommanakatte, Bhadravathi, Shivamogga for his constant support and encouragement during my research work.

I express my thanks to **Dr. R Viswanath** for his moral support and encouragement.

I would like to remember with special love and gratitude, the pleasant moment I had with my research group, Dr. Arun Kumar, Dr. I.K. Suresh Gowda, Dr. S.K. Rashmi, Dr. M. Giridhar, Dr. M. Madhukara Naik, Dr. N. Venugopal, Dr. Amith Nayak P.H, Dr. Mohammad Abdulla Mohammad Bajiri, Dr. Indrajith Naik E, Dr. M. Shashank, Dr. B.R. Kirthan, Mrs Champa, Ms Venkatalakshmi, Mrs Hena and Mr. Barikara Shivaraj, for their timely help, memorable moments spent with them and support throughout my research work.

It is to express my special gratitude to my friends, Dr. O. Nagaraja, Dr. Mamata Devendra Naik, Mrs. Priya R Kadam, for their help, everlasting support with love and gratitude.

I would like to thank the Directors, Indian Institute of Science Bangaluru, IIT Mumbai, and SAIF Dharwad for providing spectral data.

Thank God for the wisdom and perseverance that he has been bestowed upon me during this research project and indeed, throughout my life. "I can do everything through him who gives me strength".

With great love, I acknowledge the moral support of my father Sri Basavaraj K, my mother Smt. Usha, my husband Mr. Suhas D N, and my daughter Ms. Prekshika Suhas, they are the whole and sole in all of my academic aspirations, No issue have been too small for me to call home for advice, and no problem I've caused was too large for them to accept and forgive. Their belief in my abilities was expressed to me at an early age and instilled within me a desire to achieve greatness. The success that I've achieved until now is largely due to this and to the freedom, they've provided me in making my own decisions along the way.

Finally, I am truly grateful for the many hands and hearts that helped me directly or indirectly during my research work.

Great thanks to all my well-wishers.....

Mrs. Teja H B

List of research articles published and accepted

1. Study of photophysicochemical and antimicrobial photodynamic properties of visible light active azo metal(II) complexes. **H. B. Teja,** H.S. Bhojya Naik*, P.H. Amith Nayak, Prabhakara, M. C. *Asian Journal of Chemistry; Vol. 33, No. 8 (2021), 1709-1717.* https://doi.org/10.14233/ajchem.2021.23178.

2. Design, Synthesis and Pharmacological Assay of Sulfadiazine based Azo-Metal Complexes**. H.B. Teja,** H.S. Bhojya Naik*, P.H. Amith Nayak, R. Viswanath , K. Vinu, and U. Hani. *Asian Journal of Chemistry; Vol. 34, No. 6 (2022), 1443-1450.* https://doi.org/10.14233/ajchem.2022.23711.

3. Light Induced Biological Evaluation Of Schiff Base Cu(II) and Co(II) Photosensitizers. **H.B. Teja,** H.S. Bhojya Naik*, P.H. Amith Nayak, B.R. Kirthan**.** Russian journal of general chemistry (Accepted).

List of publications as Co-author

1. Synthesis, Characterization and Luminescent Properties of Mixed-Ligand Nickel Complexes for Opto-Electronic Application, P.H. Amith Nayak, H.S. Bhojya Naik, **H. B. Teja,** B.R. Kirthan and R. Viswanath, Journal of Electronic Materials, 50, 2090–2100 (2021). https://doi.org/10.1007/s11664-020-08728-0.

2. Synthesis Characterization and Photophysical Properties of Schiff Base Copper Complex, P.H. Amith Nayak, H.S. Bhojya Naik, **H.B. Teja,** B.R. Kirthan and R. Viswanath., Molecular Crystals and Liquid Crystals, 1-7 (2021), https://doi.org/10.1080/15421406.2020.1868053.

3. Synthesis, characterization,optical,electrochemical, photocatalytic, DNA interaction and biological studies of transition [3d] metal complexes having Schiff base moiety. Russian journal of general chemistry. B.R. Kirthan, M.C. Prabhakar, H.S. Bhojya Naik, R. Viswanath, P.H. AmithNayak, **H.B. Teja.**

List of papers presented in National / International Conferences

1. Synthesis and Characterization of benzimidazol derivative of azo Schiff base and their antibacterial activity "**9th KSAT Annual Conference on "Science, Technology and Innovations in the 21st Century**" Jointly organised by KATA and Christ University Bangalore Dated: 20th -21st December 2016.

2. Synthesis and characterization of novel Zn(ll) and Cu(ll) metal complexes As A Photosensitizes For Antimicrobial Photodynamic Therapy "**International conference on advances in disease management for human welfare**" Gulbarga university, kalaburagi. Dated:21st-23rd November 2017.

3. Synthesis and characterization of novel bi(lll)and Cu(ll) metal complexes and their antimicrobial activity "**10th Annual Conference of Karnataka Science and Technology Academy 2018"** Jointly organised by KATA and Reva University Bangalore Dated: 18th -19th January 2018.

4. Synthesis, Spectroscopic Characterization And Antibacterial Studies Of Azo-Metal Complex. Two-Day National Conference on "**Recent Advances in Chemical Biology and Material Science for Industry and Society"** (RACBMS-2018) Kuvempu University, Shankaraghatta, Shimoga, Karnataka. Dated: 9th & 10th February 2018.

5. Antifungal Photodynamic Inactivation Of *Candida abicans* Using Metal(ll)-Schiff Base Complexs. "**Advanced Functional Materials For Energy, Environment And Health Care(AFMEEHC)"** Mysore. Dated: 18th-20th march 2019.

6. Synthesis And Characterization Of Some Transitional Metal Complexes Derived From acetyl acetone. "**Two days national conference on recent advances in chemical biology and material engineering (RACBME)"** Veerashaiva College, Ballari. Dated: 30-31st January 2020.

7. Synthesis, spectral characterization and effect on bacterial cells of new azo metal complexes as APDT Photosensitizers. "**International Conference – Nanotechnology 2019"** – ST Aloysius college (autonomous) Mangalore, Karnataka. Dated: 10 &11 January 2019.

List of Workshops/Seminars attended

1. Spectroscopic and Microscopic Methods for the Analysis of Materials. (SMAM-2016), St. Joseph's College Bangalore in association with IAS Bangalore and INSA New Delhi and the National Academy of Science, Allahabad. Dated: 1st and 2nd December 2016.

2. One week national level workshop on "current scenario in bioenergy conversion and waste management technology" organized by department of mechanical engineering, JNNCE shivamogga and KSCST Banglore dated: 24th-28th January 2018.

ABBREVIATIONS

δ	-	Chemical shift
ν	-	Frequency
λ	-	Wavelength
ppm	-	Parts per million
m/z	-	Mass to charge ratio
FT-IR	-	Fourier transformed infra-red
NMR	-	Nuclear magnetic resonance
cm^{-1}	-	Wavenumber or per centimeter
m.p	-	Melting point
UV-Vis	-	Ultraviolet and Visible
XRD	-	X-Ray diffraction
TGA	-	Thermogravimetrc analysis
MIC	-	Minimum inhibition concentration
SEM	-	Scanning electron microscopy
EDAX	-	Energy dispersive X-ray analysis
nm	-	Nanometer
TMS	-	Tetramethylsilane
DMF	-	N,N-dimethyl formamide
DMSO	-	Dimethylsulfoxide
EDTA	-	Ethylenediamine tetraacetic acid
PSs	-	Phtosensitizers
PDT	-	Photodynamic Therapy
APDT	-	Antimicrobial photodynamic therapy
CT-DNA	-	Calf thymus – Deoxyribonuclic acid
RNA	-	Ribonuclic acid
FDA	-	Food and drug administration

Contents

	Titles	Page No.
Chapter 1	**General Introduction about metal based materials for antimicrobial pohotodynamic therapy**	**1-33**
	1.1. Antibiotics	
	1.2. Photodynamic Therapy	
	1.3. Antimicrobial Photodynamic Chemotherapy	
	1.4. Photosensitizers	
	1.5. Outsearch Of All The Chapter.	
	1.6 Reference	
Chapter 2	**Methods and Materials**	**34-46**
	2.1. Introduction	
	2.2. NMR	
	2.3. UV-VISIBLE SPECTRA	
	2.4. IR Spectra	
	2.5. Mass spectra	
	2.6. TGA spectra	
	2.7. SEM	
	2.8. Powdered XRD	
	2.9. General method involved in synthesis of azo dye	
	2.10. Biological Activity	
	2.11. Reference	

Chapter 3	**Light Induced Biological Evaluation of Schiff Base Cu(II) and Co(II) Photosensitizers** 3.1. Introduction 3.2. Experimental 3.3. Results and Discussion 3.4. Conclusion 3.5. Reference	**47-77**
Chapter 4	**Synthesis, Characterization and Pharmacological Activity of Novel Azo dye and their Metal Complexes Containing Nitrogen and Oxygen Donor Atoms** 4.1. Introduction 4.2. Experimental 4.3. Results and Discussion 4.4. Conclusion 4.5. Reference	**78-103**
Chapter 5	**Design, Synthesis and Pharmacological Assay of Sulfadiazine Based Azo-Metal Complexes** 5.1. Introduction 5.2 Experimental 5.3 Results And Discussion 5.4.Conclusion 5.5. Reference	**104-130**

Chapter 6	**Study of Photophysicochemical and Antimicrobial Photodynamic Properties of Visible Light Active Azo Metal Complexes** 6.1. Introduction 6.2. Experimental 6.3. Results and Discussion 6.4. Conclusion 6.5. Reference	**131-159**
Chapter 7	**Synthesis, Characterization and Pharmacological Activity of Cu(II) and Co(II) Transition Metal Based Azo Dye Derivatives** 7.1. Introduction 7.2. Experimental 7.3. Results And Discussion 7.4. Conclusion 7.5. Reference	**160-189**
	Publications	
	Seminars and Conferences Certificates	

Chapter-1

Introduction

1.1. Antibiotics.

Antimicrobials are possibly one of the most effective forms of chemotherapy in the history of medicine. It is not needed to repeat here, how many lives they have saved and how significantly they have contributed to the control of infectious diseases that were the important causes of human illness and death for most of human existence [1]. The research as revealed that, the traces of tetracycline, have been originated in human skeletal leftovers from ancient Sudanese Nubia dating back to 350–550 CE [2]. The spreading of tetracycline in bones is only explainable after exposure to tetracycline-containing materials in the diet of these ancient people. One more example of ancient antibiotics from a histological study of samples taken from the femoral midshafts of the Roman period skeletons from the Dakhleh Oasis, Egypt [3]. After decades some antibiotics are chemically synthesized or semi-synthesized compounds, which could inhibit growth and survival of other microorganisms [4]. The first antibiotic was Penicillin discovered by Alexander Fleming in 1929. After that different families of antibiotics have been approved in the world wide (**Fig.1.1**). After that antibiotic have become the answer of medicine and are being used to treat common and minor infections and also to cure non-bacterial infections [5,6].

Nevertheless, during the last decades, the number of clinical drug-resistant isolates such as methicillin-resistant *Staphylococcus aureus* (MRSA), cephalosporin-resistant *E. coli*, carbapenem-resistant *Pseudomonas aeruginosa,* etc., has significantly increased and grown to be a global pandemic and unavoidable problem [7-8]

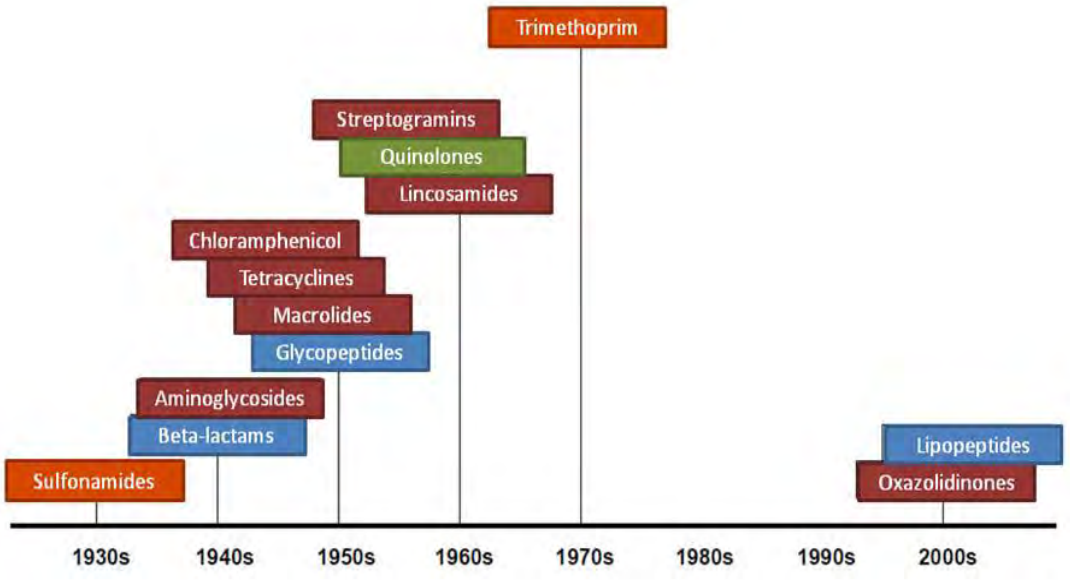

Fig. 1.1. Innovation of new classes of antibiotics. Color refers to the principal target. Orange: Inhibition of folic acid synthesis. Blue: Inhibition of cell wall synthesis. Maroon: inhibition of protein synthesis. Green: inhibition of DNA or RNA synthesis.

In 1945, Alexander Fleming warned that the incorrect use of penicillin could lead to the selection of resistant mutant forms of *S. aureus* [9]. The transfer of plasmids encoding resistance enzymes and efflux pumps that can be transferred between species, the inappropriate prescription of antibiotics and incompleted treatment, the widespread use of antibiotics in livestock feedstuff. All of them are causes by which the most resistant strain is selected. The danger of this multidrug resistance has encouraged the representatives to acknowledge this hazard to human health and gradually driving a resurgence of interest in antibiotic discovery and development [10, 11]. The UK Government-commissioned O'Neill report anticipated that without crucial action 10 million people a year will die from drug resistant infections by 2050 [12].

The problem of increased resistance is not only restricted to bacteria. Some fungal strains such as *Candida albicans* and *Kodamaea ohmeri* have been established resistance to antifungal agents such as *amphotericin B, flucytosine* and *fluconazole*

[13, 14]. It has been clinically proved that incomplete treatments of leishmaniasis with meglumine antimoniate and sodium stibogluconate for the protozoan parasites, induces selection of the drug-resistant strains increasing 50 % inhibitory concentration for *L. mexicana* and *L. braziliensis* isolates [15].

Consequently, an important research effort is being made to find alternative antimicrobial therapies to which these microorganisms cannot easily develop resistance. Therefore the most rapidly developing area of pharmaceutical research is the discoveries of novel drug are naturally occurring or synthetic antimicrobial peptides, and Photodynamic Therapy (PDT) [16-19].

1.2. Photodynamic Therapy (PDT).

In 1913, Meyer-Betz introduced photodynamic effect. He himself injected a 200 mg of haematophorphyrin and subsequently exposed himself to light, which resulted in massive swelling and blistering [20]. Further, Lipson and Schwartz in 1970 discovered that a polymeric derivative of haematoporphyrin (HpD) was selectively taken up and retained by quickly dividing cells and this observation that provoked investigations into the photodynamic therapy (PDT) of cancer. This mixture of HpD is ~ 45 % porphyrins and ~ 55 % oligomerit was purified in Photofrin [21]. Since the discovery of these compounds, the PDT of cancer has been well developed and compounds such as Photofrin and Foscan are regularly used in clinics for the treatment of cancers and many other second and third generation photosensitizers have been developed [22].

Photodynamic therapy mainly involves the photosensitizers (PS), light and molecular oxygen; it was a promising minimally aggressive therapeutic approach for the treatment of malignant as well as non-malignant tumors [23]. PDT involves the selective stimulation of the photosensitizers drug for the cancer cells leading to only a

restricted photocytotoxic effect, thus leaving the healthy cells unaffected (**Fig.1.2**) [24]. PDT justifies the elementary hypothetical requirements for successful cancer therapy such as selective damage of neoplastic tissue through direct cellular damage, vascular blocking and activation of an immune response against targeted cells and minimal toxicity towards healthy cells [25].

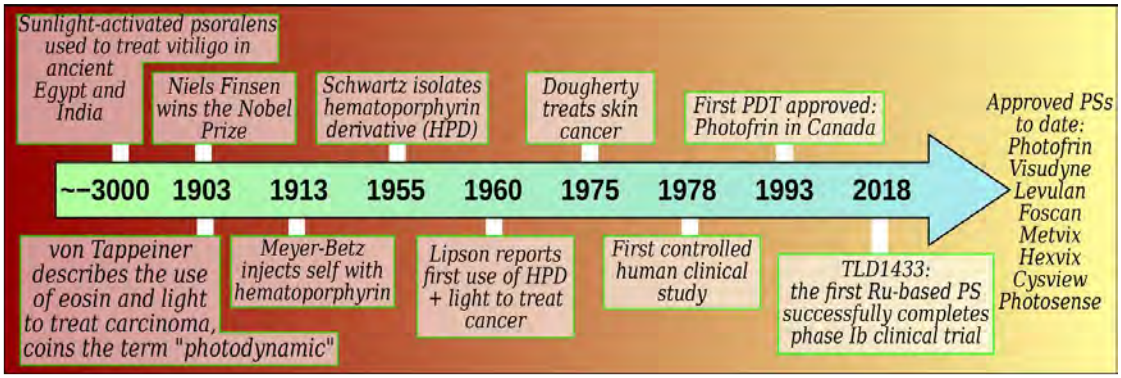

Fig.1.2. Historical development of PDT according to selected milestones. (PS = Photosensitizer)

In PDT, A non toxic photosensitizers (PS) were introduced into the target cells followed by photoirradiation. Photosensitizer molecule was excited from its ground state (S_0) because it has two electrons with opposite spins. Absorption of a photon of light with the appropriate quantum energy (620-850 nm) leads to the excitation of one electron (S_1) into a higher-energy orbital (**Fig.1.3**). This singlet excited-state is very unstable because, the short lifespan (10^{-9}s) of the singlet excited state and singlet-triple energy transfer is usually a forbidden process due to spin conservation rule. Therefore, it loses its excess energy in the form of fluorescence or internal conversion, which helps to visualize the tumor. However, the excited singlet (S_1) may undergo an intersystem crossing to form a more stable excited triplet state (T_1) with parallel spins. The triplet-state PS molecule can decay back to the ground state by the quantum selection rules, so the triplet state is more stable having lifetime of microseconds. This long lifetime of the triplet state permits it enough time to transfer its energy by

colliding with molecular oxygen (O_2), which is unique in being a molecular triplet in its ground state. This energy-transfer step leads to the formation of singlet oxygen ($^1O_2$) [26-30].

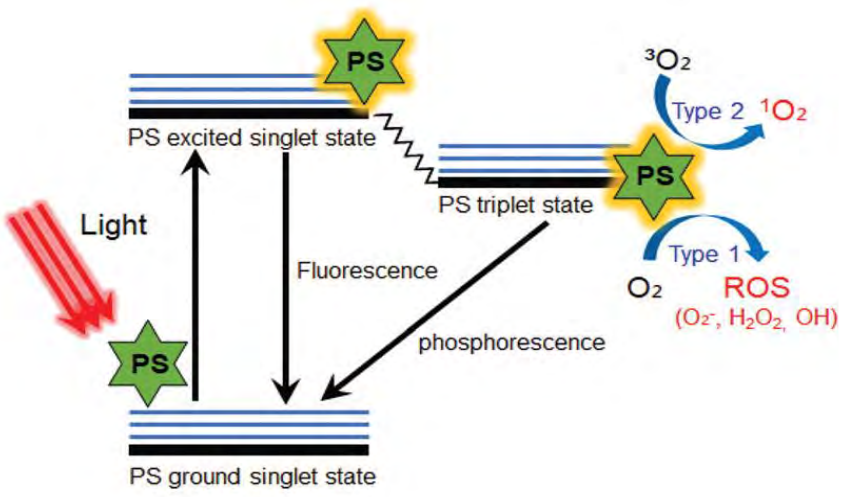

Fig 1.3. Jablonski Diagram.

In the cell the photochemical excitation of the photosensitizers was stimulates the formation of singlet oxygen ($^1O_2$), this singlet oxygen is the key for further reactions. The reactions of the excited photosensitizer can be categorized into two types, Type I reactions and Type II reactions, and examples of both of these are given in **Fig.1.4**. [31]. Type I photochemical process can also occur whereby the excited state PS undergoes electron transfer reactions that eventually forms reactive oxygen species (ROS). This mechanism may involve either gaining or donation of an electron to form the radical cation or radical anion. The radical anion can react with oxygen to produce the superoxide radical anion ($O_2^{\bullet-}$). Dismutation or one-electron reduction of $O_2^{\bullet-}$ gives hydrogen peroxide (H_2O_2), which in turn can undergo another one-electron reduction to form the powerful oxidant hydroxyl radicals ($HO^{\bullet}$). Type II reactions involved energy transfer from the triplet state to ground state O_2 forming a non-radical but highly reactive oxygen species. ROS generation via Type II reaction is

mechanistically much simpler than Type I, and most PSs used for anti-cancer PDT are believed to operate via the Type II rather than the Type I mechanism [32-35].

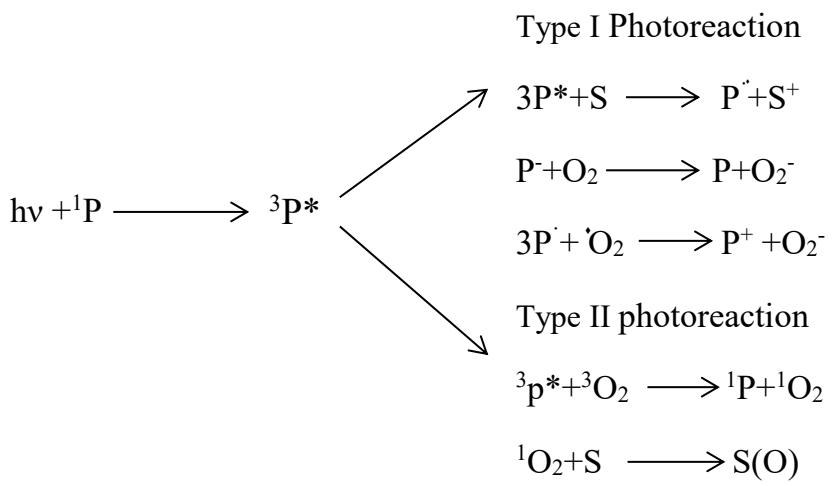

Fig.1.4. Photochemical reaction.

The photosensitizers tend to be comparatively hydrophobic compounds that rapidly diffuse into tumor cells and localize in intracellular membrane structures such as mitochondria and endoplasmic reticulum [36]. More polar compounds tend to be taken up by the active process of adsorptive or fluid phase endocytosis and this process is slower than passive diffusion, Because in polar solvents, life time of singlet oxygen are much higher than in non-polar solvents and their lifespan gets even shorter in the cells due to rapid reactions with subcellular substrates. Many theories have been suggested to account for the tumour-localizing properties that have long been observed in PDT [37-38]. These clarifications include the occurrence of leaky and tortuous tumor blood vessels that are typical of the neovascularization process happening in tumor angiogenesis and composed with the absence of lymphatic drainage in tumors are collectively known as the enhanced permeability and retention effect [39]. Some of the most effective PS compounds have been found preferentially to low-density lipoprotein among various serum proteins that are sometimes found on tumour cells could be important in tumour localization [40].

The lifetime of singlet oxygen ($^1O_2$) is very short (~10–320 ns), limiting its diffusion to only approximately 10–55 nm in cells [41]. Thus, photodynamic damage is probable to arise nearby intracellular site of the PS [42]. PDT can kill cells via apoptotic, necrotic and autophagy-associated cell death [43]. It is thought that the subcellular localization of the PS in different organelles such as mitochondria, lysosomes, endoplasmic reticulum, plasma membrane, etc., plays a major role in the type of cell death mechanism that controls, but other factors such as the overall PDT dose (PS concentration × light fluence). Overall it is accepted that apoptosis is the principal modality of cell death when cells are treated with PDT *in-vitro* [44].

1.3. Antimicrobial Photodynamic Chemotherapy (APDT).

PDT in the treatment of cancer is now widely recognised, and a number of groups have moved on to examine other fields in which the PDT principles may be used. Areas that have been looked at include age-related macular disease [45], inactivation of yeasts [46], inactivation of viruses [47], blood product disinfection [48], infected burn wounds [49] and ulcers caused by bacteria. Photodynamic antimicrobial chemotherapy (PACT) is potentially very useful in the treatment of chronic wounds or ulcers which are resistant to healing on their own or using conventional therapies and this is a growing problem in the elderly [50]. In order to address the demands of various drug resistant bacteria and the diseases they cause, the advent of bacterial resistance to traditional antibiotics has created a gap in the market [51].

Many strains of bacteria are no longer susceptible to antibiotics due to the problem of developing resistance. However, PACT is a treatment to which bacteria are less likely to develop a resistance because of the nature of the singlet oxygen generated and the ability it has to attack numerous targets inside the cell [52]. The

compounds can also potentially target anaerobic microorganisms through type I reactions. PACT is, however, limited to local, rather than systemic, infections because the body's natural flora needs to remain unaffected. There can also be problems with light delivery to internal sites, although deep-seated infections can now be treated due to the development of optical fiber technology [53].

What is important in PACT, is the capacity to excite the photosensitizer at its target site with minimal photoeffect on the surrounding tissue. But it should be remembered that the uses low-power light rather than the lasers used in ablative therapy: photokilling of microbial is attained with mille watts [54]. The power density and the illumination time both can be varied at same light dose. But, a high power density over a short time period may give dissimilar results, in terms of microbial kill, from those of a low power density over a longer time even though the light dose is the same in each case. The direct use of light against microbial pathogens may cause collateral damage [55]. This can be minimized through the light-absorption characteristics of the proposed photosensitizer and of its target environment. Although PACT is gaining increasing acceptance it is not, at present, a mainstream therapeutic option. In the field of viral decontamination the increasing use of photosensitizers may leads to remove from the clinical situation, According to recent research, the technique against a range of oral pathogens and also against drug resistant bacteria should encourage its use in a wider arena [56]. In addition, photosensitizers, are being inexpensive and should be attractive in the area of low-cost topical healthcare regimens.

1.4. Photosensitizers (PS).

Photosensitizers are compounds that are capable of absorbing light of a specific wavelength and convert it into useful energy. In the case of PDT, this would involve the production of lethal cytotoxic agents [57]. There are hundreds of natural and synthetic compounds that can function as photosensitizers, ranging from plant extracts to synthetic macrocyclic complexes. The main characteristic of any photosensitizer is its ability to specially accumulate in diseased tissue, and then generate cytotoxic agents to induce the desired biological effects [58]. A PS should preferably be a single pure compound to allow synthesis under good manufacturing practice conditions with quality control and low manufacturing costs and leading to better stability in storage [59]. The ideal photosensitizers should have a strong absorption peak in the red to near-infrared spectral region (between 650 and 800 nm) because absorption of single photons with wavelengths longer than 800 nm does not provide enough energy to excite oxygen to its singlet state [60]. The interactions of the photosensitizer excited states with endogenous oxygen in the target cells or the surrounding target tissues provide the cytotoxic effects. PSs should possess a substantial triplet quantum yield leading to good production of ROS upon irradiation [61]. Nearly all of the photodynamic action described in this perspective involves the production of either $^1O_2$ or O_2^-. However, phototherapy of severely hypoxic tissues would necessitate different mechanisms of action such as direct photoinduced charge transfer from photosensitizer to biological tissue. Molecular oxygen must be present at sufficient levels throughout irradiation of target tissues or cells to produce $^1O_2$ continuously. Depletion of molecular oxygen in tissue during high-fluence-rate irradiation has been reported to counteract the effectiveness of PDT. It should have no dark toxicity and relatively rapid clearance from normal tissues, thereby minimizing the side effects of

phototoxicity [62]. In the next sections, we shall examine the different photosensitizers including porphyrins, nonporphyrin and transition metal photosensitizers with respect to clinical or preclinical status and current research on the development of related or novel structures [63].

1.4.1. Acridine.

Acridines were first proposed by an Australian chemist Adrien Albert and it was his work that leads to the understanding of their mode of action. Adrien Albert showed that to increase the ionization of the compound the electronic conjugation between the ring nitrogen and amino group were most active with aminoacridines [64]. In bacteria, nucleic acids are the established sites of action of simple aminoacridine derivatives. This is because, the planar area of the tricyclic acridine nucleus is perfectly suitable to intercalation between nucleotide base pairs in the helix and the positive charge aids targeting [65].

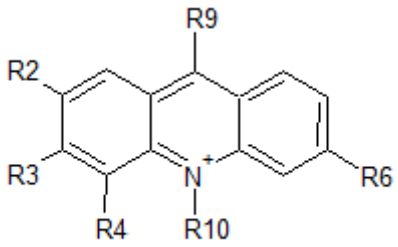

Fig 1.5. General structure of acridine**.**

	R2	R3	R4	R6	R9	R10
Proflavin	H	NH_2	H	NH_2	H	H
Aminacrin	H	H	H	H	NH_2	H

1.4.2. Azines.

Azine derivatives were the first synthetic antibacterial compounds. They have a simple tricyclic skeleton. Methylene blue is an effective nucleic acid intercalator and is comparatively non-toxic to humans [66]. It has been used for the inactivation of

numerous pathogens contained in blood plasma and for the treatment of methaemoglobinaemia. The synthesis of Methylene blue and its related phenothiazinium structures are relatively easy but are easily reduced to the neutral amine that is failed as a photosensitizer [67].

The phenothiazine derivatives associate with nucleic acids recommended that the dyes would be more specific for pathogen reduction and less damage to red blood cells. However some of the phenothiazine was associated with red blood cells and the bound form of the dye is responsible for photo induced haemolysis. Photo treated red cells exhibit high rates of potassium efflux, which is indicative of membrane damage [68]. Small pores are produced which are permeable to ions but not haemoglobin. At ionic equilibrium, the internal osmotic pressure in ion-permeable red cells is greater than the external osmotic pressure because haemoglobin contributes as anosmoticum. This imbalance in pressure leads to water influx, cell swelling and finally cell death.

	R	R^1	R^2	X	Y	λ_{Max} (nm)
Methylene blue	$N(CH_3)_2$	$N(CH_3)_2$	H	N	S	660
Toluidine blueO	$N(CH_3)_2$	NH_2	CH_3	N	S	625
Neutral red	$N(CH_3)_2$	NH_2	CH_3	N	NH	540
Proflavine	H_2N	NH_2	H	CH	NH	456
Acridine orange	$N(CH_3)_2$	$N(CH_3)_2$	H	CH	NH	492
Aminacrine	H	H	H	$C\text{-}NH_2$	NH	410
Ethacridine	H_2N	H	OC_2H_5	$C\text{-}NH_2$	NH	420

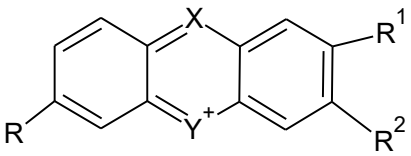

Fig 1.6. Azine photosensitizer structure with specific examples of some common azine based photosensitisers.

1.4.3. Porphyrins and Phthalocyanines.

Many researchers have shown that porphyrins are efficient photosensitizers for use in PACT. While both naturally occurring and synthetic derivatives of porphyrins can be used, the main disadvantage due to resemblances in light absorbtion spectra to endogenous porphyrins. Bamidele M. *et. al.* showed that it was possible to kill gram positive bacteria, using deuteroporphyrin [69] but the inhibition of gram negative bacteria by deuterophorphyrin is not possible. To overcome this problem, the gram negative cells were pretreating with ethylenediaminetetraacetic acid (EDTA) this was studied by Malik, *et. al.* finally he came with results that pre-treated cells were lost upto 50 %. This is due to an increased electrostatic repulsion between LPS molecules caused by the removal of the divalent cations [70].

Porphyrins and closely related chlorins have also been demonstrated as effective virucidal agents *in-vitro* apparently causing photodamage to the viral envelope [71]. Benzoporphyrin derivative has been tested against HIV in whole blood and is reported to be more selective than methylene blue against intracellular virus, giving complete inactivation.

Phthalocyanines are formed from tetrabenzotetraazaporphyrins, for these compounds aromaticity increased when compare to parent porphyrin nucleus and also the increase in the near infrared absorption. In addition to this the synthetic route for phthalocyanine is easier, so it has meant that a wide range of compounds is available in terms of the central metal/ semi-metal atom and side-chain functionality [72].

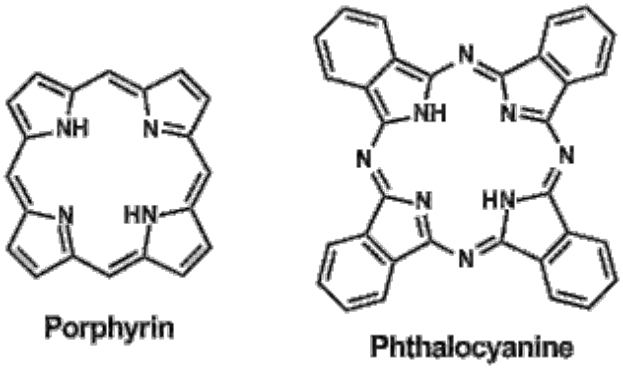

Fig.1.7. General structure of Porphyrin and Phthalocyanines.

Photofrin® is the only PS that was once approved worldwide for certain cancers, these are the clinically approved first generation PS. It has been withdrawn from use in the European Union, because of its disadvantage. This shows hepatotoxicity and reduced capacity for tumor targeting, weak absorbtion in the visible region. With these disadvantage first generation PS has been modified of form new, better second generation PSs. Second generation PSs are Visudyne®, Levulan® and porphycene® and their metallic derivatives (Al, Si, SiNCy, Sn, $SnEt_2$) were later approved worldwide for basal cell carcinoma apart from the United States [73]. But these all exhibit more intense absorbtion in visible region. But no consistence relationship between metallation and improved photoactivity was observed.

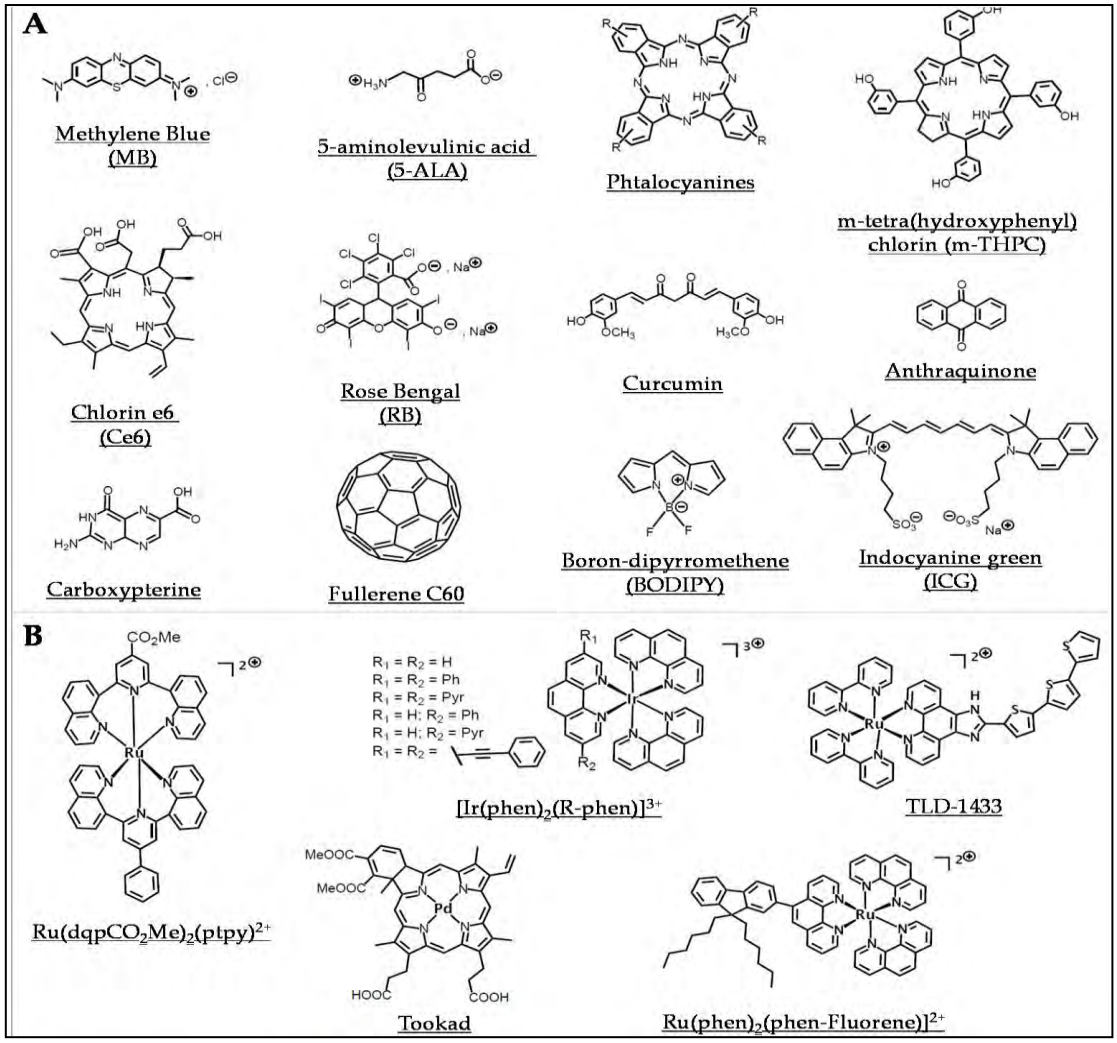

Fig.1.8. Clinically approved photosensitizers used in PDT A) Example of some organic photosensitizers, B) Examples of Some metalic photosensitizers.

From the literature survey, it is know that most of the PSs used for medical purpose belongs to three basic structure such as tricyclic dyes, tetrapyrroles and flurocoumarins and also they have approved by the food and drug administration (FDA) for clinical application, even though they have certain drawbacks, they are Single-agent, aqueous-soluble PSs that are prepared in high purity from straightforward syntheses are highly desirable [74-76]. Low photobleaching rates, high selectivity for tumors, strong PDT effects with high irradiances and favorable pharmacokinetic properties for the intended application are additional considerations [77].

1.4.4. Non porphyrinic transition metal bases photosensitizers.

After the success of cis platin (platimum basaed anticancer drugs), the chemist are interested in transition metal based compounds, which include coordination complexes and organometallic structures, there remains a universal fear that metals are too toxic to be considered in pharmaceutical formulations and consequently, the development of medicinal inorganic chemistry has lagged conventional organic chemistry in pharmaceutical development [78-80]. This ongoing worry arises from the toxicity of some heavy metals. The overall property of the transition metal complex depends on the coordinated ligands and oxidation state of the central metal ion.

As a similarity, many compounds that contain carbon are very toxic in nature, but we do not conclude that all carbon-containing compounds are dangerous [81]. Generally chemotherapeutics are toxic by design; our goal is to found an acceptable therapeutic margin, where the therapeutic benefit overshadows the negative effects. The guiding principle is the same for both organic and inorganic drug development.

Metal complexes and organometallics offer a wide range of oxidation states, coordination numbers, and geometries, yielding a virtually unlimited structural and chemical space to explore [82]. Metal complexes have been used to alter bioavailability, bind/release small molecules, inhibit enzymes, probe biological macromolecules such as DNA, label proteins, image cells and provide contrast as MRI agents, among other things [83-84]. Some act as catalysts to facilitate reactions that are simply not possible with organic compounds, and it is renowned that natural metal complexes are cofactors in their most sophisticated biological reactions [85]. Xavier Cartoixa, *et. al.* suggested that the transportation of oxygen requires a metal center. Metal-based compounds are biological and chemical diversity that is different from that of organic drugs, making them very attractive as biological agents in the detection

of new entities with novel mechanisms of action to treat drug-resistant diseases and conditions [86].

The properties of the d-block transition metal complexes can be changed drastically and owing to their modular three-dimensional architectures that can be easily modified by careful selection of ligand-metal combinations [87]. *Soliman* and *coworkers* explained on metal complexes in cancer therapy, highlighting some of these d-block properties. Structural and electronic properties can be altered by changing the identity of the metal and its oxidation state, which determines coordination number and geometry [88]. This needs changes in physical properties and chemical reactivities, including charge [89], solubility, Lewis acidity, magnetism, rates of ligand exchange, and strengths of metal−ligand bonds, metal- ligand based redox potentials, ligand conformations, and outersphere interactions [90]. In addition, the ligands can be modified to contribute to biological activity as part of the intact complex or upon ligand dissociation. Photophysical properties can also be manipulated in this way, and together these design aspects explain the attractiveness of metal complexes for photobiological applications [91].

Besides their first intended development as anticancer compounds, metal complexes have also been envisaged as potential “metallo-antibiotics”, benefiting from the knowledge accumulated about their chemical properties and biological behaviors [92]. Quite recently, several metal compounds were characterized for their activity in aPDT. For instance, platinum(II), molybdenum(II), ruthenium(II), cobalt(II) and iridium(III) were proposed as new classes of stable photo-activatable metal complexes capable of combating AMR [93-96]. In particular, many mononuclear and polynuclear Ru(II/III) complexes have been considered as potential antibiotics, antifungals, antiparasitics, or antivirals, which have been recently extensively

reviewed [97]. It is worth noticing here that, among all the metal compounds, ruthenium was the most frequent element in active antimicrobial compounds that are nontoxic to eukaryotic cells, followed by silver, palladium, and iridium its activity on all mutant strains of the SARS-CoV-2 [98].

Wanhua Lei, *et. al.* was reported the Ru(II) polypyridyl complexes (**Structure 1.1**) of mixed ligand as a photosensitizers for the inactivation gram negative bacteria such as *E.oli* at different concentration. The outcome results reported that the positive charges, the higher lipophilicity of the intercalating ligand provide $[Ru(II)(bpy)_2(dppn)]^{2+}$ with potent binding capacity to the negatively charged outer membrane of *E. coli*, leading to a remarkable photoinactivation activity [99].

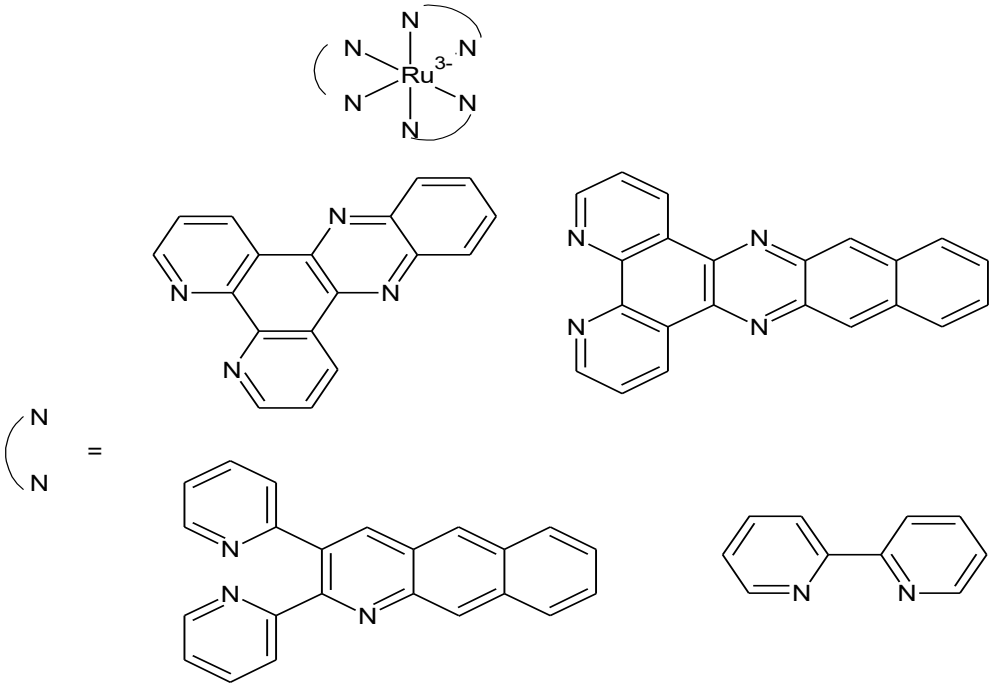

Structure 1.1. Structure of Ru(II) polypyridyl complexes.

Samantha L. Hopkins, *et. al.* have been reported the synthesis, structural investigation and photoinaction by using mixed ligand metal compex of Ru(II)-Pt(II) bimetallic complex (**Structure 1.2)**. The outcome results shows that $[Ru(Ph_2phen)_2(dpp)PtCl_2]^{2+}$ complex with *E. coli*, it is seeming that covalently

coupling a targeted bioactive site with a photosensitizer affords a photoactive antibacterial therapy, and also mixed ligand metal complexes showed enhanced antibacterial properties for the green light irradiated samples when compare to cis platin [100].

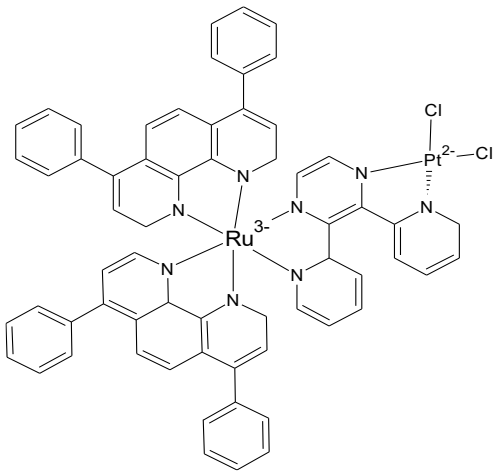

Structure 1.2. Structure of Ru(II)-Pt(II) bimetallic complex.

Chittanahalli N. Sudhamani, *et. al.* was reported a iron complex of a phenanthroline-based photosensitizers (**Structure 1.3)**. DNA binding, photo-induced DNA cleavage activity and photoinactivation of gram negative bacteria. These results reported that the planarity and extended conjugation of the phenanthroline based ligand in DNA binding and cleavage activity of the complexes. Binding study shows a minor groove-binding nature of the iron(II) complexes, due to photo induced photosensitizers effect DNA double-strand breaks leading to linear DNA. The mechanistic studies reveal direct involvement of $^1O_2$ in the photo-cleavage process. The newly synthesized iron complex proved to be potential inhibitors against photoinactivation of bacteria at 25 μM concentration. The cell reduction was found to be 80.8%. From this results iron complex was proved to be a potential APDT photosensitizers [101].

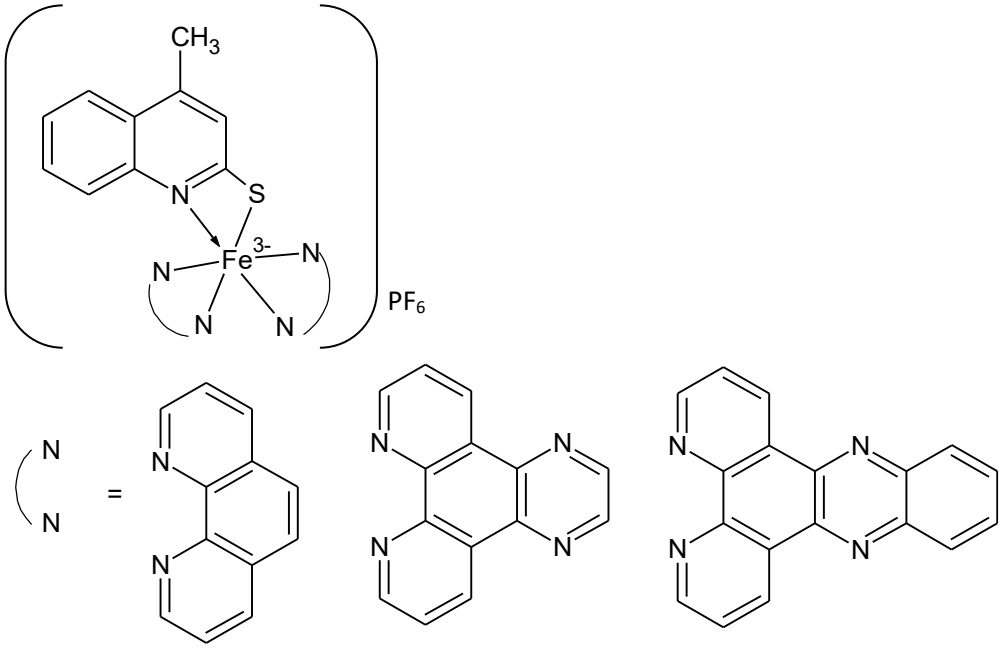

Structure 1.3. Iron complex of a phenanthroline-based photosensitizers.

1.4.5. Transition metal based Schiff base photosensitizers.

Schiff bases are the compounds containing azomethine group (-HC=N-). In 1864, Hugo Schiff which were first report the schiff base, these are formed by condensation of a primary amine with an aldehyde or a ketone under specific conditions [102]. Schiff bases are used as chelators, because of their ease of preparation, structural varieties [103]. Schiff bases have potential sites for nitrogen, oxygen and sulfur. [104]. Schiff base are widely used due to their multipurpose synthesis and soluble in most common solvents [105]. The -C=N- linkage is essential for biological activity. The nitrogen atom of azomethine may be involved in the formation of constituents and interferes in normal cell processes.

The -C=N- linkage of Schiff bases, is readily reduced by metal complexes. Consequently, Schiff bases are versatile ligands, which coordinate with almost all metal ions via nitrogen atoms located in azomethine [106]. Normally, Schiff bases are bi, tri or tetra-dentate chelate ligands and can form stable complexes with metal ions [107]. Schiff-bases play very important role in the development of coordination

chemistry, a thousand number of transition metal complexes of Schiff base have been explored widely. Thus, these are widely used in inorganic biochemistry due to their diverse biological, pharmacological, antitumor activities [108].

In addition to these, form the past decades the interaction of Schiff base metal complexes with DNA has been extensively studied, because of the specific binding properties, and also these complexes were suitable for photocleavage, antitumore drugs. The biological ativity of Schiff base will improve after coordination with different metal ion [109].

S.M. Pradeepa and coworkers have reported the synthesis of Co(II), Ni(II) and Cu(II) complexes of a tetradentate Schiff base photosensitizers having 5-bromo-2-hydroxybenzaldehyde base as DNA binder and also photosensitizers along with potential donar nitrogen and oxygen donor Schiff base (**Structure 1.4)**. From the results the DNA binding abilities resulted that the complexes bind to CT-DNA by an intercalative mode. At UV–Visible light the complexes were found to be efficient photocleaving agents of DNA. The mechanism studies reveal that singlet oxygen ($^1O_2$) plays an important role in the DNA photocleavage [110].

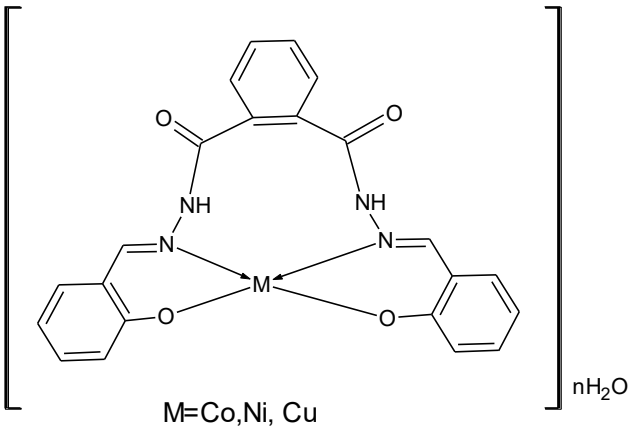

Structure 1.4. Structure of Schiff base photosensitizers.

Samya Banerjee and coworkers have reported the synthesis and characteristion of Platinum based Schiff base metal complexes and the complex

(Structure 1.5) were subjected to Photocytotoxicity and cellular imaging. From the outcome results, the Plattinum complex shows excellent photo-stability under continuous light irradiation and generated singlet oxygen with a quantum yield of ca. 50%. These complexes have potential as photosensitizers for photodynamic therapy with mitochondria and lysosome-targeting ability. Only upon light irradiation The Pt(II) complexes show anticancer activity while remaining inactive in the dark [111].

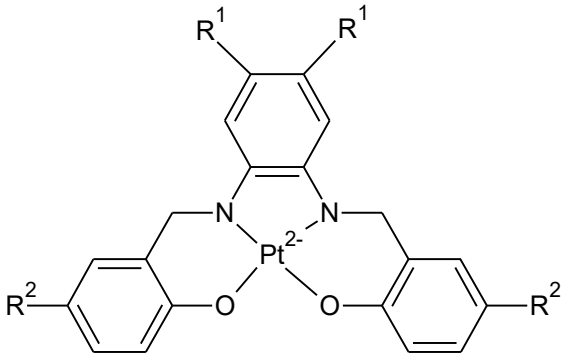

Where R^1=H,CH_3,F

R^2= H,CH_3,F

Structure 1.5 Structure of Platinum based Schiff base metal complexes.

1.4.6. Transition metal based azo photosensitizers.

Nitrogen-containing heterocyclic compounds have extensively studied owing to their interesting biological properties and their role as pharmacophores of considerable historical importance [112]. Among these compounds, the azo dyes which are colored in nature containing one or more azo (-N=N-) chromophores to form rich aromatic conjugation. In recent years, the growing interest in the synthesis of azo dyes having heterocycles in their structures have led to the design of optical recording systems and liquid crystalline devices [113].

The colour of dyes depends on their ability to absorb light in the visible range of electromagnetic radiation. Electronic absorbtion of the azo dye will show maximum absorbtion (400–700 nm) with extraordinary molar absorbtion coefficient because of

the low band gap between π-π* transition of the azo dye [114]. The colour of the dye must have a chromosphere group and an auxochrome group. Chromophores absorbs the light in the visible region (e.g., nitro, azo, quinoid groups) so they convey colour to the dye [115]. While auxochromes deepens the colour when introduced into a coloured molecule. This was explained by Witt theory, but this theory has been replaced by the modern electronic theory. According to this theory, they have extensive π conjugation between the acceptor and the donor units across the azo linkage [116].

With extinction to this Mohamed E. Khalifa, *et. al.* have worked on the synthesis of novel Azo-naphthol dyes with 1-aryazo-2-naphthol nucleus as photosensitizers (**Structure 1.6**). The azo photosensitizers are tested against Leukemia cell lines (HL-6) in photo conditions. The outcome results show that the target naphthols display higher cytotoxicity against cancer cell line under light condition than in dark condition [117].

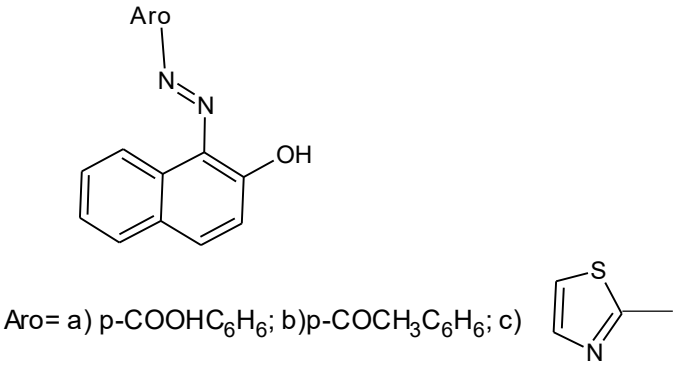

Structure 1.6. Structure of Azo-naphthol dyes derivatives.

Leli Zeng, *et. al.* have reported glutathione (GSH)-activatable dinuclear Ruthenium(II)-azo photosensitizer. This complex showed high accumulation in the mitochondria of cancer cells and produced efficient photocytotoxicity under two-photon irradiation and the complex effectively inhibited cancer growth and killed cancer cells in a 3D MCTS model. These results shows that this GSH activated Ru-azo

photosensitizer has great potential for the development of tumor-selective, two-photon photodynamic therapeutic platforms (**Structure.1.7**.) [118].

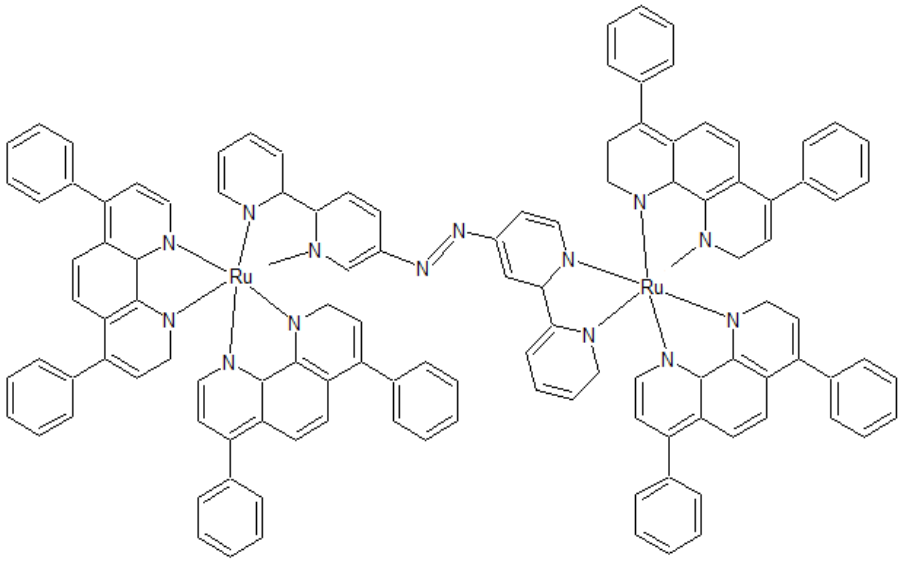

Structure. 1.7. Structure of Ruthenium(II)-azo photosensitizer.

1.5. Organization of the work.

The thesis entitled "**Development of New Metal Based Photosensitizers for Photodynamic Antimicrobial Chemotherapy; An Alternative Approach to Antimicrobial Drugs**" starts with the introduction related to the different aspect of chemistry of non-porphyrinic transition metal based phototherapitic agents. Introduction and experimental technique have been arraangerd in seven different chapter of the thesis.

Chapter-1

The highlight of the present chapter in the thesis is outlined on the detailed discussion of the metal based drugs in cancer therapy, the chemistry of the Schiff base, azo dye system is briefly reviewed. The structure features as well as their various chemical and biochemical applications of the metal complexes of these ligand systems were studied.

Chapter-2

This chapter brefly discusses about the materials used for the synthesis of compounds. The breif explanation of principle invoved in characterizing the molecules by NMR, UV-visible, FT-IR, Mass, TG-DTA, SEM and Powdered XRD are included. The general procedure involved in the preparation of azo dye and their metal complexes are also involved in this chapter.

Chapter-3

In this present chapter, we have synthesized some novel Schiff base contaning naphthalene. The aromatic amine 4-amino-3-hydroxynaphthalene-1-sulfonic acids were reacted with the two aromatic aldehyde such as salicylaldehyde and 3-bromo-4-hydroxy-5-methoxybenzaldehyde in ethanol, triether ether was used as catalyst to form a Schiff base ($HL_1$and HL_2). The formed Schiff base was reacted with Cu(II) and Co(II) metal salts to form Schiff base metal complexes. The structures of the synthesized compounds were characterized by different spectroscopic techniques. The photodynamic inactivation studies conducted against *E-Coli*. Further, all the target compounds were screened for antioxidant and DNA cleavage studies. Also, the binding capability of test compounds was checked by molecular docking studies.

Chapter-4

This chapter involves the synthesis of azo dye based transition metal complexes derived from sulfadiazine. Azo dyes were reacted with metal chloride to achieve target metal complexes. The structural aspect of the newly synthesized compounds were accomplished by various physicochemical techniques like UV-Visible, FT-IR, NMR, and mass spectroscopy, powdered XRD, TG- DTA and SEM-EDAX techniques. The newly synthesized metal complexes were screened for their photodynamic inactivation studies of *E-coli* bacteria and in-vitro antioxidant studies.

Further, the binding capability of test compounds was checked by molecular docking studies.

Chapter-5

The chapter five of the thesis describes the synthesis of heterocyclic azo dye obtained from sulfadiazine with the coupling of pyrimidine- 2,4,6(1*H*,3*H*,5*H*)-trione by diazo coupling reaction. The structures of the synthesized ligand were confirmed by different spectroscopic techiniques. The coordination of ligand to the metal ion was binuclear manner. The pharmacological efficacy of the azo metal complexes was investigated by photoinduced chemotherapy, antibacterial and antioxidant activity. The binding capacities of all the synthesized compounds with protein molecule were studied by in-silico molecular docking studies.

Chapter-6

The chapter 6 outlines the synthesis, physic-chemical characterization and biological evalution Co(II) and Mn(II) complexes of the ligand 4-[(*E*)-(8-hydroxyquinolin-5-yl)diazenyl]-1,5-dimethyl-2- phenyl-1,2-dihydro-3*H*-pyrazol-3-one. The spectroscopic data indicated that the complexes are formed in 1:2 metal to ligand ratio with the general formula of the type $[M(L)_2]$. The synthesized complexes were evaluated for *in-vitro* antimicrobial photodynamic therapy against different pathogens. The results showed that the compounds have displayed good inhibition efficiency compared with the standard. Further, all the synthesized azo compounds were screened for anti-cancer activity. The binding capacity of all the synthesized compounds with protein molecule was studied by in-silico molecular docking studies.

Chapter-7

In this chapter, the synthesis of Cu(II) and Co(II) metal complexes by azo dye derived from acetoacetanilide and indole has been reported. The synthesis of

heterocyclic azo dye was prepared by the diazotization using 4-amino-*N*-pyrimidin-2-ylbenzenesulfonamide and was coupled with 3-oxo-*N*-phenylbutanamide and indole under suitable optimized experimental conditions. Structural features of the synthesized compounds have been accomplished by the various spectroscopic, analytical techniques (UV-Visible absorption spectra, FT-IR, NMR, mass spectrometry). The pharmacological efficacy of the metal complexes was investigated by antibacterial and antituberculosis studies. All the newly synthesized complexes exhibited significant inhibitory activity against tested microbes.

1.6. Reference.

1. M. S. Brady and S. E. Katz, *Analysis of Antib. Drug Resi. in Food Prod. of Animal Orig.,* 5. **1992.**
2. *I.* Rustam Aminov*, Antimi. Resis and Chemo.,* 1, 134, **2010.**
3. J. Carratala, B. Roson, N. Fernandez-Sabe, E. Shaw, O. del Rio, A. Rivera, and F. Gudiol, *Euro. J. Cli.Micro. Infe. Dise.,* 22(3),151–157, **2003.**
4. K. Madhab Chattopadhyay, R. Chakraborty, H. P. Grossart, S. Gundlapally Reddy, and V. Medicharla Jagannadham, *BioMed Rese. Inter.*, 501658, **2015**
5. M. Hutchings, A. Truman and B. Wilkinson, *Curr. Opi, Micro.,* 51,72–80, **2019.**
6. N. Sabtu, D. A. Enoch, and N. M. *Brown British Medi. Bull.*, 116, 105–113, **2015**.
7. P. R. Moore, A. Evenson, T. D. Luckey, E. Mccoy, C. A. Elvehjem, and E. B. Hart. *J. Biolo. Chem,* 165(2), 437–441, **1946.**
8. N. C Loyd, H. W. Morgan, B. K. Nicholson and R. S. Ronimus, *The Composition of Ehrlich's Salvarsan: resolution of a century-old debate,* **2005.**
9. T. C. Smith, and S. E. Wardyn. *Curr. Envi.Heal. Rep.,* 2(1), 41–51, **2015**.
10. B. Spellberg, J. G. Bartlett, and D. N. Gilbert. *New Engl. J. Medi.,* 368(4), 299–302, **2013**.
11. G. Armelagos, *J. Scien.,* 163, 225–258. **1969.**
12. G. Garriss, M. K. Waldor and V. Burrus, *PLoS Genet.,* 5, **2009.**
13. B. G. Hall, and M. Barlow, *Drug Resist. Updat.,* 7, 111–123, 2004.
14. A. Negrea, E. Bjur and S. E. Ygberg, *Antimicrob. Agents Chemother,* **2007**.
15. J. Mahoney, R. Arnold and Harris, *Verer.Dis. Inform.* 24, 355–357, **1943.**
16. G. Hamscher, H.T. Pawelzick, S.Sczesny, H. Nau and Hartung, *Enviro. Health Perspect.,* 111, 1590-1594, **2003.**
17. A. Alaboudi, E. A. Basha and I. Musallam, *Food Cont.,* 33, 281-286. **2013**.
18. Berdy, *J. Antibiot.,* 65, 385, **2012.**
19. I. Cho and M. J Blaser, *Nat Rev Genet.,* 13, 260, **2012.**
20. J. Moan and Q. Peng, *Anticancer Res.* **23**, 3591–3600,**2003**.

21. P. Agostinis, K. Berg, K. A. Cengel, T. H. Foster, A. W. Girotti, S. O. Gollnick, S. M. Hahn, M. R. Hamblin, A. Juzeniene, D. Kessel, *Cancer J. Clin.,* **61**, 250–281, **2011.**

22. A. D. Garg, D. Nowis, J.Golab, P. Vandenabeele, D. V. Krysko and P. Agostinis, *Biochim. Biophys. Acta,* 1805, 53–71, **2010**.

23. A. R. Azzouzi, S. Lebdai, F.Benzaghou and C.Stief, *World J. Urol.*, **33**, 937–944, **2015.**

24. R. F. Donnelly, C. M. Cassidy, R. G. Loughlin, A. Brown, M. M. Tunney, M. G. Jenkins and P. A. McCarron, *Photochem. Photobio.l* B, 96, 223-231, **2009.**

25. G. Spengler, D.Takacs, A. Horvath, A. M. Szabo, Z. Riedl, G. Hajos and J.Molnar*, Burian K. In Vivo*., 28, 1071-1075, **2014.**

26. L. Huang, M. Krayer, J. G. Roubil, Y. Y. Huang, D. Holten, J. S. Lindsey, and M.R. Hamblin, *J. Photochem. Photobiol. B,* 141, 119–127, **2014.**

27. T. Dai, Y. Y. Huang and M. R. Hamblin, *Photodia. Photodyn Ther*., 6, 170-188, **2009.**

28. A. Minnock, D. I. Vernon, J. Schofield, J. Griffiths, J. H. Parish and S. T. Brown, *J. Photochem. Photobiol B*, 32. 159-164, **1996.**

29. T. Maisch, S. Hackbarth, J. Regensburger, A. Felgentrager, W. Baumler, M Landthaler and B.Roder, *J. Dtsch. Dermatol. Ges*., 9, 360-366, **2011**.

30. G. Viola and F. Dall'Acqua. *Curr. Drug Targets*, 7, 1135- 1154, **2006.**

31. M. N. Usacheva, M. C. Teichert and M. A. Biel, *Lasers Surg. Med*., 33, 311-319, **2003.**

32. M. Soncin, C. Fabris, A. Busetti, D. Dei, D. Nistri, G. Roncucci and G. Jori, *Photochem. Photobiol. Sci*, 1, 815-819, **2002.**

33. R. F. Donnelly, C. M. Cassidy, R. G. Loughlin, A. Brown, M. M. Tunney, M. G. Jenkins and P.A. McCarron, *Photochem. Photobiol.* B, 96, 223-231, **2009.**

34. L.Huang, T. G. St Denis, Y. Xuan, Y. Y. Huang, M. Tanaka, A. Zadlo, T. Sarna and M. R. Hamblin, *Free Radic. Biol. Med.*, 53, 2062-2071, **2012.**

35. P. Rothemund, *J. Ameri. Chem. Soci.,* 58. 625-627, **2015.**

36. E. Alves, L. Costa, C. M. Carvalho, J. P. Tome, M. A. Faustino, M. G. Neves, A. C.Tome, J. A. Cavaleiro, A. Cunha and A. Almeida, *Microbiol*., 9, 70, **2009.**

37. R. Dosselli, M. Gobbo, E. Bolognini, S. Campestrini , E. Reddi, *ACS Med. Chem. Lett*., 1, 35-38. **2010.**

38. D. Kessel, R. Luguya and M. G. Vicente, *Photochem. Photobiol.*, 78, 431-435, **2003**.

39. P. Mikula, L. Kalhotka, D. Jancula, S. Zezulka, R. Korinkova, J. Cerny, B Marsalek and Toman, *Photochem. Photobio.l B.*, 138, 230-239, **2014.**

40. Y. Y. Huang, S.K. Sharma, R. Yin, T. Agrawal, L.Y. Chiang and M. R. Hamblin, *J. Biomed. Nanotechnol.,* 10, 1918-1936, **2014.**

41. N. Kashef, S. Karami and G. E. Djavid, *Photodi. Photodyn. Ther.*, 12, 186-192, **2015**.

42. L. Masip, K. Veeravalli and G. Georgiou, *Antioxid. Redox Sig.*, 8, 753-762, **2006.**

43. N. C. Araujo, C. R. Fontana, V. S. Bagnato and M. E. Gerbi, *Lasers Med Sci.*, 29, 629-635, **2014**.

44. Z. Mucsi, G.A. Chass, P. Abranyi-Balogh, B. Jojart, D.C. Fang, A.J. Ramirez-Cuesta, B. Viskolcz and I.G. Csizmadia, *Phys. Chem. Chem. Phys.,* 15, 20447-20455, **2013**.

45. P. Majumdar, R. Nomula and J. Zhao, *J. Mater. Chem*, 2, 5982–5997, **2014.**

46. S. G. Awuah and Y. You, *RSC Adv.,*2, 11169–11183, **2012**.

47. A. Gorman, J. Killoran, C. O'Shea, T. Kenna, W. M. Gallagherand D. F. O'Shea, J. Am. *Chem. Soc.,* 126, 10619–10631, **2004**.

48. D. Ravelli, M. Fagnoni and A. Albini, *Chem. Soc. Rev*, 42, 97–113, **2013**.

49. L. Shi and W. Xia, *Chem. Soc. Rev,* 41, 7687–7697, **2012.**

50. Q. Zhao, F. Li and C. Huang, *Chem. Soc. Rev*, 39, 3007–3030, **2010.**

51. A. Master, M. Livingston and A. S. Gupta, *J. Controlled Release*, 168, 88–102, **2013**.

52. E. M. Sletten and T. M. Swager, *J. Am. Chem. Soc*, 136, 13574–13577, **2014.**

53. E. Boija and G. Johansson, *Biochim. Biophys. Acta,* 1758,620–626, **2006.**

54. H. D. Edwards, S. K. Nagappayya and N. L. B. Pohl, Chem. Commun, 48, 510–512, **2012.**

55. K. Reinhart, M. Bauer, N. C. Riedemann and C. S. Hartog, *Clini. Micro. Revs.,* 25 (4), 609-34, **2012**.

56. M. R. Hamblin, *Curr. Opin. Microbio.,* 33, 67-73, **2016.**

57. P. Yagupsky and F. S. Nolte, *Clini. Microbi. Rev.,* 3 (3), 269-79, **1990.**

58. M. Merchat, G. Bertolini, P. Giacomini, A. Villanueva and G. Jori, *J. Photochem. Photobiol.,* 32, 153–157, **1996**.

59. H. Gursoy, C. Ozcakir-Tomruk, J. Tanalp and S.Yılmaz, *Clinical Oral Inves.,* 17 (4), 1113-25, **2013**

60. N. A. Romanova, L.Y. Brovko, L. Moore, E. Pometun, A.P. Savitsky, N.N. Ugarova and M.W. Griffiths, *Appl Environ Microbiol.,* 69, 6393–6398, **2003.**

61. H. Abrahamse and M. R. Hamblin, *Biochem. J.,* 473 (4), 347-64, **2016**.

62. M. R. Hamblin, D. A. O'Donnell, N. Murthy, C. H. Contag and T. Hasan, *Photoche. Photobiol.*, 75, 51–57, **2002.**

63. M. Tanaka, M . Kinoshita, Y. Yoshihara, N. Shinomiya, S. Seki and K. Nemoto, *Las. Surg. Medi.,* 43 (3), 221-9, **2011.**

64. D. A. Phoenix and F. Harris, *Trends Mol. Med.*, 9, 283–285, **2003.**

65. T. G. S. Denis, K. Aziz, A. A.Waheed, Y. Y. Huang, S. K. Sharma, and P. Mroz, *Photoche. Photobio. Scie.,* 10 (5), 792-801, **2011.**

66. T.W. Wong, Y.Y. Wang, H. M. Sheu and Y.C. Chuang. *Antimicrob Agents Chemother.*, 49, 895–902, **2005**.

67. M. R. Hamblin, D. A. O'Donnell, N. Murthy, K. Rajagopalan, N. Michaud, M.E. Sherwood and T. Hasan, *J. Antimicrob. Chemother.*, 49, 941-95, **2002**.

68. G. Jori, C. Fabris, M. Soncin, S. Ferro, O. Coppellotti, D. Dei, L. Fantetti, G. Chiti and G. Roncucci, *Surg Med.,* 38, 468–481, **2006.**

69. M. Bamidele. Amos-Tautua, P. Sandile Songca and S. Oluwatobi Oluwafemi, *Molecules.*, 24(13), 2456, **2019.**

70. D. Kessel, *Med. Laser Appl.*, 21, 219–224, **2006**.

71. R. R. Allison, V. S. Bagnato and C. H. Sibata, *Futur. Oncol.,* 6, 929–940, **2010**.

72. F. Vatansever, W.C.M.A. de Melo, P. Avci, D. Vecchio, M. Sadasivam, A. Gupta, R.Chandran, M. Karimi, N.A. Parizotto, R. Yin, G.P. Tegos and M.R. Hamblin, *Microbiol. Rev*., 37, 955– 989, **2013**.

73. X. Jia, F.-F. Yang, J. Li, J.Y. Liu and J.P. Xue, *J. Med. Chem.,* 56, 5797–5805, **2013.**

74. E. Ranyuk, N. Cauchon, K. Klarskov, B. Gue and J.E. van Lier, *J. Med. Chem.,* 56, 1520–1534, **2013**.

75. S. Yano, S. Hirohara, M. Obata, Y. Hagiya, S. Ichiro Ogura, A. Ikeda, H. Kataoka, M. Tanaka and T. Joh, *Adv. Colloid Interface Sci.,* 116, 1–11, **2005**.

76. S.V. Kudrevich and J.E. Van Lier, *Coord. Chem. Rev.,* 156, 163–182, **1996**.

77. X. J. Jiang, J.D. Huang, Y.J. Zhu, F.X. Tang, D.K.P. Ng and J.C. Sun, *Bioorg. Med. Chem. Lett.,* 16, 2450–2453, **2006**.

78. J. S. Heier, D.S. Boyer, T.A. Ciulla, P.J. Ferrone, J.M. Jumper, R.C. Gentile, D.Kotlovker, C.Y. Chung and R.Y. Kim, *JAMA Ophthalmol.,* 124, 1532–1542, **2006**.

79. B. Sherlock, S.C. Warren, Y. Alexandrov, F. Yu, J. Stone, J. Knight, M.A. Neil, C. Paterson, P.M. French and C. Dunsby, *J. Biophotonics.,* 11, **2018**.

80. E. Ruggiero, S. Alonso-de Castro, A. Habtemariam and L. Salassa, *Dalton Trans.,* 45, 13012–13020, **2016**.

81. C. Sandberg, A.M. Wennberg and O. Larko, *Springer*, 91–96, **2011**.

82. N. Finsen, *Photothe.,* **1901.**

83. R. Bonnett, *Chem. Soc. Rev.,* 24, 19–33, **1995**.

84. J. Prime, Les accidentes toxiques par i'eosinate de sodium, Jouve and Boyer, Paris, **1900**.

85. L. B. Josefsen and R. W. Boyle, *Met. Based Drugs,* 276109, **2008.**

86. X. Cartoixa, R. Rurali, and J. Sune, *Phys. Rev.,* B 86, 165445, **2012.**

87. R. Ackroyd, C. Kelty, N. Brown and M. Reed, *J. Photochem. Photobiol*., 74, 656–669, **2001**.

88. A. Ahmed. Soliman, A. Saadia Ali and Adel Orabi*, Spectrochi. Acta Part A*, 65, 841–845, **2006.**

89. B. Sherlock, S.C. Warren, Y. Alexandrov, F. Yu, J. Stone, J. Knight, M.A. Neil, C.Paterson, P.M. French and C. Dunsby, *J. Biophotonics.,* 11, **2018**.

90. P. Zhang and P.J. Sadler, *J. Organomet. Chem.,* 839, 5–14, **2017**.

91. J. Fong, K. Kasimova, Y. Arenas, P. Kaspler, S. Lazic, A. Mandel and L. Lilge, *Photochem. Photobiol. Sci.,* 14, 2014–2023, **2015**.

92. S. Lazic, P. Kaspler, G. Shi, S. Monro, T. Sainuddin, S. Forward, K. Kasimova, R.Hennigar, A. Mandel, S. McFarland and L. Lilge, *J. Photochem. Photobiol.,* 93, 1248–1258, **2017**.

93. M. B. Spesia, M. E. Milanesio and E. N. Durantini, *Eur. J. Med. Chem.,* 43, 853-861, **2008**.

94. R. Yin, M. Wang, Y.Y. Huang, G. Landi, D. Vecchio, L.Y. Chiang and M. R. Hamblin, Free Radic. *Biol. Med.*, 79, 14-27, **2015.**

95. I. Garcia, S. Ballesta, Y. Gilaberte, A. Rezusta and A. Pascual, *Future Microbiol.,* 10, 347-356, **2015.**

96. V. Engelhardt, B, Krammer and K. Plaetzer. *Photochem. Photobiol. Sci.*, 9, 365-369, **2010**.

97. E. Alves, M.A. Faustino, M.G. Neves, A. Cunha, J.Tome and A. Almeida, *Future Med. Chem.*, 6, 141-164, **2014**.

98. T. J. Silhavy, D. Kahne and S. Walker, *Cold Spring Harb. Perspect. Biol.,* 2, 000414, **2010**.

99. W. Lei, Q. Zhou, G.Jiang, B. Zhang and X. Wang. *Photochem. Photobiol. Sci.,* 10, 887, **2011.**

100. L. H. Samantha Higgins, J. Allison Tucker, S. J. Brenda Winkel and J. Karen Brewer. *Chem. Commun.*, 48, 1, 67-69, 2012.

101. C. N. Sudhamani, H. S. Bhojya Naik and D. Girija, *Nucle. Nucles. Nucl. Aci.*, 31, 130–146, **2012**.

102. M. I. Souza, E. R. Silva, Y. M. Jaques, F. F. Ferreira, E. E. Fileti and W. A. Alves. *J. Pept. Sci.*, 20, 554-562, **2014**.

103. F.Gad, T. Zahra, T. Hasan and M. R. Hamblin, *Antimicrob. Agents Chemother.*, 48, 2173-2178, **2004**.

104. S. Dinicola, S.De Grazia, G, Carlomagno and J.P. Pintucci, *Eur. Rev. Med. Pharmacol. Sci.*, 18, 2942-2948, **2014**.

105. S. Aslam and R.O. Darouiche, *Int. J. Artif. Or-gans.*, 34, 752-758, **2011**.

106. L. Masip, K. Veeravalli and G.Georgiou. *Antioxid. Redox Sig.*, 8, 753-762, **2006.**

107. M. Goswami and N. Jawali. *Antimicrob. Agents Chemother.*, 54, 3529-3530, **2010.**

108. G. V. Smirnova and O. N. Oktyabrsky. *Bio-chemistry (Mosc)*, 70, 1199-1211, **2005.**

109. C. N. Sudhamani, H. S. Bhojya Naik and D. Girija, *Nucle. Nucleo.Nucl. Acis.*, 31,130–146, **2012**.

110. S. M. Pradeepa, H. S. Bhojya Naik, B. Vinay Kumar, K. Indira Priyadarsini, Atanu Barik and S. Jayakumar. *Inorg. Chim. Acta.,* 428, 138–146, **2015**.

111. S. Banerjee, S. Miles Capper, J. Guy Clarkson, H. Huang and J. Peter Sadler, *Polyhed.*, 172, 157-166, **2017**.

112. S. Winter, N. Tortik, A. Kubin, B. Krammer and K. Plaetzer, *Photochem. Photobiol. Sci.*, 12, 1795-1802, **2013**.

113. N. C. Araujo, C. R. Fontana, V. S. Bagnato, M. E. Gerbi, *Lasers Med. Sci.*, 29, 629-635, 2014.

114. M. Heger, R. F. Van Golen, M. Broekgaarden, and M.C. Michel, *Pharmacol. Rev.*, 66, 222-307, **2014**.

115. T. A. Dahl, W. M. McGowan, M. A. Shand and V. S. Srinivasan, *Arch. Microbiol.*, 151, 183-185, **1989**.

116. Z. Mucsi, G.A. Chass, P. Abranyi-Balogh, B. Jojart, D.C. Fang, A.J. Ramirez-Cuesta, B. Viskolcz and I.G. Csizmadia. *Phys. Chem. Chem. Phys.,* 15, 20447-20455, **2013**.

117. E. Mohamed Khalifa, A. Elham Elkhawass, Masayuki Ninomiya, Kaori Tanaka, and Mamoru Koketsu, *Chem. Sele., 5*, 8609 –8615, **2020.**

118. L. Zeng, S. Kuang, G. Li, C. Jin, Liangnian Ji and H. Chao, *Chem. Commun.,* 53, 1977, **2017**.

Chapter-2

Methods and Materials

2.1. Introduction.

In this chapter, we have discussed the methods, materials and analytical techniques used for the characterization of the synthesized azo dyes and their respective transition metal complexes. The solvents and reagents used are of analytical grade and obtained from sigma Aldrich, hi media and fine chemicals. All the chemicals were used without further purification. The melting points of the newly synthesized compounds were recorded in an open capillary tube on an electro thermal apparatus and are uncorrected. By using thin layer chromatography the purity of all the compounds was tested. The synthesized heterocyclic ligands and their metal complexes were characterized by different physical, analytical and spectroscopic techniques. In this chapter describes the basic principle and instrumentation used for the characterization of the synthesized compounds.

2.2. Nuclear Magnetic Resonance Spectroscopy (NMR Spectroscopy).

Model-Bruker 400 MHz high-resolution multinuclear FT-NMR spectrometer

The NMR spectroscopy is a vital analytical method, used to ascertain the composition and purity of compounds as well as the information on the structure of molecules. The ^{1}H and ^{13}C-NMR are most widely used. It is possible to determine the structure of an unknown substance by using the proton present in the molecule, which will behave differently based on the structure of the surrounding chemical environment.

Basic Principle

Firstly we start with the spin of nuclei (I) and it generates in a magnetic field without an external force. Some nuclei have integral spin (eg=1, 2, 4), some have fractional spin (e.g.=1/2, 3/2) and few have no spin I=0, in which the I= ½ are NMR active and I = 0 are NMR inactive. ^{1}H and ^{13}C have nuclear spin of ½ and they behave

similar fashion. When an external magnetic field is applied to the randomly oriented nuclie was lineup either spin aligned or spin opposed to the applied magnetic field. Further the radiofrequency is applied energy transferred between ground state to excited state which results resonance. This condition was expressed as

$$E=H\nu \quad .....Eq(2.1)$$

When the nucleus becomes equal to the frequency of the applied electromagnetic radiation then the nuclei are in resonance under the influence of magnetic field. When the spin returns to its ground state level the absorbed radiofrequency energy is emitted at the same frequency level the emitted radiofrequency signal provides the spectra of the nucleus. The intensity of signal v/s magnetic field was plotted to study the NMR signals [1]. To study the instrumentation of NMR spectra the block diagram of NMR spectra are given in **Fig 2.1**

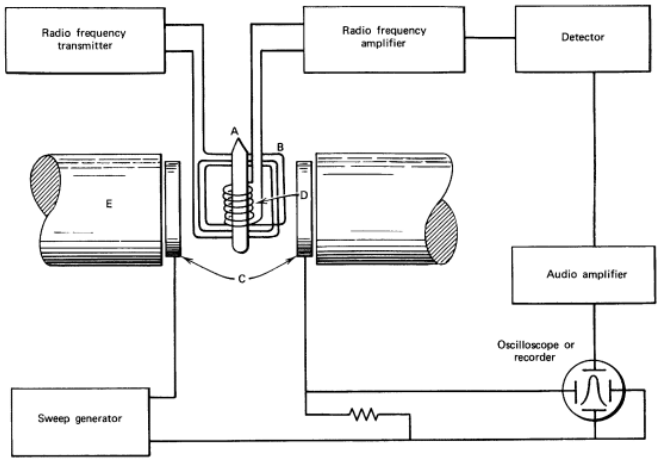

Fig. 2.1 The block diagram of NMR spectroscopy.

2.3. Electronic Absorbtion Spectroscopy (UV-Visible Spectroscopy).

Model-Shimadzu model 1650 UV-visible double beam spectrometer

The UV-Visible spectroscopy is used to detect the aromatic conjugation and multiple bonded system within the molecules by the absorbtion of energy in UV-Visible region.

Basic Principle

When light is absorbed by matter and reflected back, it results in an increased amount of energy in molecules or atoms. When ultraviolet radiations are absorbed, this causes the excitation of electrons in the ground state to the higher energy state. Molecules that contain p-electrons, or non-bonding electrons (n-electrons) are able to absorb energy from ultraviolet light that stimulates electrons into higher non-bonding orbitals. The more easily stimulated the electrons are the greater the wavelength of light that it is able to absorb. There are four types of transitions and are arranged in the following order the following order: s-s* > n-s* > p-p* > n-p* apart from this, the metal complexes exhibits d-d transition such as ligand to metal charge transfer and metal to ligand charge transfer transition. The absorption of radiation by chemical substance creates an identifiable spectrum that aids in identifying the substance [2]. The basic instrumentation of electronic spectroscopy were presented in **Fig. 2.2.**

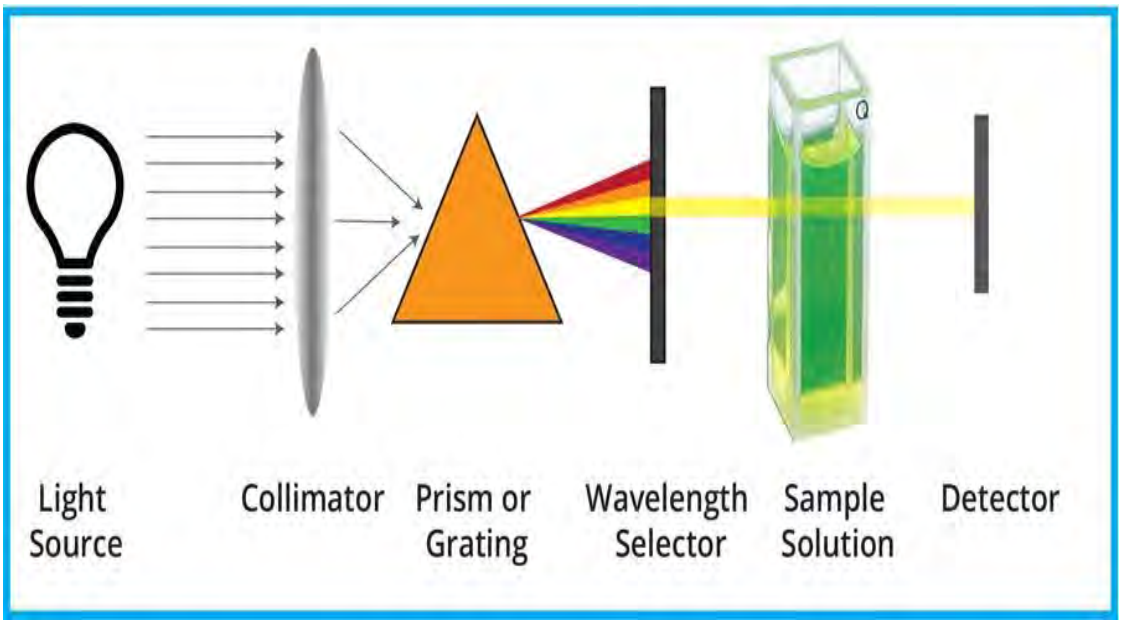

Fig.2.2 The block diagram of UV-Visible Spectroscopy

2.4. Infrared Spectroscopy (IR Spectroscopy).

Model-Thermo Nicolet Avatar IR spectrophotometer

The vibrations of the molecules can be identified by infrared radiation on the molecules. The infrared radiation of the same frequency is allowed to fall on the molecule the molecule absorbs energy and excited to higher vibrational level. The absorbtion of energy by the molecule gives rise to bands characteristic of that molecules from about 4000-400 cm^{-1}. In this region almost all the function group in a molecule exhibits their absorbtion bands respectively.

Basic Principle

When a Molecular absorbs of electromagnetic radiation in the infrared region it promotes transitions between the rotational and vibrational energy levels of the ground electronic energy state. It is well know that each vibrational level consists of various closely spaced rotational spectra. The IR spectrum of the molecule was considered vibrational-rotational spectra. In the infra-red region the molecules absorbs energy and they are constantly vibrating, ie band stretch or contrast with respect to each other, this involves a change in dipole moment as a function of time. The energy of the absorbing molecules increases with absorbed radiation by the amount proportional to the frequency of the absorbed radiation. The different types of bonds absorb radiation at different frequencies because the frequency change may depend on mass of the atom as well as strength of the bond connecting them. The vibrational motion of the molecules increases with energy of the absorbed band due to frequency of the applied was matches with the natural vibration frequency. The wavelength and stretching frequency of the vibration and the absorption frequency of the functional group can be calculated by using hooks law (Eq.2.2).

$$v = \frac{1}{2\pi c}\sqrt{\frac{k(m_1+m_2)}{m_1 m_2}} \qquad \text{.... Eq (2.2)}$$

Where v is the wave number, c the velocity of light=3×10^8 cm/sec, k is a force constant of the bond, m_1 and m_2 are masses of respective atoms [3-4]. The block diagram of FT-IR instrument was shown in **Fig. 2.3.**

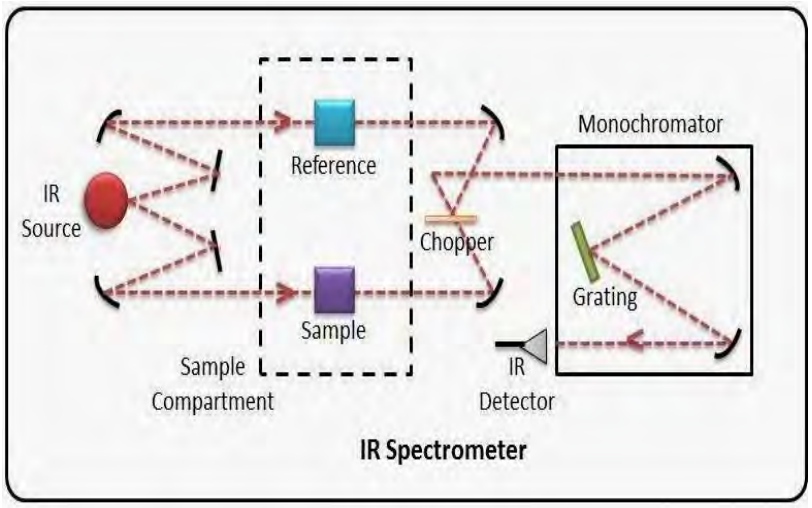

Fig.2.3. The Basic instrumentation of FT-IR Spectroscopy.

2.5. Mass Spectroscopy.

Model-LCMS 2010 SHIMADZU Mass analyzer

The Mass spectroscopy is the most accurate method of all the spectroscopic techniques and used to determine the molecular mass of the unknown compounds.

Basic Principle

When molecules are bombarded with a beam of energetic electrons from the filament, it leads to removal of one outer most electron. Due to the removal of an electron, the molecule will be positively charged and these molecules are known molecular ion or parent ion. The energy of an energetic electron should be 70ev. The excess energy of the forbidden energetic electrons was further used to break the molecular ion to get fragment ion with different molecular mass and some of these fragments are positively ions. Each ion has a particular mass to charge ratio that is

represented as m/e or m/z. For most of the ions the charge is 1 and thus m/z ratio is simply the molecular mass of the ion. The above process is represented as

$$M + e \longrightarrow M^{+\cdot} + 2e^{-}$$

In mass spectrometry, the molecular ion will provide the detailed information concerning the identity of an organic moiety and additionally the breaking of the radical cation into different fragments provides the information on structural property of the molecule [5]. The following block diagram (**Fig.2.4.**) will provide the detail instrumentation of the mass spectrometry.

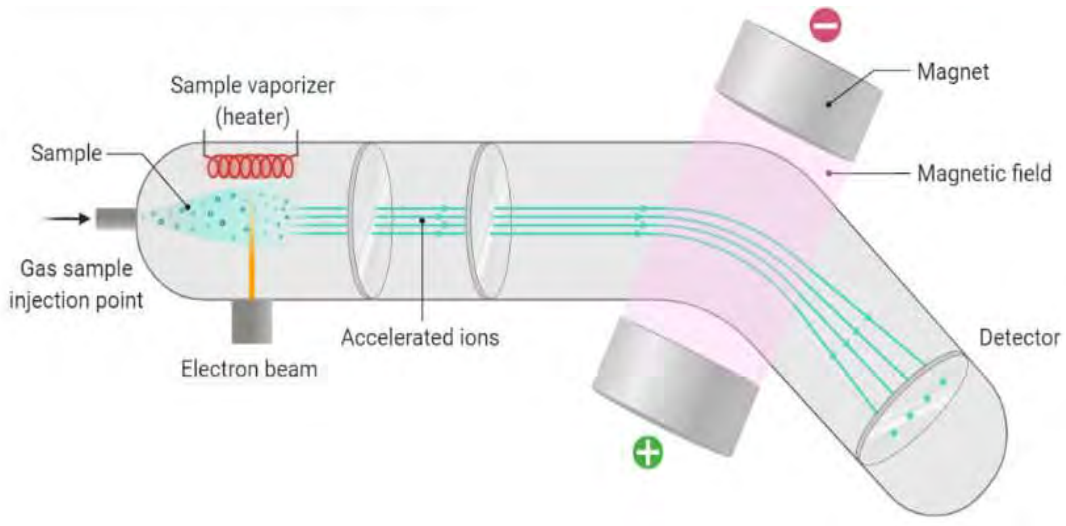

Fig.2.4. The Block diagram of Mass spectroscopy.

2.6. Thermogravimetric analysis (TGA).

Model- TG-DSC curves at a temperature ranging 30-800 ºC in Nitrogen

The Thermgravimetry is the most useful method to know the stability of the substance and also to study the degradation of the compounds with varying temperature and time. This method provides information regards absorbtion, desorption. In this technique the weight of the compound was recorded as a function of temperature and time.

Basic Principle

Tg/DTA was useful to record the thermal propertied of an organic and inorganic substance in a single investigation. In this technique the sample was heated in a given environment (Air, N_2, Ar, He etc.,) at a controlled rate, the temperature was increased at a constant rate for a known initial weight of the substance and the changes in weights are recorded as a function of temperature at different time interval. The overall analysis of this technique is to analyses the change in the weight of the sample due to decomposition, reduction, oxidation and other change in the property of the molecule which results in the decrease or increase in the weight of the substance. Further differential thermal analysis shows the degradation reaction is exothermic or endothermic. Finally the plot of weight change against temperature is known as thermogaravimetric curve or thermo gram [6]. The basic instrumentation of the TGA was presented in **Fig.2.4**

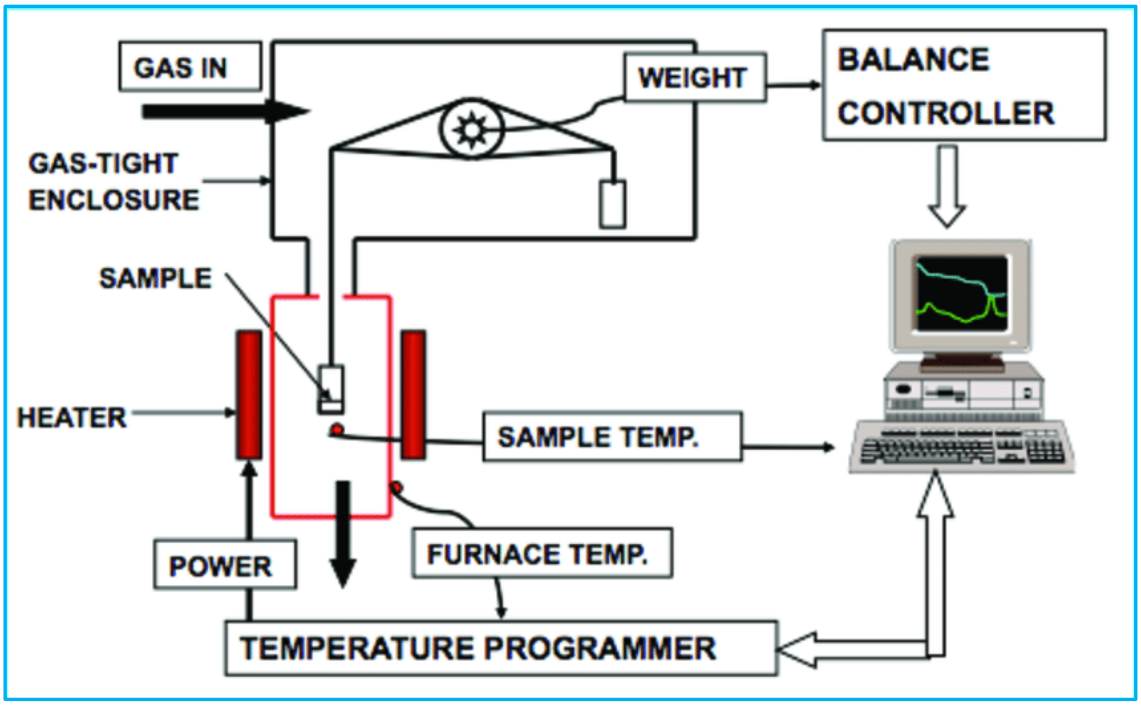

Fig.2.4. The Schematic Representation of Instrumentation of TGA.

2.7. Scanning Electron Microscopy (SEM).

Model- Zeiss scanning electron microscope.

Basic Principle

Enhanced electrons in an SEM carry significant amounts of kinetic energy and this energy is degenerate as a variety of signals produced by electron-sample interactions. When the incident electrons are slowed in the solid sample. These signals include secondary electrons (that produce SEM images), backscattered electrons, diffracted backscattered electrons, photons, visible light, and heat. Secondary electrons and backscattered electrons are normally used for imaging samples. Secondary electrons are most appreciated for showing morphology and topography on samples and backscattered electrons are most valuable for illustrating contrasts in composition in multiphase samples. X-ray generation is produced by inelastic collisions of the incident electrons with electrons in discrete shells of atoms in the sample. As the excited electrons return to lower energy states, they yield X-rays that are of a fixed wavelength. Thus, characteristic X-rays are produced for each element in a mineral that is excited by the electron beam. SEM analysis is considered to be non-destructive. That is, x-rays generated by electron interactions do not lead to volume loss of the sample, so it is possible to analyze the same materials repeatedly [7]. The instrumentation of SEM Analysire was shown in block diagram in **Fig. 2.5**.

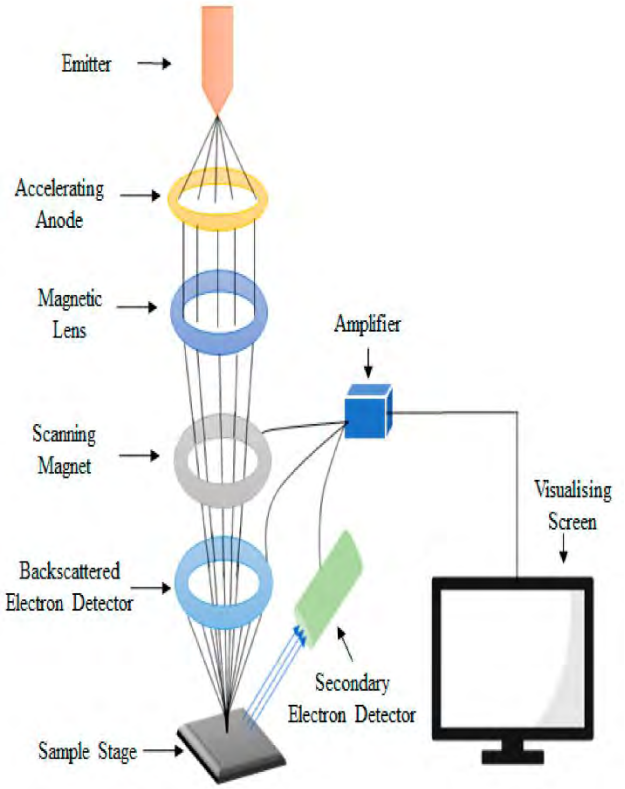

Fig.2.5. The block diagram of SEM analyzer.

2.8. Powdered X-Ray Diffraction (XRD)

Model- Rigaku Smart lab SE

The X-ray diffraction is a powerfull non distructctive technique. This provides detailed information about physical property and to study the atomic spacing of the synthesized compounds.

Basic Principle.

When a monochromatic beam of X-ray is allowed to incident on a sample. These X-rays are produced by a cathode ray tube, filtered to produce monochromatic radiation and directed toward the sample. The interaction of the incident rays with the sample produces constructive interference (and a diffracted ray) when conditions satisfy bagges law ($n\lambda=2d \sin\theta$). Bragg's law tells the wavelength of electromagnetic radiation to the diffraction angle and the lattice spacing in a powdred sample. These

diffracted X-rays are then identified, and calculated by scanning the sample over a range of 2θ angles, all the probable diffraction of the lattice should be attained due to the random orientation of the powdered material. Modification of the diffraction peaks to d-spacing allows identification of the mineral because each mineral has a set of unique d-spacing. Usually, this is achieved by comparison of d-spacing with standard reference patterns. A key component of diffraction is the angle between the incident and diffracted rays [8-9]. The instrumentation of the XRD was shown in **Fig.2.6.**

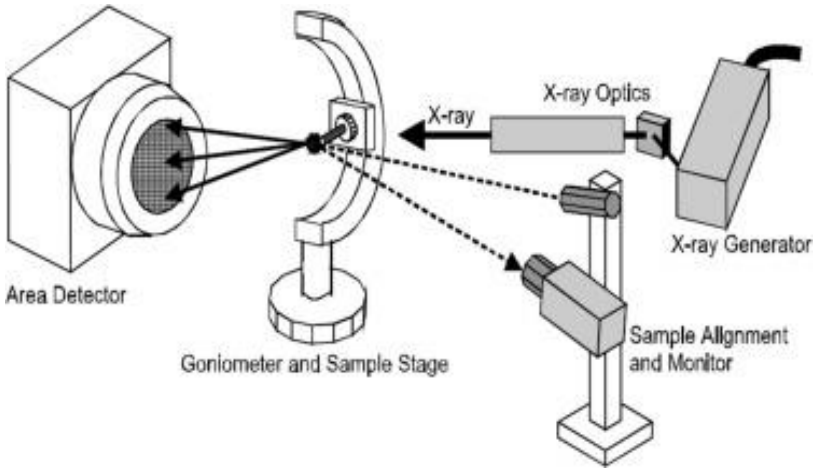

Fig.2.6. The block diagram of instrumentation of Powdered XRD.

2.9. General method of synthesis of azo dye.

The synthesis of an azo dye requires a diazonium salt, which is derived from suitable amines and a coupling component. The interaction of sodium nitrite ($NaNO_2$) with hydrochloric acid to form nitrosonium ion is the basic step in the simple diazotization method for the synthesis of an azo dye [10]. Thus, the aromatic amine reacts with nitrous acid to form N-nitroso intermediate and results in the formation of diazonium ion through protonation and elimination of water molecule.

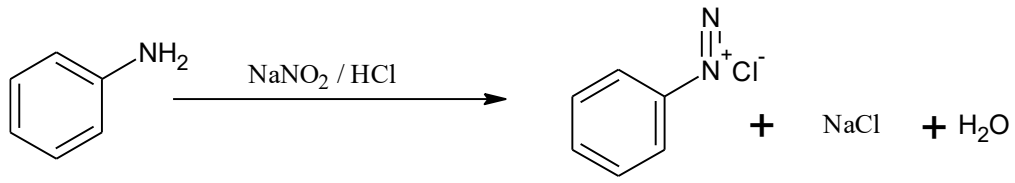

Scheme 2.1 Synthesis of azo dye

Coupling

To complete the synthesis of azo dye, the weak electrophile i.e the diazonium salt reacts with an electron rich coupling component. The coupling reaction takes place at site of increased electron density. Since the diazo ion is a weak electrophile it readily reacts with powerful electron releasing groups like –OH or $–NH_2$. The coupling of phenols takes place under alkaline condition while the coupling of amines takes place under slightly acidic condition [11].

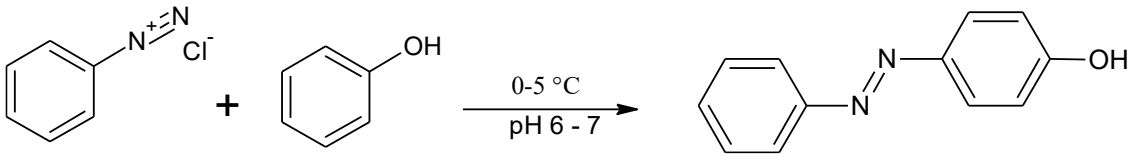

Scheme 2.1 Coupling reaction of diazonium salt with the phenol

2.10. Biological activity.

2.10.1. Antimicrobial photodynamic inactivation studies.

The photoinactivation of the microorganiscms by synthesized metal complexes were determined by Luria Bertani broth method. Briefly, a standard overnight culture containing 0.5 McFarland standards was used for all in vitro assays. Different concentaration of photosensitizers were added to the test cultures and incubated for about 3 hours in dark condition and subjected to light exposure with xenon lamp of wavelength 400-800 nm for about 15 min irradiated in the presence of foil-cover to stay away from accidental exposure to the light. After irradiation the samplese are incubated at 37 °C for 24 hours. The reduction in the planktonic cells measured [12].

2.10.2. Antimicrobial Activity.

The *in-vitro* antimicrobial activity of the tested compounds was evaluated against various bacteria and fungal strain by using agar well diffusion method at 37 °C. Briefly, the microorganism inoculums were evenly spread using sterile cotton swab on a sterile petri dish containing malt agar (for fungi) and nutrient agar (for bacteria). The plates were incubated for 24-48 h at 37 ºC (for bacteria) and at 28 ºC (for fungi). After incubation, microorganism growth was observed. Inhibition of the bacterial and fungal growth were measured in mm. The minimal inhibitory concentration (MICs) was determined after incubation period [13].

2.10.3. In-silico molecular docking studies

Molecular docking is a software based computer program used to understand the interaction between the standard and the synthesized compunds. Therefore, it became clear that molecular docking studies should be carried out to show the *in-vitro* results. The structures of the studied compounds were built in ChemBioOffice Ultra 14.0 software which provides 2D orientation. Further, for carring out the docking simulation, the energy of each molecule was minimized using Avogadro in an open source molecular builder which was used as a input for AutDockVina [14].

2.11. Reference.

1. O. Zerbe and S. Jurt, *Applied NMR Spectro. for Chem. and Life Sci.*, **2013.**
2. H.H.Perkampus, *Uv-Visible Spectroscopy and Its Applications,* Springer Laboratory.
3. A.I. Vogel, A Text Book of Quantitative Inorganic Analysis, vol. 433, third ed., Longmans, London, 443, **1975**.
4. S. Sharma. S. Jaiswal, B. Duffy and A. K. Jaiswal, *Bioeng.,* 6 (1), **2019.**
5. Subramani Parasuraman, Anish R, Subramani Balamurugan, Selvadurai Muralidharan, Kalaimani Jayaraj Kumar and Venugopal Vijayan**,** *Pharmaceutical Methods*, 5(2), **2014.**
6. H. R. Prakash Naik, H. S. Bhojya Naik, T. R. Ravikumar Naik, H. Raja Naika, K. Gouthamchandra, R. Mahmood and B.M. Khadeer Ahamed. *Eur. J. Med. Chem.,* 44, 981–989, **2009.**
7. A. Mohammed and Avin Abdullah, *Proceedings of 2018 International Conference on Hydraulics and Pneumatics – HERVEX,* **2018.**
8. A. Chauhan and P. Chauhan, *J Anal Bioanal Tech,* 5, 5, **2014**.
9. Andrei A. Bunaciua, Elena gabriela Udriştioiub & Hassan Y. Aboul-Eneinc, *Critical Reviews in Analytical Chemistry,* 45, 289–299, **2015.**
10. N. K.Thakral,L. Roger Zanon Ron and C.Kelly SeemaThakral, J Pharma.Sci., 107(2), 2969-2982, 2018
11. E. Ispir, M. Ikiz, A. Inan, A. Burak Sunbul, S. Erden Tayhan, S. Bilgin, Muhammet, Kose and M. Elmastas, *J. of Mole. Struc.,* **2019**
12. V.T. Anju, P. Paramanantham, SB Lal Sruthil, Alok Sharan, Marzouq H.Alsaedi, Turki M.S.Dawoud, Asad Syed, Busi Siddhardha, *Photodia. and Photodyn. Ther.,* **2018.**
13. S. Khlood and Abou Melha, *J. of Enz. Inhi. and Medi. Chem.,* 23(4), 493–503, **2008**
14. A. De, H. Prakash Ray, P. Jain, H. Kaur and N. Singh, *J. of Mole. Stru.,* 1199, 126901, **2020**.

Chapter-3

Light Induced Biological Evaluation of Schiff Base Cu(II) and Co(II) Photosensitizers

3.1. Introduction.

Metal complexes are recognized as efficient photosensitizers and have been successfully used in many fields such as non-linear optics, photocatalytic degradation of pollutants, dye-sensitized solar cells (DSSCs), organic light-emitting diodes, PDT, APDT and semiconductors amongst others [1-3]. APDT is based on the utilization of specific wavelength of light to excite the photosensitizers to generate Reactive oxygen species i.e. singlet oxygen. These ROS are highly reactive in nature so that they can oxidize biomolecules such as protein, nuclic acid, lipids, amino acids etc., resulting in cell death [4]. Thousands of drugs have been tested for PACT including porphyrins, chlorins, bacteriochlorins, texaphyrins, phthalocyanines and metal complexes [5]. So far the preponderance of photosensitizers are stand on rare and precious metals, like ruthenium, iridium, platinum, limiting their large-scale application. In this regard, transition metals such as Cu(II) and Co(II) are contemplate as a very promising alternative, as evidenced by a strongly increasing number of publications in recent years [6].

The great potential of transition metal complexes are already shown in the field of medicinal chemistry. The drawback of transition metal complexes are these are does not effciently generate hydroxyl radicals [7]. However, in the presence of a chelating agent it can abel to form a ROS, to overcome this, Schiff base are used as a chelating agent, Due to synthetic resilience, selectivity and sensitivity towards a different of metal atoms, the metal complexes derived from Schiff base are extensively studied as PSs[8]. It has been reported that the transition metal complexes of nitrogen, oxygen-donor Schiff base ligands are exhibits various biological applications such as antitumor, antioxidant, antibacterial, antifungal and antiviral properties [9-11]. In fact, several metal complexes with Schiff base ligands have proved its ability to break DNA

chains on UV–visible light irradiation [12]. Furthermore, amino naphthalene derivatives are reported to have wide spectrum of biological activities [13]. In the present study, we have reported that the newly synthesized transition metal complex can indeed be used to kill the bacterium *E.coli*. Further, these complexes were investigate for the pharmacological activities such as; antioxidant, DNA cleavage, which were further evaluated by in silico molecular docking in order to recognize the possible relations between the target compounds with protein RpsA.

3.2. Experiment.

3.2.1. Methods and materials.

The selected metal salts like Copper Chloride hexahydrite and Cobalt chloride hexahydride, 4-[(E)-benzylideneamino]-3-hydroxynaphthalene-1-sulfonic acid were purchased from Sigma–Aldrich. The employed aldehydes were of analytical grade. Other chemicals and solvents were of highest purity and used without further purification. The techniques which are used to conform the structure of the ligand and metal complexes are discussed in **Chapter 2.**

3.2.2. Synthesis of Schiff bases ligand (HL_1 and HL_2).

Synthesis of 4-[(E)-benzylideneamino]-3-hydroxynaphthalene-1-sulfonic acid derivative precursors was accomplished using a modification of the previously reported procedure [14]. As reproduce in **Scheme 3.1**. briefly, the ethanolic solution of aromatic aldehyde (0.01mol) was added to the stirring ethanolic solution of 4-amino,3-hydroxynaphthalene sulphnolic acid (0.01 mol) in presence of tryethyl amine (0.02 mol) and was stirred for about 24 hour at ambidendent temperature which results as yellow solid compounds followed by their filtration, wash with ethanol and diethyl ether, dried and recrystallize with ethanol.

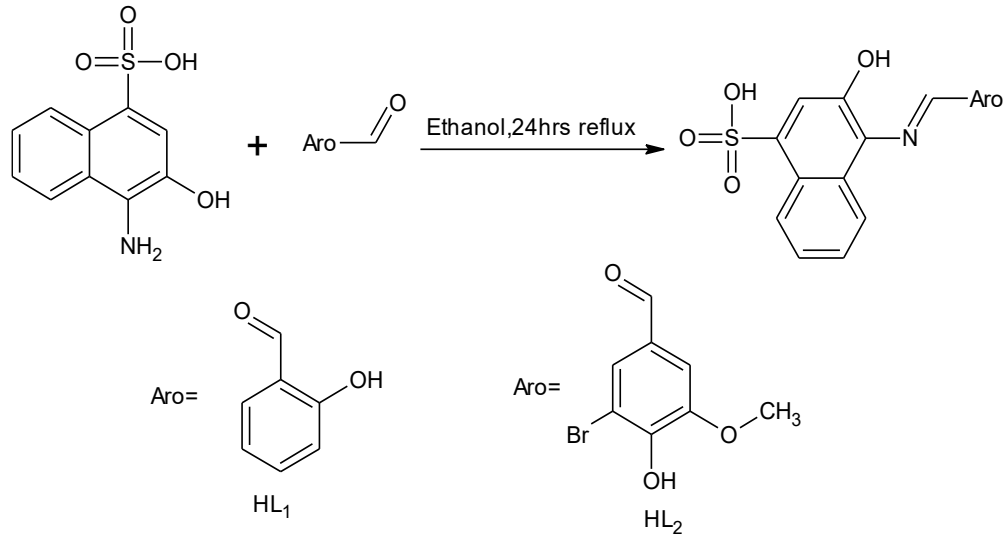

Scheme 3.1. Schematic representation for the syntheses HL_1 and HL_2

3.2.3. Synthesis of metal complexes.

The complexes [$(ML_2)n$] were prepared by the following general method, in which the hot ethanolic solution of the ligands HL_1 (0.001mol) and HL_2 (0.002mol) was added to the stirring ethanolic solution of the metal(II) chloride (0.001 mol). The reaction mixture were heated under reflux for 2 hours then the volume of the mixture was reduced to half of the initial volume under reduced pressure, then the reaction mixture was cooled overnight, then the precipitate was filtered off, washed with water and ethanol, and dried in desiccators [15]. As depicted in **Scheme 4.2.**

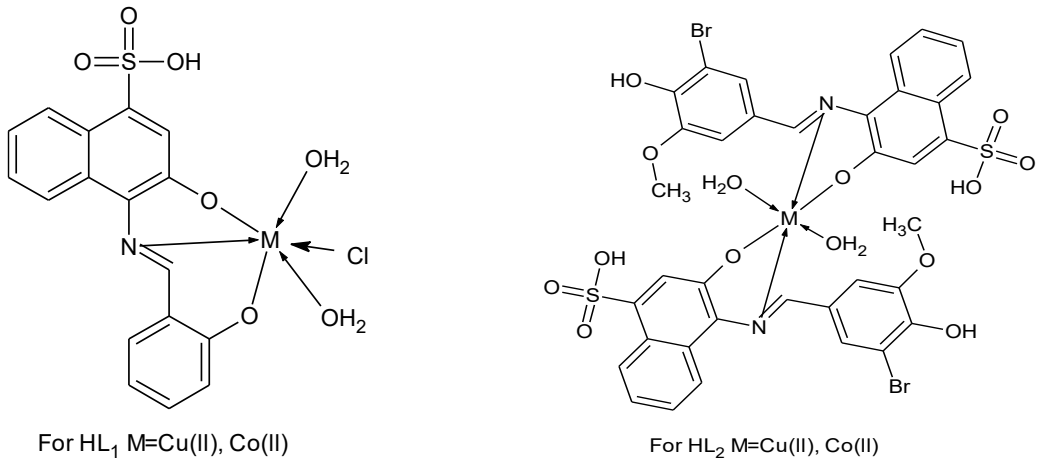

Scheme 4.2. Structures of Metal complexes

3.3. Result and Discussion.

This chapter deliberates the synthesis of heterocyclic Schiff base ligands (HL_1 and HL_2) and their solid complexes have been synthesized. The Physical and analytical data of the Schiff base ligand and their related metal complexes are given in **Tables 3.1.** Both the ligand and the complexes are air stable. The ligand is soluble in EtOH, Et_2O, $CHCl_3$, acetone and CCl_4 whereas complexes are soluble in DMF and DMSO. Assessment of the elemental analysis for both the calculated and found percentages indicates that the compositions of the synthesized complexes coincide well with the proposed formulae.

Tables 3.1. Physical and analytical data of the synthesized azo dye and their metal complexes.

Ligand/ complexes	Mol. wt	M P	Colour	Elemental analysis(%) calcd.(found)						
				C	H	N	O	S	Br	M
Ligand (HL_1)	343	282-284	Yellow	59.45 (58.94)	3.85 (4.04)	4.08 (4.10)	23.30 (23.20)	9.34 (9.30)	--	--
Cu(II) complex (3a)	476	>300	Light Green	42.86 (42.29)	3.17 (3.10)	2.94 (2.88)	23.51 (25.8)	6.73 (6.48)	--	13.34 (13.28)
Co(II) complex (3b)	471	>300	Brown	43.28 (43.24)	3.20 (3.30)	2.97 (2.82)	23.74 (23.70)	6.80 (6.60)	--	12.49 (12.40)
Ligand (HL_2)	452	226-228	Orange	47.80 (46.98)	3.12 (3.01)	3.10 (3.00)	21.23 (21.04)	7.09 (6.86)	17.67 (17.40)	--
Cu(II) complex (3c)	998	>300	Green	43.15 (43.0)	3.02 (3.00)	2.80 (2.84)	22.35 (22.30)	6.40 (6.42)	15.95 (15.92)	6.34 (6.32)
Co(II) complex (3d)	997	>300	Brown	43.35 (43.30)	3.03 (3.00)	2.81 (2.80)	22.46 (22.10)	6.43 (6.50)	16.02 (16.0)	5.91 (5.88)

3.3.1. NMR Spectra.

The *^{1}H-NMR* spectra of the synthesized ligands HL_1 and HL_2 shows signals at ambient temperature in $CDCl_3$ using TMS as a internal standard. The ^{1}H-NMR spectra of the ligand HL_1 and HL_2 show important signals at their respective positions, confirming the structures of Schiff base. The ^{1}H-NMR spectra of the free Schiff base

ligand as shown in **Fig. 3.1a. Fig. 3.1b** and in **Table 3.2**. The NMR spectra contained the signals corresponding to the aromatic protons which were observed in the range of d 7.17-7.76 ppm as a multiplet. At 10-13 ppm the hydroxyl proton will appeared as a singlet. The hydrogen of the imide showed signals at 8.9 ppm [16]. The phenolic -OH appeared at 9.06-9.08 ppm [17]. Additionally methoxy proton of the ligand HL_2 appeared at 3.003 with a singlet [18].

The ^{13}C-NMR spectra of HL_1 and HL_2 were taken in $CDCl_3$. ^{13}C-NMR spectra of the schiff base ligand are depicted in **Fig. 3.2a** and **Fig. 3.2b.** HL_1 of the ligand showed multiplet signals in the region of 110-160 ppm due to aromatic carbon. Methoxy carbon of the ligand HL_2 was observed in the region of 56 ppm [19]. The signal at 157 ppm was assigned to the imine carbon atom [20]. For the ligand HL_1 the signal at 161ppm was due to the carbon attached to the hydroxyl group (C-OH).

Table 3.2. ^{1}H-NMR spectral data of ligand HL_1 and HL_2

Ligand	^{1}H-NMR spectral data
HL_1	10 (S, 1H -OH), 9.082-9.084 (d, 1H,-OH), 8.892-8.899 (d, 1H,NH=CH), 7.53-7.51 (d, 1H, Ar-H), 7.35-7.28 (t, 2H, Ar-H)
HL_2	11.50 (S, 1H -OH), 10.5 (S.1H. –OH) , 9.09 (S, 1H,-OH), 8.54 (d, 1H,NH=CH), 7.53-7.51 (d, 1H, Ar-H), 7.35-7.28 (t, 2H, Ar-H), 3.16(S, 3H, O-CH_3)

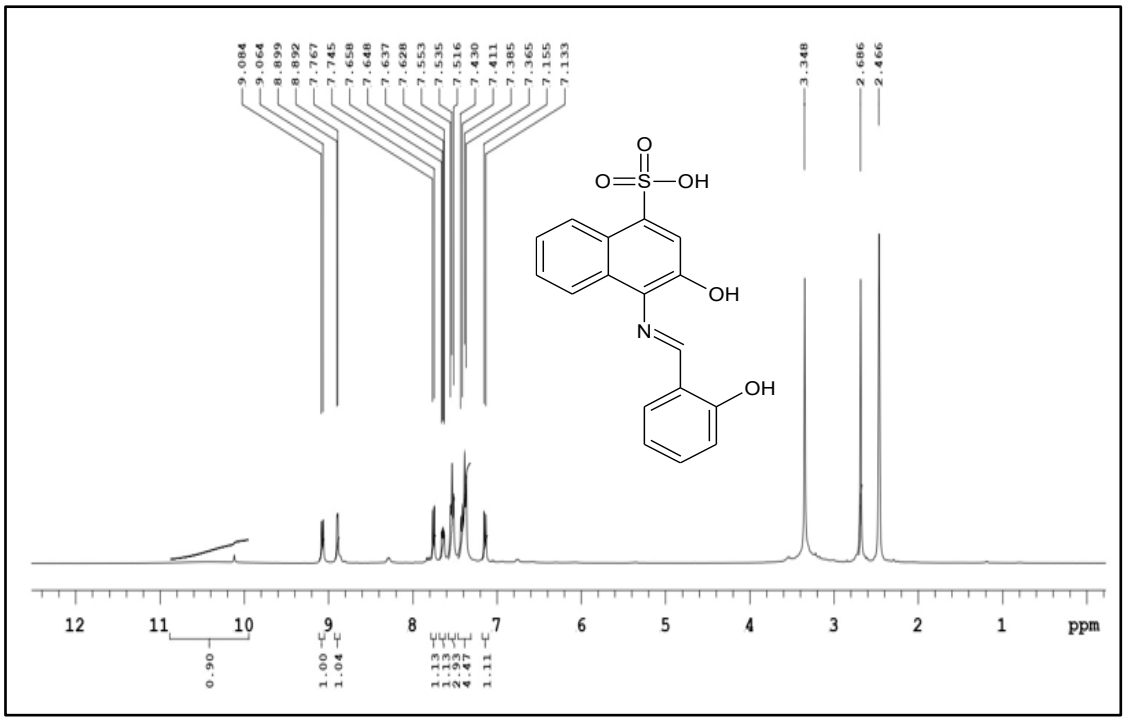

Fig 3.1a- ^{1}H-NMR spectra of HL_1.

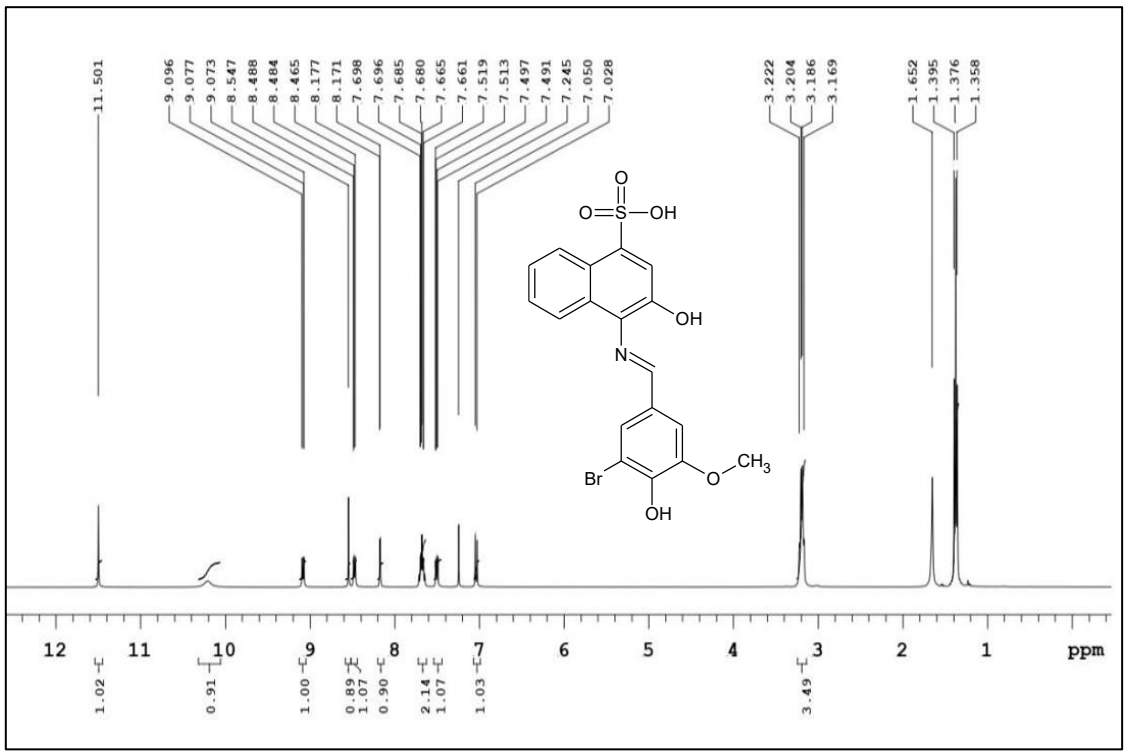

Fig. 3.1b- ^{1}H-NMR spectra of HL_2.

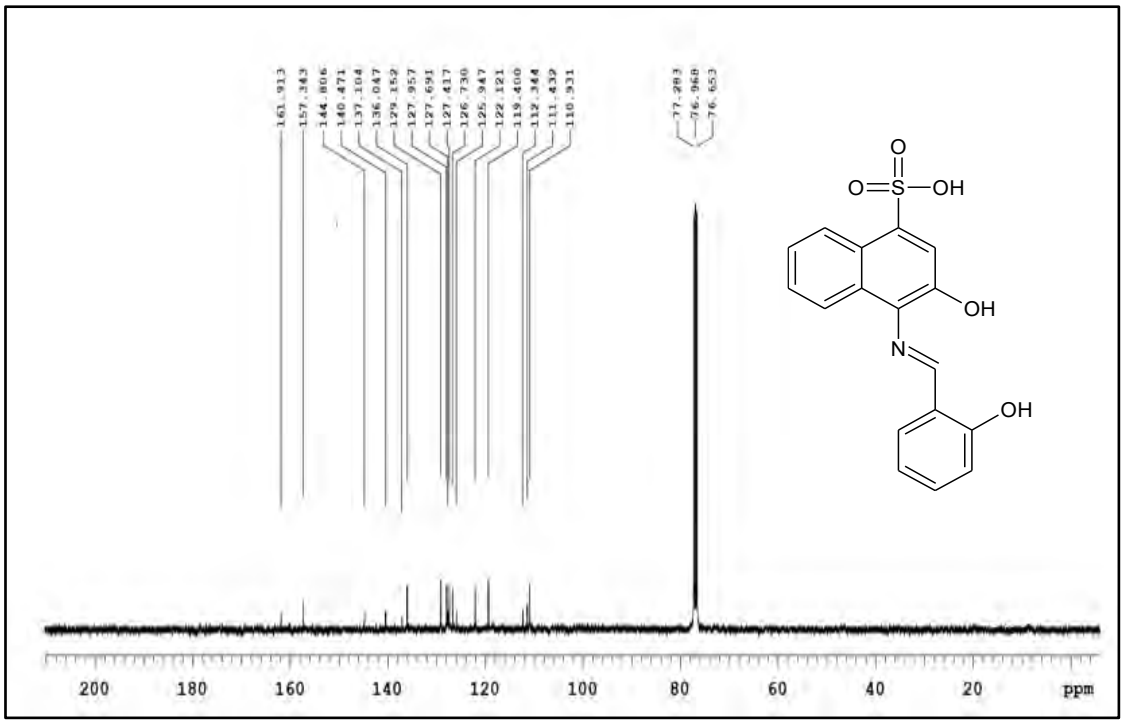

Fig.3.2a. ^{13}C-NMR spectra of HL_1.

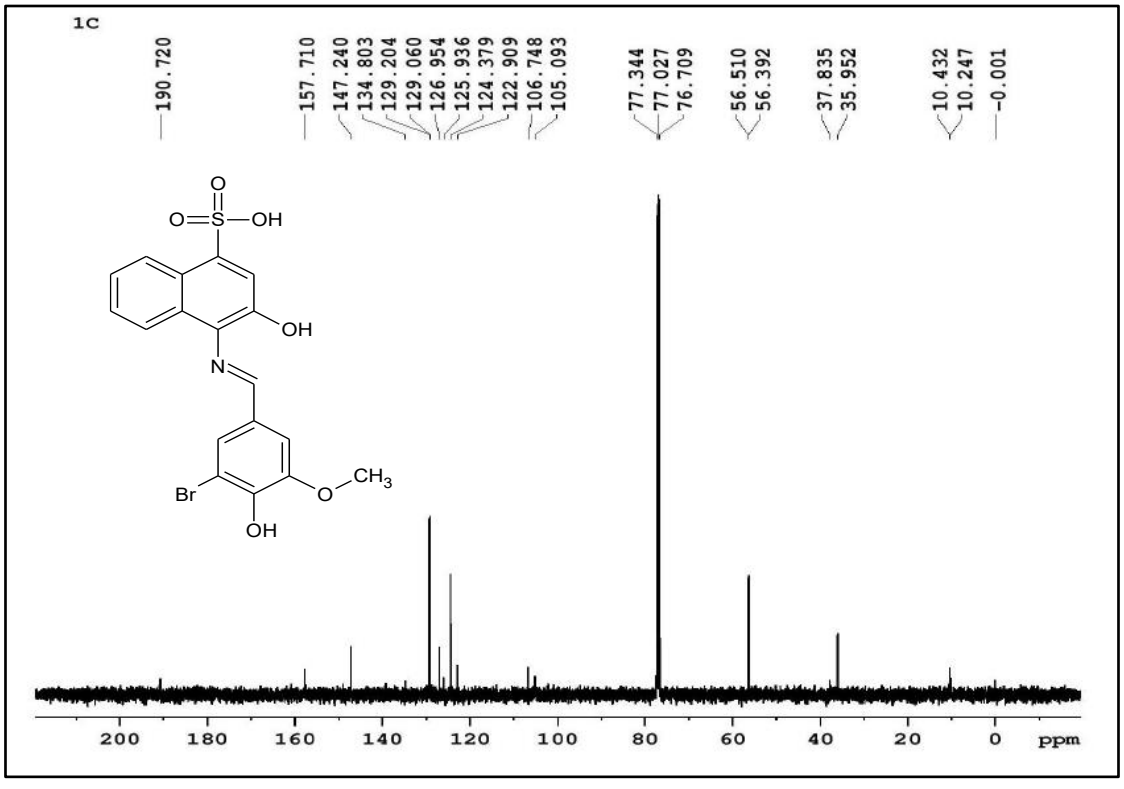

Fig.3.2b. ^{13}C-NMR spectra of HL_2.

3.2.2. Electronic Absorbtion Spectra.

The UV-Visible spectral of the synthesized compounds were recorded in DMF (10^{-3}) mol solution. All the compounds displayed an absorption band in the range 290 and 530 nm. The electronic transition of the free schiff bases, Cu(II) and Co(II) Complexes are shown in **Table-3.3** and **Fig.3.3a- Fig 3.3b**. The absorption maximum of the ligand HL_1 showed broad band observed at 387.9 nm which was assigned to n–π* transition of azomethane. The absorbtion maximum of the ligand HL_2 displayed two bands in the range of 299 and 389 nm, these bands were assigned to π–π* intraligand transitions of aromatic moiety and n–π* transition of the C,N chromophore [21]. In complexes, ligand-based emission band shifted to the longer wavelength region for about 10-15 nm proposing the coordination of azomethine nitrogen to the central metal ion [22]. The Cu(II) complex (3a) of HL_1 showed three bands in the region 344, 361 and 403 nm are assigned as $^2B_{1g}\rightarrow{}^2A_{1g}$, $^2B_{1g}\rightarrow{}^2B_{2g}$, and $^2B_{1g}\rightarrow{}^2E_g$ transitions [23]. The electronic spectra of Cu(II) (3c) complexes showes a broad band in the region 334 and 421 nm, were one is from intra ligand charge transition and the other broad band in the high-energy region can be assigned to the ligand-to-metal charge transition (LMCT). This indicates octahedral geometry for the Cu(II) complexes for HL_2 ligand [24]. The Cobalt complex of HL_1 and HL_2 exhibit bands at 347, 525 and 397, 492 nm these bands were assigned as $^4T_{1g}$ (F) $\rightarrow{}^4A_{2g}$ (F) (ν2) and $^4T_{1g}$ (F) $\rightarrow{}^4T_{2g}$ (P) (ν3) transitions [25]. These values proposed the distorted octahedral geometry for Co(II) complexes. The predictable characteristic d-d transitions in the visible region for the complexes were not detected when different concentrated solutions were used [26].

Table.3.3. UV-Visible spectra of the synthesized ligand and metal complexes.

Compound	λmax (nm)	Transition
HL_1	387	n–π*
HL_2	299, 389	π–π*, n–π*
3a	344, 361, 403	π–π*, n–π*, $^2B_{1g}\rightarrow{}^2A_{1g}$, ($^2B_{1g}\rightarrow{}^2A_{1g}$, $^2B_{1g}\rightarrow{}^2B_{2g}$, and $^2B_{1g}\rightarrow{}^2E_g$)
3b	397, 492	$^4T_{1g}$ (F) $\rightarrow{}^4A_{2g}$ (F) (ν2) and $^4T_{1g}$ (F) $\rightarrow{}^4T_{2g}$ (P) (ν3)
3c	334, 421	$^2B_1g \rightarrow {}^2A_1g$ INCT
3d	347, 525	$^4T_{1g}$ (F) $\rightarrow{}^4A_{2g}$ (F) (ν2) and $^4T_{1g}$ (F) $\rightarrow{}^4T_{2g}$ (P) (ν3)

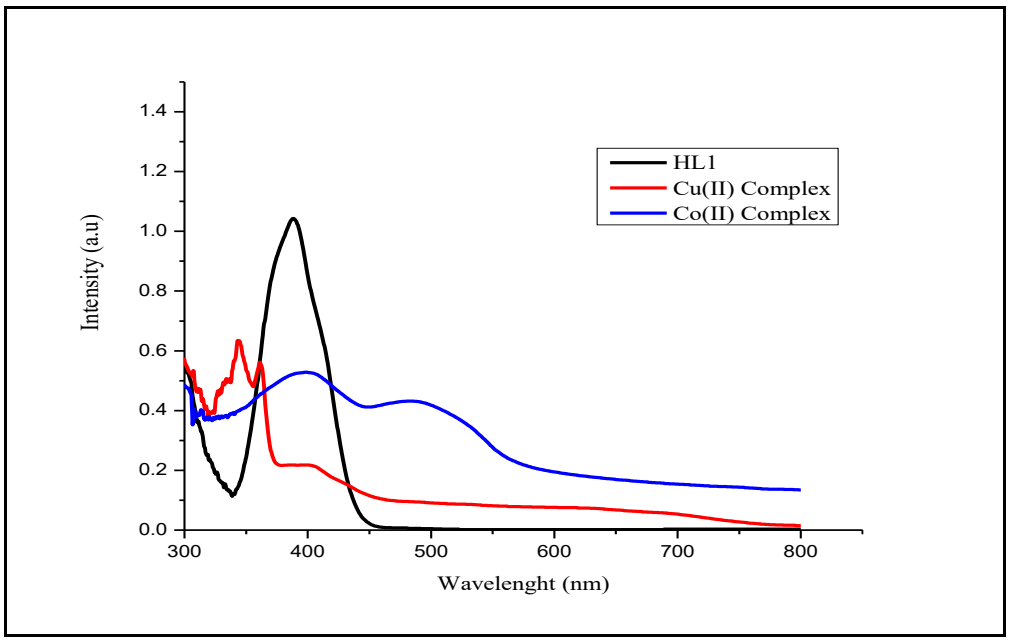

Fig. 3.3a- Uv-Visible spectrum of **HL_1** and its metal complexes.

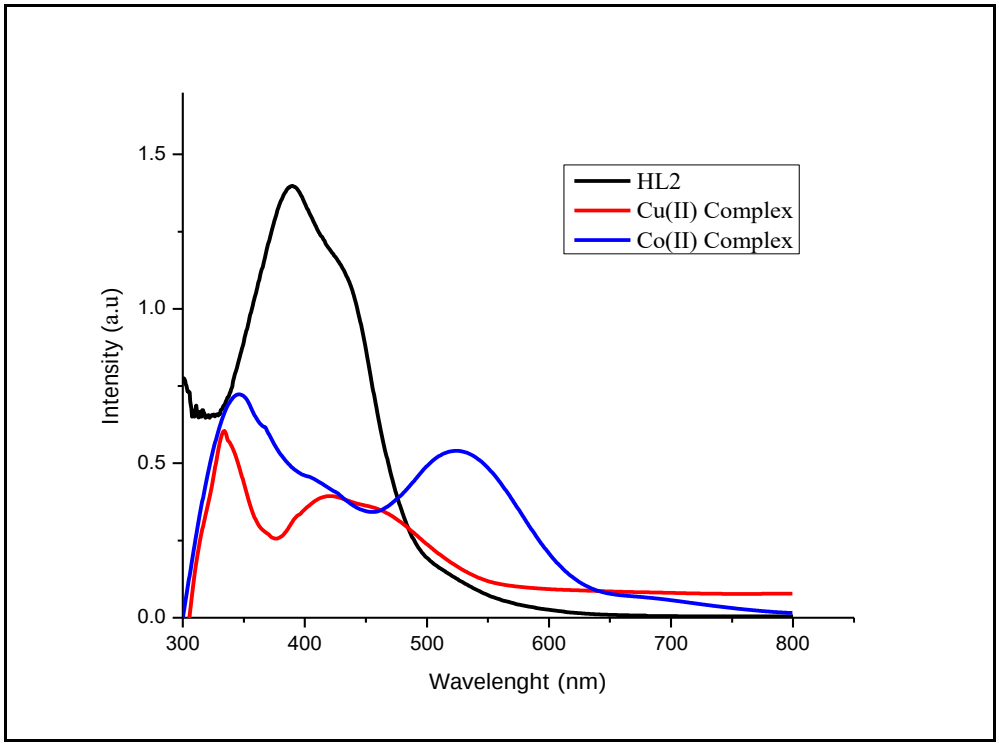

Fig. 3.3b. Uv-Visible spectrum of **HL_2** and its metal complexes.

3.3.3. FT-IR spectra

The FT-IR spectroscopy technique has been used extensively for the identification of functional group of the synthesized compounds. The important tentative assignments of the FT-IR spectra are presented in **Table 3.4.** and the spectra data were shown in **Fig.3.4a** to **Fig.3.4f.** The ligand HL_1 and HL_2 showed absorption band at 1633 and 1524 cm^{-1} due to imide group of (C=N) and it shifted to lower frequency in all the complexes, indicating the involvement of (C=N) of the imide group in the formation of metal complexes [27]. The strong absorption band at 1588 cm^{-1} was due to aromatic C=C stretching vibration of the synthesized compounds. In case of HL_1 and HL_2 the absorbation band at 3172 and 3232 cm^{-1} for phenolic -OH group of the free ligand disappeared for all the metal chelates which indicates the formation of bonds between the metal ion and phenolic oxygen atom [28]. The absorption due to phenolic C-O stretching vibrations was observed in the region 1381

and 1352 cm^{-1} which shifted towords lower region in the complexes, this conforms the formation of M-C-O bond in all the complexes [29]. A new broad band due to the coordination of water molecules appeared in the complexes at 3400 cm^{-1}. The existence of water molecule in complexes was confirmed by thermogravimetry and photoluminescence study. The absorption band due to metal-nitrogen and metal-oxygen in complexes were confirmed by the appearance of new band in the regions 484-430 cm^{-1} and 542-513 cm^{-1}. The IR data revealed the formation of tridentate nature of the ligand to the metal ion

Table 3.4. FT-IR bands and tentative assignments of the ligand and its metal complexes

Synthesized Compound	ν(OH/H_2O)	νphenolic C-O	ν(C=N)	ν(M-N)	ν(M-O)
HL_1	3172	1381	1633	-	-
HL_2	3413	1352	1524	-	-
3a	3423	1331	1493	696	466
3b	3137	1365	1540	633	461
3c	3423	--	1590	696	466
3d	3448	1332	1512	662	457

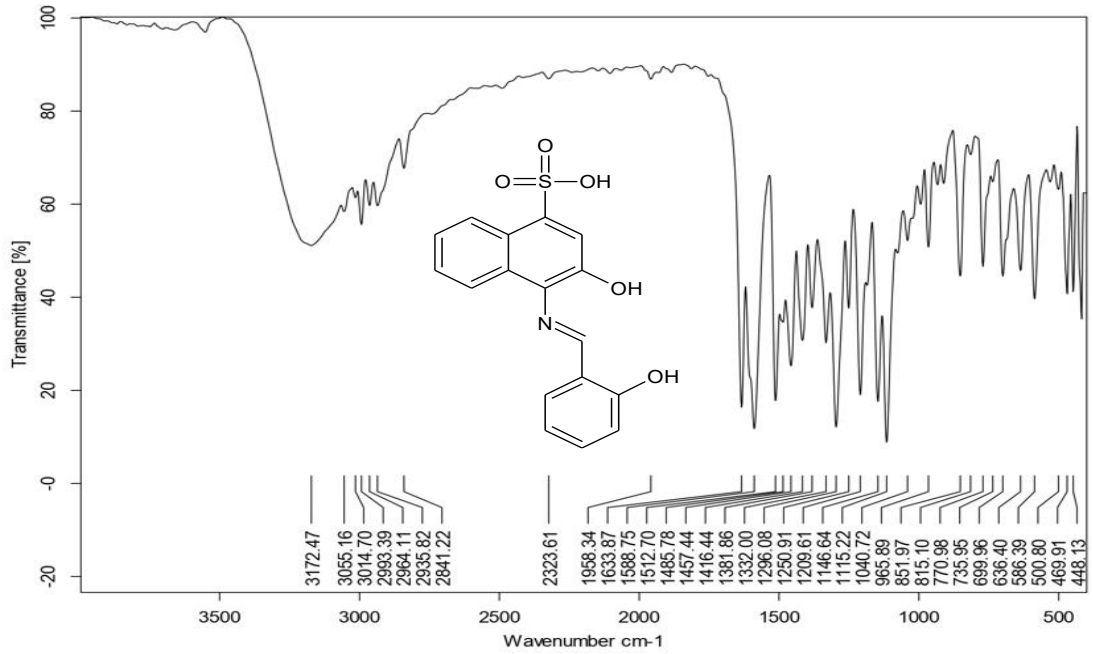

Fig.3.4a. FT-IR spectra of the free Schiff base ligand (**HL_1**).

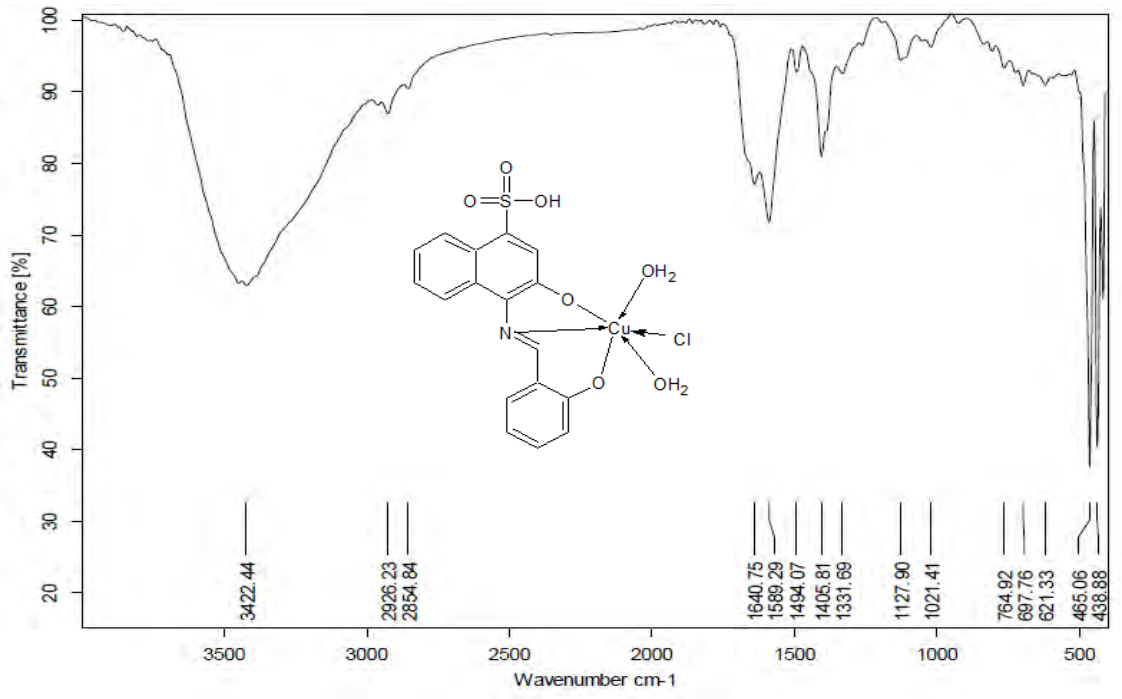

Fig.3.4b. FT-IR spectra of the Cu(II) complex of the HL_1 ligand (**3a**).

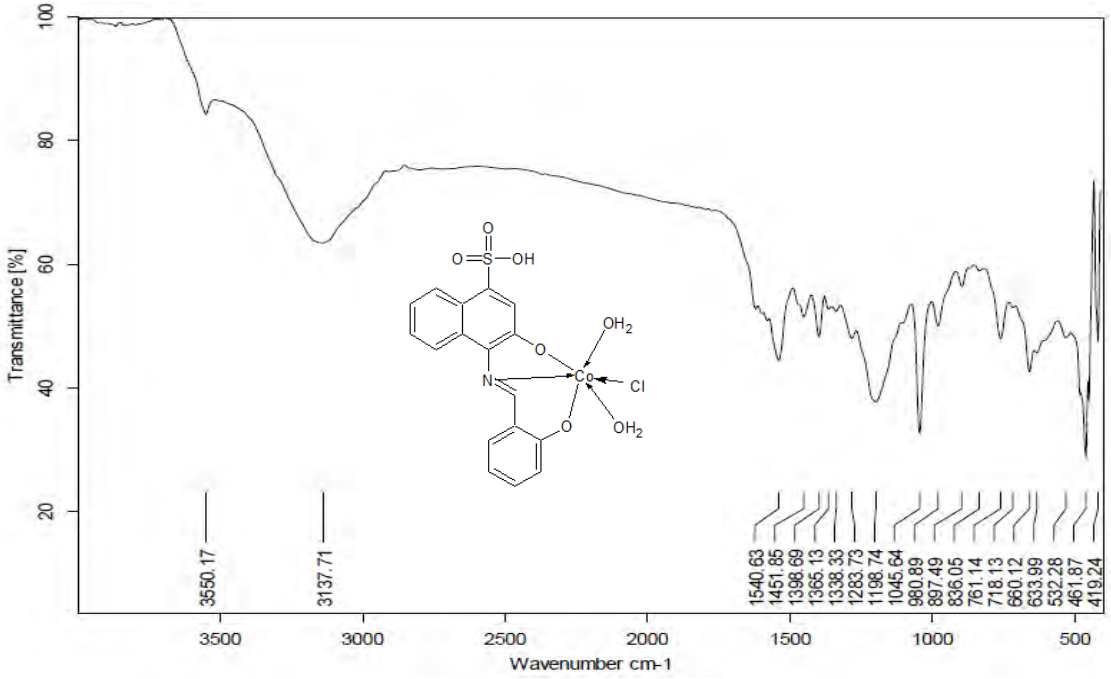

Fig.3.4c. FT-IR spectra of the Co(II) complex of the HL_1 ligand (**3b**).

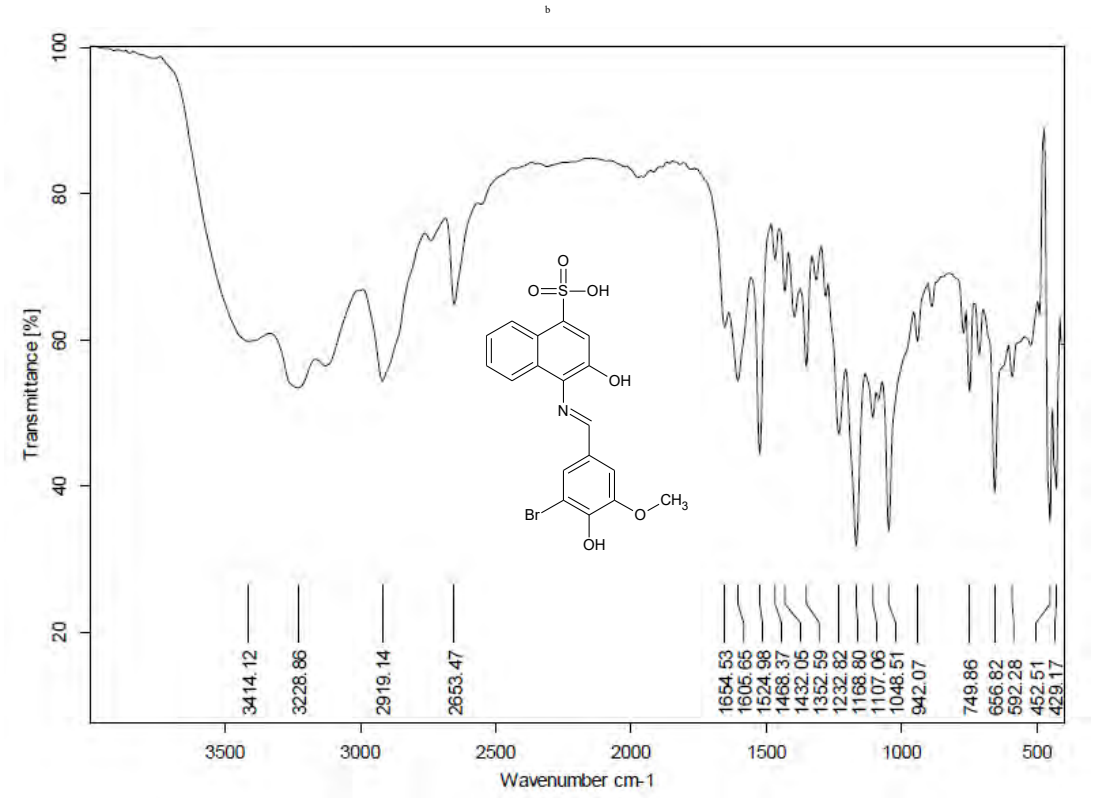

Fig.3.4d. FT-IR spectra of the free Schiff base ligand (**HL_2**).

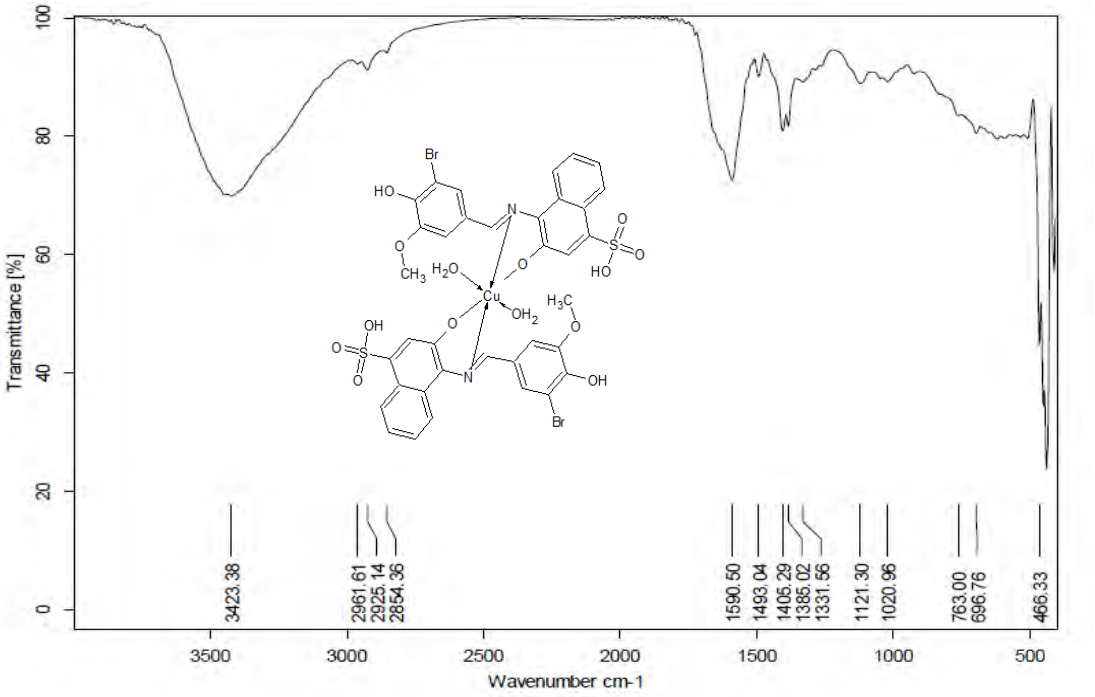

Fig.3.4e. FT-IR spectra of the Cu(II) complex of the ligand HL_2(**3c**).

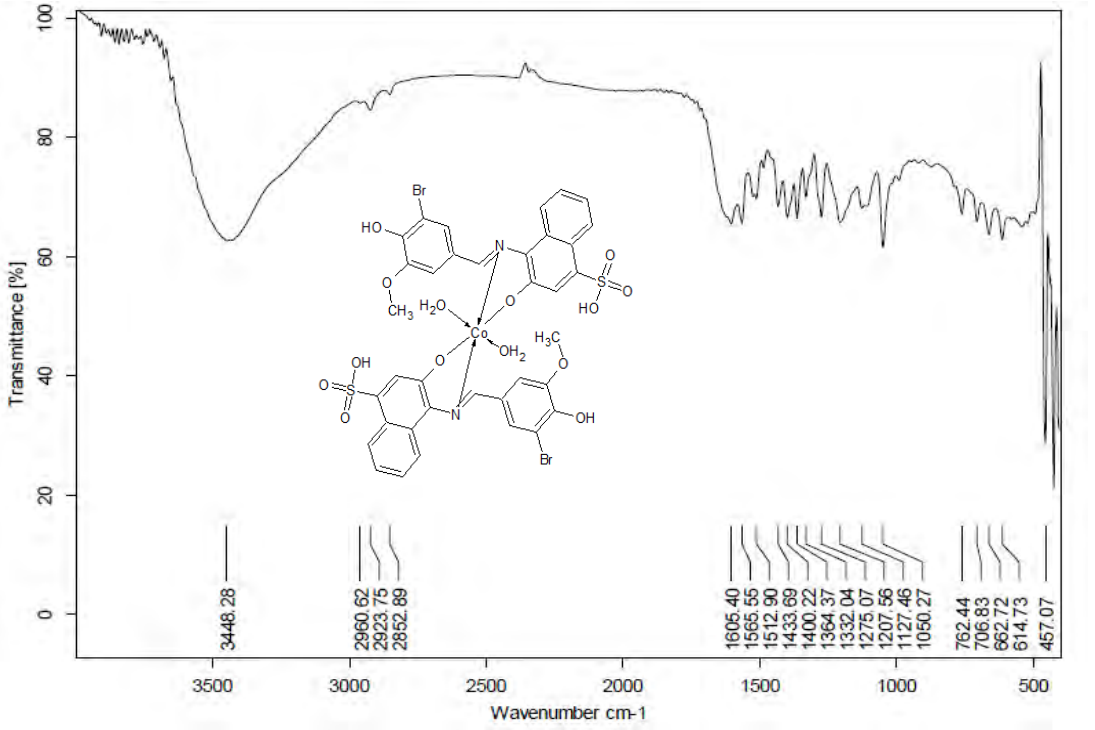

Fig.3.4f. FT-IR spectra of the Co(II) complex of the HL_2 ligand (**3d**).

3.3.4. Mass spectra

The mass spectrum of the Schiff base ligands and their Cu(II) metal complexes showed molecular ion peak corresponding to their molecular mass. The mass spectra of the organic ligand and the metal complexes are showed in **Fig.3.5a** to **Fig 3.5d.** The mass spectrum of the Schiff base ligand HL_1 displayed a molecular ion peak observed at m/z 344[M+H], for the ligand HL_2 the molecular ion peak observed at m/z 451[M-H] both the ligands are coincides to its molecular mass of the ligand. The molecular ion peaks of the Cu(II) complex of HL_1 ligand were found to be m/z 478. For complex of ligand HL_2 molecular ion peak at m/z 996 for Cu(II) complexes. Which are synchronized with the stoichiometric configuration of [M(L)] for HL_1 ligand $[M(L)_2]$ type for ligand HL_2. Furthermore, the experimental molecular ion peaks in all the spectra are in good agreement with the suggested molecular formula indicated from elemental analyses.

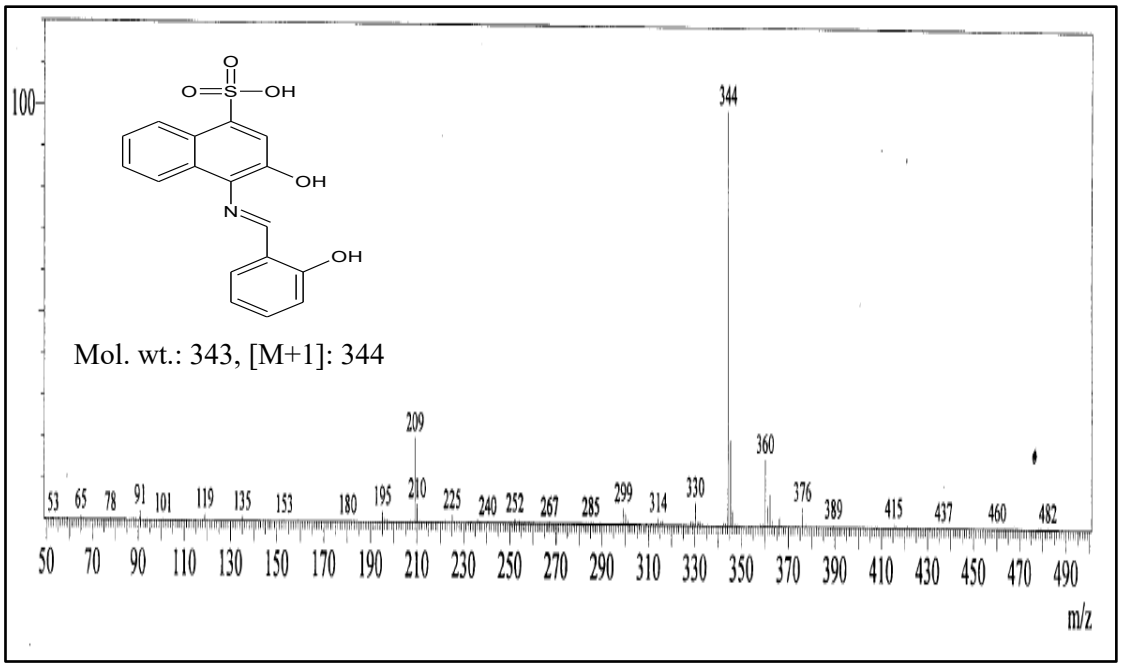

Fig.3.5a. Mass spectra of the free Schiff base ligand (**HL_1**).

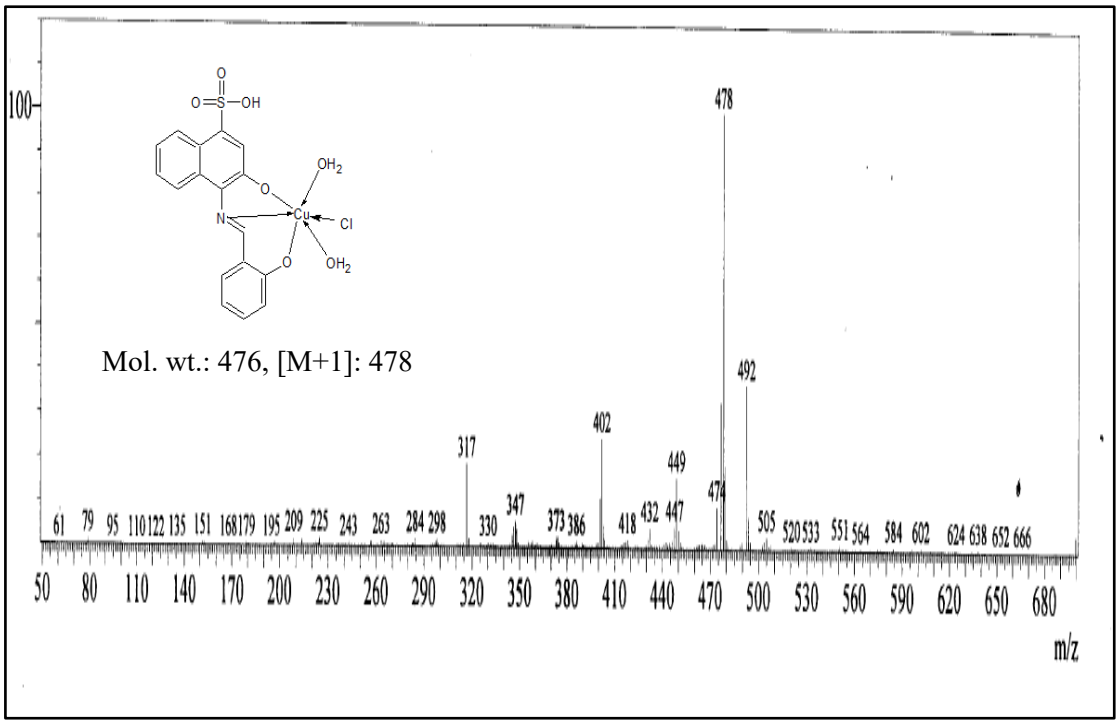

Fig.3.5b. Mass spectra of the Cu(II) complex of the HL_1 ligand (**3a**).

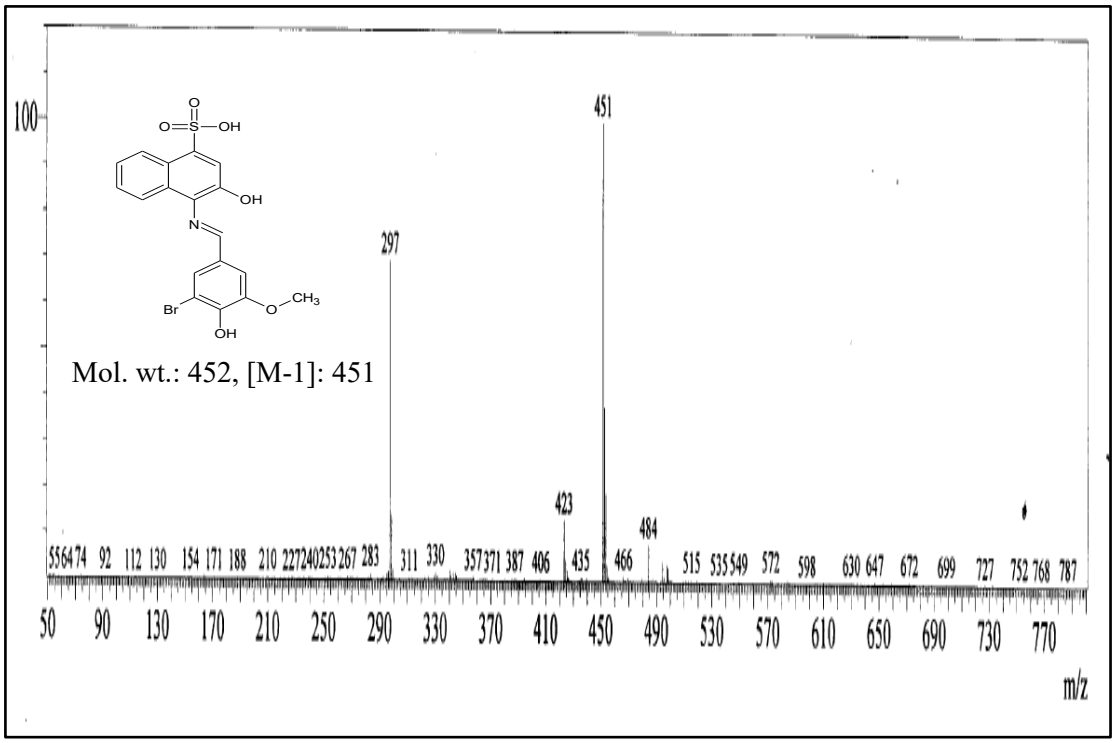

Fig.3.5c. Mass spectra of the free Schiff base ligand (**HL_2**).

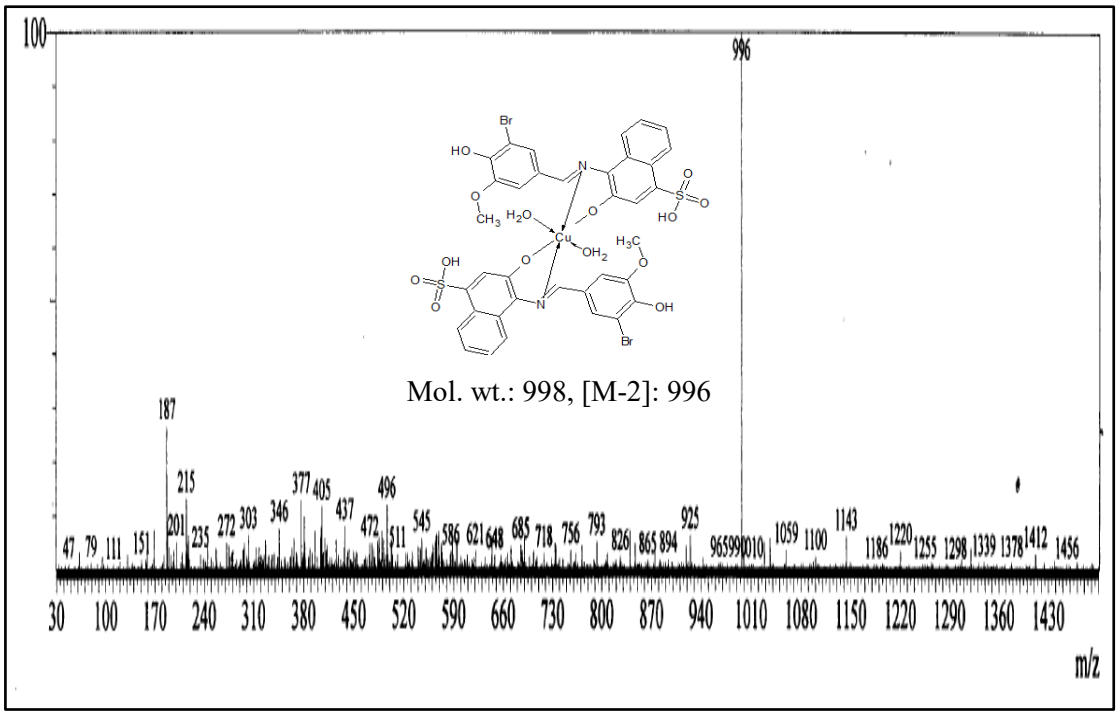

Fig.3.5d. Mass spectra of the Cu(II) complex of the HL_2 ligand **(3c).**

3.3.5. Thermo gravimetric analysis.

The TG curve of selected metal complexes were recorded in nitrogen atmosphere, heat flow was to be 10 $^{\circ}C\ min^{-1}$. The weight loss was measured from 30-800 $^{\circ}C$. The mass loss was calculated and compared with those theoretically calculated values were summarized in **Table 3.5.** The results showed that the complexes were hydrated in nature. **Fig. 3.6** shows the Cu(II) complex of HL_1 dissociated in three stages. In the first stage, the complexes detaches the coordinated two water molecule at a range of 30-135$^{\circ}C$ and the calculated mass loss was to be 8.1 % (calculated 7.9 %). Some part of organic moiety (C_7H_8O) was dissociated in 2nd stage at 136-305 $^{\circ}C$ with a weight loss of 24.34 % (calculated 24.569 %). The temperature at 305-370 $^{\circ}C$ showed the loss of organic moiety ($C_{11}H_9NO_4S$) with mass loss of 86 % (calculated 86.94 %). Further the dissociation takes place to form the oxides of copper. The overall decomposition was 90 %.

The *Tg* curve of Cu(II) complex of HL_2 showed a total mass loss of 85.7% which took place in three stages. In the first stage, the loss of lattice water molecule with a weight loss of 3.43 % (calculated 3.59 %) at a temperature range of 30-72.93 °C. At temperature range of 73-307.9 °C the decomposition of some part of the organic ligand ($C_{12}H_{10}Br_2O_2$) takes place and the weight loss was to be 19.037 % (calculated 19.24 %). In the third stage the loss of remaining organic ligand ($C_{22}H_{18}N_2O_8S_2$) was dissociated in the temp range of 308-445.43 °C with a mass loss of 52.45 % (calculated 52.94 %). Further, decomposition takes place to form CuO as a residue.

Table 3.5. Thermal decomposition of the Cu(II) metal complexes at nitrogen.

Complexes	Stages	Decomposition Temp (°C)	Probable Assignment	Loss Of Mass In (%)	Residual Species
3a	1st 2nd 3rd	30-135 136-305 Above 306	2 H_2O C_7H_8O $C_{11}H_9NO_4S$	8.1 24.56 86.94	CuO
3c	1st 2nd 3rd	30-120 121-362 363-462	2 H_2O $C_{12}H_{10}Br_2O_2$ $C_{22}H_{18}N_2O_8S_2$	6.4 36.9 57.05	CuO

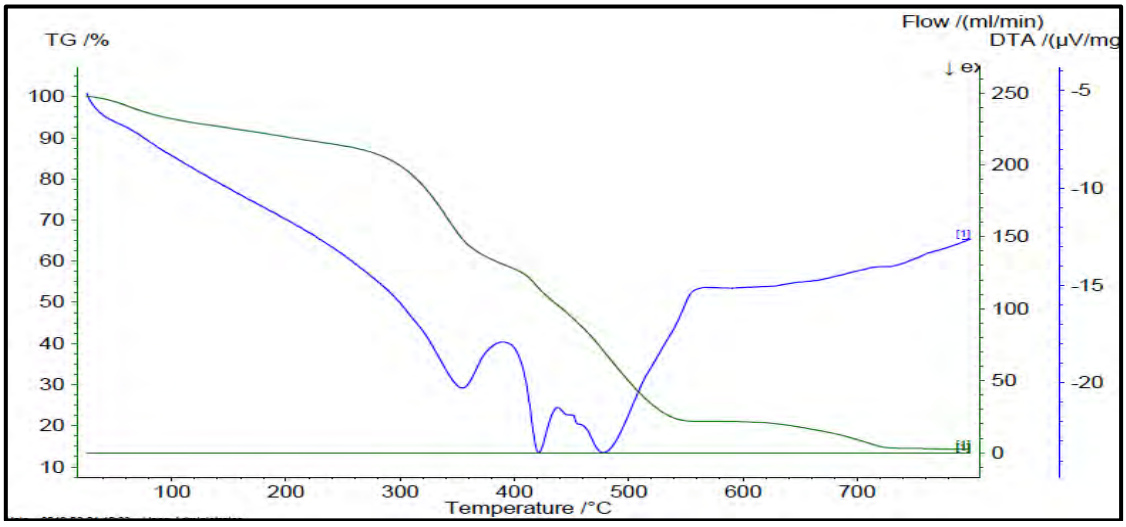

Fig.3.6a TG/DSC curve of Cu(II) Complex of HL_1 (**3a**).

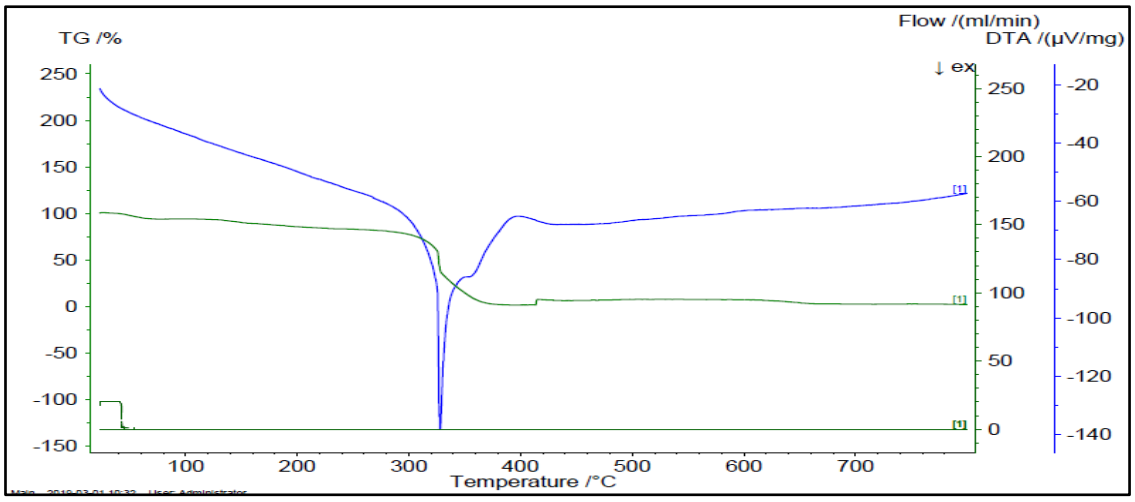

Fig.3.6b TG/DSC curve of Cu(II) Complex of HL_2 (**3c**).

3.3.6. Photoluminesons Spectra.

The emission spectra of ligand and metal complexes were investigated in DMF (10^{-5} M) at ambidendate temperature. **Fig.3.7** shows the emission spectra of ligands and their metal complexes. From the fig.3.7 it can be seen that the emission spectra of ligands HL_1 and HL_2 showed a band at 394 and 439 nm at excitation wavelength of 380 nm. This can be assigned to the $\pi \rightarrow \pi^*$ electronic transition. The Cu(II) complexes of ligand HL_1 and HL_2 exhibited significant emission peaks at 467, 516 nm and 439, 494 nm at the excitation of 380 nm. On complexation, the band shifted towards lower wavelength with fluorescence quenching which was explained by Esin Ispir, *et. al.* [30], where they stated that fluorescence quenching is a common phenomenon, during complexation the excited state charge transfer from ligand to metal ions, leading to a decrease in the intensity, which also conforms the complexation. Co(II) complexes of HL_1 and HL_2 exhibited a band in the region of 420 nm and 506 nm, and a broad band at 620-650 nm. In all the complexes the new band was observed that is π-π^* transition of the schiff base ligands with metal ion charge transitions. In addition to this, the noticeable broadening of the spectra of all the complexes could be attributed to the existence of water molecule in the complexes,

this also conforms the presence of water molecule in complexes [31]. Thus, Schiff base and metal complexes are fluorescent in nature and they open a way for photochemical and cancer applications of the complexes.

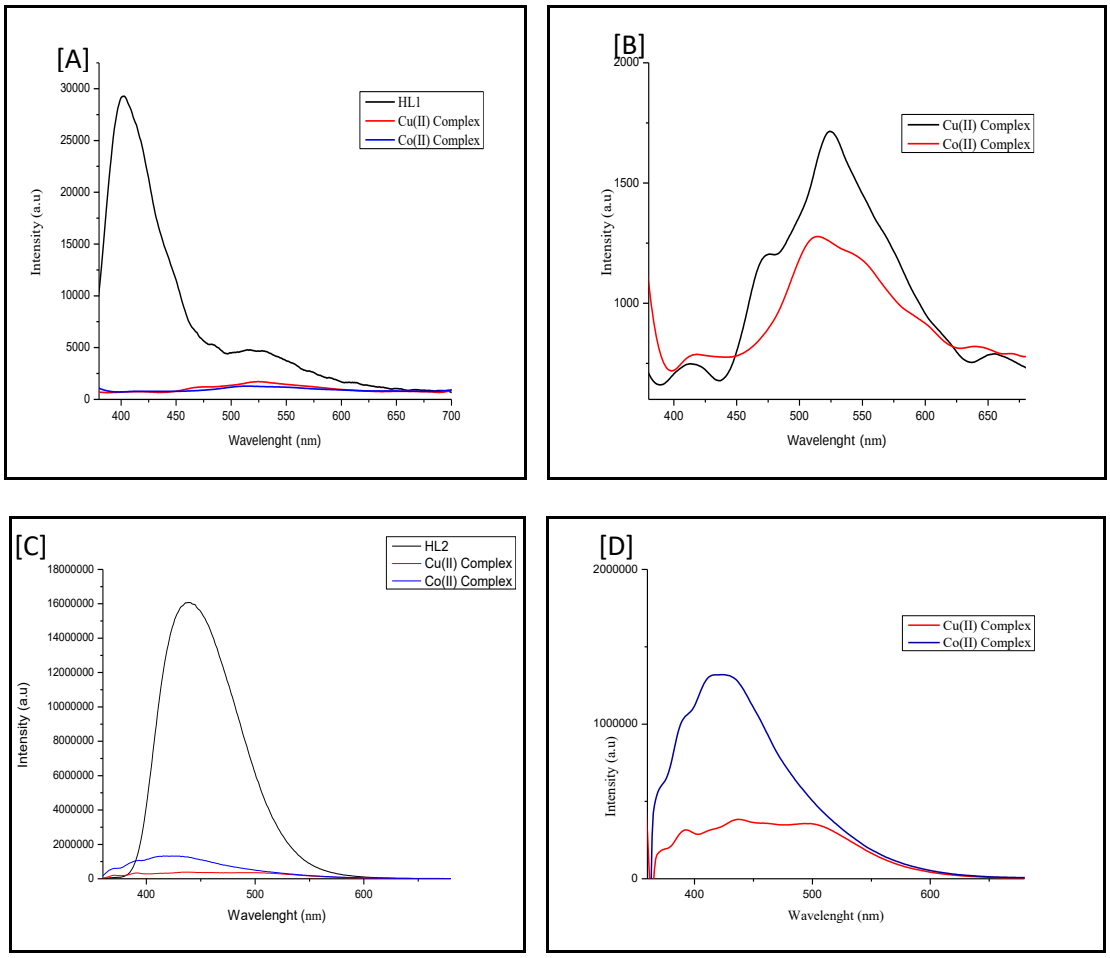

Fig.3.7. Photoluminescence spectra of the Ligands (HL_1 and HL_2) and their metal complexes [A-D].

3.3.7. Biological application.

3.3.7.1. Invitro antimicrobial inactivation studies.

Microorganisms and Culture Conditions.

Microorganism utilized in the experiments was *E. coli* (E. coli, ATCC 25922) were routinely subcultured in Luria Bertani broth under shaking conditions at 37 °C for 24 hour. A standard overnight culture containing 0.5 McFarland standards was used for all *in-vitro* assays.

Photosensitizer and Light Source.

The newly synthesized metal complexes were used as a photosensitizer. A stock solution of metal complexes at a different concentration (1, 2, 5, 7, 10, and 20 μg/mL) and the final volume was 0.1mg/mL was prepared by using non-toxic concentration of dimethyl sulfoxide. Xenon lamp emitting wavelength over the range 400 to 800 nm was used as a radiation source. According to V.T. Anju, *et. al.* the maximum light expose time for the bacterial was 10 to 15 min [32].

Photoinactivation on Planktonic Cells.

From previous report [33], planktonic cell of *E. coli* were analyzed. An overnight bacterial suspension (100 μL) with a 0.5 McFarland standard containing 1.5 $\times 10^8$ CFU/ mL of bacteria and 1.5×10^7 CFU/mL fungi was transferred to 96 well multitier plates. Test cultures were then treated with photosensitizer of different concentration of Photosensitizers were prepared by using non-toxic concentration of dimethyl sulfoxide. The samples were pre incubated for about 3 hours in dark condition and subjected to light exposure with xenon lamp of wavelength 400-800 nm for about 15 min irradiated in the presence of foil-cover to stay away from accidental exposure to the light. Control cultures, with absence of phtosensitizers, were also induced for the same period. The irradiated samples were serially diluted in LB broth and incubated at 37 °C for 24 hours. The reduction in the planktonic cells was calculated by measuring the optical density at 560 nm and expressed as percentage reduction by comparing with the OD values of control [34].

Result and Discussion.

PDT activity of 3a-3d was evaluated by photo-induced cell death of *E.coli* ATCC 25922 under irradiation by a xenon lamp with a wavelength range of 400-800 nm with a intensity 350 Mw\cm^2. The percentage cell inhibition has been shown in

Fig.3.8. It could be seen that the cell death rate was found to be for 3a 82 % for 3b 64 %, for 3c 80 % for 3d its 70 %. Our results showed that all the complexes inhibited the growth of *E-coli* bacteria, but the effectiveness was not same. The pronounced PDT effect of the complexes on gram-negative bacteria may be due to the electrostatic attraction between the photosensitizers and the negatively charged membrane of the bacteria [35]. An apparent dose dependent inhibition curve was observed, this is because of self-shielding of the photosensitizer, where the molecules will absorbs the light at top of the sample which will prevent the light penetration through the sample and initiation of the photosensitizer below it leads to the generation of ROS at proximal location to the targeted [36].

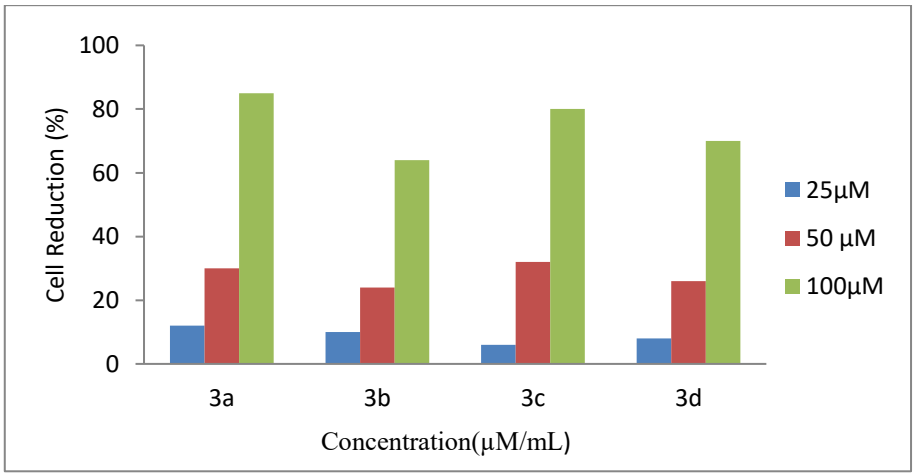

Fig.3.8. Effect of different concentrations of metal complexes on *E.coli*

3.3.7.2. DPPH radical scavenging activity.

All prepared metal complexes were examined for *in-vitro* antioxidant activity by 2,20- diphenyl-1- picrylhydrazyl (DPPH) assay. The presence of electron donating group in the synthesized compounds will exhibits free radical scavenging capacity in comparison with the standard Butylated Hydroxytoulene (BHT). In the present investigation, a stock solution of metal complexes with different concentration (10, 50 and 100 µg) were prepared by using DMSO and dilute by using methanol (500µL) to

the sample solution 0.1 mM ethanolic solution of 1,1-diphenyl-2-picryl hydrazyl was added, then stirred for minute and kept at ambidendate temperature for about 30 minute in the dark to complete the reaction. The decolorization of DPPH solution was determined by measuring the absorbance at the wavelength of 517nm. The % inhibition was calculated by using the formula

$$\% \text{ inhibition} = (Ao - A_t) / A_o \times 100$$

Where, A_o is the absorbance of blank and A_t is the absorbance of tested sample. Percent inihibition plot ted against log concentration and the equation for the line was used to get IC_{50} value. A lower IC_{50} value pointed higher scavenging activity [37].

Result and Discussion.

The fast method to evaluate antioxidant activity is DPPH radical method. The DPPH radical had an absorbance at 517 nm which vanished after acceptance of an electron or hydrogen radical from an antioxidant compound to become a stable diamagnetic molecule. It would be recorded in the visible region, during free radical scavenger the unpaired electron becomes paired off and the absorbance reduces with respect to the number of electron capture. All the complexes showed good antioxidant properties as shown in **Fig.3.9**. The order of reactivity was as follows 3a>3c>3b>3d. The highest percentage of free radical scavenging of all the complexes were 54 %. The standard drug Butylated Hydroxy Anisole (BHA) was 89.69 %. The complexes from HL_1 showed high activity compared to HL_2. The presences of electron donating groups are responsible for increased antioxidant activity [38]. In addition to this, the increasing activity shows concentration dependent manner.

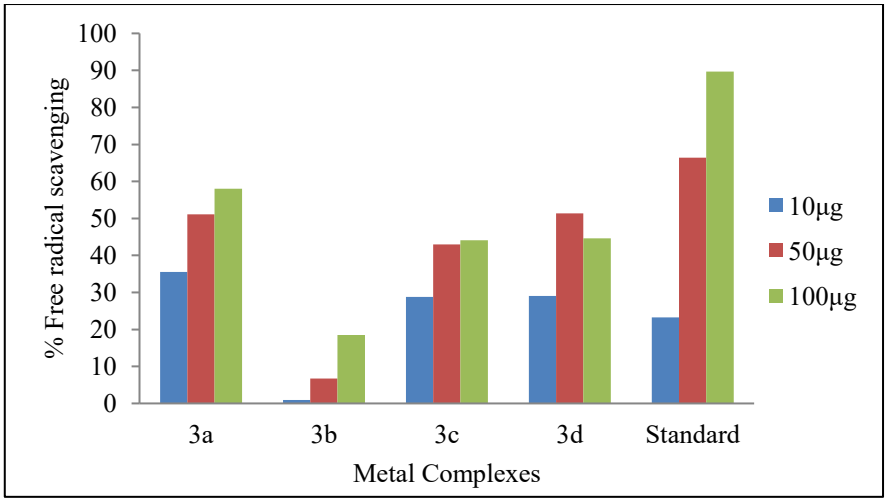

Fig.3.9. DPPH Scavenging activity of Metal Complexes

3.3.7.3. DNA Cleavage Studies.

The DNA cleavage study of synthesized ligand and their metal complexes with supercoiled pBR322 DNA was carried out by using agaros gel-electrophoretic technique. pBR322 DNA (0.5 µg) in ltris-HCl buffer (50 mM) with 50 mM NaCl (pH 7.2) was treated with metal complex (50 µM), followed by dilution with tris-HCl buffer to a total volume of 20 µl after that the content was incubated to 1 hour at 37 °C. After incubation a loading of buffer containing 25 % bromophenol blue, 0.25 % xylene cyanol and 30% glycerol was added in 1:1 ratio, DNA without metal complex is served as a control and the samples were poured into the well along with standard DNA marker electrophoresis was carried out for 2.5 hours at 50 V. The wells were strained with ETBR solution (10µg/ml) for 10-15 min. Bands were visualized using UV light and photographed. By using cleavage efficiency of the metal complexes we can determine the ability to convert the pBR322 DNA to nicked circular (NC) form and Linear (LC) form [39].

Result and Discussion.

The investigation of cleavage study of HL_1 and HL_2 with their metal complexes against supercoiled pBR322 DNA to other forms such as; nicked circular and linear

conformations in DMSO. The pBR322 DNA was subjected to electrophoresis, supercoiled DNA quickly migrates than other forms, if one strand is cleaved, and the supercoiled will unwing to generate a slower moving NC form (Form II). If both strands are cleaved, supercoiled DNA will produce linear form (Form III) [40].

As presented in **Fig. 3.10** the gel electrophoretic results of the interaction of complexes with pBR322 DNA. Lane-1 was employed to unrefined pBR322 DNA (control DNA), lane-2 standard markers DNA, Lane (II-VII) ligands and their metal complexes. It has been observed that Cu(II) complexes (3a and 3c) will effectively cleave pBR322 DNA to nicked-circular and linear DNA. Whereas, the 3b, 3d and the ligands HL_1 and HL_2 will effetely cleave DNA to form nicked DNA (Form 2). The effectiveness of DNA cleavage may vary with different metal complexes may due to the different binding affinity of the complexes to DNA. From DNA cleavage studies, we concluded that 3a and 3c metal complexes will suppress the growth of pathogen by cleaving the supercoiled DNA.

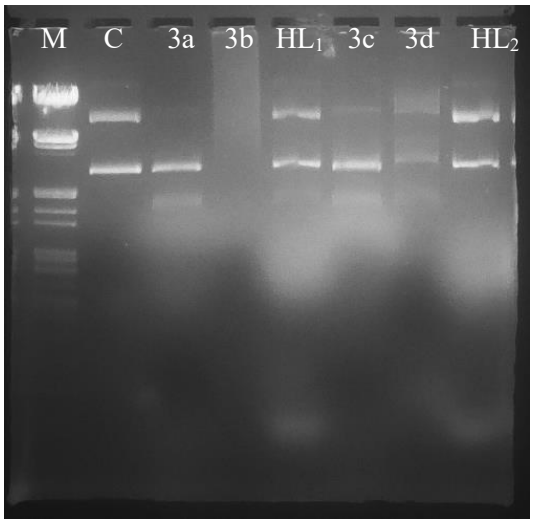

Fig.3.10. Cleavage of supercoiled pBR322 DNA (20 µl) M: Marker, Lane 1: DNA control (pBR322), lane 2: DNA+3a complex, lane 3: DNA+3b complex, lane 4: DNA+ HL_1 ligand, lane 5: DNA+3c complex, lane 6: DNA+3d complex, lane 7: DNA+ HL_2 ligand.

3.3.7.4. In-silico Molecular Docking Studies.

AutoDock4 with MGL tools 1.5.4 were used to achieve blind docking calculations. By using chemsketch software the structures of molecules was drawn and cleaned and convert it into PDB format from mol format by online OPENBABEL. From the Protein Data Bank (PDB id: 423D) was originated from the DNA sequence d(ACCGACGTCGGT)2 at a resolution of 1.6°A was used for the docking studies. First of all the water molecules were deleted, polar hydrogen and Kollman charges were added, non-polar hydrogens were merged into their analogous carbons using AutoDock Tool, then rotatable bonds in ligands were assigned. All the intentions were carried out on an Intel Pentium 4, 2.4 GHz based machine running MS Windows XP SP2 as operating system. The output results from AutoDock were analysed by ligplot and paymol software. According to the autodock score, the lowest energy docked conformation was selected as the binding mode [41].

Result and Discussion

Molecular docking plays a key role in the drug design this is an estimated computational method to investigate the binding site offered at the molecular target DNA. All the synthesized metal complexes were employed to recognize the interaction between the metal complexes with the target receptor molecules (RpsA). The binding sites of complexes (3a-3d) on DNA are shown in **Fig.3.11.** All the synthesized complexes have the capacity to interrelate with DNA through electrostatic interactions, hydrogen bonding, and hydrophobic bonding. All the complexes subjected for docking studies showed at least one H-bond with the enzyme active site. All the synthesized complexes exhibited a firmly-established interaction with the amino acids such as; Vog502, Arg356, Arg357, Tyr280, Arg355, Glu354, Glu381, Asp352 Vog501, The binding energies of the complexes (3a-3d) are presented in

Table 3.6. The Cu(II) complexes (3a) showed the highest binding energy of -5.78 and showed good interactions with the binding site of DNA.

Table 3.6. Docking energy data of the synthesized complexes (3a-3d).

Compounds	Binding Energy (kcal/mol)	H-bonds	H-bond length (å)	H-bond with	Hydrophobic interactions
3a	-5.78	2	2.76 2.83	Arg555, Asp352.	Vog501, Arg357
3b	-5.41	3	2.85 2.69 2.73	Asp352, Arg357, Arg355.	Vog501,Vog502
3c	-4.76	2	2.71 3.33	Glu354, Glu381.	Vog502,Arg356,Tyr280, Arg355
3d	-3.04	1	2.58	Arg356.	Vog501, Arg255, Arg357

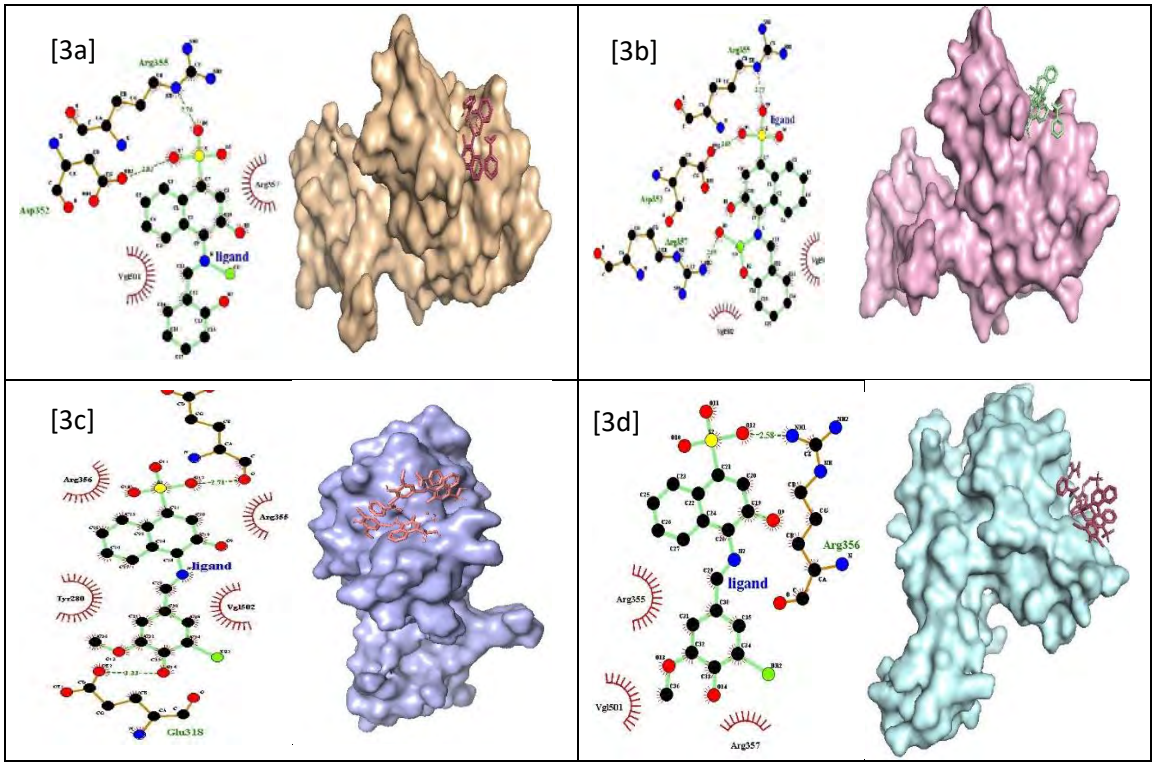

Fig.3.11. Three-dimensional representation of the synthesized compounds [3a-3d] with protein RpsA

3.4. Conclusion.

Based on the spectroscopic studies, these newly synthesized schiff base ligands formed a stable complexation with metal ions to form a octahedral metal complexes with ONO donar sites. The thermal data and photoluminescence spectra of complexes reveled the existence of water molecule in the complexes (3a-3d). The pharmlogical behavior of the complexes was more efficient in comparison to parent ligand. Biological data reveled that, all the metal complexes showed good effectiveness towards DNA cleavage. The antimicrobial photodynamic activity of *E.coli* was tested. Among the studied compounds, 3a exhibited the highest cell reduction was found to be 82% in at a concentration of 200 µg/mL. The Cu(II) and Co(II) complexes of ligand HL_1 showed efficient antioxidant activity. Molecular docking studies were carried out to explore the binding interactions between the synthesized complex and the target receptor RpsA. It showed that the tested compounds fit into the receptor active site with complimentary binding energy. It was concluded that the Schiff base ligand (HL_1 and HL_2) and its metal complexes proves to be promising candidates as photoactive antimicrobial activity and also great biological agents with reduced toxicity.

3.5. Reference.

1. Y. Zhang, P.Traber, L. Zedler, S. Kupfer, S. Grafe, M. Schulz, W. Frey, M. Karnahl and B.Dietzek, *Chem.Phys.,* **2018**.
2. M. Cheng, M. Wanhong, C. Chen, J. Yao and J. Zhao, *App. Catal. B: Envir.,* 65, 217–226, **2006**.
3. L. Samantha Hopkins, L. Stepanyan, N. Vahidi, A. Jain, S. J. Brenda and J. Karen Brewer, *Inorg. Chim. Act.,* **2016**.
4. C. Cheng Liu, L.Sheng Zhou, J. Yun Liu. J. Min Xiao, H. Zhou Gao and K.Wu Yang, *New.J.Chem.,* 37, 575, **2013**.
5. J. Dlugaszewska, W. Szczolko, T. Koczorowski, P. S. Mrugalska, A. T, K. Konopka, M. Kucinska, M. Murias, N. Duzguneş, J. Mielcarek and T. Goslinski., *J. Inorg. Biochem.*, **2017**.
6. R. Giereth, I. Reim, W. Frey, H. Junge, S. Tschierlei and M. Karnahl, *Susta. Energy Fue.,* 3, 692–700, **2019**.
7. S. Leonard, P.M. Gannett, Y. Rojanasakul, D.S. Berry, V. Castranova, V. Vallyathan and S. Xianglin, *J. Inorg. Bioche.,* 70, 239-244, **1998**.
8. S. M. Pradeepa, H. S. Bhojya Naik, B. Vinay Kumar, K. Indira Priyadarsini, Atanu Barik, T. R. Ravikumar Naik and M. C. Prabhakara, *Spectro. Acta Part A: Mole. Biomole. Spectro.,* 115,12–21,**2013**.
9. K. Mohanan, N. Subhadrambika, R. Selwin Joseyphus, S.S. Swathy and V.P Nisha, *J. Saudi Che. Soci.,* **2012**.
10. Y. Sindhu, C.J. Athira, M.S. Sujamol, R.S. Joseyphus and K. Mohanan, *Syn,Rea. Inorg. Metal-Organic. and Nano-Metal Chem.,* 43, 226–236, **2013**.
11. N. Raman, A. Kulandaisamy and C.Thangaraja, *Trans. Metal Chem.,* 28, 29–36, **2003**.
12. C. N. Sudhamani, H. S. Bhojya Naik, K. R. Sangeetha Gowda, M. Giridhar, D. Girija and P. N. Prashanth Kumar, *Med. Chem. Res.*, 26, 1160–1169, **2017**.
13. B. Karami and M. Kiani, *Polyc. Arom. Comp.,* 37(4), 257-266, **2017**.
14. S. Neeraj, S. K. Asthana, R. K. Mishra and K.K. Upadhyay, *RSC Advances.,* 1-3, **2013**.
15. S. Kiran, R. Thakur and Vikas Kumar*, beni-suef unive. J. of basic and appli. scien.,* 21–30, **2016**.
16. G.Y. Nagesh and B.H.M. Mruthyunjayaswamy, *J. Mol. Stru.*, 1085, 198–206, **2015**.

17. S. Harisha, J. Keshavayya, B.E. Kumara Swamy and C.C. Viswanath, *Dyes and Pig.,* 136, 742-753, **2017**.
18. A. A. Amer, H. Ilikti and U. Maschke, *J. Mol. Stru.*, 1147, 177-184,**2 017**.
19. U. D. Kamaci, M. Kamaci and A. Peksel, *J. Fluoresc.,* 16, 18, **2016**.
20. B. Vinay Kumar, H.S. Bhojya Naik, D. Girija, N. Sharath and S.M. Pradeepa, *Macromol. Sci. Part A Pure Appl. Chem.,* 49, 139–148, **2012**
21. M. A. Abdel Nasser, A. Alaghaz Badr, E. Sayed, A, Ahmed, E. Henawy and A.A. Reda Ammar, *J. Mol. Stru,*1035, 83–93, **2013**.
22. P. H. Amith Nayak, H. S. Bhojya Naik, H. B. Teja, B. R. Kirthan and R. Viswanath, *J.Elec.Mat.,* **2021.**
23. G.Y. Nagesh, K. Mahendra Raj and B.H.M. Mruthyunjayaswamy, *J. Mol. Stru.,* 1079, 423–43, **2015**.
24. W. H. Mahmoud, N.F. Mahmoud and G. G. Mohamed, *J. of Organo.Chemi.,* 848, 288-301, **2017**.
25. E. Ispir, M. Ikiz, A. Inan, A. Burak Sunbul, S. Erden Tayhan, S. Bilgin, Muhammet, Kose and M. Elmastas, *J.of Mole. Struc.,* **2019.**
26. E. Sundaravadivel, G. Ramanjaneya Reddy, D. Manoj, S.Rajendran, M. Kandaswamy and M. Janakiraman, *Inorg. Chim. Acta.,* 482, 170–178, **2018**.
27. M. C. Prabhakara, B. Basavaraju and H. S. Bhojya Naik, *Bioinorg. Chem. Appl*., 7–13, **2007.**
28. K. R. Sangeetha Gowda, H. S. Bhojya Naik, B. Vinay Kumar, C. N. Sudhamani, H. V. Sudeep, T. R. Ravikumar Naik and G. Krishnamurthy, *Spectrochim. Acta Part A: Molec. and Biomolec. Spectro.,* 105, 229–237, **2013**.
29. H. R. Prakash Naik, H. S. Bhojya Naik, T. R. Ravikumar Naik, H. Raja Naika, K. Gouthamchandra, R. Mahmood and B.M. Khadeer Ahamed. *Eur. J. Med. Chem.,* 44, 981–989, **2009.**
30. E. Ispir, M. Ikiz, A. Inan, A. Burak Sunbul, S. Erden Tayhan, S. Bilgin, Muhammet, Kose and M. Elmastas, *J.of Mole. Struc.,* **2019.**
31. D. Majumdar, S. Das, R. Thomas, Z. Ullah, S.S. Sreejith, D. Das., Pooja Shukla, Kalipada Bankura, and Dipankar Mishra, *Inorg. Chim. Acta.,* **2019**.
32. F. Fayyaz, R. Rahimi, M.Rassa and R. H. Yaghoobi, *1st Intern. Elect. Conf. on Mole. Scie.Cell Sign. Su.r and Gro.,* **2015**.
33. W. M. Sharman, M. Cynthia Allen and Johan E. *Van Lier Therapeutic Focus DDT,* 4, **1999**.

34. S. Nazzal, C.P. Chen and Tsuimin Tsai, *J. of Food and Drug Anal.,* 19, 4, 383-395, **2011.**

35. G.Y. Nagesh, U.D. Mahadev and B.H.M. Mruthyunjayaswamy. *Int. J. Pharm. Sci. Rev. Res.,* 31(1), 190-197, **2015**.

36. M. Cleiton, Da Silva, L. Daniel, da Silva, V. Luzia Modolo, B. Rosemeire Alves, A. Maria de Resende, V.B. Cleide Martins and Angelo de Fa tima. *J. of Adv. Res.,* 2, 1–8, **2011**.

37. A. Kajal, S. Bala, S. Kamboj, N. Sharma and V. Saini, *Hind. Publ. Corpo. J. of Catalysts*, 893512, **2013**.

38. J. Liua, T. Zhangb, T. Lua, Q. Lianghu, H. Zhouc, Q. Zhanga and J.Liangnian, *J. of Inorg.Bioche..,* 91, 269–276, **2002.**

39. M. Gul, I. Ozturk Cali, A. Cansaran, O. Idil, I. Kulu and U. Celikoglu, *Cog. Chemi.*, 3, 1337293, **2017**.

40. S. Abdul Malek. Y. Al-Tamimi, Sheena Mary, M. Hanan. K.S. Hassan, A. Resmi, B. A. El Emam, B.K. Narayana and Sarojini, *J. of Mole. Struc.,* **2018**.

41. O. I. Edozie1, O. J. Godday, A.K. Chijioke, I. O. Uchenna and N.Felix Chigozie, *Bull. Chem. Soc. Ethiop.,* 34(1), 83-92, **2020**.

Chapter-4

Synthesis, Characterization and Pharmacological Activity of Novel Azo Dye Ligand and Their Metal Complexes Containing Nitrogen and Oxygen Donor Atoms

4.1. Introduction.

Resistance of bacteria against current antibiotics is a common and huge problem. This chapter focused on azo dye of sulfadiazine and acetyl acetone to explore their potential to substitute their parent drug so that bacteria may be destroyed rapidly and effectually [1]. The Resistance development against antibacterial drugs. Sulfonamides having amide functional group have improved [2] pharmacological, toxicological properties and are being used as drugs. Domagk got his Nobel prize in the year 1939 for discovery of sulfonamides are active chemotherapeutic ingredient [3].

Sulfadiazine was presented in medical therapy from 1940 onwards because of its biological activity in the prevention and cure of bacterial infections in humans. Sulfadiazine is a pyrimidinyl sulfonamide derivative is very popular synthetic bacteriostatic antibiotic [4]. The presence of sulfonamide unit in the azo dye exhibit excellent pharmacological properties and has been used as effective drugs for the treatment of various diseases. Yet, the applicability of these compounds shows allergic side effects to many body organs such as lymphadenopathy, hepatotoxicity, and haematological disorders [5]. In order to overcome these sulfonamide derivatives and their transition metal complexes were in clinical trials. The presence of several potential donor sites e.g., amino, pyrimido, sulfonamidic nitrogen and sulfonyl oxygen atoms make them versatile complexing agents [6]. A large number of metal sulfonamide complexes were found to be more potent than the parent drugs. Due to these challenges, there is needed to design novel drugs with multiple medicinal properties.

The coordination chemistry of transition metal ions has been extensively investigated in recent years because of its useful magnetic and optical behaviors. It

could display coordination numbers 1-12, with 2, 4 and 6 being ubiquitous [7]. Wide selection of azo dye ligands have been employed for the synthesis of transition metal complex. Over the last few years, the growing interests in the synthesis of azo dyes having heterocycles have led to the design of optical recording systems and liquid crystalline devices (LCDs) [8]. The Azo dye ligands with N, O donors have often been used since the azo dye ligands may gather coordination architectures focused by the transition metal ion. because, these are showed potential applications in number of biological reactions such as inhibition of RNA, protein synthesis and nitrogen fixation, antibacterial, antifungal, anticancer and antituberculosis agents etc., [9-10].

Here in this Chapter, we present a series of Cu(II), Co(II) and Ni(II) azo based metal complexes using organic ligands prepared with sulfadiazine and acetyl acetone by diazotization method. The structures of the newly synthesized dyes were confirmed by various physico-chemical techniques. The antimicrobial photoinactivation, antioxidant and Insilco molecular docking studies of the metal complexes were studied in order to explore their potentiality to inhibit the respective pathogens.

4.2. Experimental.

4.2.1. Materials and Methods.

The Sulfadiazine, Acetyl acetone and the selected metal salts like $CoCl_2.6H_2O$, $CuCl_2.6H_2O$ and $NiCl_2.6H_2O$ were purchased from Sigma– Aldrich. All the solvent used with high purity. The synthesized azo dye and its metal complexes were characterized by different analytical and spectroscopic techniques are described in **Chapter 2.**

4.2.2. Synthesis of azo dye ligand (HL_3).

The azo dye 4-[(*E*)-(1-acetyl-2-oxopropyl)diazenyl]-*N*-pyrimidin-2-ylbenzenesulfonamide were prepared according to the general procedure in the

literature. Briefly, a mixture of sulfadiazine (0.01mol) and concentrated hydrochloric acid (5 ml) were stirred at 0–5 °C until a clear solution was obtained. A solution of sodium nitrite (0.01 mol) in 10 mL ice cold water were then added drop wise, retaining the temperature below 5 °C. The resulting mixture was stirred for an additional 1 hour in an ice bath to form a diazonium salt solution. The Coupling Resultant acetyl acetone (0.01 mol) were dissolved in 10 ml of ethanol, and cooled to 0–5 °C in an ice bath. This solution was then gradually added to the cooled diazonium salt solution and the resulting mixture were stirred at 0–5 °C for further 2 hour. The resulting precipitate were filtered, washed with cold water and recrystallized from ethanol, DMF mixture to yield azo dye ligand. The schematic representation was depicted in **Scheme 4.1** [11].

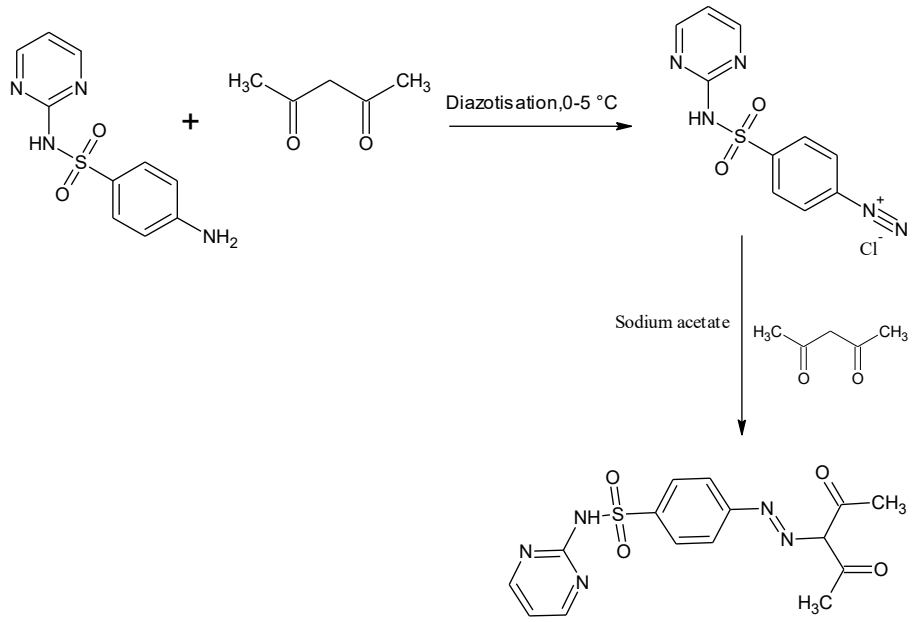

Scheme 4.1. Synthesis route of azo dye ligand (HL_3)

4.2.3. Synthesis of metal complexes.

A solution of 0.05 mol of [$CoCl_2.6H_2O$, $CuCl_2.6H_2O$ and $NiCl_2.6H_2O$] metal salts in 50 mL ethanol was added to a magnetically stirred suspension of the azo ligand (0.1 mol) in 20 mL of ethanol and the reaction mixture were refluxed for 24 hour at a temperature 60 °C. After completion of the reaction, 50 ml of water was added. The

colored precipitate of the respective complexes separated from the reaction mixture which were filtered, washed with water, ethanol and dried in vacuum oven for 24 hour at 70 °C [12].

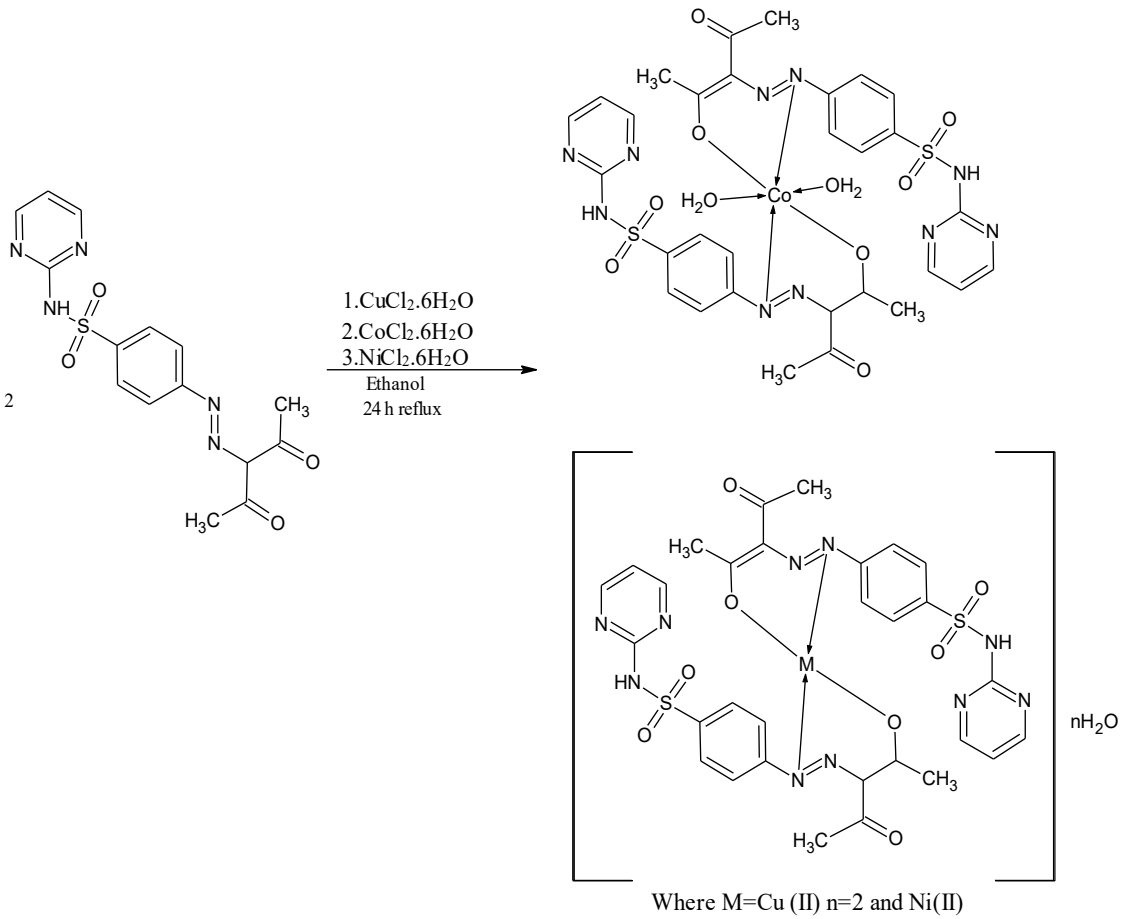

Scheme 4.2. Synthetic route for azo dye metal complexes.

4.3. Results and Discussion.

The azo-dyes having sulfadiazine and acetyl acetone moieties as prepared. The synthesized compounds were obtained in reasonable yield. The bright yellow colored azo dye ligand (HL_3) is stable in room temperature and found to be soluble in chloroform and other common organic solvents like ethanol, DMF, and DMSO. All the azo metal complexes are colored solids, non-hygroscopic, amorphous in nature and found to be soluble in DMF, DMSO. Melting points of the metal complexes were found to be above 300 ºC. The results of the elemental analysis of the synthesized

compounds were presented in **Table 4.1**. From the results, the complexes suggest that the metal to ligand ratio is 1:2 stoichiometry of the type $[M(L)_2]$ for all the complexes, where L stands for the deprotonated ligand.

Table 4.1. Yields and Elemental analysis data for azo-dye ligand and its metal complexes.

Sl No	Synthesized Compound	Molecular Weight	Yield In%	Melting Point In ^{0}C	Elemental Analyzer % Found (Calculated)					
					C	H	N	O	S	M
1	$C_{15}H_{15}N_5O_4S$ (HL_3)	361	78	258-260	49.80 (49.85)	4.16 (4.18)	19.36 (19.38)	17.70 (17.71)	8.86 (8.87)	-
2	Cu(II) Complex	788	70	>300	45.70 (45.71)	4.04 (4.09)	17.11 (17.77)	16.04 (16.24)	8.12 (8.14)	8.04 (8.06)
3	Co(II) Complex	817	65	>300	44.04 (44.06)	4.18 (4.19)	17.12 (17.13)	19.58 (19.57)	7.82 (7.84)	7.20 (7.21)
4	Ni(II) Complex	782	75	>300	45.90 (45.99)	4.10 (4.12)	17.84 (17.88)	16.36 (16.34)	8.20 (8.19)	7.50 (7.49)

4.3.1. ^{1}H-NMR spectral studies.

The proton NMR spectrum is an outstanding tool to check the purity of the organic compounds. ^{1}H-NMR spectra of the azo dye obtained at ambient temperature in DMSO-d6 at 400 MHz using BRUKER-400 spectrometer, using TMS as an internal standard. The values of the chemical shifts obtained were matches with the expected theoretical values of the compounds. The ^{1}H-NMR spectra of the ligand is shown in **Fig 4.1**.The aromatic protons were observed in the range of 7.14 to 7.85 ppm. The two methyl proton of the acetyl acetone moiety had showed a singlet at 2.41 ppm and at 3.20 ppm (3H each) [13]. The -NH of the sulfadiazine moiety had showed a signal at 10.63 ppm(s, ^{1}H,-NH). The azo dye ligand displayed a singlet at 14.94 ppm (s, ^{1}H, -OH) [14] is due to hydroxyl group of acetyl acetone this suggest the tatomeric form of acetyl acetone this was also supported by FT-IR spectroscopy.

Keto-Enol Tautomerism.

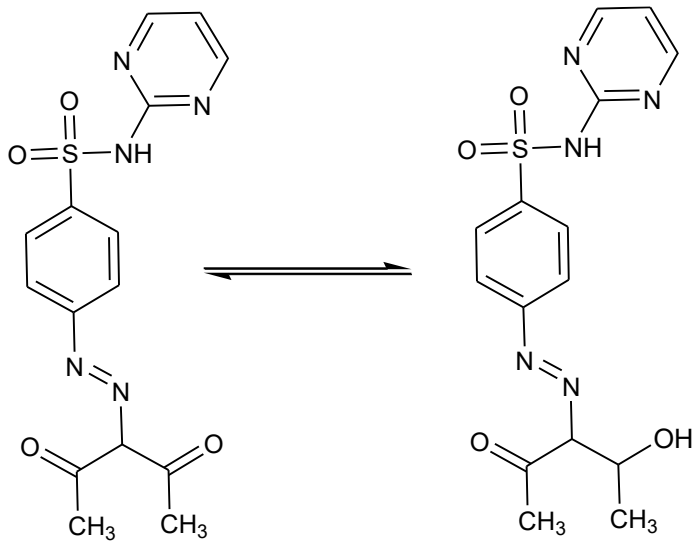

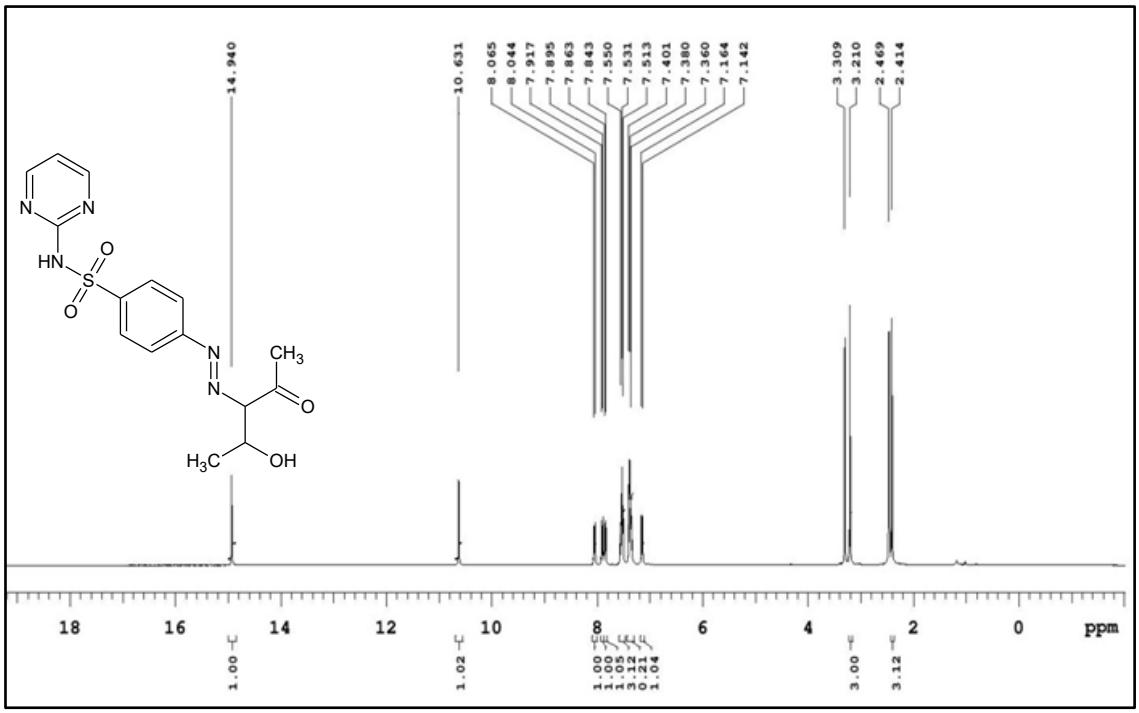

Fig.4.1.[1]H-NMR Spectra of the azo dye ligand (**HL_3**)

4.3.2. Electronic absorption spectra.

The electronic absorption spectra in the UV-visible region for the free ligand as well as their metal complexes were recorded in DMSO solution. The electronic

absorbtion spectral results of ligand and its metal complexes are given in **Tale 4.2** and the characteristic electronic spectra are shown in **Fig 4.2**. The absorption spectrum of the free ligand, showed a band 356 nm due to the transition involving electron migration along the entire conjugate system of the ligand. This band shift towards longer wavelength in all the complexes. According to Molecular orbital theory explains the impact of center metal(II) ions on the absorption bands of the complexes. The metal complexes exhibited new bands in the range of 496-505 nm assigned to charge transfer spectrum (LMCT), which were absent in ligand [15]. The Cu(II) complex showed a well-defined band at 387 and 496 nm which was assigned to the transitions of $^2B_{2g} \rightarrow {}^2B_{1g}$ and $^2B_{2g} \rightarrow {}^2A_{1g}$ region disclose that the presence of square planar geometry of complex. The Co(II) complex showed the absorption of 380 and 495 nm and the bands were assigned as $^4T_{1g}(F) \rightarrow {}^4T_{2g}(F)$ and $^4T_{1g}(F) \rightarrow {}^4A_{2g}(F)$, [16] which are supporting the octahedral geometry. From the electronic spectrum of the Ni(II) complex, it is observed that the bands at 393 and 505 nm are assigned to INCT and $^1A_{1g} \rightarrow {}^1B_{1g}$ respectively. All these transitions are characterized for square planar geometry for Ni(II) complex [17]

Table 4.2. Electronic absorbtion data of azo dye and its metal complexes.

Compound	λmax (nm)	Transition	Geometry
HL_3	356	π→π*	
Cu(II) Complex	387 496	$^2B_{2g} \rightarrow {}^2B_{1g}$ $^2B_{2g} \rightarrow {}^2A_{1g}$	Square planar
Co(II) Complex	380 495	$^4T_{1g}(F) \rightarrow {}^4T_{2g}(F)$ $^4T_{1g}(F) \rightarrow {}^4A_{2g}(F)$,	Octahedral
Ni(II) Complex	393 505	INCT and $^1A_{1g} \rightarrow {}^1B_{1g}$	Square planar

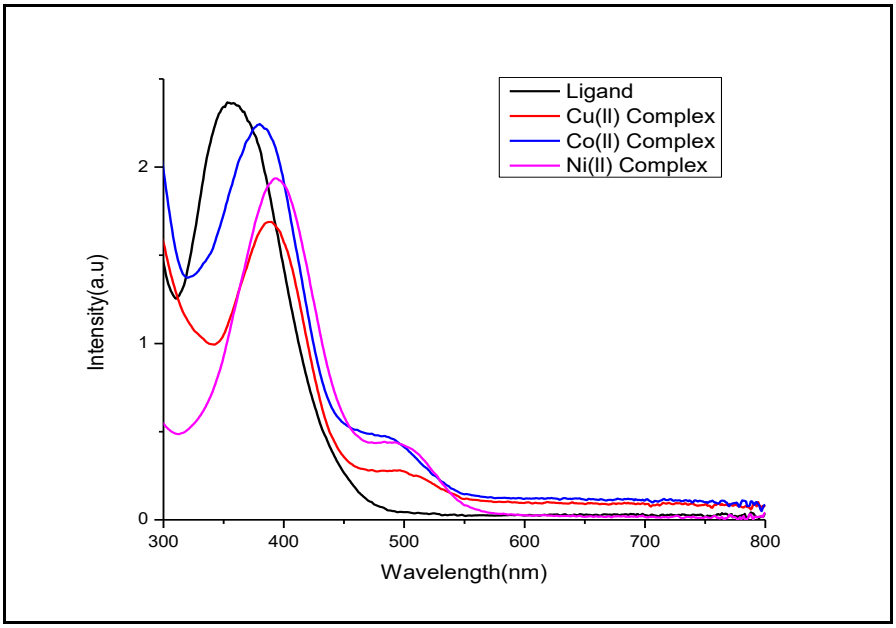

Fig. 4.2. UV-Visible spectrum of azo dye ligand (HL_3) and its metal complexes.

4.3.3. FT-IR Spectra.

The IR spectra of the synthesized azo compounds were recorded in the region of 4000 cm^{-1} to 400 cm^{-1} on a FTIR-ALPHA BRUCKER IR spectrometer in KBr pellets. For mononuclear metal complexes the metal ion forms a bond with azo dye center or with sulfanilamide part. The FT-IR spectrum of the azo dye shows vibrational peaks at 3402 cm^{-1} due to -OH group conforming enolization of C=O through keto-inol tautomirsm. A sharp peak at 1673 cm^{-1} was assigned as a carbonyl stretching vibration (C=O) conversely, this vibrational frequency of the carbonyl is conspicuously decreases in the metal complexes. Moreover, the peak at 1516 cm^{-1} are assigned as N=N stretching vibrations, this vibrational frequency was shifted by ca. 30 cm^{-1} to a lower frequency on complexation [18], due to the involvement of one of the azo nitrogen atoms in coordination with metal ion. In the free ligand three essential absorption bands centered around 3034 cm^{-1}, 2930 cm^{-1} and 2868 cm^{-1} are assigned as the CH aromatic, CH_2 and CH_3. The medium intensity band at 1314 cm^{-1} are assigned as S=O, in complexes this vibrations remain unchanged this is evidenced that S=O

group are not contributed in coordination. Compared to the free ligand, some shifted bands in the spectra of the azo metal complexes were observed, as shown in **Table 4.3**, and depicted in **Fig.4.3a-4.3d**. The IR spectrum of complexes showed a broad band at 3400-3435 cm^{-1}, due to vibration of water molecule connected with complexes [19]. This was moreover supported the existence of weak coordinated water molecules (H_2O) at 730-750 cm^{-1}. Undoubtedly, the appearance of new metal-oxygen and metal-nitrogen vibrational frequency was observed in all the metal complexes. This result emphasizes the contribution of ester carbonyl group and one nitrogen of the azo group in bonding with metal complexes.

Table 4.3. FT-IR Spectrum of azo dye ligand and Cu(II), Co(II) and Ni(II) complexes.

Sl No	Compound	OH/H_2O	N=N	S=O	C=O	M-O	M-N
1	Ligand (HL_3)	3402	1516	1314	1673	--	---
2	Cu(II) complex	3412	1442	1316	1587	598	683
3	Co(II) complex	3438	1465	1310	1598	591	627
4	Ni(II) complex	3418	1448	1316	1592	571	671

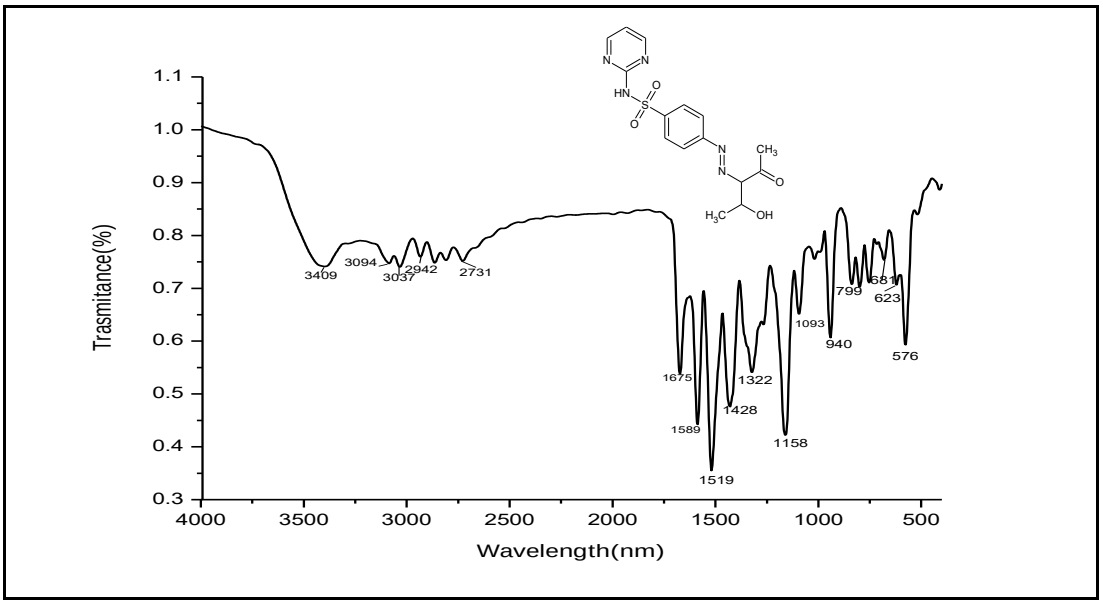

Fig.4.3a. FT-IR spectrum of azo dye ligand (HL_3).

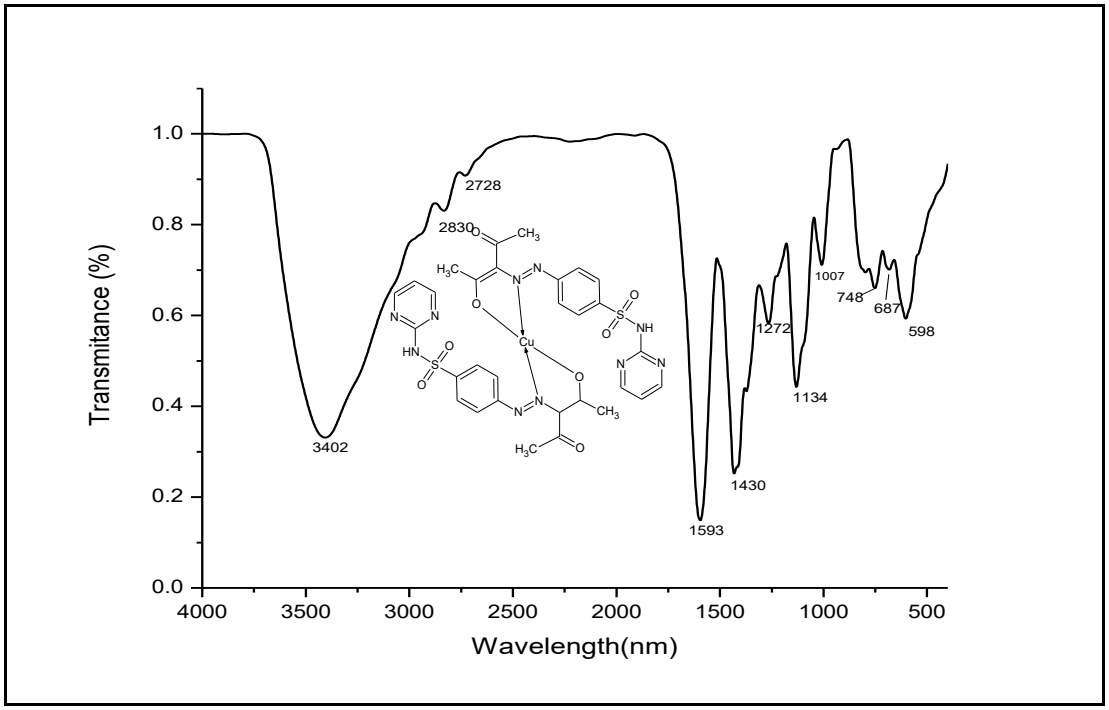

Fig.4.3b. FT-IR spectrum of Cu(II) complex.

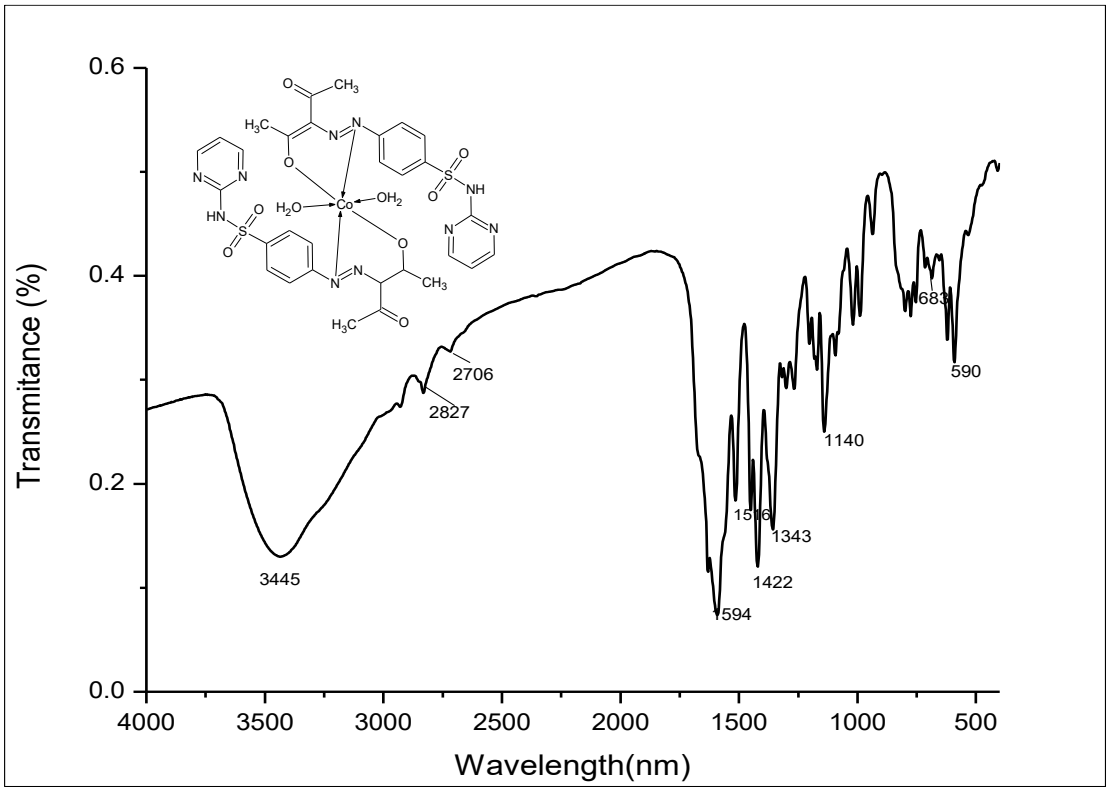

Fig.4.3c. FT-IR spectrum of Co(II) complex

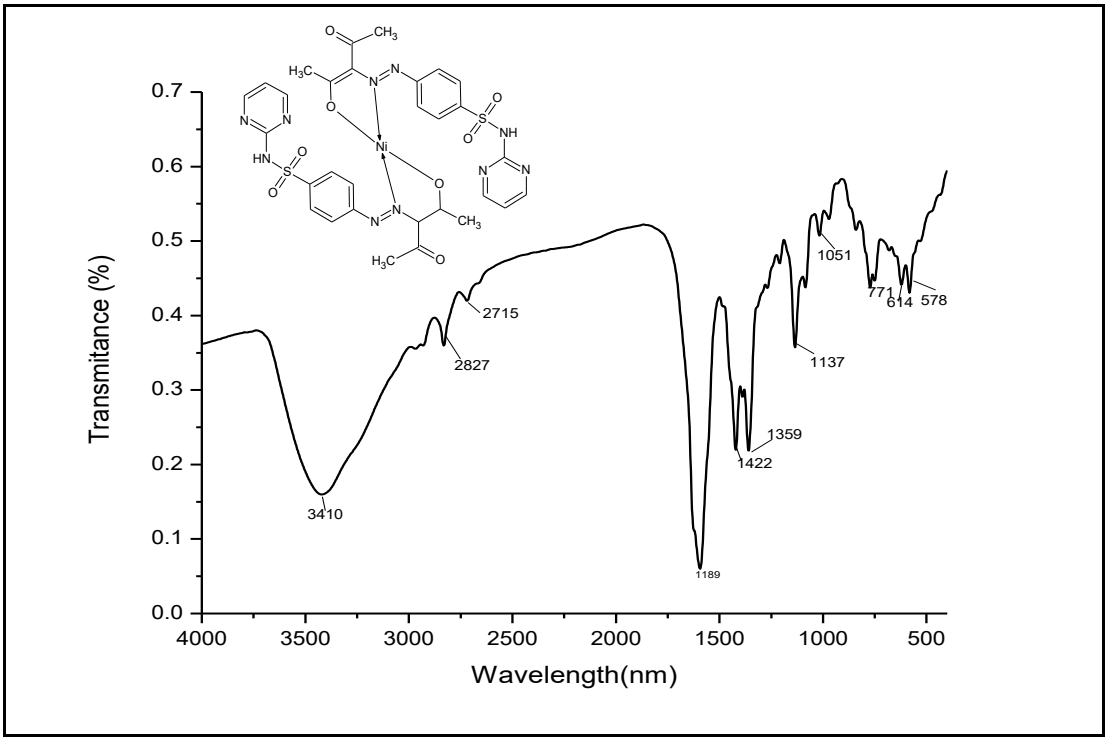

Fig. 4.3d. FT-IR spectrum of Ni(II) complex.

4.3.4. Mass spectra.

The mass spectra of the free ligand and its metal complexes were recorded, and they are depicted in **Fig.4.4a-4.4d.** The mass spectrum of the azo dye ligand were measured to confirm their structure all most all the azo compounds have the same molecular formula and formula weight ($C_{15}H_{15}N_5O_4S$ M.Wt. 361 g/mol), their mass spectra showed a molecular ion peak observed at m/z 361. This molecular ion peak is in good agreement with the expected molecular mass as showed from elemental analyses, as shown in **Table 4.1.** The Cu(II), Co(II) and Ni(II) complexes of the ligand showed a molecular ion peak at m/z at 788, 817 and 782 respectively. The molecular mass of the complex shows that the stoichiometric composition of $[M(L)_2]$ type. In addition, the molecular ion peaks in all the complexes at are in good agreement with empirical formula.

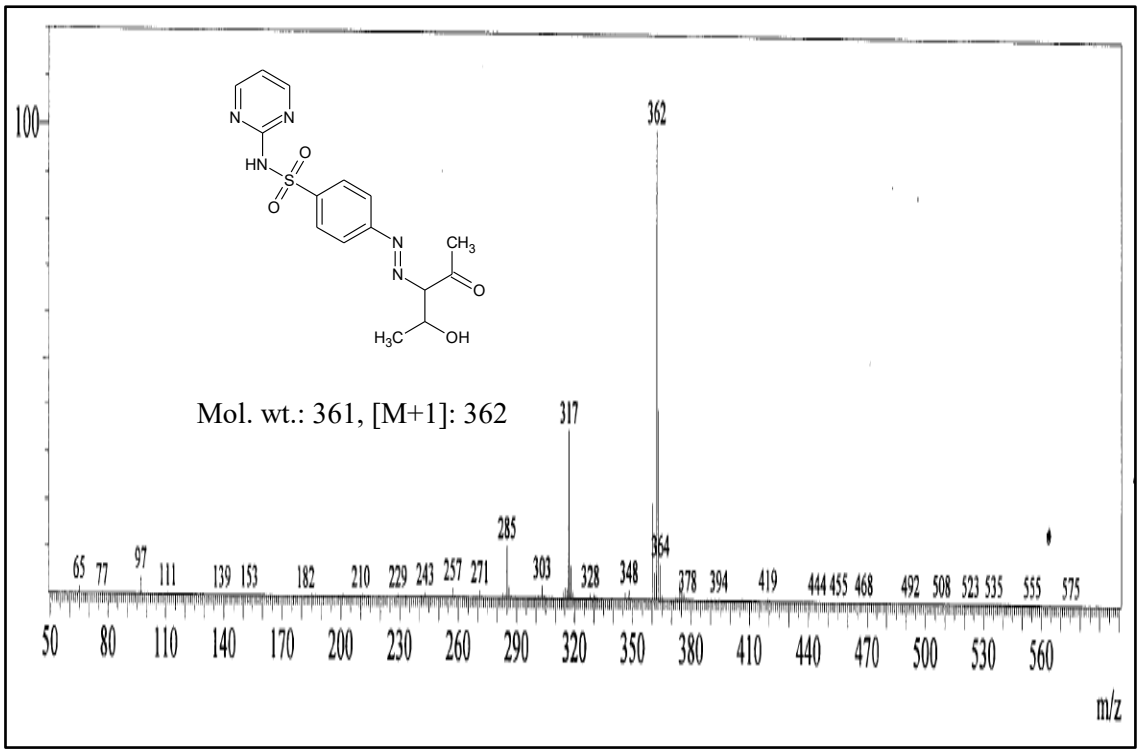

Fig. 4.4a- Mass spectrum of azo dye ligand (HL_3).

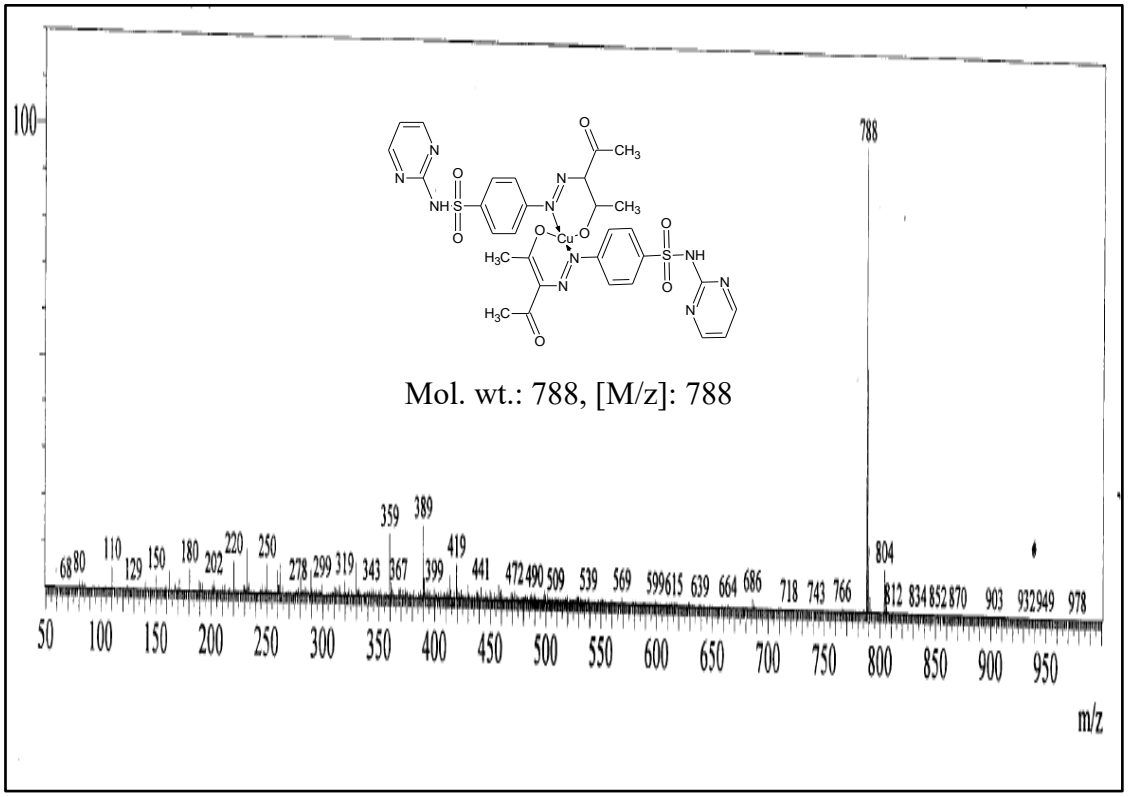

Fig. 4.4b. Mass spectrum of Cu(II) complex.

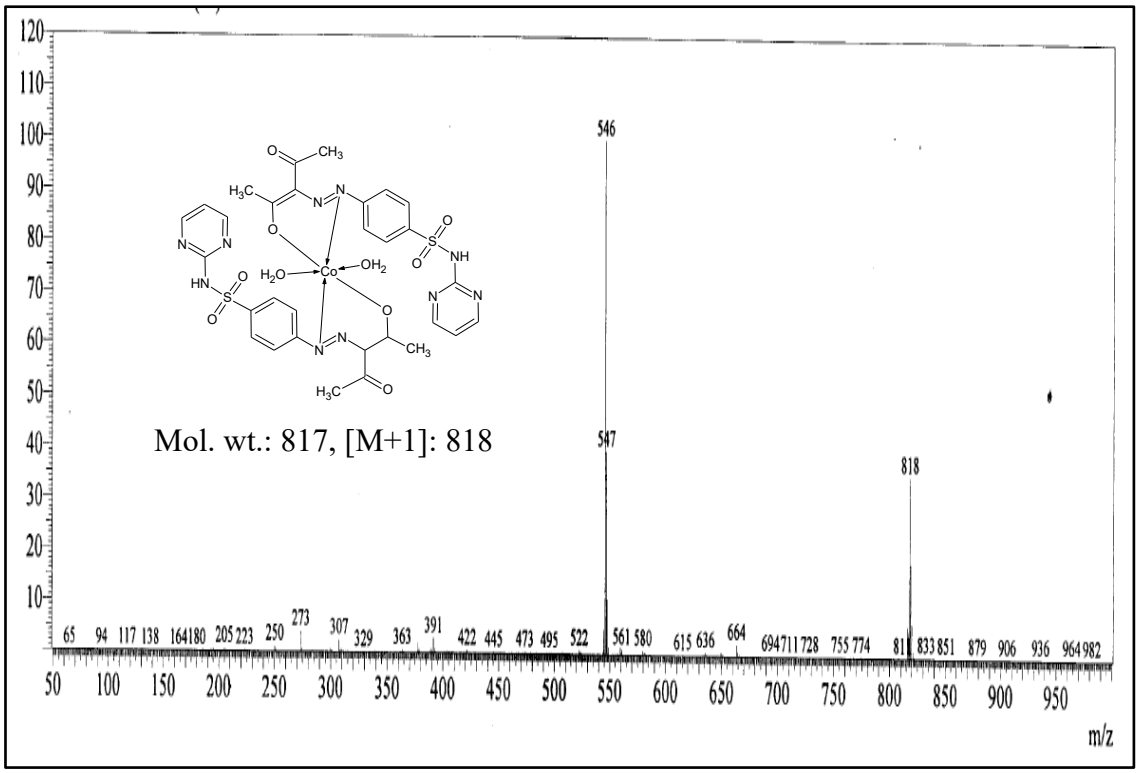

Fig.4.4c. Mass spectrum of Co(II) complex.

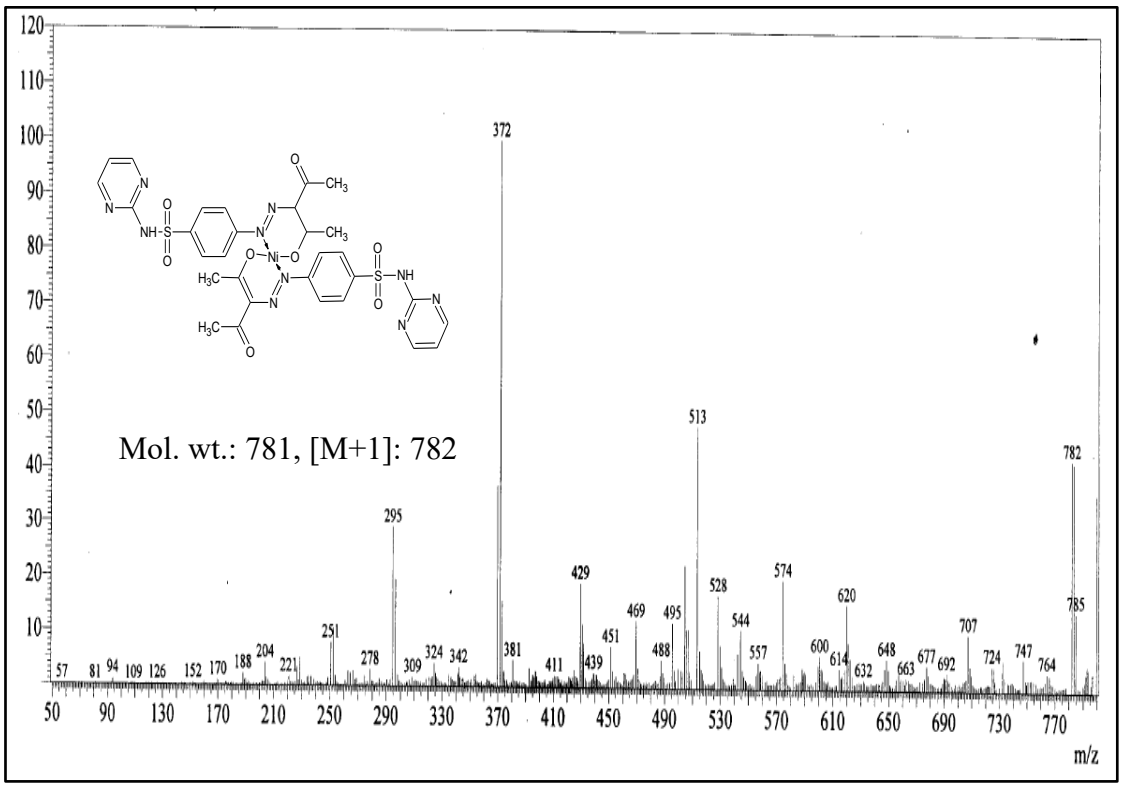

Fig. 4.4d. Mass spectrum of Ni(II) complex.

4.3.5. Thermogravimetric analysis.

The thermal behavior of metal complexes was carried out to confirm their molecular structures and thermal stability. The TGA of the complexes were studied at a rating of heating 10 ^{o}C min^{-1} under nitrogen atmosphere within temperature range 30-750 ^{o}C. The tentative assignments of metal complexes with respect to temperature and formation of the respective metal oxides are displayed in **Table 4.4 and Fig 4.5**

The TG graph of Cu(II) complex gave three stages of disintegration. In the first stage the loss of two moles of lattice water molecule with the mass loss was found to be 3.9 % (calcutated 4.35%) at a temperature range 30-156 ^{o}C. The second stage of degradation corresponds to the loss of organic moiety $C_8H_6N_4$ in the complex with the mass loss of 24.89 % (calculated 24.76%) temperature ranging from 115-314 ^{o}C. The loss of $C_{22}H_{26}N_4O_8S_2$ takes place in third step with the loss of 58.4 % (Calculated 57.6 %) with in the temperature range 315-731 ^{o}C. The gradual decomposition of the Azo dye complex with the formation of CuO.

The thermogram (TGA) data of Co(II) exhibited four stages of decomposition at different temperatures. In the first stage the loss of two moles of coordinated water molecules with the loss mass was found to be 4.33 % (calculated 4.41 %) ranging 30-75 ^{o}C. The second stage corresponds to the loss of organic moiety $C_4H_8O_2$ with the loss of 11.1 % (calculated 11.3%) at temperature ranging from 76-254^{o}C. The loss of $C_8H_{10}N_6$ was taken place in the third step ranging 255-330 ^{o}C with the mass loss of 27.0% (calculated 27.1%). In the last step correspond to the gradual decomposition of the complex with the formation of CoO with the mass loss at temperature ranging 330-700^{o}C.

TGA curve of Ni(II) complex gave four stages of disintegration started at 36, 96, 315, 373 ^{o}C. The loss of two crystalline water molecules was takes place in first

step at temperature 36-108 ºC with the mass loss of 4.2 % (calculated 4.41 %). The second stage of decomposition appeared in the temperature 108–314 °C with a mass loss of 10.54 % (calculated 11.3%) corresponds to removal of $C_{12}H_{18}N_6O_2$. The gradual decomposition of the Azo dye complex with the formation of NiO + $NiCO_3$ mixture was takes place in last two stages.

Table 4.4. Thermal analysis data of metal complexes.

Complexes	Stages	Decomposition Temp (°c)	Probable Assignment	Loss Of Mass In (%) Found (Calc)	Residual Species
Cu complex	1st 2nd 3rd	30-156 156-314 315-731	2 H_2O $C_8H_6N_4$ $C_{22}H_{26}N_4O_8S_2$	3.90(4.35) 24.89(24.76) 58.4(57.6)	CuO
Co complex	1st 2nd 3rd 4th	30-76 76-254 254-330 331-500	2 H_2O $C_4H_8O_2$ $C_8H_{14}N_6$ $C_{10}H_{14}O_4S_2$	4.33(4.4) 11(11.3) 26(26.2) 52.0(52.11)	CoO
Ni Complex	1st 2nd 3rd 4th	30-95 96-314 314-372 373-748	2 H_2O $C_4H_8O_2$ $C_8H_{14}N_6$ $C_{10}H_{14}O_4S_2$	4.23(4.41) 10.54(11.03) 27.17(27) 52.34(52.11)	NiO + $NiCO_3$

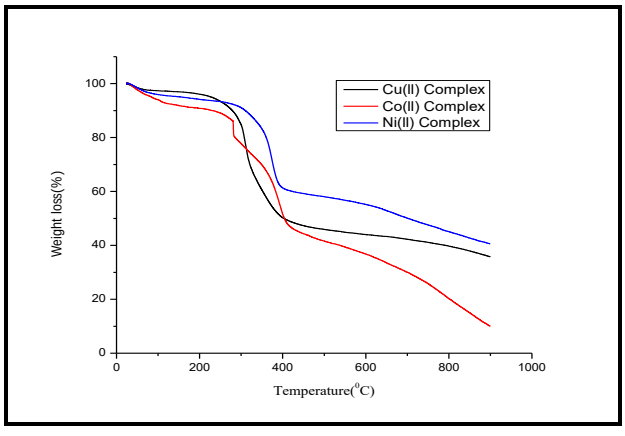

Fig. 4.5. TG curves of metal complexes.

4.3.6. SEM with EDAX.

The morphology and particle size of ligand and metal complexes have been illustrated by the scanning electron micrography. **Fig 4.6** shows the surface

morphology of the synthesized free ligand and their metal complexes. We noted that a uniform bricks like structure was observed in free ligand. The size of the particle decrease after complexation. A ice rock like shape is observed in the Co(II) complex. Rough and damaged images were seen for Cu(II) complex. The Ni(II) complexes show a small granular structure [20].

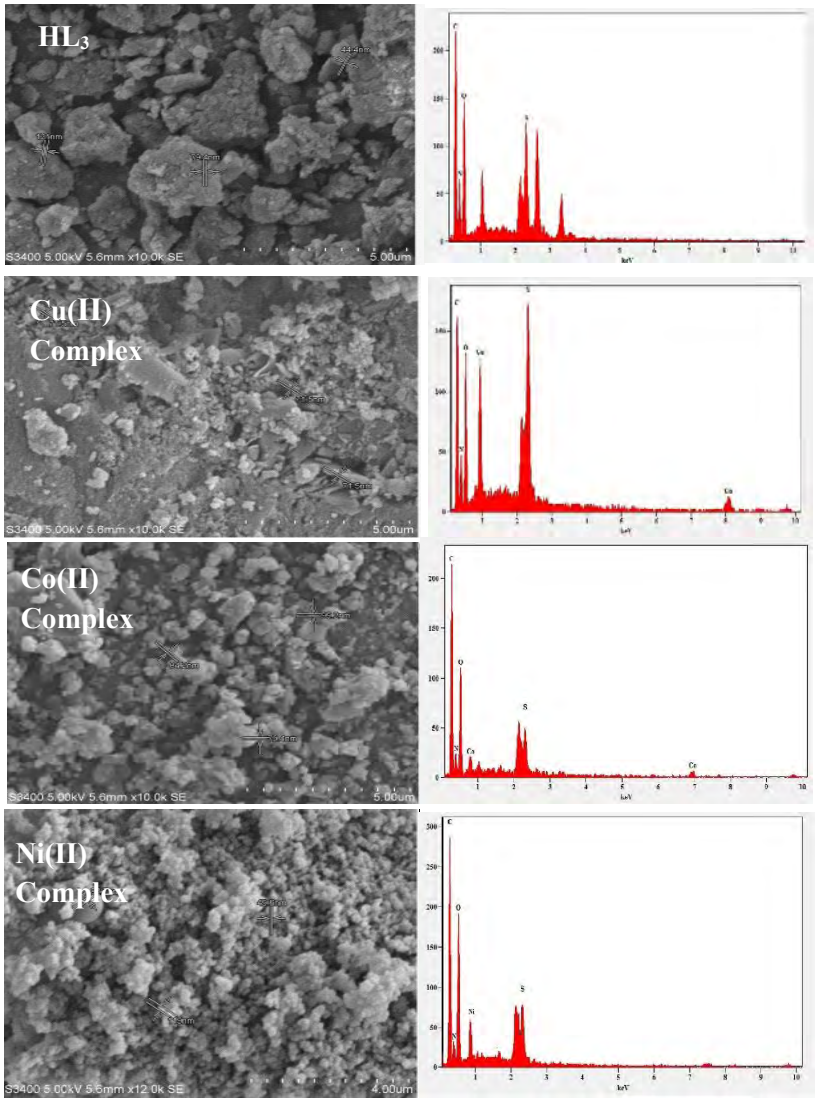

Fig.4.6. The SEM-EDAX spectrum of the azo dye ligand and its metal complexes.

4.3.7. XRD

The synthesized Cu(II), Co(II) and Ni(II) complexes were soluble in certain polar solvents, but crystals that are appropriate for single-crystal studies were not obtained. Therefore, Powder X-ray diffraction patterns of metal complexes were

obtained to study the degree of crystallinity of the complexes. The powered XRD patterns of azo metal complexes were recorded over 7- 40 positions at wavelength 1.54 Å. The powdered XRD pattern of Cu(II), Co(II) and Ni(II) are shown in **Fig 4.7** . The XRD pattern of Cu(II) complex shows 11 reflection in the range of 9-25 (2θ). The inter-planar spacing was calculated by using Bragg's Equation $2d \sin\theta = n\lambda$. by knowing the most intense peak (2θ) [21]. The inter-planar spacing together with the relative intensities was calculated and depicted in **Table 4.5a-4.5c**. From all the highest intense peak the Miller indices (*h k l*) along with $h^2+k^2+l^2$ were also determined. The $h^2 + k^2 + l^2$ values of Cu(II) complexes are 1, 2, 3, 6, 8, 10, 10, 11, 13 and 15. The lattice parameter for Cu(II) complex is calculated to be *a*=*b*=*c*= 9.976. From the results, it is evident that the presence of forbidden number 15 indicates that the Cu(II) complex may belong to hexagonal or tetragonal system.

Similar calculations were carried out for Co(II) and Ni(II) complexes and displayed 11 and 8 reflexation in the range in the range 6-40^o (2θ) the important peaks have been recognized. The unit cell calculations were obtained and the $h^2+k^2+l^2$ values were determined. The $h^2+k^2+l^2$ values for Co(II) complexes are 1, 2, 3, 4, 6, 8, 12, 13, 15 and 18 and for Ni(II) complex are 1, 2, 3, 5, 6, 7 and 8. The presence of forbidden numbers like 15 for Co(II) complex and 7 for Ni(II) complex indicates both the complexes may belong to hexagonal or tetragonal systems. The calculated lattice parameter for Co(II) and Ni(II) complexes are *a*=*b*=*c*= 8.99 and 5.43 respectively. The Cu(II) and Co(II) metal complexes exhibits sharp crystalline peaks representing their crystalline nature, whereas Ni(II) complexes do not exhibit sharp crystalline peak due to their amorphous nature.

Table 4.5a. Powder X-ray spectral data of Cu(II) complex.

Sl no	2Θ	Θ	sin Θ	Sin^2 Θ	$Sin^2Θ$× 1000	$h^2+ k^2+l^2$	h k l	D in Å	a in Å
1	7.14	3.57	0.0622	0.00387	3.877	1(1)	100	12.384	9.976
2	9.14	4.57	0.0796	0.00634	6.348	1.63(2)	110	9.668	9.928
3	11.40	5.70	0.0993	0.00987	9.878	2.55(3)	111	7.751	9.971
5	17.26	8.63	0.1505	0.02251	22.515	5.81(6)	211	5.133	9.974
6	19.26	9.84	0.1708	0.02923	29.235	7.55(8)	220	4.509	9.974
7	21.99	10.99	0.1907	0.03635	36.359	9.56(10)	310	4.039	9.822
8	22.66	11.33	0.1964	0.03859	38.596	10.15(10)	310	3.922	9.859
9	23.18	11.59	0.2009	0.04036	40.363	10.62(11)	311	3.851	9.956
10	26.18	13.09	0.2264	0.05129	51.293	13.49(13)	320	3.402	9.874
11	28.25	14.125	0.2439	0.05951	59.513	15.37(15)	-----	3.158	9.974

Table 4.5b. Powder X-ray spectral data of Co(II) complex.

Sl no	2Θ	Θ	sin Θ	Sin^2 Θ	$Sin^2Θ$× 1000	$h^2+ k^2+l^2$	h k l	D in Å	a in Å
1	7.917	3.958	0.06903	0.00476	4.765	1(1)	100	11.2028	8.990
2	11.90	5.95	0.1037	0.01075	10.756	2.25(2)	110	7.4534	8.978
3	13.78	6.89	0.1199	0.01439	14.399	3.023(3)	111	6.447	8.995
4	16.73	8.36	0.1454	0.02116	21.164	4.44(4)	200	5.3163	8.991
5	18.72	9.36	0.1626	0.02645	26.450	5.55(6)	211	4.7539	8.989
6	19.46	9.73	0.1690	0.02856	28.562	6.00(6)	211	4.5739	8.996
7	22.96	11.48	0.1990	0.03986	39.867	8.37(8)	220	3.8669	8.993
8	28.094	14.045	0.2426	0.05945	59.454	12.49(12)	222	3.1863	8.997
9	29.319	14.65	0.2530	0.06466	64.660	13.445(13)	320	3.0553	8.949
10	31.527	15.76	0.2716	0.07377	73.771	15.42(15)	--	2.8460	8.991
11	34.046	17.023	0.2927	0.08687	86.870	18.25(18)	330	2.6409	8.996

Table 4.5c. Powder X-ray spectral data of Ni(II) complex.

Sl no	2Θ	Θ	sin Θ	Sin^2 Θ	$Sin^2Θ\times$ 1000	$h^2+k^2+l^2$	h k l	D in Å	a in Å
1	13.097	6.548	0.1140	0.01303	13.033	1(1)	100	6.7570	5.436
2	16.307	8.153	0.1418	0.02011	20.11	1.54(2)	110	5.4322	5.436
3	19.145	9.572	0.1662	0.02777	27.77	2.13(2)	110	4.6325	5.437
4	24.579	12.285	0.2126	0.04526	45.26	3.47(3)	111	3.6232	5.434
5	29.028	14.514	0.2506	0.06344	63.44	4.88(5)	210	3.0738	5.443
6	32.299	16.1495	0.2779	0.07827	78.72	6.006(6)	211	2.7718	5.437
7	36.156	18.078	0.3103	0.09775	97.75	7.50(7)	---	2.4824	5.436
8	39.5936	19.796	0.3386	0.1146	114.69	8.80(9)	300	2.2749	5.438

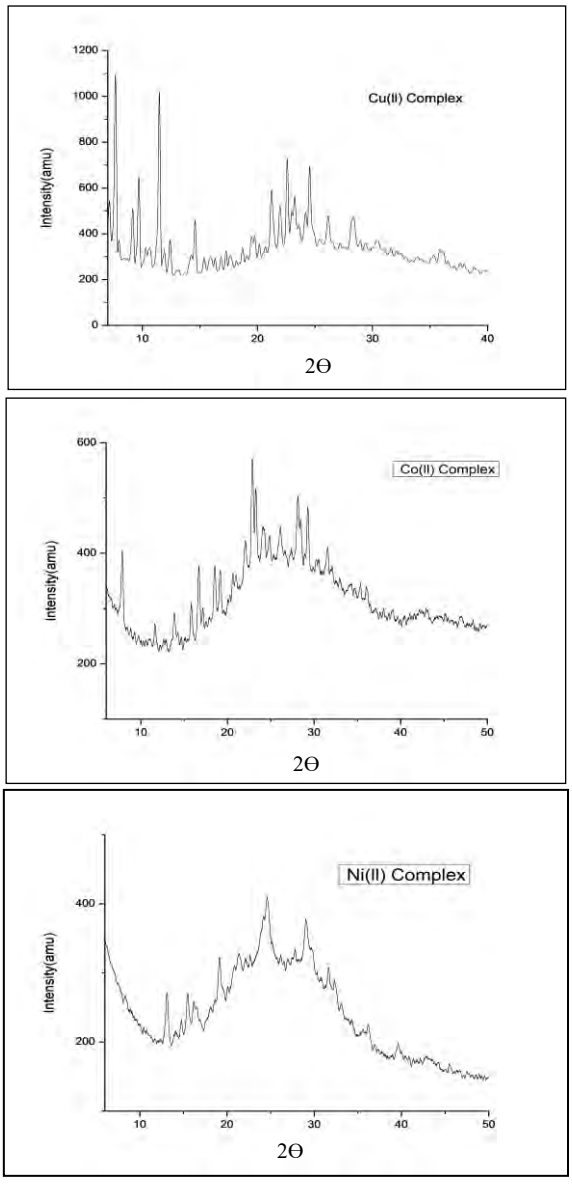

Fig. 4.7. X-ray diffraction pattern of metal complexes in powder form.

4.3.8. Biological evolution.

The synthesized azo metal complexes possessing important heteroatoms like nitrogen, oxygen and sulfur groups proved to be a significant biomolecules as it exhibits a number of biological properties, such as antimicrobial, anticancer activity. Therefore based on the above observation, some of important biological activities such as photoinactivation of bacteria, antioxidant and Insilco molecular docking studies were examined and their detailed experimental results discussed below.

4.3.8.1 Photo inactivation of *E.Coli* Bacteria.

The azo metal complexes were screened for their photodynamic inactivation studies against gram negative bacteria *E. coli* species in DMSO, and the detailed procedure was described as **Section 3.3.7.1** of **Chapter 3**.

The PACT activities of the three complexes were preliminarily assessed in the following way. Photo-induced cell death of *E.coli* ATCC 25922 under irradiation by a xenon lamp with a wavelength range of 400-800 nm with a intensity 350 Mw\cm^2 at different concentration (25, 50 and 100 μM) of the complex. The cells were then irradiated 15 min in xenon lamp. The percentage cell inhibition has been shown in **Fig.4.8.** Cobalt Complex leads to 72% of cell reduction in planktonic cell at concentration of 100 μM. whereas a moderate photo inactivation was observed for Cupper and Nickel complexes with a approximately 50% cell reduction. With this context Cobalt complex will prove to be better photosensitizers for the reduction of plantonic cells. For PACT application in localized infection, an important prerequisite is that the microbes are selectively killed while mammalian cells are spared.

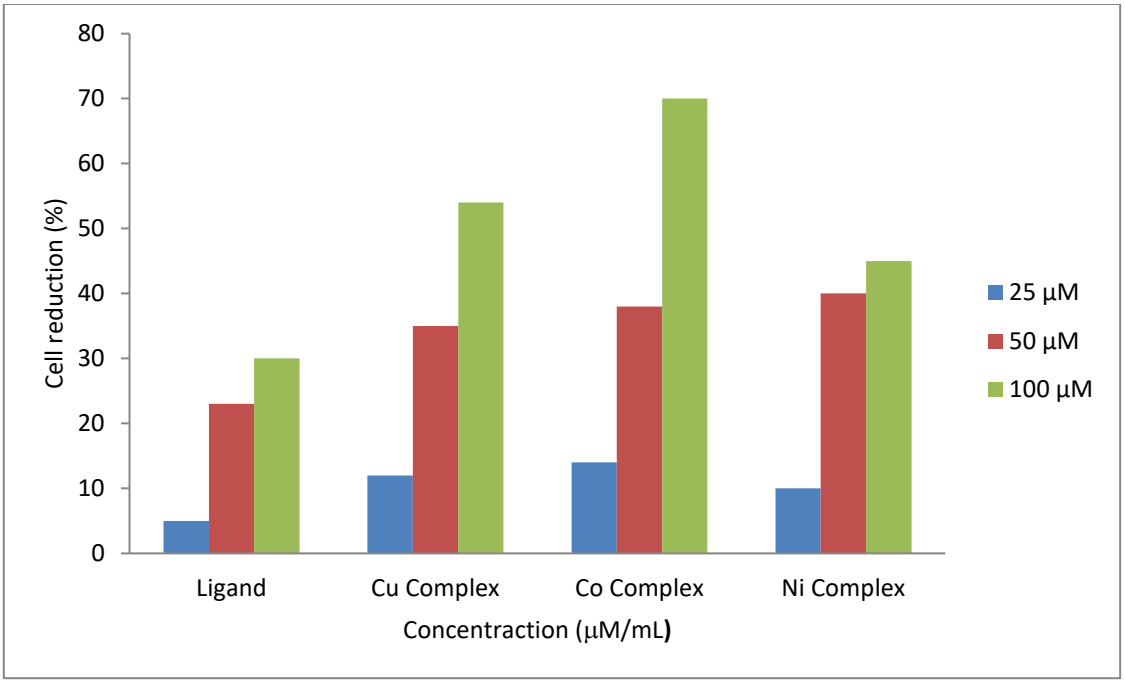

Fig.4.8. Photoinactivation metal complex on *E. coli* bacteria.

4.3.8.2. DPPH activity.

The DPPH radical scavenging activity is a simplest method to check the antioxidant activity of the synthesized molecules. Antioxidants are available as a biomolecules as well as synthetic molecules. Synthetic molecules are also evidenced to be best agents in eradicating the annoying toxic radical from biological system [22]. In this connection we have tested the antioxidant activity of azo dye ligand and its metal complexes. The DPPH free radical scavenging activity of the synthesized compounds as per the procedure explained in **Section 3.3.7.2** of **Chapter 3**. The graphical representations of the synthesized compounds are shown in **Fig. 4.9**. In this assay, the red coloured solution changes its color to different shags depending on the reducing power. The antioxidants can convert the ferricyanides to ferrous form by measuring at 700nm [23]. From the results, all the tasted compounds exhibits a significant reducing power when compare with standard ascorbic acid. The order of reactivity was as follows Cu(II) >Co(II) >Ni(II) >HL_3. In addition to this, the graph showed the activities of the compounds are concentration dependent manner.

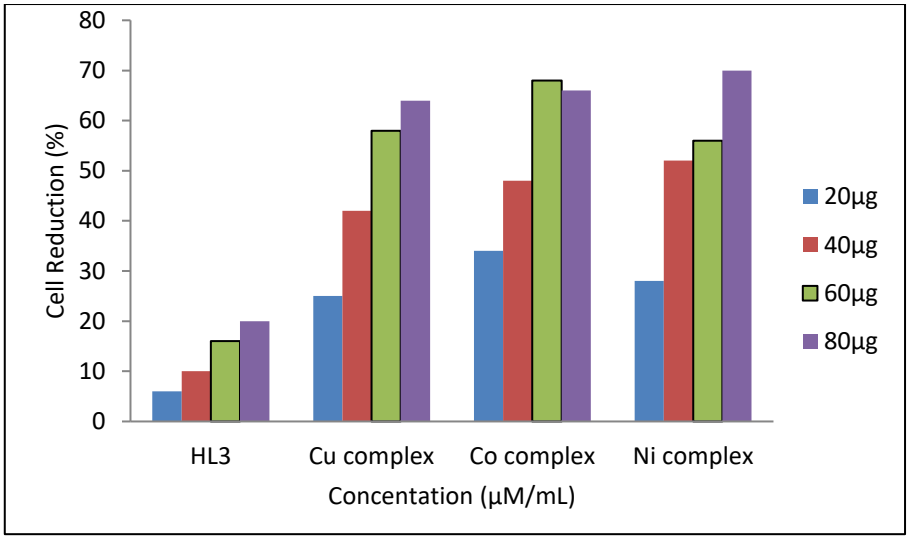

Fig.4.9. DPPH Free radical activity of azo free ligand and its metal complexes.

4.3.8.3. Molecular docking studies.

Molecular docking study is a fundamental tool in the drug design. Molecular docking studies were employed to detect the relationship between the metal complexes and the target receptor [24]. To recognize the mechanism of drug action, the molecular docking studies were carried out for the synthesized compounds with the target receptor RpsA. Its experimental procedure was discussed in detail in **Section 3.3.7.4** of **Chapter 3.**

All the synthesized metal complexes showed well recognized hydrophobic interactions to amino acids such as Asp350, Ser359, Arg357, Arg355, His322, Glu325, Gln364, Ile349, Leu320 and Tyr280 in the target enzyme active pockets (**Fig 4.10**). All the complexes well established bonds with amino acids such as Asp352, Arg357, Glu318, in the receptor active pockets as displayed in **Table 4.6.** The relative binding affinities of all the complexes were accomplished in the range of −2.74kcal/mol to -4.01kcal/mol, respectively. From the results, Cu(II) complex shows the highest −ve relative binding energy that indicated it may be considered as a good inhibitor glucose-amine-6-phosphate synthase.

Table 4.6. Molecular docking scores of the metal complexes.

Compounds	Binding Energy (kcal/mol)	H-bonds	H-bond length (å)	H-bond with	Hydrophobic interactions
Cu(II) Complex	-4.01	1	2.08	Asp352	Asp350,Ser359,Arg357, Arg355.
Co(II) Complex	-2.74	2	2.90 2.80	Arg357, Arg357.	Arg355,His322,Asp350,Glu325, Gln364,Ile349,Ser359,Leu320
Ni(II) Complex	-3.28	1	2.85	Glu318.	Tyr280

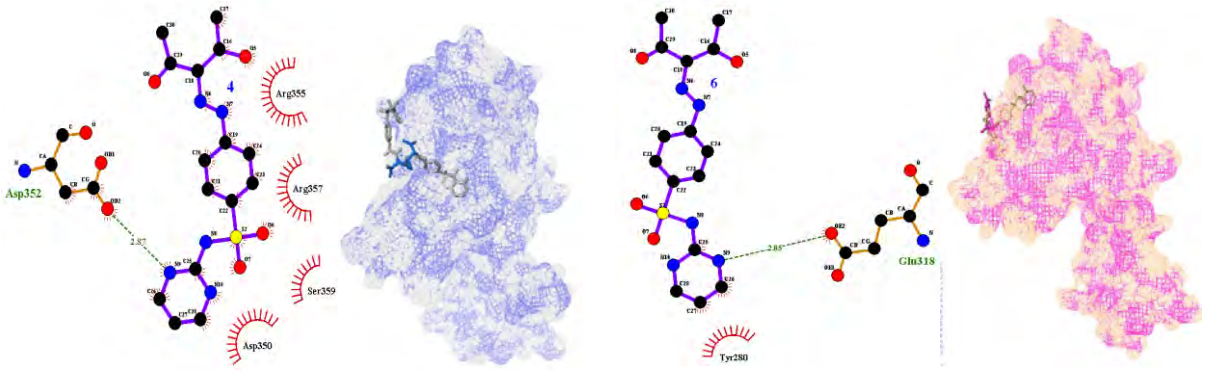

Cu(II) Complex

Co(II) Complex

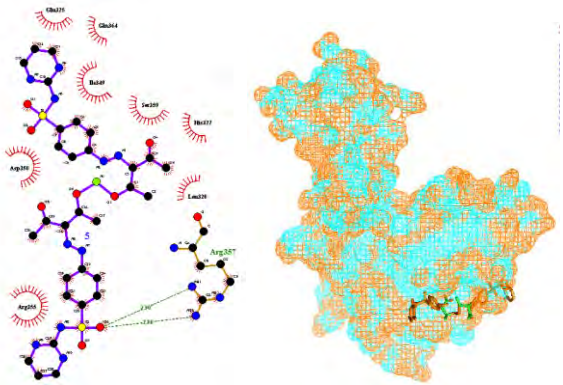

Ni(II) Complex

Fig 4.10. Three-dimensional representation of the metal complex into active site RpsA.

4.4. Conclusion.

The novel azo chromophore containing sulfadiazine was synthesized by diazo-coupling reaction. The reactions of azo-dye ligand with Cu(II), Ni(II) and Co(II) ions yielded a colored complexes and the azo dye ligand and its complexes are characterized by elemental analysis, FT-IR, ^{1}H-NMR, mass, UV–Vis, XRD, SEM, EDX spectroscopy and thermal gravimetric analysis (TGA) techniques. From these analytical date the structures of the Cu(II) and Ni(II) complexes were possess square planer and octahedral geometry for Co(II) complexes. By knowing mass spectra the ligand attached to the metal a bidendate manner with a stoichiometric ratio ML_2 type. The azo dye metal complexes were evaluated for antibacterial activity against Gram negative bacteria. Amongst the tested compounds Co(II) revealed highest photoinactivation than Cu(II) and Ni(II) complex. The antioxidant potential of the compounds was studied by DPPH radical scavenging activity. All the metal complexes showing promising antioxidant activity than free ligand. Lastly, in-silico molecular studies were carried out to identify the binding modes and interaction with the target enzyme. The results demonstrated that all the metal complexes exhibited good binding affinity. Furthermore all the complexes were able to form H-bonds with the several amino acids in the enzyme active site.

4.5. Reference.

1. M. Vathanaruba, P. Muthukumar and P. Tharmaraj, *Der Pharma Chem.*, 10(1), 54-59, **2018**.
2. N.M. Mallikarjuna and J. Keshavayya, *J. of King Sau. Univ.,* **2018**.
3. N.C. Desai, Atul H. Makwana and R.D. Senta, *J. of Sau. Chem.Soc.,* 20, 686–694, **2016**.
4. G.M. Golzar Hossain, A.J. Amoroso, A. and Banu, K.M.A. Malik, *Polyhed.,* 26, 967–974, **2007**.
5. H. E. Gaffer, *Colo. Tech.,* 12437, **2019.**
6. M. S. Refat, T. Sharshar, K. M. Elsabawy and Abdel Majid Adam. *J. of Mole. Liqu.,* 1, **2016**.
7. K. Y. E. Baradie and Monatshefte, *fur Chem.,* 136, 1139–1155, **2005**.
8. H. M. Patel and C. Bharat Dixit, J. *of Sau. Chem. Soci*., 18, 507–512, **2018**.
9. H. Khanmohammadi and A. Abdollahi, Dyes *and Pigm.,* 94, 163-168, **2012**.
10. G. Feng, H.F. Qian, G. Bai, Y.C. Liu and H. Ling Ling, *Dyes and Pigm.,* 129, 54-59, **2016**.
11. M. Szala, J. E. Nycz, G. J. Malecki, R. Sokolova, S. Ramesova, A. Switlicka Olszewska, R. Strzelczyk, R. Podsiadly and B. Machura. *Dyes and Pigm.,* **2017**.
12. H. A. El Wahaba, M. Abd El Fattahb, H.M.Z. El alfya, M.E. Owdaa, L. Linc, and I. Hamdya*, Progress in Orga. Coati.,* 142, 105577, **2020**.
13. H. B. Teja, H. S. Bhojya Naik, P. H. Amith Nayak and M.C. Prabhakara. *Asian J. of Chem.,* 33, 1709-1717, **2021**.
14. M. S. Sujamol, C.J. Athira, Y. Sindhu and K. Mohanan, *Spectrochi, Acta Part A,* 75, 106–112, **2010**.
15. K. M. Khalifa, A. M. Hamil, A. Qasem Ali, N. Mohamed, Y. A. Alkhayali and A. Shamsi Saad, *J. of Sebha Univ.,*1, 2, **2016**.
16. A. Palanimurugan, A. Dhanalakshmi, P. Selvapandian and A. Kulandaisamy, *Heliy.,* 5, 02039, **2019**.
17. A. A. E. Asmy, A. Z. A. Abdeen, W.M. A. Elmaaty and M. M. Mostafa, *Spectrochim. Acta Part A,* 75, 1516–1522, **2010**.
18. A. Pilar Sonza, Garcia-Vfizquez and R. Jose Masaguer, *Tran. Met. Chem. 10,* 410-412, **1985**.

19. Y. K. Abdel Monem, S. A. Abou ElEnein, and M. M. ElSheikh Amer, *J. of Mol. Stru.,* 1127, 386-396, **2017**.
20. P. Anand Mishra, Rudra Mishra, Rajendra Jain and Santosh Gupta, *Mycobio.,* 40, 20-26, **2012**.
21. S. M. E. Megharbel, A. S. Megahed, M. S. Refat, *J. of Mole. Liq.,* 216, 608–614, **2016**.
22. M. L. Sundararajan, T. Jeyakumar, J. Anandakumaran and B. Karpanai Selvan, *Spectrochi. Acta Part A: Mole. and Biomol. Spectro.,* 131, 82–93, **2014**.
23. Rajesh Kumar, Pradeep Kumar, Mahesh Kumar and Balasubramanian Narasimhan, *Med. Chem. Res.,* 21, 4301–4310, **2012**.
24. Emin Erdem, Eylem Yildirim Sari, Rafet Kilinc¸arslan and Nilgun Kabay, *Trans. Met Chem*., 34, 167–174, **2009**.

Chapter -5

Design, Synthesis and Pharmacological Assay of Sulfadiazine Based Azo-Metal Complexes

5.1. Introduction.

Azo chromospheres are a group of colorant ingredients characterized by the presence of an azo group (N=N) group. Azo compounds have been widely used as a dying agent and accounting for over 50% of all commercial dyes [1]. These azo dyes have played an important role in the expansion of coordination chemistry. Azo metal complexes have also increasing attention due to their interesting electronic and geometrical features [2]. The significance of these compounds may steam from their biological activity and analytical investigations. Also, it is well known that heterocyclic azo compounds have been used to stabilize the low oxidation states of different metal ions [3-4]. Azo dyes derived from numerous heterocyclic coupling components such as thiazole, thiophene and pyrazole are the instances of chosen constituents [5]. On the other hand, the possibility of tautomerism in hetarylazo compounds which induce light fastness. It is well known that azo dyes with heterocyclic components exhibit good tinctorial strength and brighter dyeing than those derived from benzenoids [6].

Barbituric acid belongs to the family of 2, 4-pyrimidione derivatives which play an important role in nature and in technical or pharmaceutical applications. Barbituric acid is mainly derived from barbiturate drugs, although barbituric acid himself is not bioactive, and the bioactivity of barbiturates mainly depends on the side groups attached to the C-5 atom of the pyrimidine ring. Azo-barbituric acid derivatives are characterized to show various tautomeric structures in their free acid form [7-8]. Sulfa drugs are the most extensively used antimicrobial agents in the world, because of their low cost, low toxicity: Sulfonamides drugs working scientifically as chemotherapeutic agents to prevent and cure bacterial infections in humans. Sulfadiazine is a sulphanilamide derivative, is renowned as an antimalarial drug. The biological activity of the sulfadiazine is because of the structure resemblance between

the sulfanilamide group and the 4-amino benzene which is a good inhibitor, it stops the synthsis of dihydropteroate and also it prevents the synthesis of folic acid path and blocks the cell division which causing cell death [9-11]. The increase in the pharmacological activity of these drugs due to coordination with metal ions [12]. Some of the azo dyes from sulfa drugs exibits chelating properties with the number of metal ions. Sulphanilamide azo dye forms thermally stable and better chelating agents for complexation. When a metal ion enters into the ligand system, it will enhance the pharmacological properties and thereby become more effective than its corresponding ligand. In particular, metal complexes with silver and sulfonamides as ligands have proved to be effective topical anti-bacterial agents, especially Agsulfadiazine (Ag-SDZ) used in burn therapy [13]. All thought both sulfadiazine and barbutaric acid have donor atoms (N and O) at different positions and this will enhance them to act as multidentate ligands. Hence they can coordinate with different metal ions [14, 15]. It was seen that, after the coordination with the metal ion the pharmacological activity of the azo dye have been improved. The activity of the sulfonamide metal complexes was depended on the gentle release of metal ions and also more prominently, depends on the nature of the molecules to which the metal ion is bound [16]. Therefore coordination of sulfa drugs to these important metals leads to important biological purposes.

From the above observation, the azo dyes having sulphonyl group with various heterocyclic molecules will intensifies the color of the molecule and also it improve the pharmacological effectiveness of the azo dyes. Thus in accordance with the literature survey and from the above report, in this chapter, we tried to explore the pharmacological properties of the sulfadiazine azo dye, in the newly synthesized azo dye and its metal complexes of Cu(II), Co(II) and Ni(II) were synthesized and

characterized by different physical and analytical and spectroscopic method. All the synthesized metal complexes were subjected into pharmacological studies like antibacterial, antifungal and Insilco molecular docking studies.

5.2. Experimental.

5.2.1. Material and Analytical Methods.

All the chemicals used for the preparation of the azo dye ligand and their metal complexes were purchased from Sigma– Aldrich. Other chemicals and solvents were of high purity and used without further purification.

5.2.2. Synthesis of azo dye ligand (HL_4).

The synthesis of azo dye involves two steps [17], in which a primary aromatic amine in acid media was treated with the nitrous acid ($NaNO_2$ in 2 mL of H_2SO_4) to produce a week electrophile diazonium salt at below 5 °C temperature. In the second step, the obtained diazonium salt was treated with a strong nucleophile to get coloured azo dye.

Step I: Diazotization

A mixture of 4-amino-N-pyrimidin- 2-yl-benzenesulfonamide (0.01mol) and concentrated hydrochloric acid (5 mL) was stirred in ice bath until a clear solution was obtained. This mixture was added dropwise to a cold sodium nitrate (0.1 mol) in 10 ml of ice cold water with constant stirring. The resulting mixture was stirred for 1 hour. The temperature of the mixture was maintained at 0 to 5 $^{\circ}$C, the resulting mixture was stirred for an additional 1 hour in an ice bath.

Step II: Coupling

The barbutaric acid (0.01 mol) was dissolved in 10 mL of 10% potassium hydroxide, and cooled to 0–5 °C in an ice bath. This solution was then gradually added to the cooled diazonium salt solution and the resulting mixture was stirred at 0–5 °C

for 1 hour. The pH of the reaction mixture was maintained at 5-6 by adding saturated sodium bicarbonate solution. The resulting crude precipitate was filtered, washed several times with cold water and recrystallized from hot ethanol to yield azo dye. The reaction pathway of the specified procedure is represented in **Scheme 5.1.**

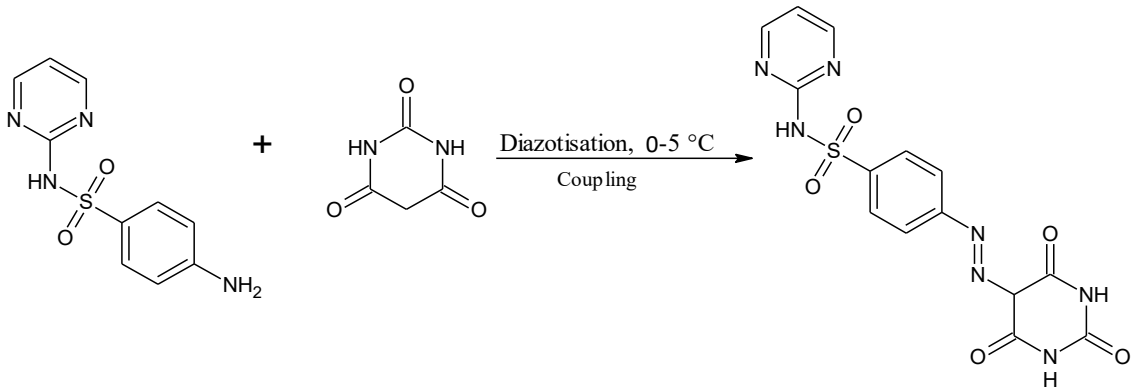

Scheme 5.1. Synthetic route for the preparation of azo dye (HL_4)

5.2.3. Synthesis of Cu(II), Co(II) and Ni(II) metal complexes.

The metal complexes were synthesized by the addition of hot ethanolic solution of azo ligand (0.02 mol) to a hot ethanolic solution of metal chlorides (0.01 mol) at 2:1 stoichiometric ratio of the ligand to metal complex respectively and the resulting solution was refluxed for 4-5 hour with constant stirring at 60 $^{\circ}$C. After that the reaction mixture was allowed to stand overnight. The coloured solution was filtered and washed with distilled water and ethanol mixture and dried over anhydrous $CaCl_2$ in the vacuum desiccator [18]. The structures of the complexes were depicted in **Scheme 5.2**

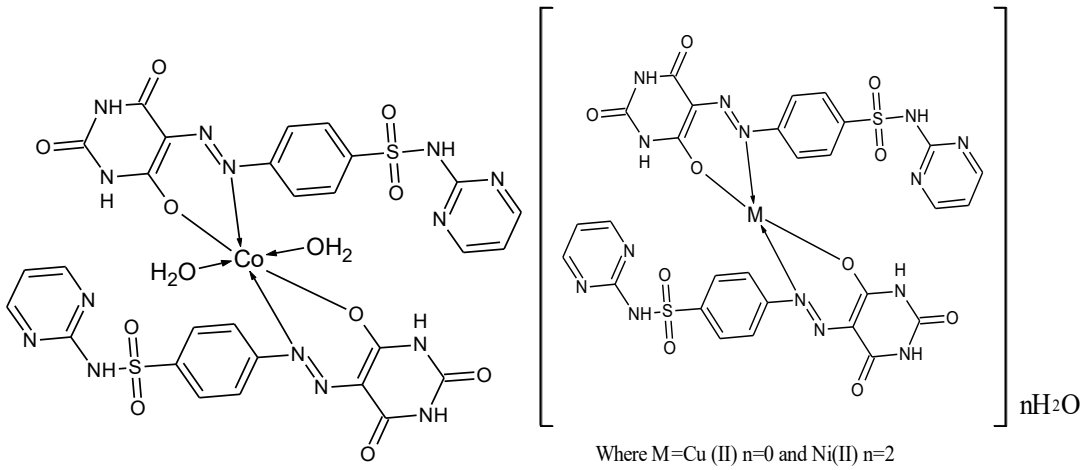

Scheme. 5.2. Structure of Metal Complexs.

5.3. Result and discussion.

The successful syntheses of azo metal complexes of sulfadiazine have been carried out as per the reaction formulated in **Scheme 5.1** and the products were obtained in good yield. All the complexes were found to be coloured solid and stable at ambidentade temperature. The synthesized compounds are soluble in organic solvents like ethanol, DMF and DMSO. The synthesized compounds were stable in both solid and in solution phase. The physico-analytical data of the ligand HL_4 and its metal(II) complexes are presented in **Table.5.1.**

Table 5.1. Physical and analytical data of the synthesizes azo dye and its metal complexes

Ligand/ complexes	Mol. wt	M P	Colour	Elemental analysis(%) calcd.(found)					
				C	H	N	O	S	M
Ligand (HL_4)	389	196	Orange	43.19 (43.02)	2.85 (2.65)	25.18 (25.14)	20.55 (20.50)	8.24 (8.20)	--
Cu(II) complex	840	300	Pale green	40.03 (40.00)	2.40 (2.38)	23.34 (23.32)	19.04 (19.02)	7.63 (7.60)	7.56 (7.54)
Co(II) complex	871	300	Reddish brown	38.58 (38.54)	2.78 (2.76)	22.50 (22.54)	22.03 (22.00	7.36 (7.34)	6.76 (6.73)
Ni(II) complex	835	300	Pale Yellow	40.26 (40.24)	2.41 (2.40)	23.47 (23.45)	19.15 (19.14)	7.68 (7.64)	7.03 (7.04)

5.3.1.^{1}H and ^{13}C NMR Spectral studies.

^{1}H-NMR and ^{13} C-NMR spectra of the free ligand was recorded using DMSO as a solvent, and TMS as an internal standard. The spectra were recorded from 0-15 ppm, the chemical shift were reported in parts per million (ppm). The spectra of the azo ligand were presented in **Fig 5.1**. ^{1}H-NMR spectra of the ligand showed a singlet at 13.97 ppm clearly attributed to NH of the sulfadiazine [19]. The signal corresponding to hydrogen devoted to nitrogen of the pyrimidinetrione ring was observed at 11.57 and 11.35 ppm [20]. The aromatic protons show signals at 7.68-8.48 ppm.

The ^{13}C- NMR spectra of free ligand (HL_4) **(Fig 5.2)**, the signal at 162, 160, and 158 ppm corresponds to carbon of the pyrimidine ring [21]. The signals at 158.6, 157.2, 150.1 ppm corresponds to C=O of the pyrimidinetrione ring. The signals at 145.27 and 136.88 ppm are due to the carbon atom adjacent to the diazo group (N=N). The peak in the range of 112.61 to 130.22 ppm corresponds to aromatic region [22].

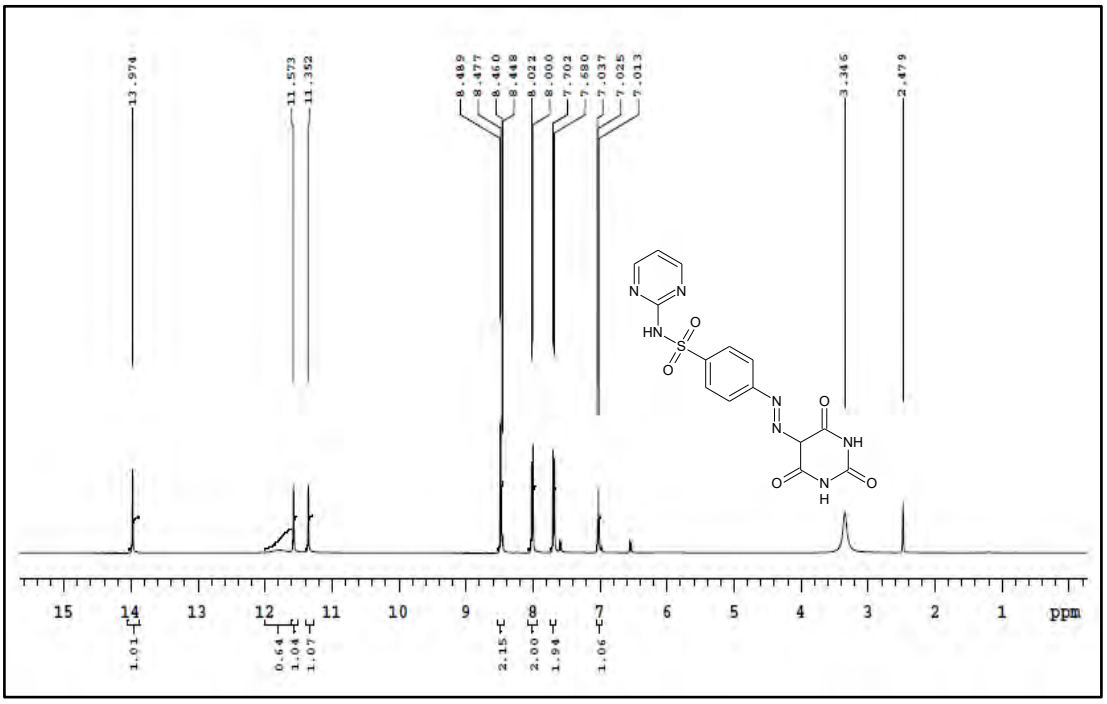

Fig 5.1. ^{1}H-NMR Spectra of azo dye ligand (HL_4).

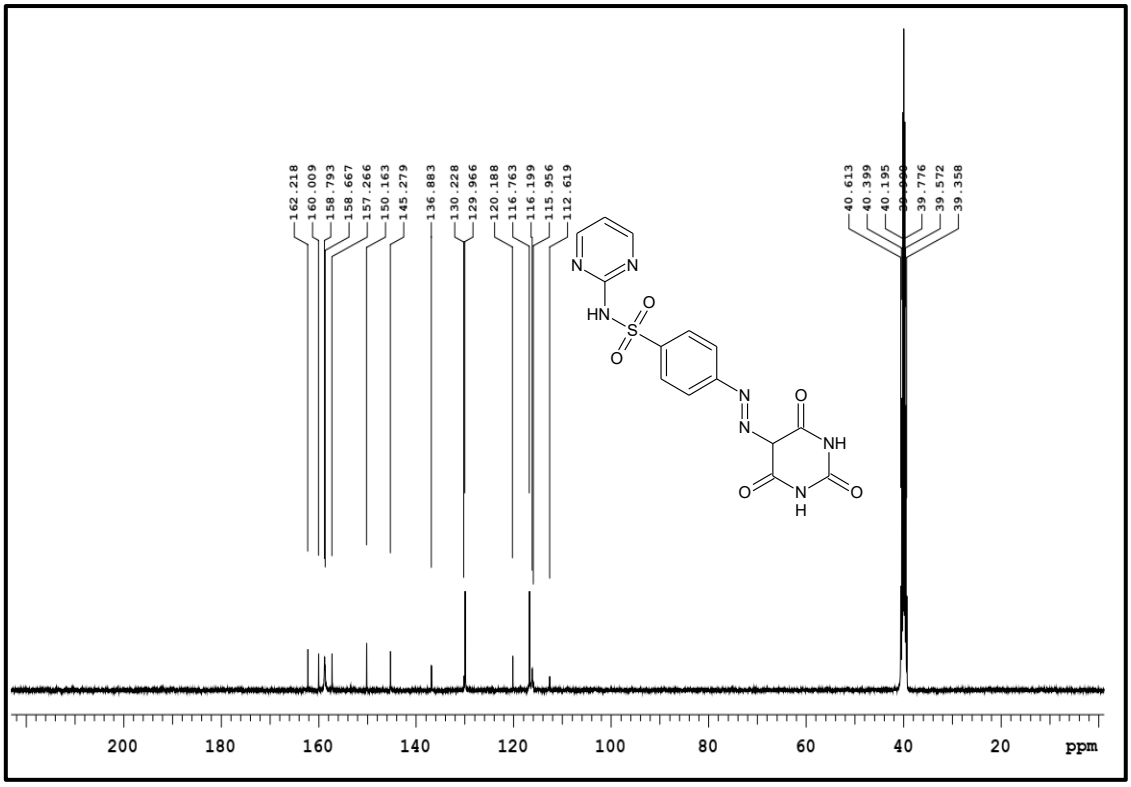

Fig 5.2. ^{13}C-NMR Spectra of azo dye ligand (HL_4).

5.3.2. Electronic Absorbtion Spectra.

The electronic absorption spectra in the UV-visible region for the ligand precursor, as well as their corresponding complexes, were recorded in DMF (10^{-3}) solution in the Range of 250-300 nm at room temperature. The assignments of the observed absorption bands of the azo dye and their metal complexes are shown in **Table 5.2** and **Fig 5.3**. The electronic spectral data of the free azo ligand (HL_4) displays two recognizable absorption bands. The absorption band at λ_{max} 299 nm attributed to n→ π* transitions arrived due to the azo group, while another band at 383 nm corresponds to π→ π* transition of the aromatic ring. The Cu(II) complex of the azo dye shows three electronic absorption bands at 305, 322 and 411 nm are assigned as $^2B_{1g} \rightarrow {}^2A_{1g}$ (υ1) $^2B_{1g} \rightarrow {}^2B_{2g}$ (υ2) and $^2B_{1g} \rightarrow {}^2E_g$ (υ3). The observation of this band suggested a square planar geometry around the Cu(II) ion [23]. In the electronic spectra of Co(II) complex shows three bands which are assigned $^4T_{1g}$ (F) → $^4T_{2g}$ (F)

(υ1) $^4T_{1g}(F) \rightarrow {}^4A_{2g}$ (F) (υ2), and $^4T_{1g}$ (F) $\rightarrow {}^4T_{2g}$ (P) (υ3) transitions. The position of these bands conforms the octahedral geometry around the Co(II) ion. The electronic spectrum of Ni(II) complex shows broad band at 304 nm and 414 nm. These bands may be assigned to the inter ligand charge transfer and $^1A_{1g} \rightarrow {}^1B_{1g}$ transitions. These transitions suggested the square planar geometry around Ni(II) ion [24,25].

Table 5.2. Electronic absorbtion spectra of azo dye (HL_4) and their Metal complexes.

Compound	λmax (nm)	Transition
HL_4	299, 383.	n–π* π–π*
Cu(II) Complex	305, 322, 411,	$^2B_{1g} \rightarrow {}^2A_{1g}$ (υ1) $^2B_{1g} \rightarrow {}^2B_{2g}$ (υ2) $^2B_{1g} \rightarrow {}^2E_g$ (υ3)
Co(II) Complex	292, 306, 387.	$^4T_{1g}$ (F) $\rightarrow {}^4T_{2g}$ (F) (υ1) $^4T_{1g}(F) \rightarrow {}^4A_{2g}$ (F) (υ2), $^4T_{1g}$ (F) $\rightarrow {}^4T_{2g}$ (P) (υ3)
Ni(II) Complex	304, 414.	INCT $^1A_{1g} \rightarrow {}^1B_{1g}$

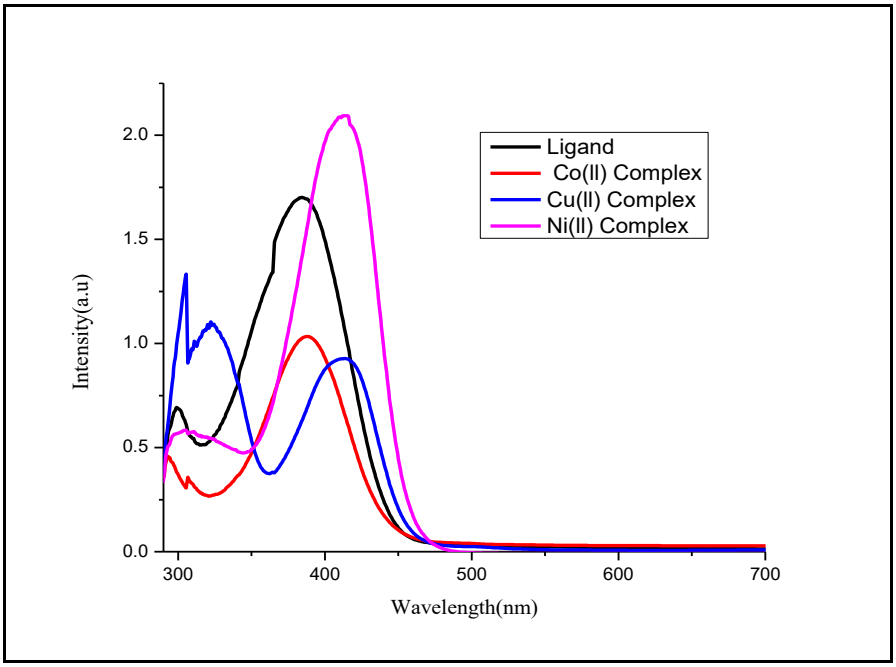

Fig 5.3. Electronic absorbtion spectra of ligand and their metal complexes.

5.3.3. FT-IR Spectra.

The Solid-state infrared spectra of the azo dye ligand and its metal complexes were recorded with a Thermo Nicolet Avatar IR spectrophotometer using KBr pellets in the range of 4000-400 cm^{-1}. The main characteristic bands and their tentative frequencies are summarized in **Table 5.3.** The obtained IR spectra of the synthesized compounds were displayed in **Fig.5.4a-5.4d.** The IR spectrum of the free ligands showed a strong band at 1725 cm^{-1}, 1682 cm^{-1}, and 1596 cm^{-1} corresponds to ν(C=O) vibrations of the barbutaric acid [26]. The ligand exibits a strong absorbtion at band 1431 cm^{-1} which can be assigned to the ν(-N=N-) of azo group, and a medium intense band at 1245 and 1151 cm^{-1} corresponds to the ν_{asym} and ν_{sym} of the (O=S=O) moiety. The other band observed in the spectrum at 304 cm^{-1} due to aromatic ν(C–H). In the spectra of metal chelates the two carbonyl carbons appear in the region of 1587-1724 cm^{-1} and the third carbonyl carbon disappeared in all the complexes [27]. The appearance of new band at 1107-1135 cm^{-1} for all the complexes attributed to ν(C-O) vibration which indicates coordination through carbonyl carbon of the barbuaric acid. The absorption band with in the range 1431 cm^{-1} due to -N=N- vibration are showed blue shift in all the metal complexes compared to free ligand, implying the coordination through azo nitrogen [28]. Furthermore, the appearance of new band in the region of 554-591 cm^{-1} corresponds to metal-oxygen bond and frequency at 602-683 cm^{-1} due to metal-nitrogen bond, which supports the contribution of nitrogen and oxygen in coordination. In complex the appearance of strong band at 3422-3431 cm^{-1} attributed to water molecule. This was strongly supported the appearance of new band at 999 cm^{-1}. These overall data propose that the -N=N- and carboxylate–O groups are involved in coordination in the complexes with bidentate mode.

Table 5.3. Important vibration frequencies of the azo dye and their metal complexes.

Compounds	ν(O-H)/H_2O	ν(N=N)	ν(M-O)	ν(M-N)
Ligand	---	1431	--	--
Cu(II) complex	--	1424	685	578
Co(II) complex	3432	1421	682	585
Ni(II) complex	3444	1412	655	598

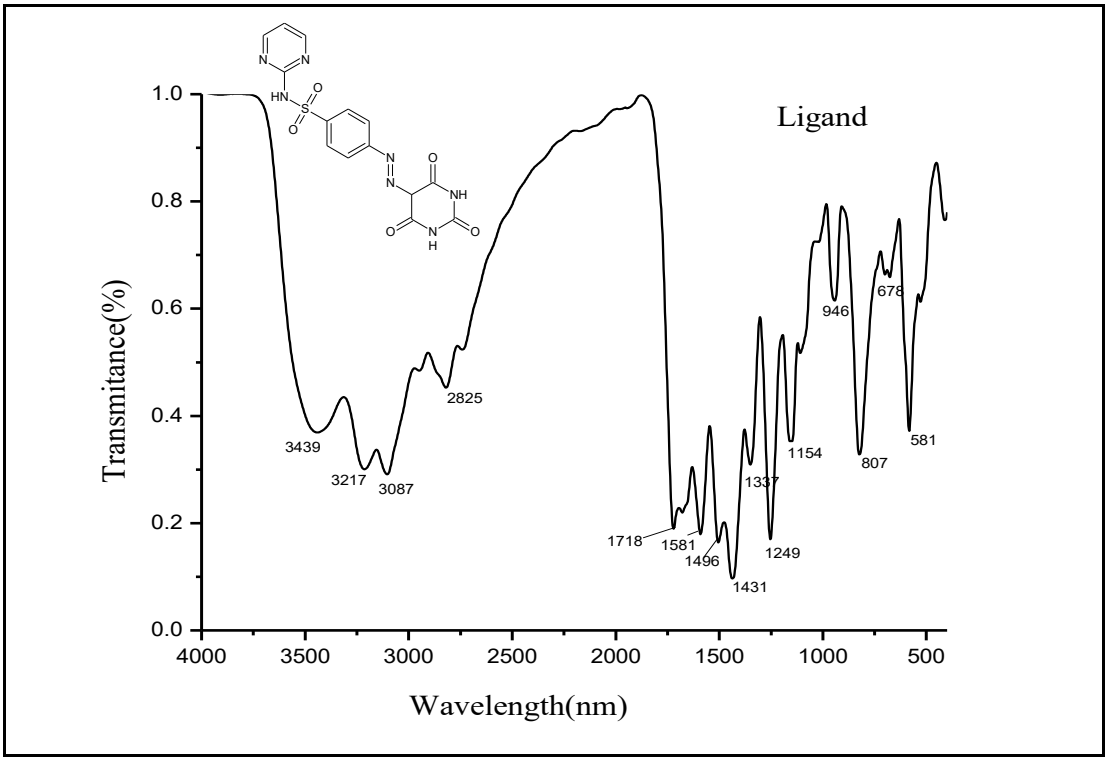

Fig.5.4a. FT-IR spectrum of free azo dye ligand (HL_4).

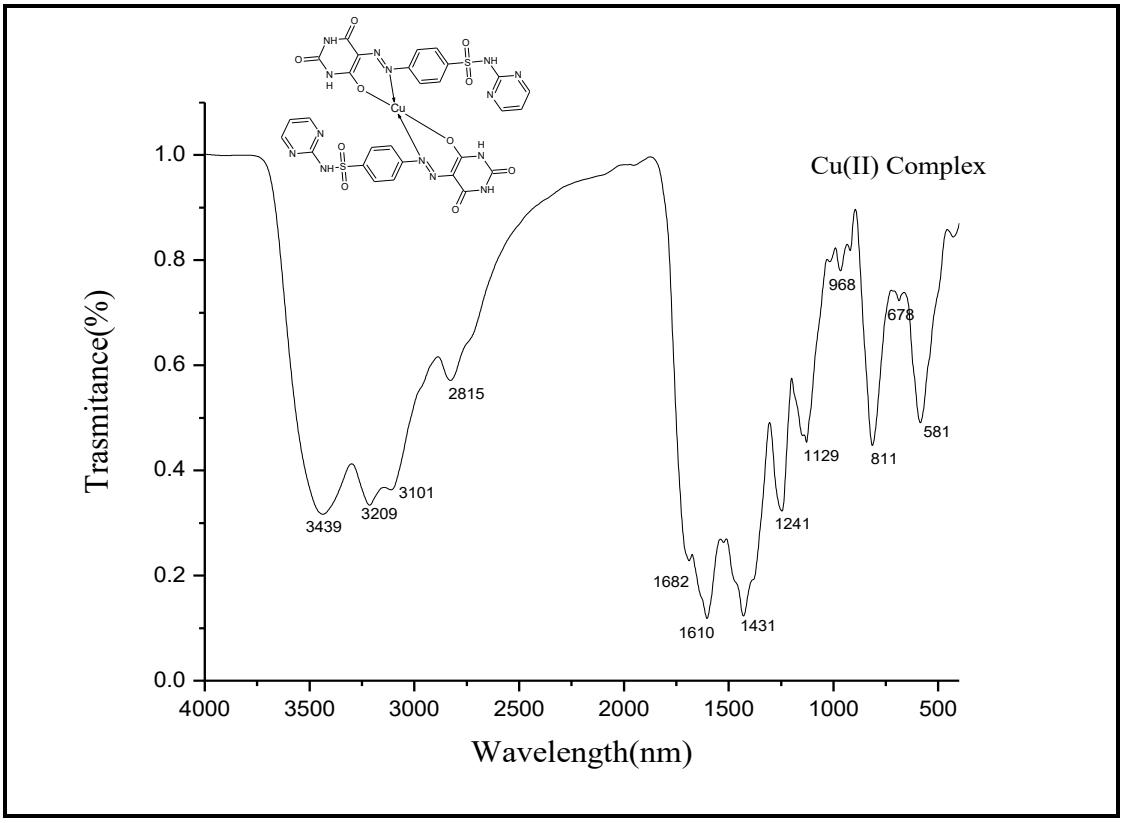

Fig.5.4b. FT-IR spectrum of Cu(II) complex.

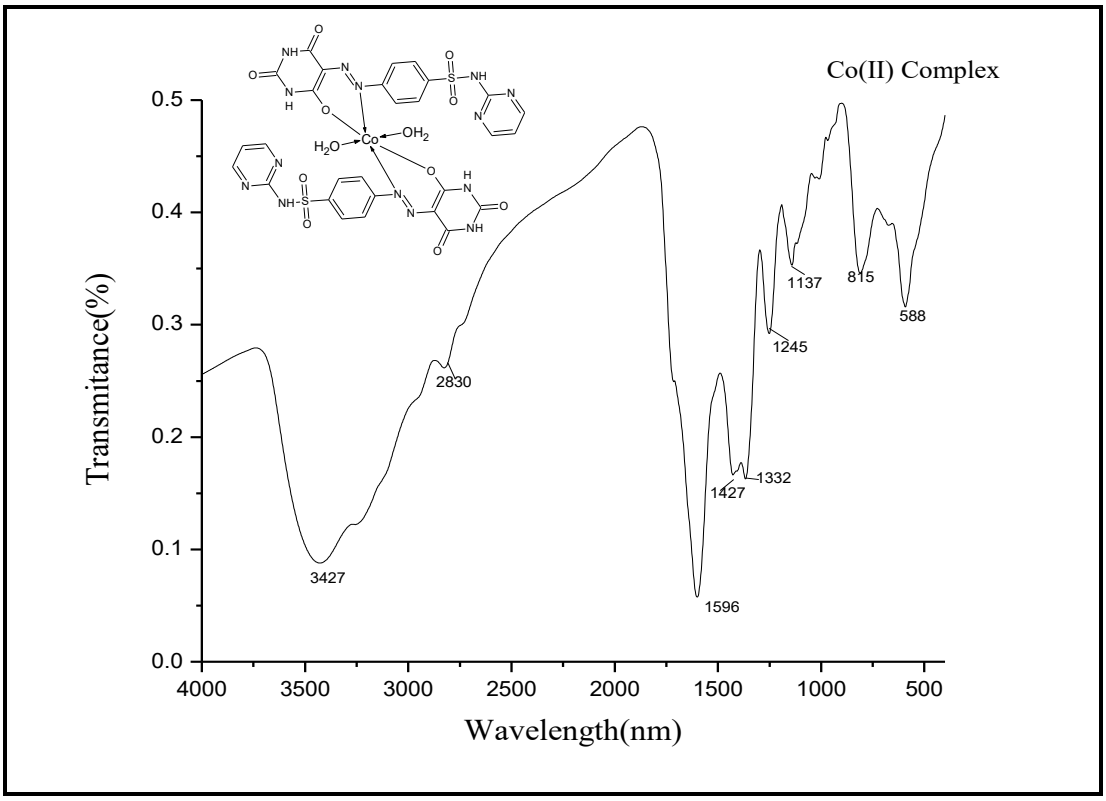

Fig.5.4c. FT-IR spectrum of Co(II) complex.

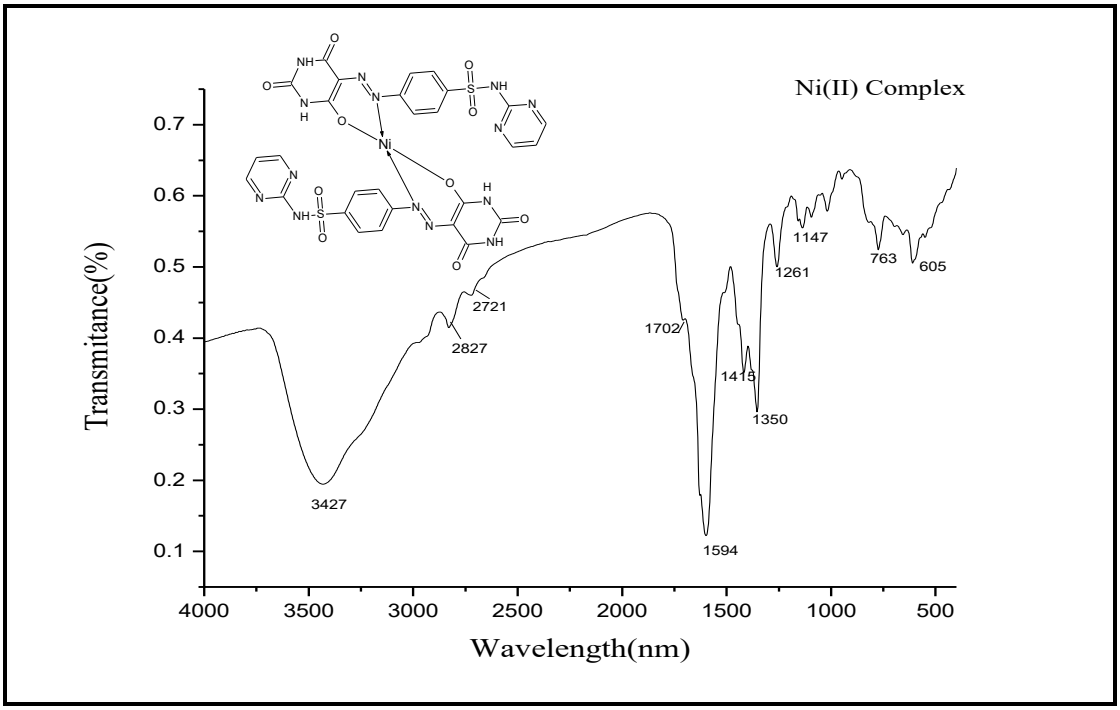

Fig.5.4d. FT-IR spectrum of Ni(II) complex.

5.3.4. Mass spectra.

The mass spectrum of the organic ligand (HL_4) and the metal complexes showed molecular ion peak analogous to their molecular mass. The mass spectrum of the organic ligand exhibited a apparent molecular ion peak observed at m/z 389[M+H], which is similar to its molecular mass of the ligand showed in **Fig.5.5a-5.5d**. In addition, the complex formed with the ligand were also studied for their mass spectral studies and the molecular ion peak of the synthesized complexes were found to be m/z 871 for Co(II) complex, for Cu(II) complex shows a molecular ion peak at m/z 840, for Ni(II) complexes will display a molecular ion peak at m/z 835 respectively, which are synchronized with the stoichiometric configuration of $[M(L)_2]$ type. The observed molecular ion peaks in all the spectra are in good agreement with the recommended molecular formula indicated from elemental analyses.

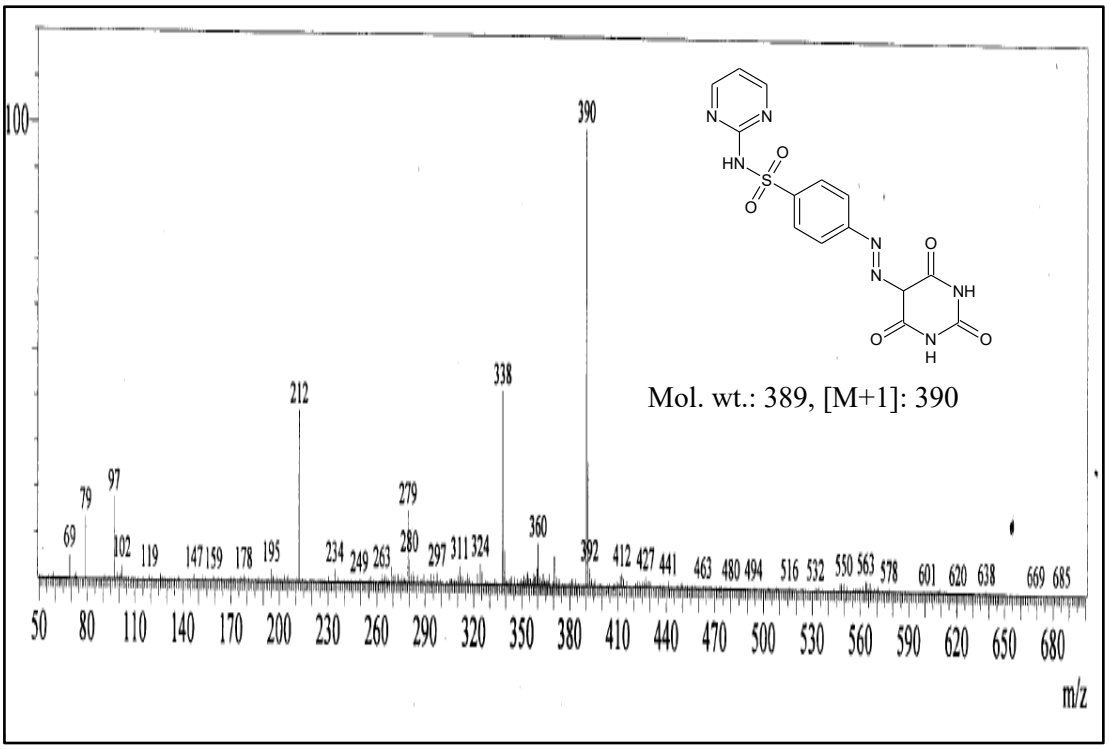

Fig.5.5a. Mass spectrum of azo dye ligand (HL_4).

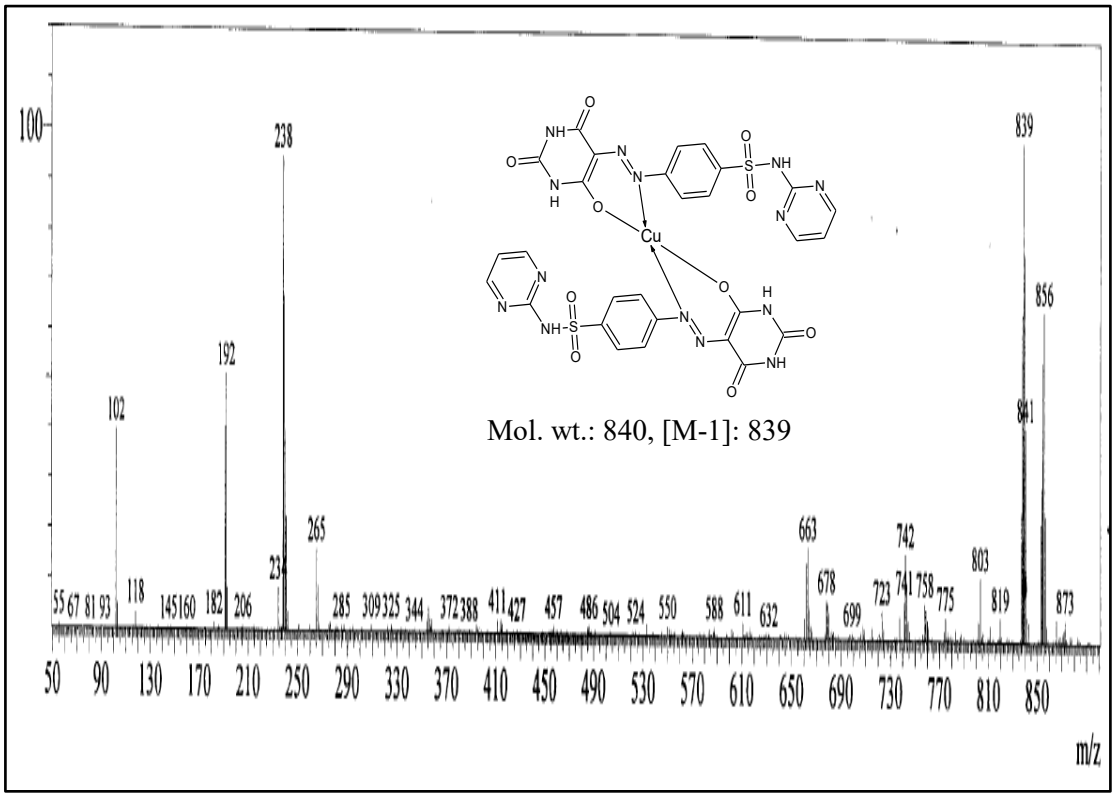

Fig.5.5b. Mass spectrum of Cu(II) complex.

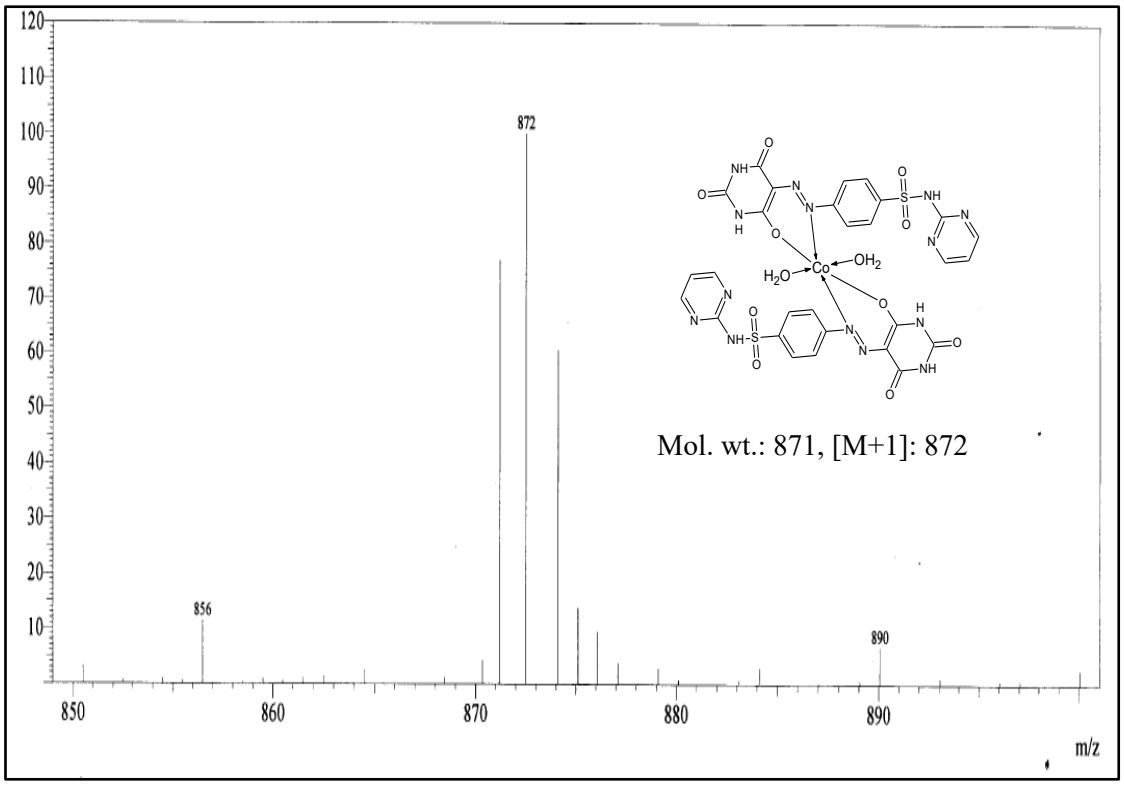

Fig.5.5c. Mass spectrum of Co(II) complex.

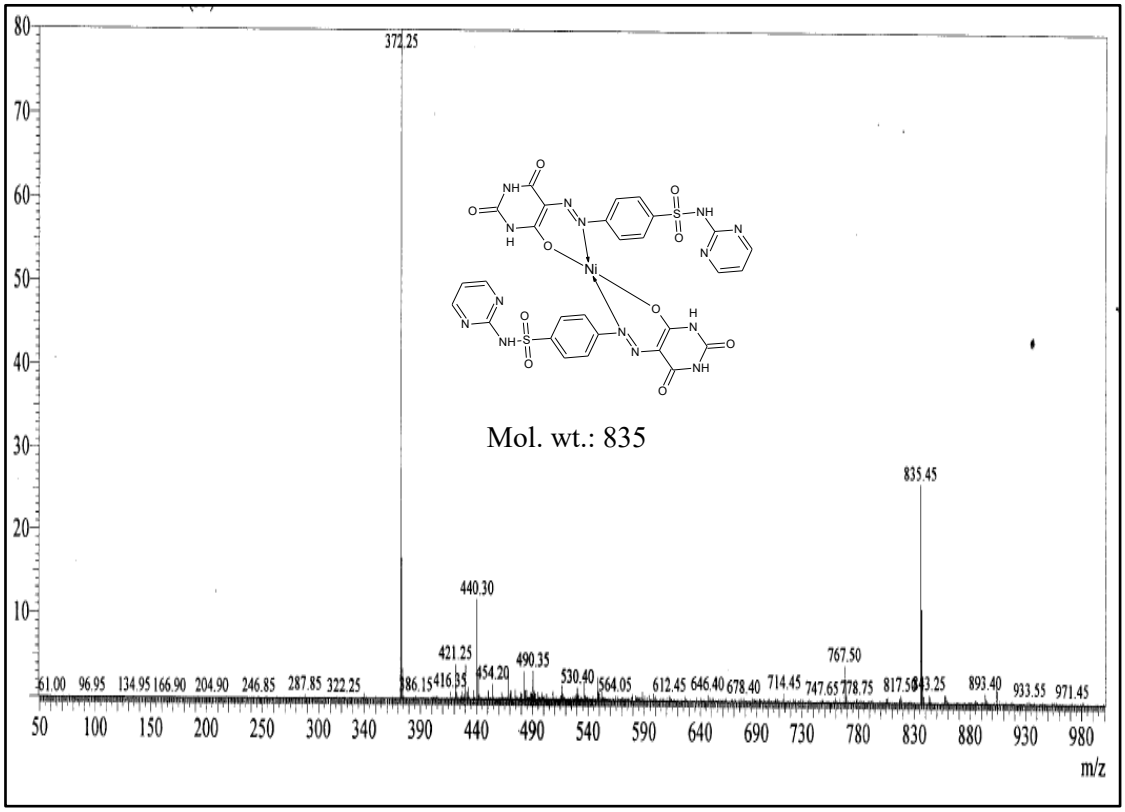

Fig.5.5d. Mass spectrum of Ni(II) complex.

5.3.5. Thermo gravimetric analysis.

The Thermo gravimetric analysis (TGA) gives proof relating to the thermal stability of the metal complexes. To get essential physicochemical indication and the presence of inner coordinated water molecules in the central metal ion carried out by using TGA. The TGA of metal complexes was taken over a temperature range from 30 to 900 °C at a scan rate of 10 °C/min in nitrogen atmosphere on TG-DSC curves. All the prepared complexes of azo dye exhibited high thermal stability as shown in **Fig. 5.6** and the percentage of decomposition is given in **Table 5.4.**

The Cu(II) complex shows three stages of disintegration. The first stage resembles to the loss of pyridine ring of the ligand with a weight loss of 18.88 % (calculated 18.97 %) at temp 30-346.89. At temperature 347-355 with a loss of 23.44 % (calculated 23.55 %) was observed in the 2nd stage, after the elimination of the fragments of the ligand the decomposition of the remaining portion of the complex started simultaneously between temperature 355.68-367 $^{\circ}$C with a weight loss 32.95 % (calculated 33.14 %) a further more the complex shows a gradual decomposition from and above 400 $^{\circ}$C owned the loss of remaining organic moiety the final mass of the scum corresponds to copper oxide.

The TGA of Co(II) complex showed three stages of decomposition. In the first step the loss of coordinated water molecule was takesplace at temperature 30 - 66°C. In the 2nd step the loss of some part of the ligand ($C_8H_5N_3$) takes place with a loss of 22.7 % (calculated 22.5 %) at temperature ranging 67 to 351 $^{\circ}$C. In the third stage the dissociation of complete ligand temperature ranging 352-800 $^{\circ}$C corresponds to $C_4H_8N_4O_8S_2$ with a mass loss 47.11 % (calculated 47.16 %) leaving behind the stable CoO as a residue.

Similarly TGA graph of Ni(II) complex, the first stage corresponds to the decomposition of water with a loss of 4.1 % (calculated 4 %) at 95 $^{\circ}$C. The resulting

complex undergo degradation at 2nd stage the loss of two pyridine was takes place with a mass loss 19.2 % (calculated 19.17 %) at temp 96-343 °C. The loss of SO_2NH was takes place in 3rd step with 23.52 % (calculated 23.7 %) temp ranging 344-351 °C. The final step the decomposition occurred with mass loss of 40.2 % (calculated 40.30 %) with temp ranging 352 to 750 °C due to complete decomposition of organic part leaving behind one mole of NiO.

Table 5.4. Thermal decomposition of metal complexes at nitrogen atmosphere.

Complexes	Stages	Decomposition Temp (°C)	Probable Assignment	Loss Of Mass In (%)	Residual Species
Cu(II)	1st	30-346	$C_8H_8N_4$	18.88	CuO
Complex	2nd	347-355	$S_2O_4N_2H_2$	23.44	
	3rd	Above 356	$C_4H_8N_4O_4$	32.95	
Co(II)	1st	30-66	2 H_2O	4.1	CoO
Complex	2nd	67-351	$C_8H_8N_3$	22.76	
	3rd	Above 357	$C_4H_8N_4O_8S_2$	47.16	
Ni(II)	1st	30-95	$2H_2O$	4.1	NiO
Complex	2nd	96-343	$C_8H_8N_4$	19.2	
	3rd	344-351	$H_4N_2O_4S_2$	23.7	
	4th	352-750	$C_4H_8N_4O_4$	40.3	

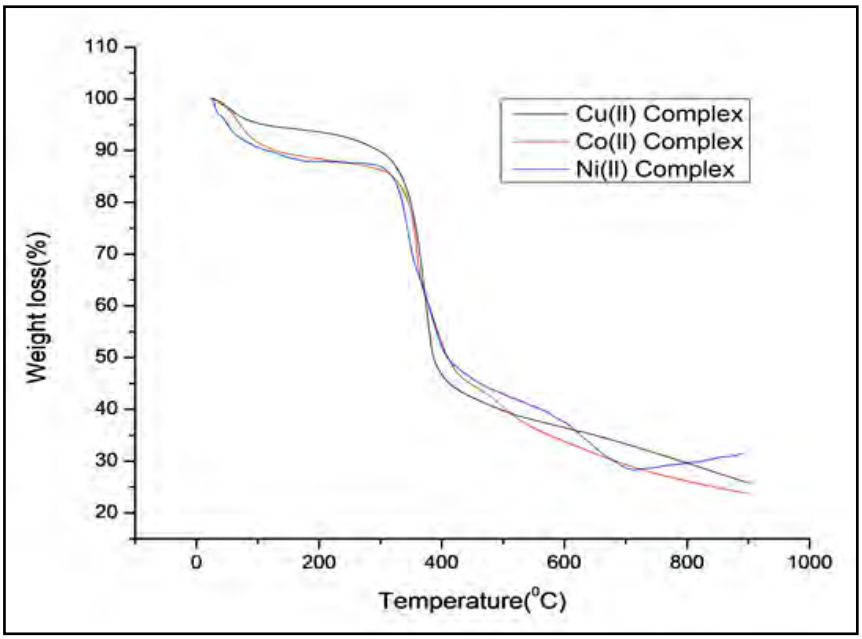

Fig.5.6. Thermal decomposition of metal complexes.

5.3.6. SEM with EDAX.

The syntheised ligand and their metal complexes were analyzed using scanning electron microscope with EDAX spectra to study their surface morphology and to determine the elements present on the surface of the compounds. The SEM images with EDAX spectra are shown in **Fig 5.7.** For the ligand the broken ice like structured particles are observed. Small granule like structure was observed for Ni(II) complex, for Co(II) complex layer by layer chip like structure was observed. Uniformed granules are formed in Cu(II) complex. Therefore clear changes in the structure of the ligand after the formation of metal complex were detected by using SEM [29]. EDX analysis of metal complexes showed the metal content along with nitrogen, carbon, and oxygen proposing the formation of metal complex.

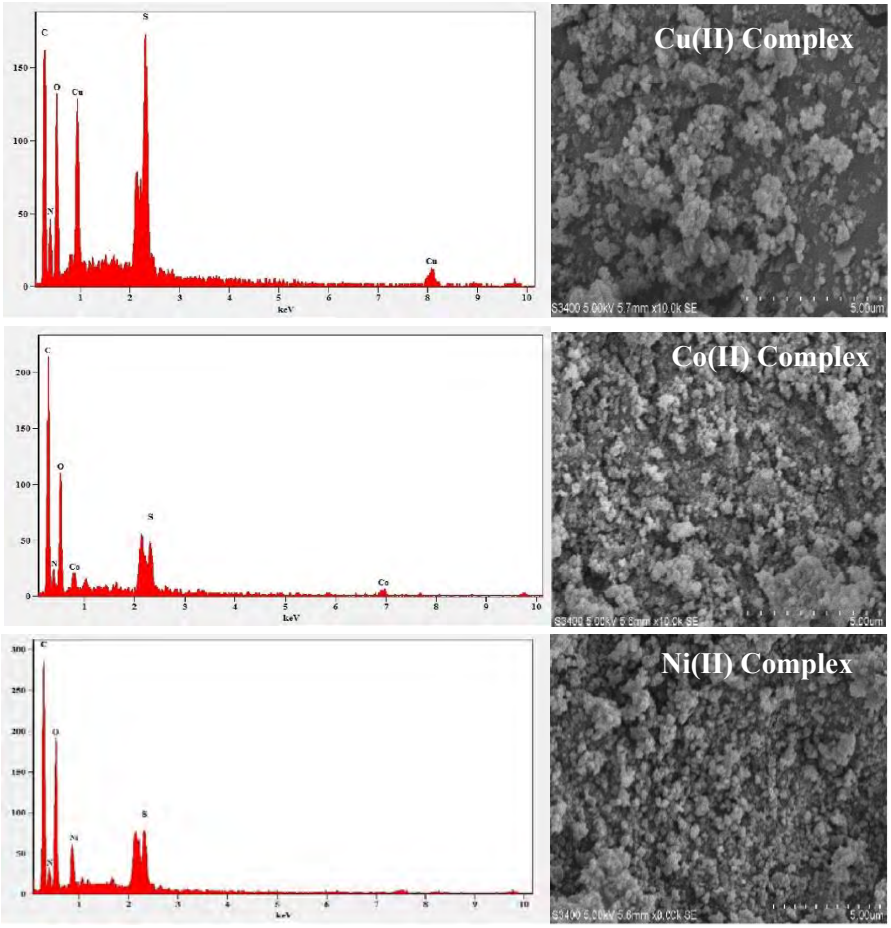

Fig. 5.7. The SEM-EDAX Spectrum of the Metal Complexes.

5.3.7. XRD.

The degrees of crystallinity of the azo metal chelates were studies by using powdered XRD. The XRD pattern of Cu(II), Co(II) and Ni(II) is depicted in **Fig. 5.8a-5.8c**. and the calculated XRD data for the selected high intensity peaks for all the complexes were tabulated in **Table 5.5a-5.5c.** From the data it is shown that all the metal complexes show certain amount of crystallinity.

The XRD pattern of Cu(II) complexes showed 7 reflections in the range 9 to 40° (2θ). By using bragg's equation **2dsinθ = nλ** the inter planar spacing was calculated. The miller indices (*h k l*) values were evaluated and the unit cell parameters are also determined. The lattice parameters was found to be a=b=c=5.44. The calculated $h^2+k^2+l^2$ was 1, 2, 3, 4, 6 and 7. The forbidden number 7 indicates that the complex belongs to hexagonal or tetragonal system [30].

Likewise, the above calculations were carried out for the Co(II) and Ni(II) complexes showed 9 and 6 reflections at 7-40. The unit cell parameters with the miller indices (*h k l*) values were determined. For Co(II) $h^2+k^2+l^2$ values are 1, 2, 3, 4, 6, 8, 10, 14 and 15, and for Ni(II) complex are 1, 1, 4, 5, 6 and 7. The existence of forbidden numbers like 15 for Co(II) complex and 7 for Ni(II) complex confirms that both the complexes may belong to hexagonal or tetragonal systems. The calculated lattice parameter for Co(II) are a=b=c=7.4 Å and Ni(II) complexes are a=b=c= 5.4Å, respectively.

Table 5.5a. Powder X-Ray spectral data of Cu(II) complex.

Sl no	2Θ	Θ	sin Θ	Sin^2 Θ	$Sin^2Θ\times 1000$	$h^2+k^2+l^2$	*h k l*	D	a in Å
1	13.1	6.55	0.114	0.01301	13.01	1	100	6.7570	5.440
2	19.17	9.58	0.1664	0.02769	27.69	2.1(2)	110	4.629	5.275
3	22.24	11.12	0.1928	0.03719	37.19	2.8(3)	111	2.0712	5.384
4	24.75	12.37	0.2142	0.04589	45.89	3.51(4)	200	3.594	5.419
5	29.07	14.535	0.2509	0.06294	62.94	4.8(5)	210	3.070	5.419
6	32.42	16.2	0.2789	0.07783	77.83	5.9(6)	211	2.7619	5.401
7	34.30	17.15	0.2948	0.08695	86.95	6.68(7)	--	2.6129	5.401

Table.5.5b. Powder X-Ray spectral data of Co(II) complex.

Sl no	2Θ	Θ	sin Θ	Sin^2 Θ	$Sin^2Θ\times 1000$	$h^2+ k^2+l^2$	*h k l*	D	a in Å
1	9.6	4.8	0.0836	0.0070	7.0	1	100	9.214	7.416
2	14.4	7.2	0.1253	0.0157	15.7	2.24(2)	110	6.1476	7.410
3	17.92	8.96	0.1557	0.02406	24.06	3.4(3)	111	4.9473	7.377
4	19.17	9.58	0.1655	0.0276	27.6	3.9(4)	200	4.6543	7.37
5	23.03	11.51	0.1995	0.0398	39.8	5.68(6)	211	3.8611	7.412
6	28.06	14.03	0.2424	0.05877	58.77	8.39(8)	220	3.1778	7.414
7	31.54	15.52	0.2675	0.07159	71.59	10.22(10)	310	2.8796	7.415
8	36.04	18.02	0.3093	0.09569	95.69	13.67(14)	321	2.4904	7.397
9.	36.95	18.47	0.3168	0.10036	100.36	14.5(15)	--	2.4315	7.341

Table.5.5c. Powder X-Ray spectral data of Ni(II) complex.

Sl no	2Θ	Θ	sin Θ	Sin^2 Θ	$Sin^2Θ$× 1000	$h^2+k^2+l^2$	h k l	D	a in Å
1	13.18	6.59	0.1147	0.01317	13.17	1(1)	100	6.7157	5.40
2	19.31	9.655	0.1676	0.02809	28.09	2.1(1)	110	4.5960	5.42
3	24.82	12.41	0.2149	0.04618	46.18	3.52(4)	200	3.5844	5.41
4	29.35	14.675	0.2533	0.06479	64.17	4.8(5)	210	3.0410	5.43
5	31.58	15.79	0.2721	0.07404	74.04	5.65(6)	211	2.8309	5.42
6	33.25	16.62	0.2861	0.08185	81.85	6.61(7)	---	2.6924	5.41

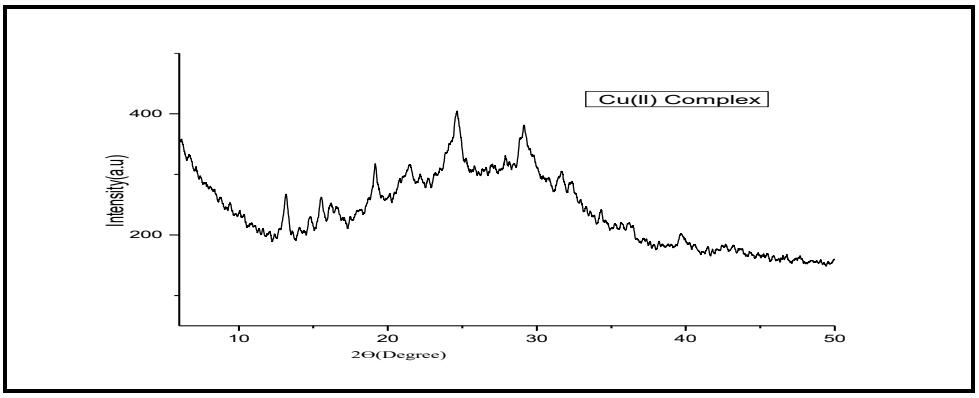

Fig. 5.8a-XRD pattern of Cu(II) complex of HL_4

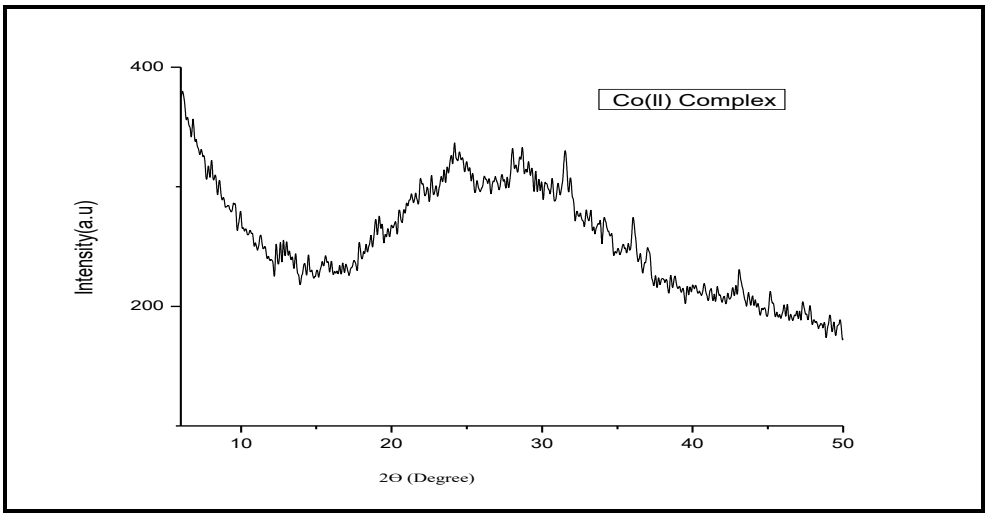

Fig. 5.8b-XRD pattern of Co(II) complex of HL_4

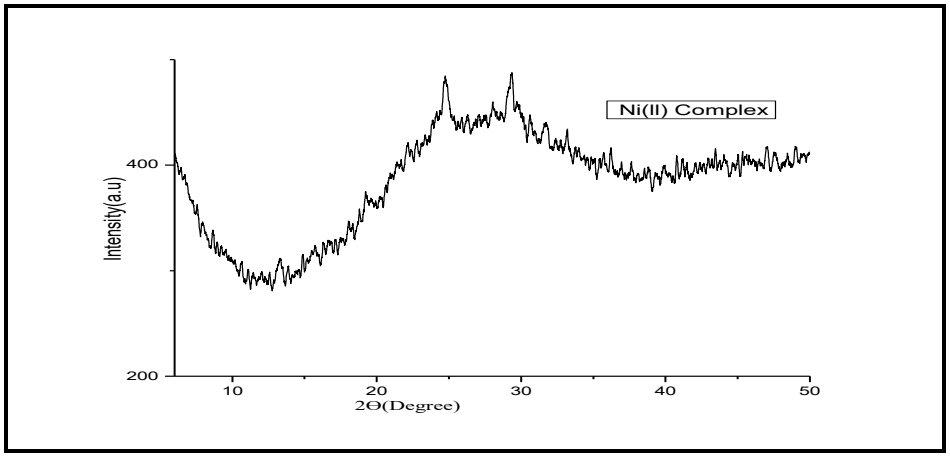

Fig. 5.8c-XRD pattern of Ni(II) complex of HL_4

5.3.8. Biological Evoluation.

The azo-sulphonamide moiety displays a efficient chemotherapeutic drugs and some of the drugs were designed based on the excellent pharmacological property of the sulphonamide molecule. In order to improve the biological activity and to overcome the limitation such as parasitic resistance strains increase toxicity. Thus observance the above disadvantage in the present study we are concentrate on the biological studies of the metal chelates which includes antibacterial, antifungal, and Insilco molecular docking studies.

5.3.8.1 Antimicrobial Studies.

The synthesized complexes were screened for their antimicrobial activity against *staphylococcus aureus, E-coli, xanthomonas ampestris, klebsiella pneumonia,* and antifungal activity against *C.albicans* and *A. flavus* by agar well diffusion method. Briefly, the micro-organism inoculums were evenly spread using sterile cotton swab on a sterile Petri dish containing malt agar (for fungi) and nutrient agar (for bacteria). Different concentration of metal chelates were added to each well (6 mm diameter holes cut in the agar gel, 20 mm apart from one another). The plates were incubated for 24–48 hour at 37 °C (for bacteria) and at 28 °C (for fungi). After incubation, micro-organism growth was observed. Inhibition of the bacterial and fungal growth

were measured in mm. Tests were performed in triplicate. The minimal inhibitory concentration (MICs) was determined after incubation period [31].

Result and Discussion

The potency of the metal chelates with the reference Amoxicillin (antibacterial drug) and Fluconazole (antifungal drug) were tested against gram positive (*staphylococcus aureus*,) gram negative (*E.coli, xanthomonas ampestris, klebsiella pneumonia*) bacteria and two fugal strain (*C.albicans and A. flavus*). The zone of inhibition (mm) was used to compare the antimicrobial activity of the synthesized compounds with reference drug. Results of the antimicrobial activity are presented in **Table.5.6** and **Table 5.7.** From the data, it is observed that all the metal chelates exhibited significantly enhanced antibacterial activity against selected bacterial strains. In general, the *in-vitro* Bacterial activity of Co(II) and Cu(II) exhibited higher antibacterial activity than Ni(II) complex.

Moreover, towards fungi species the metal chelates are more active than the standard drug, with Ni(II) Complex being supreme active. Whereas ligand shows least activity compared to all complexes against both the strains. This showed that reaction of metal ions with the ligands plays an key role in increasing its pharmacological activity. The increase in pharmacological activity could be due to the occurance of electron delocalization within the metal complexes. This reduces the polarity of the metal ion. Polarity decreases due to the sharing of positive charge with the ligand donor atoms. This may upsurge the hydrophobic and lipophilic character of the metal complex, permitting it to the lipid layer of the organism killing them more effectively [32]

Table 5.6. Antibacterial activity of metal complexes.

Bacteria		Cu(II) Complex	Co(II) Complex	Ni(II) Complex
Staphylococcus Aureus	25 mg/mL	06	13	02
	50 mg/mL	12	14	06
	100 mg/mL	18	22	11
	Amoxicillin	14	15	11
Escherichia Coli	25 mg/mL	04	7.5	02
	50 mg/mL	16	12	05
	100 mg/mL	19	17.5	10
	Amoxicillin	17	15	13
Xanthomonas Ampestris	25 mg/mL	03	08	01
	50 mg/mL	12	16	06
	100 mg/mL	13	17	09
	Amoxicillin	14	21	08
Klebsiella Pneumonia	25 mg/mL	05	12	03
	50 mg/mL	11	14	12
	100 mg/mL	15	19	14
	Amoxicillin	17	15	12

Table 5.7. Antifungal activity results of the synthesized compounds.

Compounds	% of inhibition			
	C.albicans		A. flavus	
	50 µg/mL	100 µg/mL	50 µg/mL	100 µg/mL
HL_4	22±0.20	41±0.27	19±0.46	46±0.31
Cu(II) Complex	38±0.25	62±0.15	25±0.21	67±0.22
Co(II) Complex	32±0.33	64±0.21	31±0.64	66±0.32
Ni(II) Complex	37±0.14	68±0.33	41±0.13	78±0.21
Fluconazole	39±0.13	79±0.13	37±0.14	89±0.13

Values are symbolized as the mean±SEM
Values are significant for the standard at 0.005 level of significance

5.3.8.2. Insilco Molecular docking.

The molecular docking studies have become a more suitable method to relate the experimental *in-vitro* biological results with the theoretical results. The detailed protocol of molecular docking studies was described in **Section 3.3.7.4** of **Chapter 3**.The results shows that the Co(II) complex shows the highest binding energy.

All the synthesized metal complexes were employed to recognize the interaction between the metal complexes and the target receptor. The docking studies showed significance interaction with the target receptor RpsA [33]. All the metal chelates showed well recognized aquaphobic interactions such as His322, Ile349, Glu325, Ser359, Arg355, Asp350, Arg357 Asp352, Arg357 and Gln3649 in the target enzyme active pockets (**Fig. 5.9** and **Table 5.8**). The relative binding affinities of all the complexes were accomplished in the range of −2.51 kcal/mol to -3.90 kcal/mol respectively. From the results, Co(II) complex shows the highest –ve relative binding energy that indicated it may be considered as a good inhibitor glucoseamine-6-phosphate synthase.

Table 5.8. Docking Energy Data of the Synthesized Complexes.

Compounds	Binding Energy (kcal/mol)	H-bonds	H-bond length (å)	H-bond with	Hydrophobic interactions
Cu(II) Complex	-2.51	1	3.08	Gln364	His 322,Ile349,Glu325, Ser359
Co(II) Complex	-3.90	2	3.02 3.20	Ser359, Ser359	Arg355,His322,Asp350, Arg357
Ni(II) Complex	-3.45	1	2.51	Arg355.	Asp352,Asp350,Ser359, Arg357

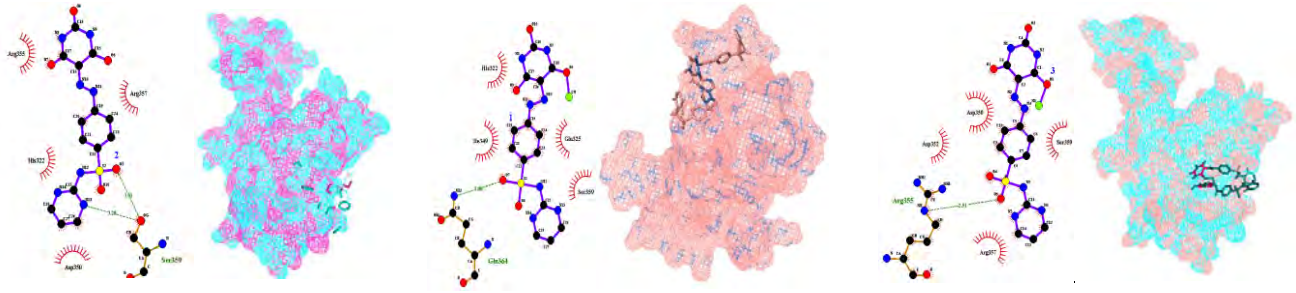

Cu(II) Complex Co(II) Complex Ni(II) Complex

Fig. 5.9. Three-Dimensional Representation of the Metal Complex into Active Protein RpsA.

5.4. Conclusion.

To conclude, a successful synthesis of novel azo derivatives of sulfadiazine (HL_4) with their Cu(II), Co(II) and Ni(II) complexes were achieved with good yield. All the synthesized compounds were characterized by conventional spectroscopic and analytical techniques. From elemental analysis and mass spectroscopic measurements, it is determined that the metal to ligand ratio is 1:2 stoichiometry of the type $[M(L)_2]$. Based on the results the Cu(II) and Ni(II) Complexes exhibits square planar geometry. Whereas The Co(II) ion in the complex adopts a octahedral environment. The thermal properties of metal complexes are investigated by TGA, result showed high thermal stability and suggested molecular formulae of the complexes. Metal complexes were tested against Gram-negative bacteria, Gram-positive bacteria and two strains of fungi, all the complexes showed enhanced activity against standard drug and can be used as a potent antimicrobial agent against selective pathogens. A molecular docking study was carried out to explore the binding interactions between the synthesized complex and the target receptor RpsA. It showed that the tested compounds fit into the receptor active site with complimentary binding energy.

5.5. Reference.

1. M. Hassan, S.M. Nasr, S.E. Abd-El Razek, M.S. Abdel-Aziz and S.M. El-Gamasy, *Arab. J. Chem.*, 13, 7324, **2020**.
2. M. Rocha, O.E. Piro, G.A. Echeverría, A.C. Pastoriza, M.A. Sgariglia, J.R. Soberon and D.M. Gil, *J. Mol. Struct.*, **2018**.
3. T. N. J. I. Edison, R. Atchudan, M. G. Sethuraman and Y. R. Lee, *J. Photochem. Photobiol. B*, 162, 604, **2016**.
4. K. J. Al-Adilee and H. A. K. Kyhoiesh, *J. Mol. Struct.*, 1137, 160, **2017.**
5. Y. K. Abdel-Monem, S. A. Abou El-Enein and M. M. El-Sheikh-Amer, *J. Mol. Struct.*, 1127, 386, **2017**.
6. H. E. Gaffer, *Color. Technol.*, 135, 484, **2019**.
7. B. R. Kirthan, M. C. Prabhakara, H. S. Bhojyanaik, P. H. Amith Nayak, R. Viswanath, H. B. Teja and Ereshanaik, *Inorg. Chem. Commun.*, 135, 109109, **2022**.
8. P. A. Ajibade, G. A. Kolawole, P. O'Brien, M. Helliwell and J. Raftery, *Inorg. Chim. Acta*, 359, 3111, **2006**.
9. A. W. Bauer, W. M. M. Kirby, J. C. Sherries, M. Turck, Am. *J. Clin. Pathol*. 45, 493–496, **1966**.
10. A. I. Vogel, A Text Book of Quantitative Inorganic Analysis, vol. 433, third ed., Longmans, London, 443, **1975**.
11. B. Katia, L. Simon, R. Anne, C. Gerard, D. Francoise and M. Bernard, *Inorg. Chem*. 35 387, **1996**.
12. N. Raman, A. Kulandaisamy, A. Shanmugasundaram, and K. Jeyasubramanian, *Trans. Met. Chem*. 26, 131, **2001**.
13. A. Cukurovali, I. Yilmaz, H. Ozmen, and M. Ahmedzade, *Trans. Met. Chem.* 27, 171, **2002.**
14. A. Garcia-Raso, J.J. Fiol and B. Adrover, *J. Inorg. Biochem*., 95, 77-86, **2003**.
15. S. Dhar and A.R. Chakravarty, *Inorg. Chem*., 42, 2483-2485. **2003**.
16. P. B. Dervan, *Scien.,* 232, 464-471, **1986**.
17. L. P. Lu, M. L. Zhu and P. Yang, *J. Inorg. Biochem.,* 95, 31-36, **2003**.
18. J. Z. Wu, H. Li and J.G. Zhang, *J. Inorg. Chem Commun.,* 5, 71-75, **2002**.
19. P. M. Burrows and B. Meunier, *Nucle. Acids Res.,* 28, 4856-4864, **2000**.
20. M. Navarro, E. J. Cisneros-Fajardo and A. Sierralto, *J. Biol. Inorg. Chem.,* 8, 401-408, **2003**.

21. C. A. I. Detmer, F.V. Pamatong and J. R. Bocarsly, *Inorg. Chem.,* 35, 6292-6298, **1996**.
22. S. Mahadevan and M. Palaniandavar, *Inorg. Chem.,* 37, 693-700, **1998**.
23. A. Mohammadi and M. Safarnejad, *Spectrochim. Acta A Mol. Biomol.Spectrosc.*, 126, 105, **2014**.
24. P. H. Amith Nayak, H. S. Bhojya Naik, H. B. Teja, B. R. Kirthan and R. Viswanath, *J. Electron. Mater.*, 50, 2090, **2021**.
25. K. E. Baradie, R. E. Sharkawy, H. E. Ghamry and K. Sakai, *Spectrochim. Acta A Mol. Biomol. Spectrosc.*, 121, 180, **2014**.
26. P. H. Amith Nayak, H. S. Bhojya Naik, H. B. Teja, B. R. Kirthan and R. Viswanath, *Mol. Cryst. Liq. Cryst.*, 722, 67, **2021**.
27. N. Venugopal, G. Krishnamurthy, H.S. Bhojyanaik and P. Murali Krishna, *J. Mol. Struct.*, 1183, 37, **2019**.
28. M. C. Prabhakara and H. S. Bhojya Naik, *Biometals.,* 21, 675–684, **2008**.
29. N. M. Mallikarjuna, J. Keshavayya and B. N. Ravi, *J. Mol. Struct.*, 1173, 557, **2018**.
30. N. M. Mallikarjuna, J. Keshavayya, M. R. Maliyappa, R. A. Shoukat Ali and T. Venkatesh, *J. Mol. Struct.*, 1165, 28, **2018**.
31. M. C. Prabhakara, and H. S. Bhojya Naik, *Main Group Chem.,* 7, 97–107, **2007**.
32. H. B. Teja, H. S. Bhojya Naik, P.H. Amith Nayak and M.C. Prabhakara, *Asian J. Chem.*, 33, 1709, **2021**.
33. N. Venugopal, G. Krishnamurthy, H.S. Bhojya Naik and J.D. Manohara, *J. Inorg. Organomet. Polym. Mater.*, 30, 2608, **2020**.

Chapter-6

Study of Photophysicochemical and Antimicrobial Photodynamic Properties of Visible Light Active Azo Metal Complexes

6.1. Introduction.

Photoactivation has attracted researches from last few decades because of its application from medicine to energy harvesting. Light is the important key for photoactivation [1]. Light as an external, temporally controllable, non-invasive and this is the motivation to succeed precise control over specific processes. Because of its specificity and selectivity this method provides a safe to achieving accurate control over processes like drug or gene delivery, cell killing etc., thereby reducing side effects and improving therapeutic efficacy [2-4]. Photoinactivation is the principel of techniques such as photodynamic therapy, photo-triggered release systems, photocaging, photoisomerization etc. in all these techniques light is used in different ways to achive specific outcomes [5]. Photodynamic therapy (PDT) has garnered enormous interest; PDT is a local technique for cancer treatment. Usually, in PDT non-toxic photosensitizers was irradiation with the appropriate wavelength is provided, usually in the UV or near-infrared region, in order to activate the ground state photosensitizer to the excited triplet state. The triplet-state photosensitizer can participate in a one electron oxidation–reduction reaction with a adjacent molecule [6]. Subsequently, free radical intermediates are generated which can react with oxygen to form peroxy radicals and various reactive oxygen species (ROS). Alternatively, the triplet-state photosensitizer can also transfer energy to ground state oxygen, producing singlet oxygen. The highly reactive singlet oxygen can destroy the tumor cells and tissues through damage of various biological molecules including lipids, proteins and nucleic acids [7].

The effectively and efficiency of PDT is mainly depend upon the photosensitizer. Selection of a suitable photosensitizer is more important. An ideal photosensitizer should not only have high efficiency in generating ROS within aerobic

tissues, high molar extinction coefficient, and also inherently nontoxic in the dark and soft tissue penetration depth [8]. The toxixity of the induced light can be controlled by confined area through directing light irradiation. Subseqently, PDT has its own advantages compared to conventional chemotherapy and radiotherapy, including minimum side effects, researches confirm that PDT can even activate the immune response of the body to kill tumor cells. indeep PDT is still considered as an alternative remedy due to certain limitations like most traditional chemotherapy drugs, photosensitizers also have unacceptable tumor efficacy after in vivo injection [9].

To solve these dilemmas, the development of photosensitizers by using Organic dyes is growing in research field, because the organic dye has several advantages such as the effortlessness synthesis, handling and hydrophobicity [10]. To develop environmental friendly, safer and more efficient photosensitizers for antimicrobial PDT is a challenge for the researchers. But the efficacy of dye is still relatively low when compared to their inorganic counterparts, which may be due to the highly bonded nature of the electrons in the metal-free organic materials [11]. So; we design the photosensitizers in which the aromatic peripheral ligands around the heavy central metal make it possible to design transition-metal complexes [12]. In these photosensitizers, the transition-metal atom effect facilitates intersystem crossing (ISC) of a photosensitizer to produce its triplet state after photoexcitation. Additionally, the derivatives of 4-amino antipyrine compounds are applicable as potential ligands for numerous metal complexes having great significance in the field of biochemistry [13]. On the other side, quinoline and related heterocyclic systems are found in a large number of biologically active natural products and pharmaceuticals [14-16]. The nitrogen-containing metal complexes deserve a massive significance, because it as ability to break DNA chains and protein. Our intrest is to develop transition metal

complexes of organic dye as a binder considering the biocompatibility of both the metal and the ligands.

Here, we have attempted the synthesis and characterization of a azo base ligand 4-[(E)-(8-hydroxyquinolin-5-yl)diazenyl]-1,5-dimethyl-2-phenyl-1,2-dihydro-3H-pyrazol-3-one and its Co(II) and Mn(II) complexes. The lignd and complexes are conformed by spectral characterization. Furthermore; the cytotoxicity was tested against human melanoma (A-375) and human primary glioblastoma (U-87) cell lines and invitro antimicrobial PDI toward gram-positive bacteria *S.aureus*, gram-negative bacteria *E.coli* and fungus *C.albicans* were investigated.

6.2. Experiment.

6.2.1. Methods and materials.

The selected organic compounds and the metal salts are purchased fron sigma Aldrich.the structure of the ligand and the metal complexes are conformed by spectroscopic techniques which are discussed in **Chapter 2**.

6.2.2. Synthesis of azo-dye (HL_5).

The azo dye -[(E)-(8-hydroxyquinolin-5-yl)diazenyl]-1,5-dimethyl-2-phenyl-1,2-dihydro-3H-pyrazol-3-one was synthesized by using heterocyclic amine 4-Aminoantipyrine was coupled with 8-hydroxy quinolone. The schematic representation of the azo dye was depicted in **Scheme 6.1**. The heterocyclic amine (0.1 mol) in 10 % HCl at temperature 0 to 5 $^{\circ}$C. The $NaNO_2$ (0.1 mol) in 10 ml of ice cold water, which was then added gradually to HCl mixture. The reaction mixture was stirred for about 1 hour was the temperature was maintained at below 5 $^{\circ}$C. By adding urea the excess nitrous acid was removed, then stir for about 30 mins. The resulting diazonium salt solution was then added dropwise to a well-cooled solution of 8-

hydroxyquinoline (0.1mol) in potassium hydroxide (5% in 20 ml water) by adding saturated sodium bicarbonate the pH of the reaction mixture was maintained at 6. The reaction mixture was further stir for about 1 hour the coloured precipitate separates and then crude dyes were filtered, washed with water and purified by recrystallization from DMF-ethanol [17].

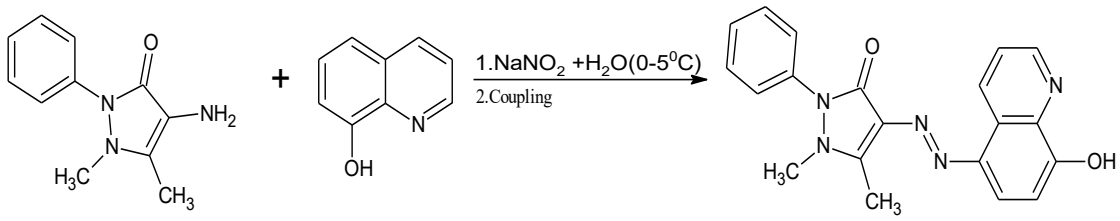

Scheme 6.1. Synthesis of azo dye ligand (HL_5)

6.2.3. Synthesis of photoreactive Co(II) and Mn(II) complexes.

A solution of the metal salt $CoCl_2.6H_2O$ (0.005 mol) and $Mn(CH_3COO)_2.4H_2O$ (0.005 mol) was taken in in 20 ml of absolute ethanol and added drop wise to a stirred solution of 0.01 mol of free azo dye. This mixture was then refluxed for about 2 hour at 70 °C and then concentrated by heating to reduce its volume. The precipitate obtained was filtered and washed with hot ethanol product was then dried under vacuum [18]. The schematic resprentation of metal complexes are depicted in **Scheme 6.2.**

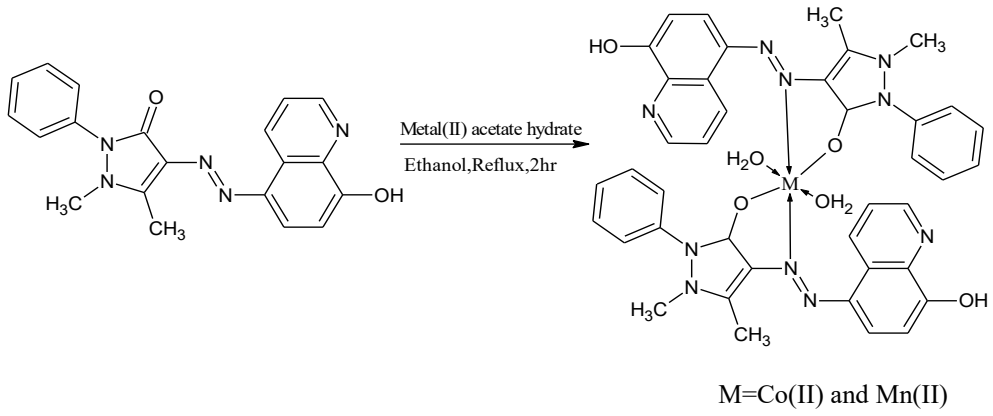

Scheme.6.2. Metal complexes synthesis by using azo dye ligand.

6.3. Results and Discussion.

The synthesis of ligand HL_5 was based on the fact that the electrophilic aromatic diazonium ions reacts with the nucleophilic activated aromatics at 0 °C. The results of this amine group was concerted into azo group that is -N=N-. The azo dye was characterized using different spectroscopic techniques described in **Chapter 2**. The results which were obtained were consistent with the structure. The azo dye was then reacted with metal salts to form octahedral azo metal complexes. The analytical & physical data of the ligand HL_5 and its metal(II) complexes are presented in **Table 6.1.**

Table.6.1. Physical and Analytical data of the synthesized azo ligand and its metal complexes.

Sl No	Synthesized Compound	Molecular Weight	Yield In%	Melting Point In ^{0}C	Colour	Elemental Analyzer Found (Caclculated)				
						C	H	N	O	M
1	HL_5 ($C_{19}H_{15}N_5O_2$)	359.14	80	258-260	Orange	67.0 (66.84)	4.64 (4.77)	19.5 (19.49)	8.88 (8.90)	-
2	Co(II) Complex	815	75	>300	Brown	55.0 (55.05)	4.42 (4.39)	16.11 (16.05)	11.04 (11.0)	13.61 (13.51)
3	Mn(II) Complex	811	60	>300	Yellow	55.49 (55.56)	4.32 (4.43)	16.16 (16.20)	11.08 (11.10)	12.8 (12.71)

6.3.1. ^{1}H-NMR and ^{13}C-NMR Spectra.

To elucidate the number and position of hydrogen atom in the synthesized compounds the ^{1}H-NMR spectra were important. ^{1}H-NMR spectra of ligand HL_5 obtained at ambient temperature in DMSO-d6 as solvent. the spectra of the ligand were presented in **Fig 6.1.** The azo dye ligand displayed signals at 9.06-9.08 ppm (doublet) which corresponds to -N-CH- of the quinoline ring [19]. The downfield shift of the -OH proton of 8-hydroxyquinoline ring was resonated at 8.89 ppm in ^{1}H-NMR spectrum indicated that the -OH proton was possibly in the formation of strong

intramolecular hydrogen bonding [20]. The Aromatic protons showed a signal at 7.3-7.7 ppm as a multiplet [21]. A singlet at 3.34 and 2.68 ppm were resonated as methyl protons of 4-Aminoantipyrine moiety [22].

The ^{13}C-NMR of the free azo dye displayed a signal at 151 ppm which attributes to -N-CH of the quinoline ring. The Carbon attached to the -OH of the 8-hydroxyquinoline was resonated at Signal at 155.5ppm [23]. The adjacent carbon atom of the -N=N- group are assigned as signal at the 111 ppm and 122ppm[24]. The methyl carbon of the 4-amino antipyrine were assigned at 34 ppm (-N-CH_3) and 11ppm (-C-CH_3). **Fig.6.2.** Shows the ^{13}C-NMR spectra of qunoline azo dye. Due to paramagnetic nature the NMR spectra of the complexes cannot be obtained.

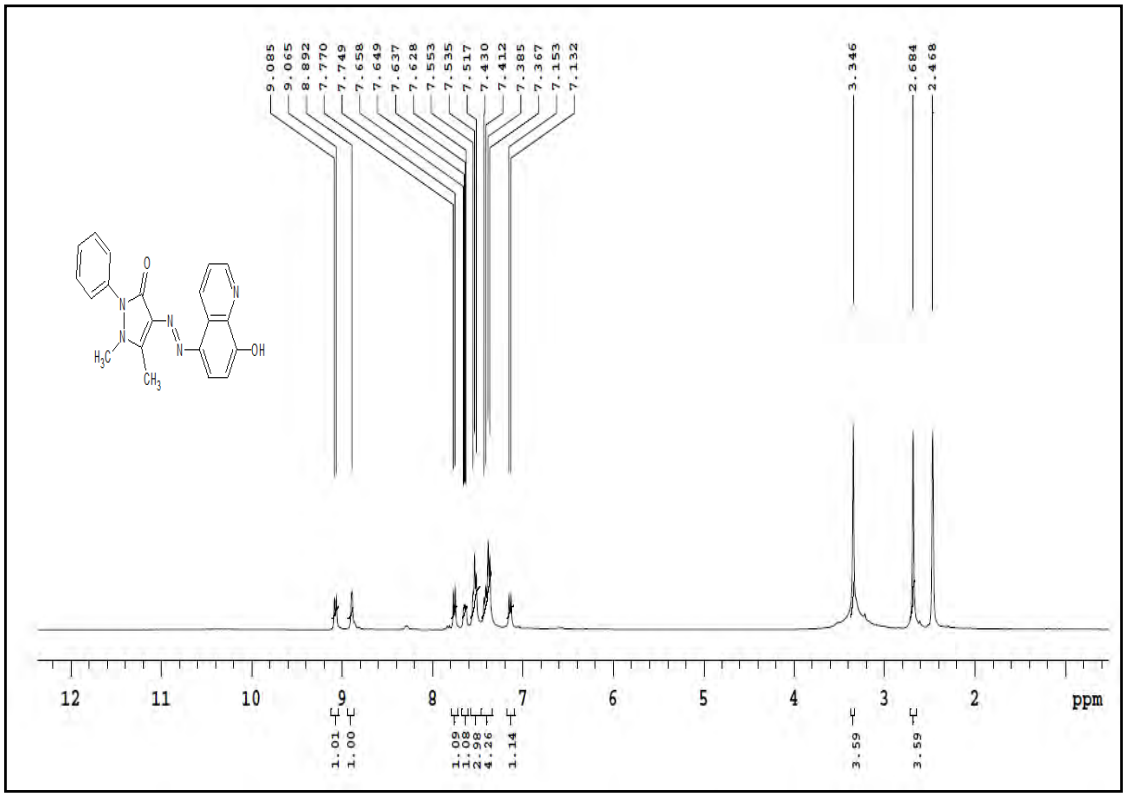

Fig.6.1.^{1}H-NMR Spectra of azo dye ligand (HL_5).

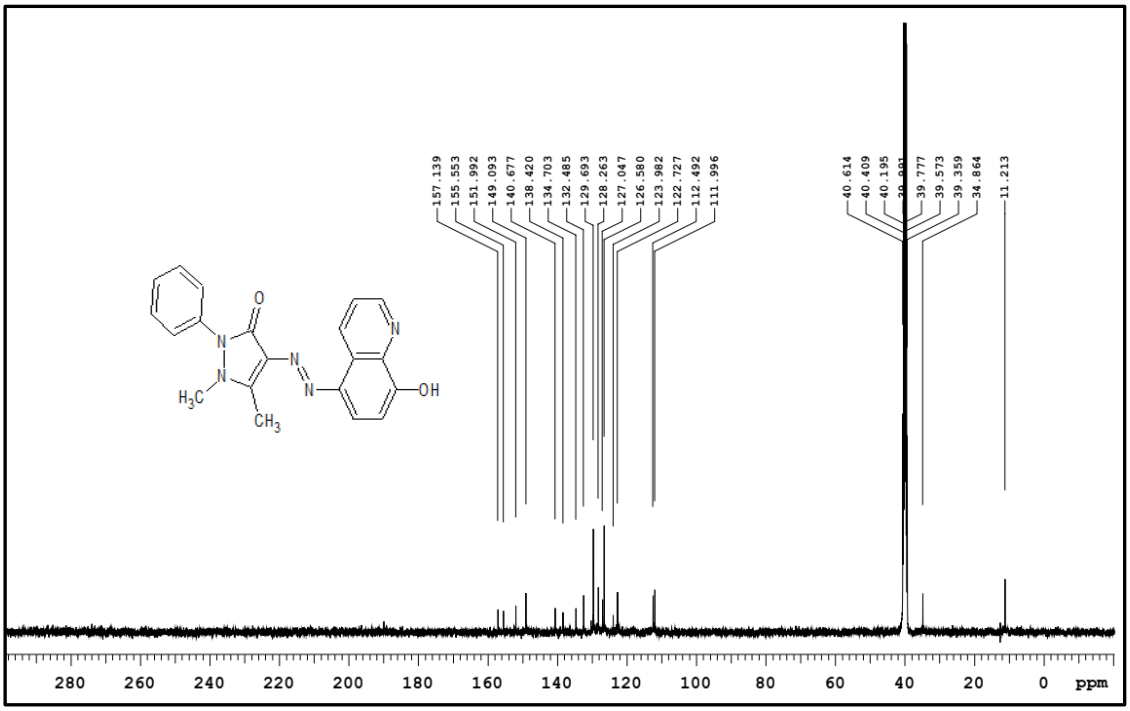

Fig.6.2. ^{13}C-NMR Spectra of azo dye ligand (HL_5).

6.3.2. Electronic Spectra.

The electronic absorption spectra in the UV-visible region for the ligand precursor, as well as their corresponding complexes. The formation of the metal complexes was also confirmed by UV-vis spectra. **Fig.6.3** gives the UV-visible spectra of the ligand and its metal complexes in DMSO solution and the spectral data were depicted in **Table 6.2**. The absorbtion of the free ligand was at 408 nm arises due to transition involving electron migration along the entire conjugate system of the ligand. In the spectra of the metal complexes, this absorption bands are shifted to longer wavelengths relative to their metal free ligand. From **Fig.6.3.** which shows that the metal complexes showed red shift of 4 nm when compared to that of free ligand [25]. According to modern molecular orbital theory the center metal ions have influence on the absorption bands of the complexes. The differences in the absorbtion band of the complexes are due to electronegativity, the radius and electronic configuration of the metal ion that can influence the electronic density of a conjugated system.

The metal complexes exhibited new bands in the range of 490- 500 nm assigned to charge transfer spectrum (LMCT) of complexes which were absent in ligand [26]. The Co(II) complex showed the absorption at 406 and 492 nm the bands were assigned as $^4T_{1g}(F) \rightarrow {}^4T_{2g}(F)$ and $^4T_{1g}(F) \rightarrow {}^4A_{2g}(F)$ which showed a distorted octahedral geometry [27]. The spectrum of the octahedral Mn(II) complex shows two bands at 411 and 494 nm due to $^6A_{1g} \rightarrow {}^4T_{1g}$ and $^6A_{1g} \rightarrow {}^4T_{2g}$ transitions. Mn(II) complex has ground state $^6A_{1g}$, hence the transition from this ground state $^6A_{1g} \rightarrow {}^4E_g$ (d) is forbidden and band intensity was very low[28].

Table.6.2. Electronic spectral date of the azo dye ligand and its metal complex.

Compound	λmax (nm)	Transition
HL_5	408	electron migration
Co(II) complex	406 and 492	$^4T_{1g}(F) \rightarrow {}^4T_{2g}(F)$ $^4T_{1g}(F) \rightarrow {}^4A_{2g}(F)$
Mn(II) complex	411 and 494	$^6A_{1g} \rightarrow {}^4T_{1g}$ $^6A_{1g} \rightarrow {}^4T_{2g}$

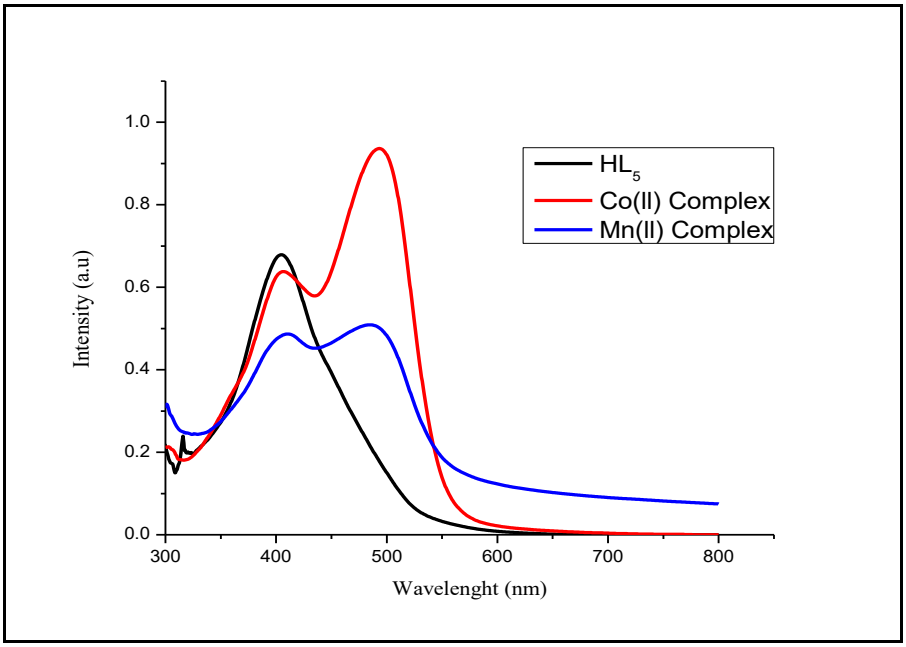

Fig.6.3. UV-visible spectra of the Ligand (HL_5) and their metal complexes.

6.3.3. FT-IR spectra.

To study the nature of the ligand metal ion bonding IR spectra has been proven to be the most suitable technique for elucidation of the structure. The main characteristic bands and their tentative frequencies were summarized in **Table 6.3**. The FT-IR spectra are shown in **Fig 6.4a** to **Fig 6.4c**. The IR spectra of the azo metal complexes were analogous to each other, apart from some slight shifts and intensity changes of a few vibration frequency's produced by different metal ions, which specifies that the complexes were of similar structure. However, there were some important differences between the free ligand and the azo metal complexes. The coordination mode and sites of the ligand to the metal ions were investigated by comparing the IR spectra of the free ligand with its metal complexes. The IR spectra of the ligand the band at 1634 cm^{-1} was assigned to the stretching frequency of carbonyl group present in the 4-amino antipyrin moiety. In the spectra of all the complexes, the carbonyl stretching bands shifted significantly towards lower energy, which specifies a reduction in the stretching force of (-C=O). As a result, coordination occurs through the carbonyl oxygen atoms [29]. In the free ligand the stretching frequency at 1492 cm^{-1} corresponds to the azo group (-N=N-), this band also shifted towards lower energy in the complexes, it conforms that the azo nitrogen group was involved in the complex formation. In the ligand a broad peak at 3422 cm^{-1} corresponds to –OH of the quinoline ring which was because of the –OH group involved in inter or intra molecular hydrogen bonding. Mohammed Khaled bin Break, *et. al.* [30] suggested that stable azo form is due to inter molecular hydrogen bonding at solid state. The broad peak at 3350- 3400 cm^{-1} presents in both complexes attributes to the presence of water molecule in the coordination with the metal ion. The presence of water in these complexes was also confirmed by thermal analysis. The presence of

new band in metal complexes at 488-693 and 483-618 cm^{-1} assigned to M–N of the azo nitrogen and M–O of the antipyrine moiety respectively [31].

Table 6.3. FT-IR bands and tentative assignments of the ligand and its metal azo complexes.

Compounds	ν(–OH)	ν(C=O)	ν(N=N)	ν(M-N)	ν(M-O)
HL_5	3422	1634	1492	-	-
Co(II) complex	3377	1563	1458	488	693
Mn(II) complex	3390	1563	1461	443	515

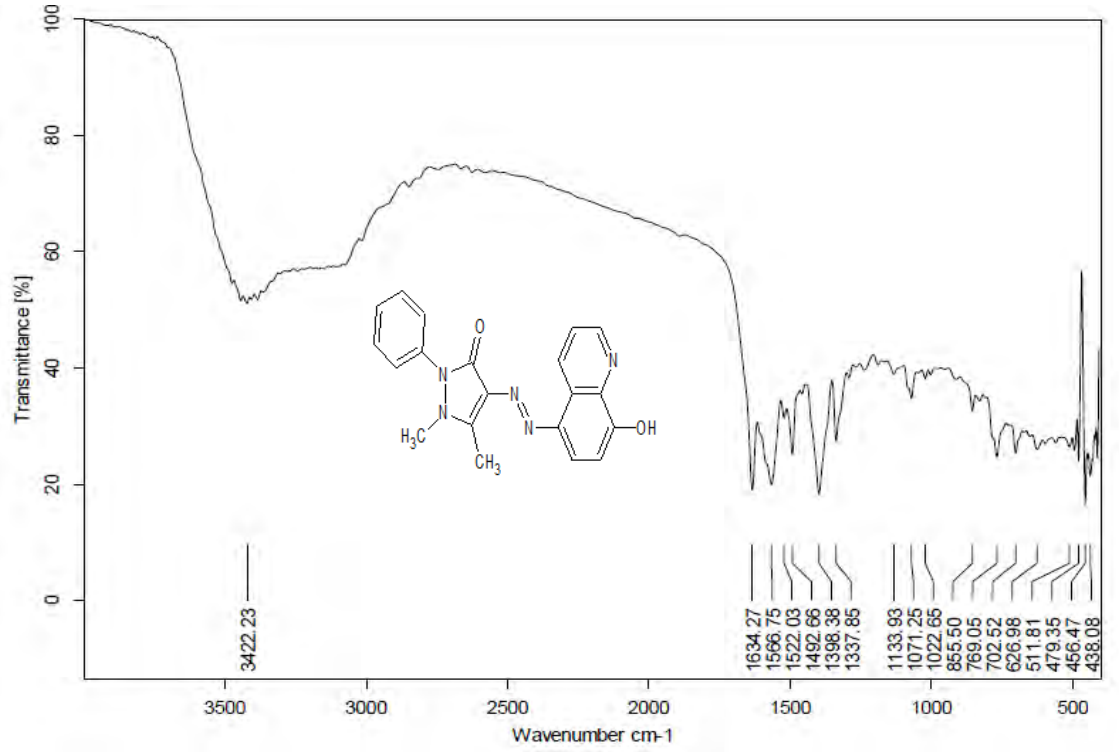

Fig.6.4a FT-IR Spectrum of free azo dye.

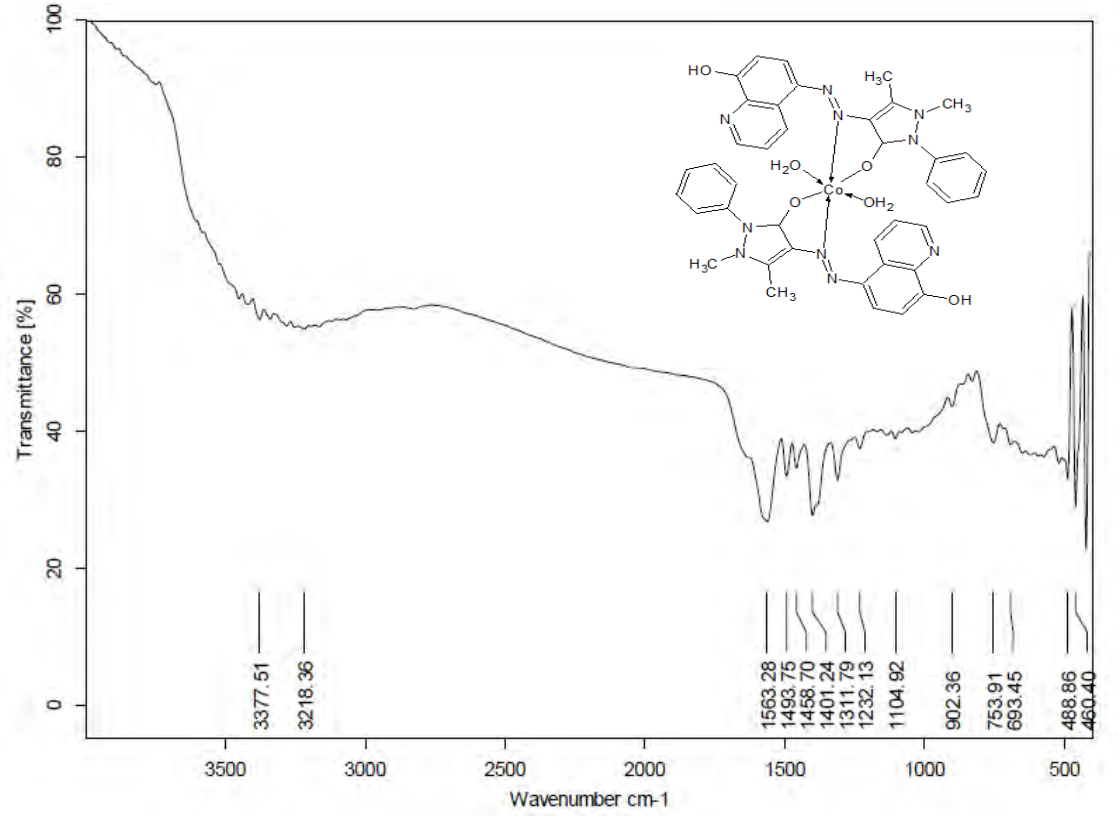

Fig.6.4b. FT-IR Spectrum of Co(II) Complex of ligand HL_5.

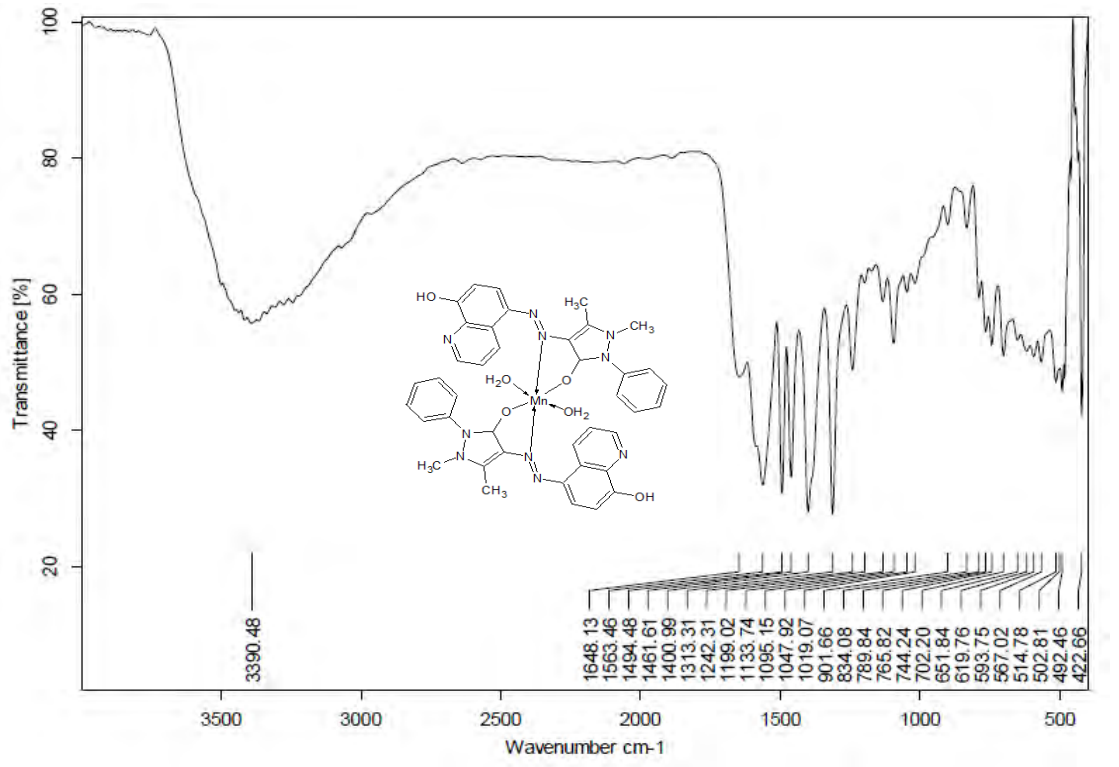

Fig.6.4c. FT-IR Spectrum of Mn(II) Complex of Ligand HL_5.

6.3.4. Mass spectra.

The data showed that the molecular ion peaks are in good agreement with their recommended empirical formula depicted in **Fig.6.5a** to **Fig 6.5c**. The mass spectra of the ligand exhibited a well-defined molecular ion peak at m/z = 359 molecular ion (parent peak), peak at 360 m/z was due to (M+1) which agree with the molecular weight of the ligand. The fragment peak corresponds to $C_{13}H_{13}N_4O$ at m/z = 241 which indicates the formation of azo compound. The mass spectra of the Co(II) and Mn(II) complex exhibited molecular ion peak at m/z valve 815 and 811 respectively. This supports the ligand to metal stoichiometric ratio of 1:2 that is ML_2 type.

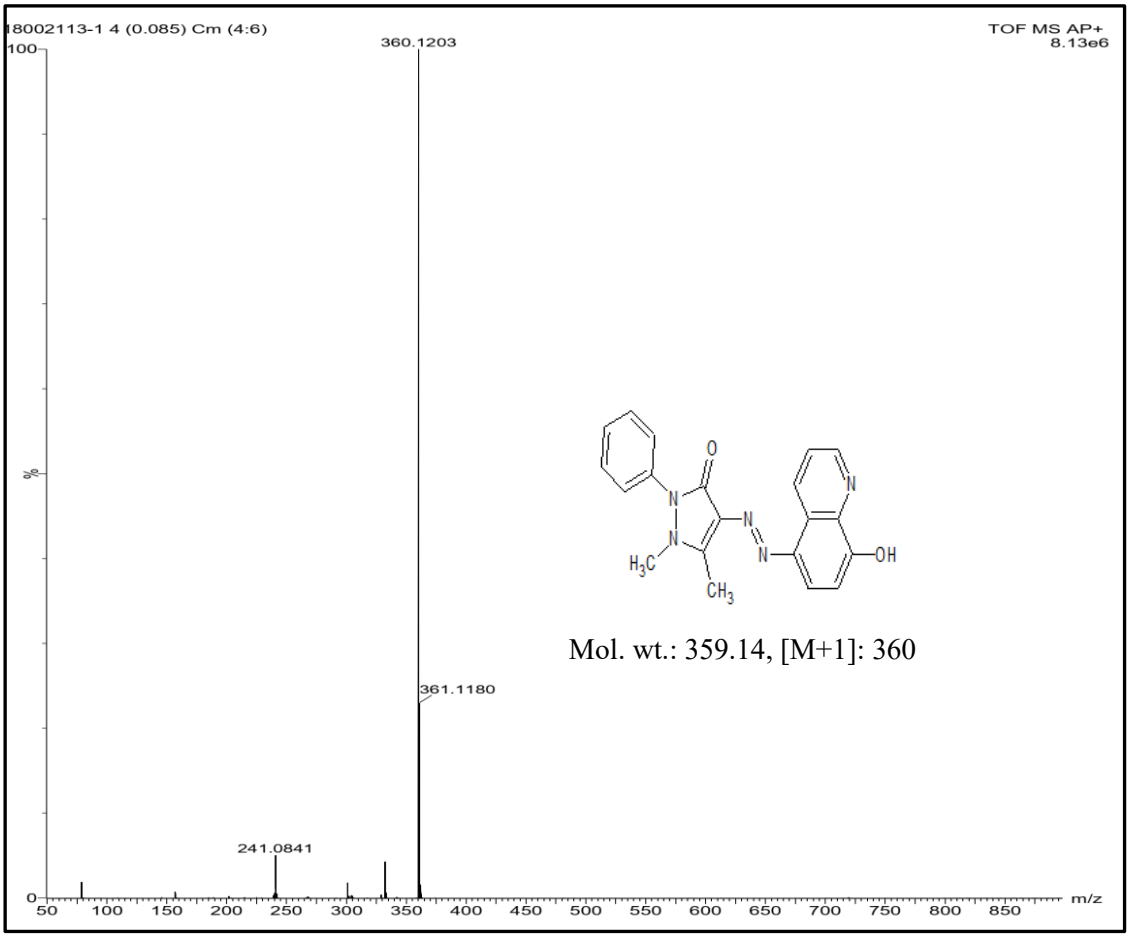

Mol. wt.: 359.14, [M+1]: 360

Fig.6.5a. Mass Spectrum of azo dye HL_5.

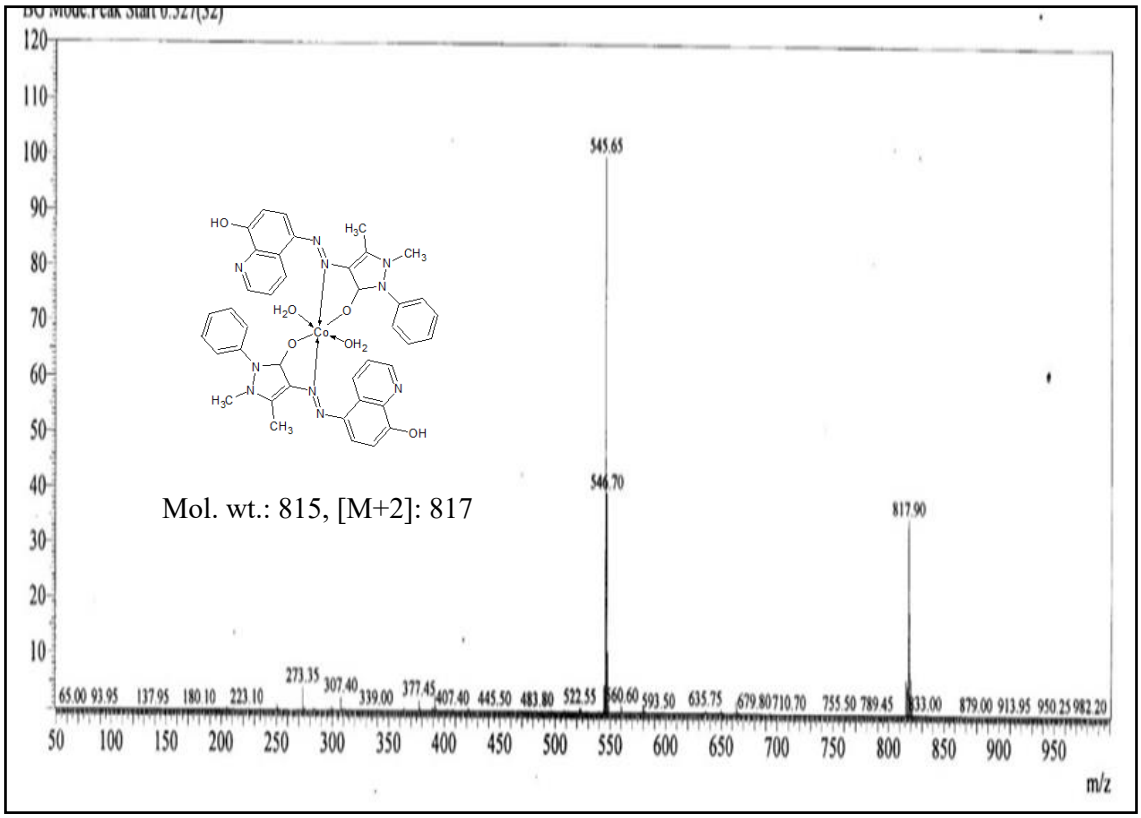

Fig.6.5b. Mass Spectrum of Co(II) Complex of ligand HL_5.

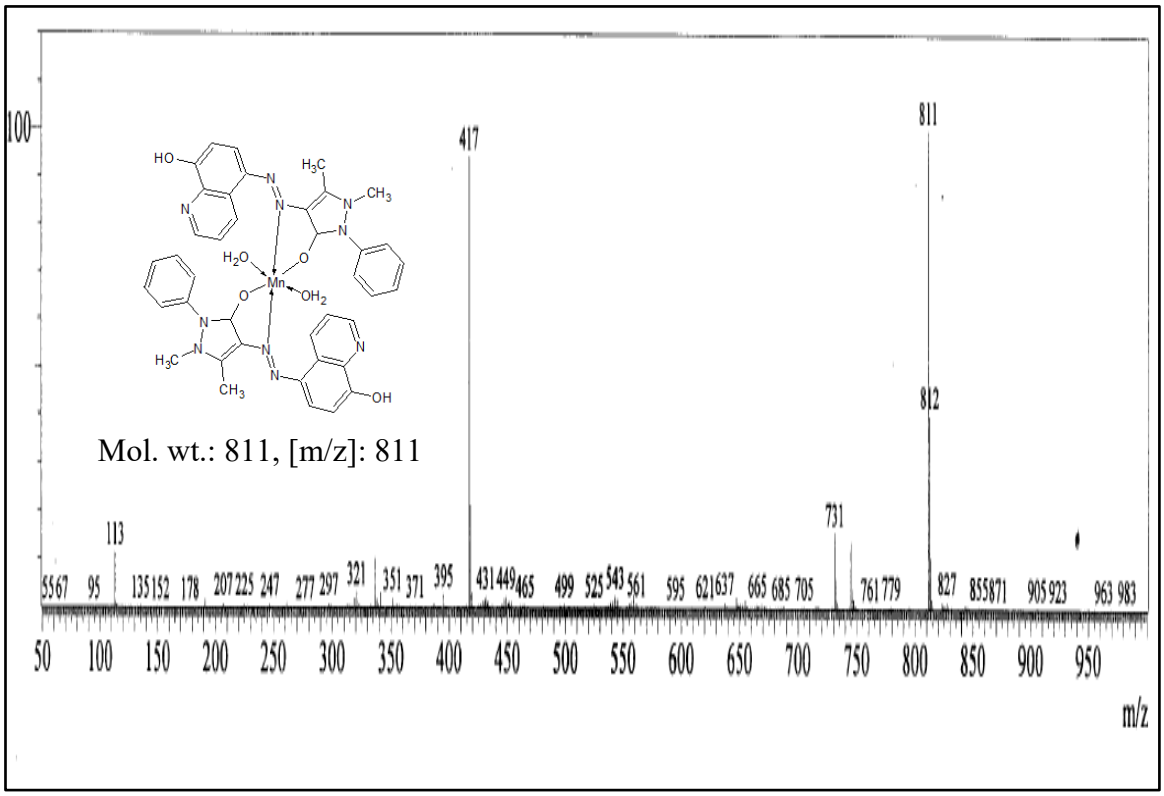

Fig.6.5c. Mass Spectrum of Mn(II) Complex of ligand HL_5.

6.3.5. Thermal Studies.

The thermal properties of metal complexes were investigated by Thermogravimetric (TG) Analysis and Differential Scanning Calorimetry (DSC) in the temperature range of 30-800 °C at nitrogen atmosphere and the weight loss was observed in room temperature as given in **Fig.6.6a- 6.6b** and summarized in **Table 6.4.**

The Co(II) complex showed three stages of decomposion. The first step attributed to the loss of strongly coordinated water molecule (found / calc 6.46/6.52) with in the temperature range of 40-110 °C, in the second stage the dissociation of organic part that is, the non-Coordinated quinolin-8-ol group ($C_{18}H_{14}N_2O_2$) (found /calc 34.67/35.02) takes place within the temperature range 111-370 °C. In the third step the dissociation coordinated heterocyclic moiety (found/calc 53.4/52.18) with in the temperature range 370-440 °C. Further, heating resulted in continuous loss of mass, indicating the decomposition of the molecules, which was not complete up to 800 °C due to the presence of metal oxide. The overall dissociation was found to be ~93 %.

The Mn(II) complex also shows three stages of decomposition in the first stage the loss of weekly coordinated water molecule (found/ calc 6.47/6.53) at a temperature range 47-90 °C. In second stage ~320 °C intimates the dissociation of non-coordinated quinolin-8-ol group (found/ calc 36.7/35.081) at a temperature range 91-390 °C. In third step, the loss of aminophenazone moiety (found/ calc 51.4/52.23) attributed at high temperature ~450 °C, probably was due to the intermolecular π interation. Further, heating was continues to 800 °C to form a nickel oxide.

Table 6.4. Thermal decomposition of the metal complexes at nitrogen.

Complexes	Stages	Temp Range In (^{0}C)	Dsc Peak	Mass Loss (%) Found (Calc)	Probable Assignments	Residue
Co(II) Complex	Stage1 Stage2 Stage3	34-110^{0}C 111-370^{0}C 370-440^{0}C	114.8 317 434	6.46(6.52) 34.67(35.02) 53.4(52.18)	loss of $2H_2O$ Loss of $C_{18}H_{14}N_2O_2$ Loss of $C_{22}H_{24}N_8O_2$	CoO
Mn(II) Complex	Stage 1 Stage 2 Stage 3	47-90^{0}C 91-390^{0}C 390-450^{0}C	54 266 361 461	6.47(6.53) 36.7(35.081) 51.4(52.23)	loss of $2H_2O$ Loss of $C_{18}H_{14}N_2O_2$ Loss of $C_{22}H_{24}N_8O_2$	MnO

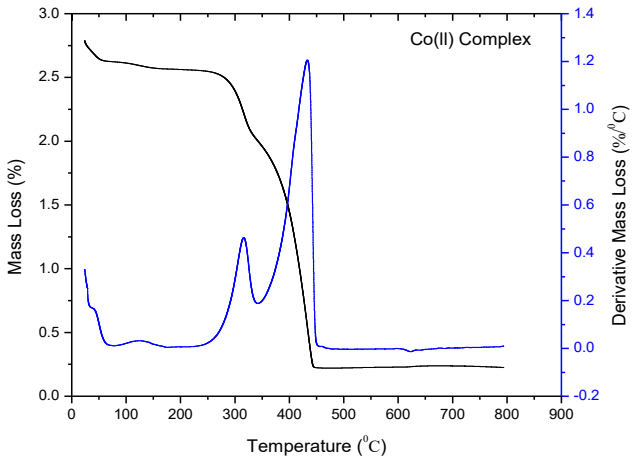

Fig. 6.6a. TG/DSC curve of Co(II) metal complex.

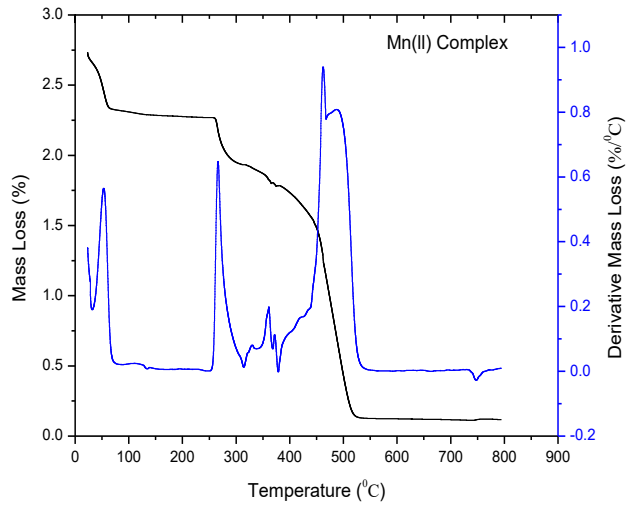

Fig. 6.6b. TG/DSC curve of Mn(II) metal complex.

6.3.6. SEM Images.

Scanning electron micrograph (SEM) has been used to study the morphology and the grain size of the ligand and the metal complexes. The SEM photograph of the complexes was shown in **Fig. 6.7** which was taken in different scale ranges from 10 μm to 100 μm. The SEM photography of the ligand demonstrated nonuniform platelet-like structure with variable lateral dimensions [32]. For Co(II) complex niddle shaped structure was observed and irregular shaped grains were seen in Mn(II) complexs.

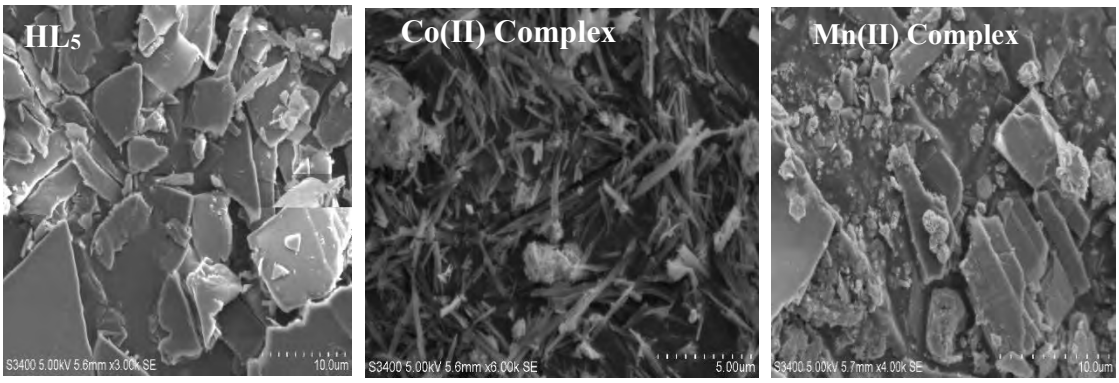

Fig. 6.7. SEM image of azo dye ligand and its metal complexes.

6.3.7. XRD studies.

To check the crystallinity of the synthesized metal complexes the powdered X-ray diffraction spectroscopy was used. The metal complexes are partially soluble in organic solvents single crystals are not obtained to study single crystal XRD. There four we recorded the powdered XRD pattern of the Co(II) and Mn(II) complexes and their respective data were shown in **Fig.6.8a and 6.8b.** And the data was recorded in **Table 6.5**a and **Table 6.5b**. The Cobalt complex shows certain amount of crystallinity whereas Mn(II) complex was amorphous in nature.

The X-ray diffractogram of metal complexes were obtained in the range of 10-80 (2θ) at a wavelength of 1.54 Å. The XRD pattern of Co(II) and Mn(II) complexes shows 10 and 9 reflection in the range 9 to 40^0(2θ). The inter planar spacing were

calculated by means of Bragg's equation nλ= 2dsinθ (where λ=1.5406 Å). The obtained and calculated d-spacing values were found to be in good agreement. The unit cell calculations were calculated for cubic symmetry by all the obtained peaks, miller indices (*h k l*) values were determined. The $h^2+k^2+l^2$ values of Co(II) 1, 6, 7, 8, 11, 13 and 16. For Mn(II) was found to be 1, 3, 8, 10, 11, 15, 17, 21 and 22. The calculated lattice parameter for Co(II) complex found to be a=b=c= 12.8 and for Mn(II) Complex a=b=c= 17.1. The existence of forbidden number 7 for Co(II) and 15 for Mn(II) indicates that complexes may belong to hexagonal or tetragonal systems.

Table 6.5a. Powdered XRD data of Co(II) Metal complexes.

Peak number	2Θ	Θ	SinΘ	Sin^2 Θ	1000 sin^2 Θ	$h^2+k^2+l^2$ (1000sin^2 Θ/CF)	*h k l*	D Obs	D cal	a in A^0
1	6.9057	3.452	0.0602	0.003625	3.625	1(1)	100	12.793	12.800	12.79
2	16.2760	8.138	0.1415	0.02003	20.03	5.52(6)	211	5.441	5.446	13.33
3	18.8127	9.406	0.163	0.02671	26.71	7.36(7)	--	4.713	4.717	12.46
4	19.6690	9.834	0.1708	0.02917	29.17	8.04(8)	220	4.510	4.513	12.75
5	22.7479	11.373	0.1972	0.03888	38.88	10.72(11)	311	3.906	3.909	12.95
6	25.7479	12.593	0.2180	0.04753	47.53	13.11(13)	320	3.533	3.235	12.73
7	27.4482	13.724	0.2372	0.05628	56.28	15.52(16)	400	3.246	3.249	12.98
8	29.4582	14.729	0.2542	0.06464	64.64	17.83(18)	411	3.029	3.032	12.85
9	32.6210	16.310	0.2808	0.07887	78.87	21.75(22)	332	2.742	2.745	12.86

Table 6.5b. Powdered XRD data of Mn(II) Metal complexes.

Peak number	2Θ	Θ	SinΘ	Sin^2 Θ	1000 sin^2 Θ	$h^2+k^2+l^2$ (1000sin^2 Θ/CF)	h k l	D Obs	D cal	a in A^0
1	5.1632	2.5816	0.0450	0.00202	2.028	1(1)	100	17.101	17.116	17.10
2	9.3787	4.6893	0.0817	0.00668	6.683	3.29(3)	111	9.422	9.422	16.31
3	14.3955	7.1977	0.1252	0.01569	15.69	7.74(8)	220	6.147	6.153	17.39
4	16.1954	8.0976	0.1408	0.01984	19.84	9.78(10)	310	5.468	5.473	17.29
5	17.3696	8.6848	0.1509	0.02280	22.80	11.24(11)	311	5.101	5.105	16.91
6	19.9378	9.9689	0.1731	0.02996	29.96	14.77(15)	---	4.449	4.449	17.23
7	21.2131	10.6068	0.1840	0.03388	33.88	16.70(17)	410	4.184	4.188	17.25
8	23.6635	11.8317	0.2050	0.04204	42.04	20.72(21)	421	3.756	3.759	17.21
9	24.6174	12.3087	0.2131	0.04544	45.44	22.40(22)	332	3.613	3.613	16.94

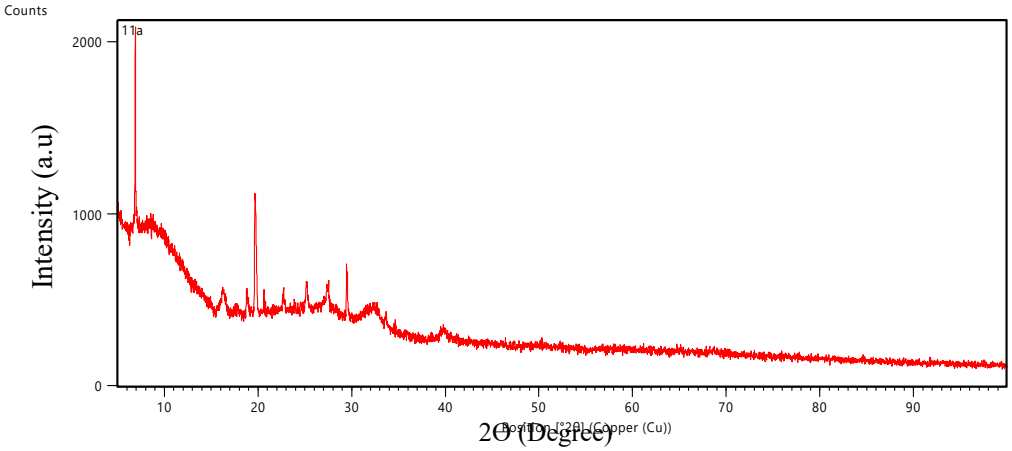

Fig.6.8a.Powdered XRD data for Co(II) metal complex.

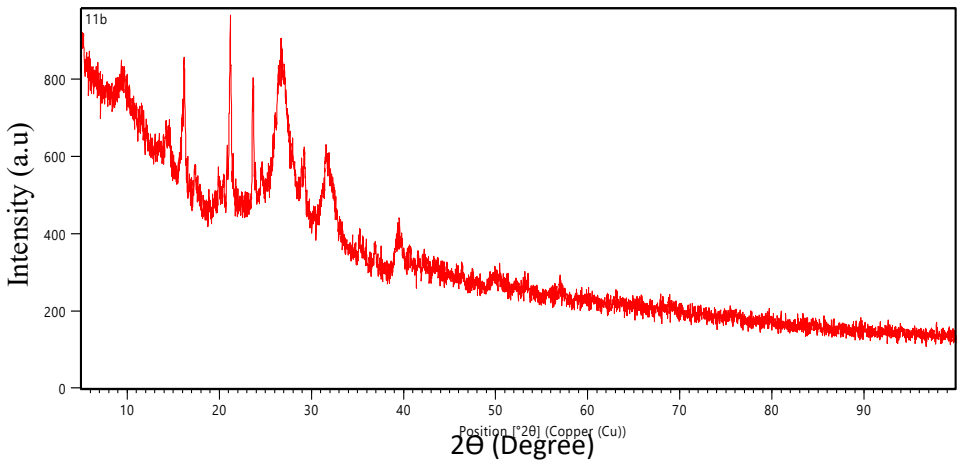

Fig.6.8b. Powdered XRD data for Mn(II) metal complex.

6.3.8. Photoluminescence Spectra.

Photoluminescence Spectra of the ligand and azo metal complexes were recorded in room temperature using DMSO as a solvent. The samples were excited by single excitation wavelength of 400 nm with the excitation source of 450 W Xenon lamp as shown in **Fig.6.9**. The emission spectra of the ligand showed the excitation at 400 nm. The free azo dye ligand exhibited intraligand π-π* transitions. The emission spectrum of Co(II) showed strong emission peck at 530 nm at the excitation of 400 nm. But Mn(II) complexes showed emission peak at 700 nm at the excitation of 400nm. The decreased intensity of Mn(II) complex may be due to the formation of metal complexes and the energy transfers from the excited ligand to the metal ion [33]. The significant difference in position and intensity of the metal complexes shows the coordination of the metal ion to the peripheral ligand. In general, all the synthesized compounds can serve as potential photoactive materials, as indicated from their characteristic photoluminescence property.

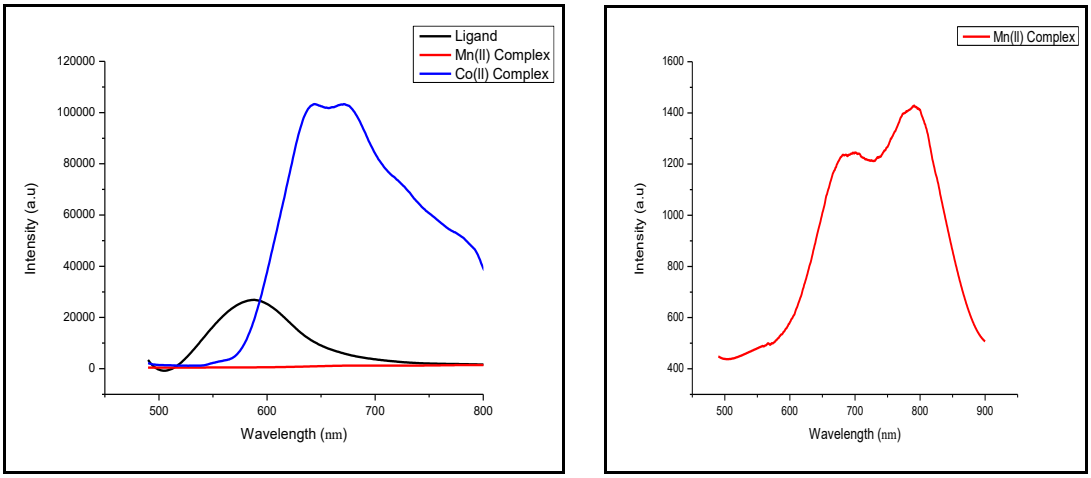

Fig. 6.9. Photoluminescence spectra of the HL_5 and its metal complexes.

6.3.9. Biological Activity.

The transition metal complexes exhibit a significant biological activity. Many of the reports published a biological activity of the metal complexes having heterocyclic ligand. Transition metal complex shows excellent antimicrobial, anti-oxidant, antituburculosis activity. In order to know the phtosensitising activity we have carried out antimicrobial PDT, anticancer activity and also insico molecular docking studies.

6.3.9.1. Antimicrobial photodynamic therapy.

The azo metal complexes are screened for their photodynamic inactivation studies against *E. coli, S. aureus and C. albicans* species in DMSO. And the detailed procedure was described in **Section 3.3.7.1** of **Chapter 3.** The results were displayed in **Fig.6.10a-6.10c.** Photodynamic therapy with synthesized metal complexes at high concentration promotes a significant reduction in the number of CFU mL^{-1} of bacteria and fungi.

Result and Discussion.

The results of this demonstrated that photosensitizers with xenon lamp at the concentration of 200 μg/mL showed significant reduction in plantonic cells when compared to the MB. The antimicrobial photodynamic therapy is an operative process in presence of light. Based on these results, order of susceptibility of bacteria towards photolysis in presence of Co(II) and Mn(II) complex is given as *S: aureus > E: coli >C.albumin*

The percentage inhibition of metal complexes over bacterial species *S. aureus* was high when compare to gram negative bacteria *E. coli.* This is because gram negative bacteria was more resesistance than gram positive bacteria, due to the structural difference of the gram negative bacteria and the presence of an additional

and more negatively charged outer layer, serves as a barrier to prevent the entry of outer species. The percentage inhibition of *S. aureus* of Co(II) complex was high when compared to Mn(II) complex this may due to the high abortion in fluorescence, the photons will not have sufficient energy for the ground state oxygen molecule to excite the singlet oxygen and shorter wavelength leads to less tissue penetration and more likely leads to skin photosensitivity, The cell death rate of *C.albumin* was absorbed to be 74 and 70% for Co(II) and Mn(II) metal complexes. Where the percentage death was decreased compared to bacteria. Antifungal APDT involves more complex mechanisms.

For both the complexes the concentration dependents on growth inhibition trend as observed. This is because of self-shielding of the photosensitizer, molecules will absorbs the light at top of the sample which will prevent the light penetration through the sample and activation of the photosensitizer below it leads to the generation of ROS at aproximal location to the targeted bacteria [34].

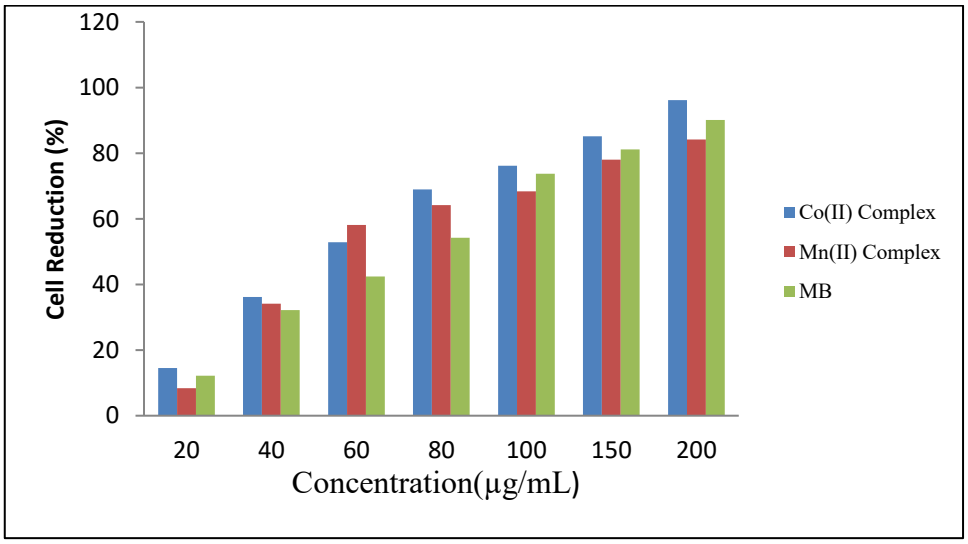

Fig.6.10a. Relative cell reduction of *Staphylococcus aureus.*

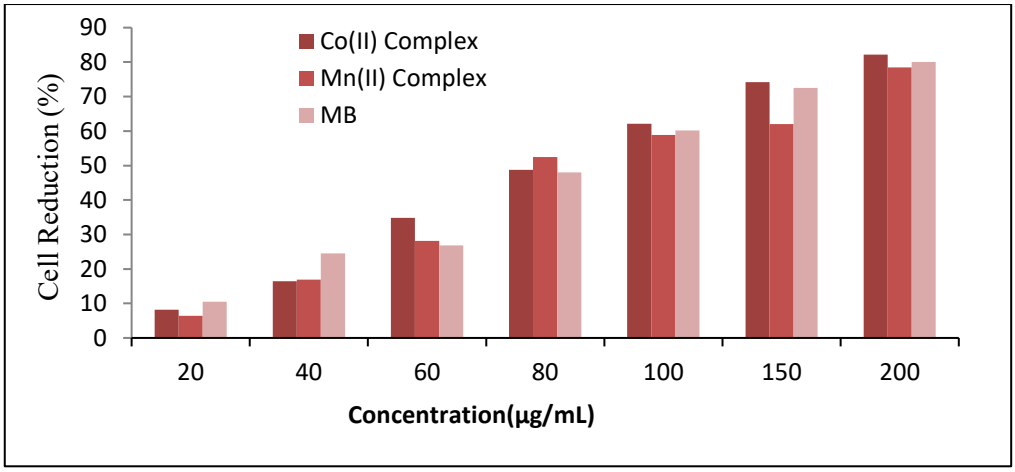

Fig.6.10b. Relative cell reduction of *E. coli.*

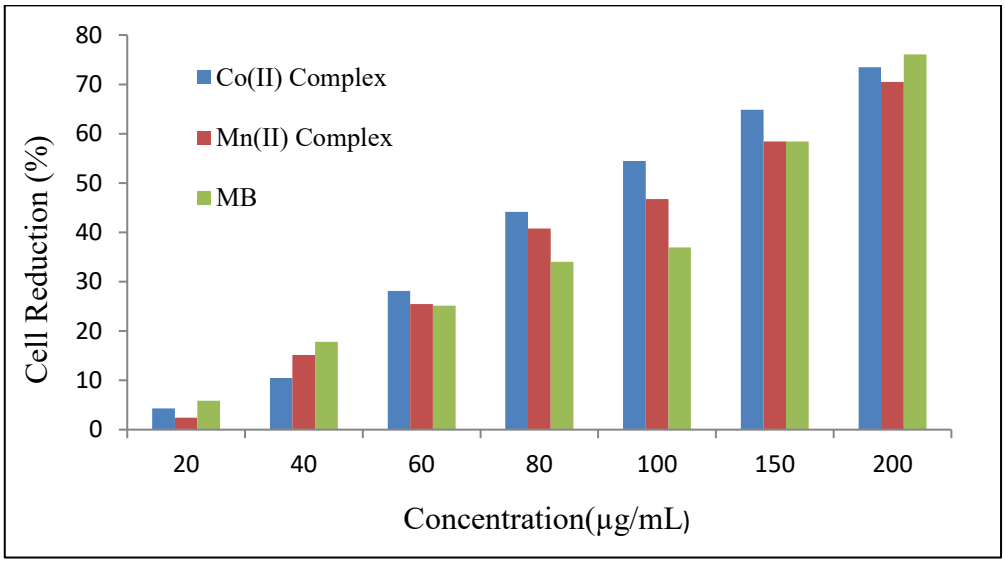

Fig.6.10c. Relative cell reduction of *C.albumin* fungi.

6.3.9.2. *In-Vitro* Anti-Tumor Activity.

It has been known from the decades that cancer is deadly disease in spite of having many advanced treatments. The treatment of this disease remains a interesting, due to various factors like lack of selectivity in drug design, toxicity. In spite of having the most advanced technology to cure cancer, at some point emergency of old and new antibiotic resistance created in the last few years [35]. This leads to lots of interest to develop a drug. Therapeutic potential of metal complexes in cancer therapy has attracts a researcher, mainly because metals exhibit unique characteristics, such as

redox activity, variable coordination modes and reactivity toward the organic substrate. These properties help to bind the metal complexes to bimolecular target with a resulting modification in the cellular mechanism of proliferation [36]. Numerous metal-based compounds have been synthesized with promising anticancer properties i.e., cis-platin and carboplatin, but in the mean while they also have limitation [37]. Therefore, it is more important to design a drug which kills the cancer cell by inhibiting the activity of the protein that causes the disease. Herein, we tried to test the anticancer activity of the synthesized metal complexes against Human melanoma (A-375) and human primary glioblastoma (U-87) cell line by MTT assay.

The well-established method to evaluated viability of the cell is MTT assay methods. Human melanoma (A-375) and human primary glioblastoma (U-87) were used as cell lines. The cell pellets were maintained in DMEM-HG, the cells were grown in 96 well tissue culture plates. The metal complex of different concentration (50, 100, 150, 200 and 250 µg/mL) and Cis-platin the final volume of 200 µL were treated with selected cell lines for about 24hrs. After incubation 20 µL of MTT reagent 0.5mg/mL concentration was added to each well and incubated for further 3hrs. The medium was replaced with DMSO (100µL/well) to dissolve the formazan crystals. The effects of the different test compounds on the viability of the tumor cell lines were measured at 540 nm using a multimode reader. All samples (five concentrations of each sample) were tested in triplicate and using origin software, IC_{50} values with standard deviation were calculated [38].

Result and Discussion.

The anticancer activities of metal complexes were analyzed against two tumour cell lines using MTT assay. Different concentrations of complexes (50, 100, 150, 200 and 250 µg/mL) were treated with the tumour cell lines and clinical drug Cis Platin

was used as a controle. The metal complex's inhibited the growth of cancer cells with the increase in concentration of the drug. At higher concentration, IC_{50} values and cell viability were given in **Table 6.6. Fig.6.11a-6.11b** shows that metal complexes exhibited good cytotoxic activity.

The synthesized compound showed good cytotoxic activity but lesser activity when compared to standard drug. The Co(II) complex shows better activity than Mn(II) complex. This selectivity may be explained based on the mode of action of cobalt complex. The Co(II) ions are able to induce in the formation of ROS in physiological conditions, thus the increase of ROS levels leads to oxidative macromolecular damage and elimination of cancer cells. Thus, increasing the ROS levels is a promising anticancer strategy. For the complex the IC_{50} value was more than 100, this indicated that the complex probably was non-toxic in nature [39].

Table.6.6. IC_{50} values of azo metal complexes on A-375 and U-78 cancer cells.

Compound	A-375 (IC_{50})	% Inhibition	U-78(IC_{50})	% Inhibition
Co(II) Complex	74	92	115	84
Mn(II) Complex	50.5	74	42	64

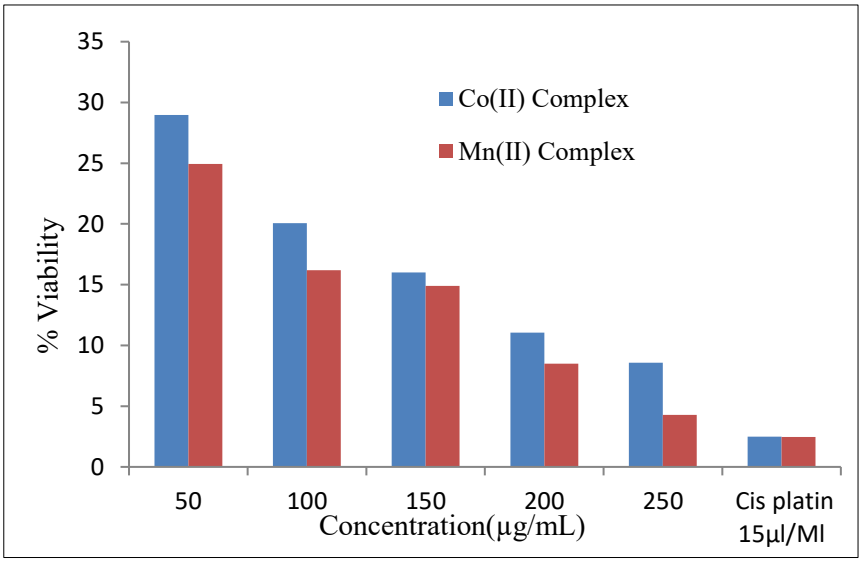

Fig.6.11a. Cytotoxicity activity of metal complex with U-87 cell line

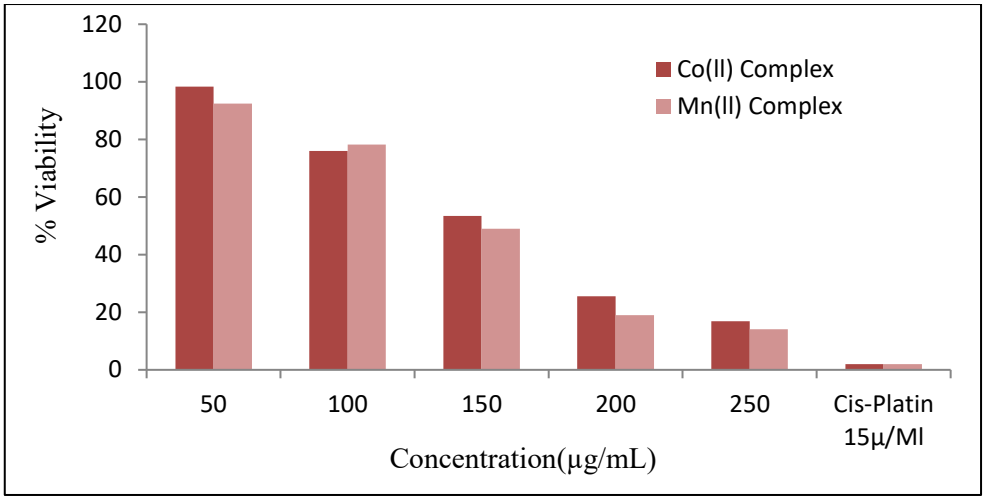

Fig. 6.11b. Cytotoxicity activity of metal complex with A-378 cell line

6.3.9.3. Insilico Molecular Docking Studies.

Molecular docking plays a key role in the drug design, this is an estimated computational method to investigate the drug-nucleic acid interactions for the modern drug design and also to discover the exact binding site offered at the molecular target DNA. The detailed protocol of molecular docking studies was described in **Section 3.3.7.4** of **Chapter 3**. The results shows that the Co(II) complex shows the highest binding energy.

Result and discussion.

All the synthesized metal complexes were employed to understand the interaction between the metal complexes with the target receptor molecules (RpsA). The binding sites of complexes on DNA are shown in **Fig.6.12**. All the synthesized complexes have the capacity to interrelate with DNA through a small groove. The metal complexes shows a hydrophobic interation with Arg 350, Arg 355, Arg 356,Arg 357, Ile 349, Ser 359, Tyr 280, Vgl 502 and vgl 1051. The Co(II) complex showed the highest binding energy of -3.55 and showed good interactions with the DNA.

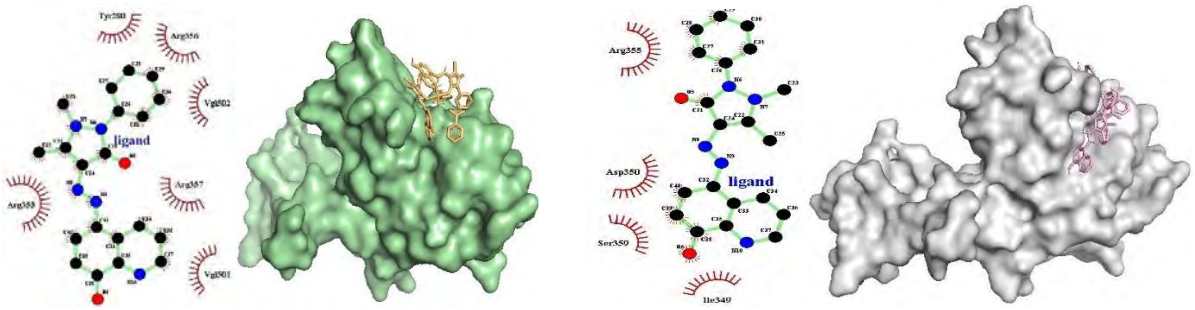

Co(II) Complex **Ni(II) Complex**

Fig.6.12. Three-dimensional molecular docking studies of synthesized metal complexes

6.4. Conclusion.

In conclusion, a series of novel photosensitizes based on azo derivatives were synthesized, and their photo physical and photochemical properties were investigated. The spectral studies suggest that the ligand was coordinated with the metal ion through the oxygen of the 4-aminoantipyrin and the nitrogen of the azo group with the octahedral geometry. The thermal data of complexes demonstrate the presence of water molecule in the complex. The synthesized complexes were evaluated for cytotoxicity and APDT studies. Both the complexes showed cytotoxic activity, but Cobalt complex was more active towards human melanoma cell line. The antimicrobial photodynamic activity of *S.aureus, E.coli* and fungus *C.albicans* was tested. The highest cell reduction was found to be 96% in S.aures at a concentration of 200 µg/mL. The effective binding interactions between the tested compounds and the target receptor RpsA was studied by using insilico molecular docking studies. This shows that metal complexes with azo ligand, proves to be promising candidates as photoactive antimicrobial activity and also alternatives to the anticancer drug.

6.5. Reference.

1. A. Juarranz, P. Jaen, F. Sanz Rodriguez, J. Cuevas and S. Gonzalez, *Clin. Transl. Oncol*., 10, 148-154, **2008**.
2. R. R. Allison, H. C. Mota and C. H. Sibata, *Photodia. Photodyn. Ther*., 1(4), 263-77, **2004.**
3. M. D. Ron, R. Allison and H. Claudio Sibata*, Photodia. Photodyn. Ther.,* 7, 61-75, **2010**.
4. L. C. Izekova, A. Grolmusova, Z. Ipothova, Z. Barbierikova, V. Brezova, L. Hunakova, J. Imrich, L. Janovec, I. Dovinova and H. Paulikova, *Bioorg. Medic. Chem.,* 22, 4684–4693, **2014**.
5. A. Gasparetto, T. F. Lapinski, S. R. Zamuner, S. Khouri, L. P Alves, E. Munin, Marcos and J. Salvador, *J. of Photochem. Photobio. B: Biol.,* 99, 15–20, **2010**.
6. N. Barbero, S. Visentin and G. Viscardi, *J. of Photochem. Photobio. A Chem.*, 299, 38–43, **2015**.
7. A. P. Castano, T. N. Demidova and M. R Hamblin, *Photodia. Photodyn. Ther.,* 1, 279, **2004**.
8. M. S. Baptista and M. Wainwright Braz, *J. Med. Biol. Res.,* 44(1), 1-10, **2011**.
9. M. S. Muthumuni Managa, K. Edith Amuhaya and Tebello Nyokong, *Spectrochim. Acta Part A: Mole. Biomole. Spectr*., 151, 867–874, **2015**.
10. Y. D. Kim, J. H. Cho, C. R. Park, J. H. Choi, C. Yoon and J. P. Kim, *Dyes and Pigm.,* 89, 1-8, **2011**.
11. K.Vinod, M. Gohain, H. Johannes Van Tonde, S. Ponra, B.C.B. Bezuindenhoudt and O.M. Ntwaeaborwa, *Opti. Mate*., 50, 275–28, **2015**.
12. N.C. Warshakoon, J. Sheville, R. T. Bhatt, J. W. Mendez-Andino, K. M. Meyers, N.Kim, J. A. Wos, C. Mitchell, J. L. Paris, B. B. Pinney, O. Reizes and Hu XE, *Bioorg, Med. Chem. Lett.* 16(19), 5207-11, **2006**.
13. M. Manjunath, D. Ajaykumar Kulkarni, B. Gangadhar Bagihalli, Shridhar Malladi and A. Sangamesh Patil, *J. of Mole. Stru.,* **2016**.
14. S. Kumar, S. Bawa and H. Gupta, *Mini-Reviews in Med. Chem.,* 9, 1648-1654, **2009**. ·
15. H. R. Zhang, K.B. Huang, Z.F. Chen, Y.C. Liu, Y.N. Liu, T. Meng, Q.P. Qin, B. Q. Zou and H. Liang, *Med. Chem. Commun.* 1-3, **2016**.
16. M. C. Prabahkara and H. S. Bhojya Naik, *Biometals.,* 21, 675–684, **2008**.

17. M. A. Gouda, H. F. Eldien, M. M. Girges and M. A. Berghot, *J. of Saudi Chem. Soci*., 20, 151–157, **2016.**
18. C. N. Sudhamani, H. S. Bhojya Naik and D. Girija, *Synth. React. Inorg. Met. Org. Nano Met. Chem.*, 42, 518–524, **2012**.
19. A.Vakhid Mamedov, R. Venera Galimullina, A. Nataliya Zhukova, F. Saniya Kadyrova, V. Ekaterina Mironova, I. K. Rizvanov and K. Shamil Latypov, *Tetrahed. Let.,* 55, 4319–4324, **2014**.
20. A. Saylam, Z. Seferoglu and N. Ertan, *J. of Mole. Liq.,* **2014**.
21. S.Grazyna Karpin, P. Aleksander Mazurek and J. Dobrowolski. *J. of Mole. Stru.,* 961, 101–106, **2010**.
22. M. Manjunath, D. Ajaykumar Kulkarni, B. Gangadhar Bagihalli, Shridhar Malladi and A.Sangamesh Patil, *J. of Mole. Stru.*, **2016**.
23. N. Venugopal, G. Krishnamurthy, H.S. Bhojyanaik and P. Murali Krishna, *J. of Mole. Struc.,* **2019**.
24. C.N. Sudhamani, H.S. Bhojya Naik, T.R. Ravikumar Naik, M.C. Prabhakara. *Spectrochim Acta A,* 72, 643–647, **2009**.
25. S.M. Pradeepa, H.S. Bhojya Naik, B. Vinay Kumar, K. Indira Priyadarsini, Atanu Barik and M.C. Prabhakara, *Spectrochim. Acta Part A: Molec. Biomole. Spectr.,* 141, 34–42, **2015**.
26. S.M Pradeepa, H. S. Bhojya Naik, B. Vinay Kumar, K. Indira Priyadarsini, Atanu Barik, T.R. Ravikumar Naik, M.C. Prabhakara. *Spectrochim. Acta A,* 115, 12–21, **2013**.
27. A. Kavitha, A. Sanmugam, E. Deivanayagam, K. Karuppasamy, H. S. Kim and D. Vikramanb, *Scientific Repo*., 8, 3054, **2018**.
28. T. Manjuraj, G. Krishnamurthy, D.Yadav Bodke, H.S. Bhojya Naik and H.S. Anil Kumar, *J. of Mole. Stru.,* 1171, 481-487, **2018**.
29. M. Sennappan, P. Murali Krishna, R. Ranganathan and P. Sivakami sundari, *Jnal of Molecular Structure*, **2018**.
30. A. F. Sherif Rostom, M. Ibrahim El-Ashmawy, A. Heba Abd El Razik, H. Mona Badr, M. A. Hayam Ashour, *Bioorg. Medi. Chem.,* 17, 882–895, **2009**.
31. L. Xiaoyi, W.Yiqun, G. Donghong, and Fuxi Gan, *Dyes and Pigm.*, 86, 182-189, **2010**.
32. C. Narendra Kumar and M. Parashuram, *Hindawi Bioinor. Chem. and Appl.,* **2017**.

33. S. Zhiyuan, S. Zhou, H. Qiu, G. Ying and Yuxia Zhao, *RSC Adv*. 8, 17073, **2018**.

34. M. Corona Cassidy, F. Ryan Donnelly, J. Stuart Elborn, D. Nicholas Magee, M. Michael Tunney, *J. of Photoche. Photo. B: Biol.,* 106, 95–100, **2012**.

35. S. Leonard, P. M. Gannett, Y. Rojanasakul, D. Schwegler Berry, V. Castranova, V. Vallyathan, X. Shi, *J. of Inorg.Bioche.*, 70, 239-244, **1998**.

36. A. Hanakovaa, K. Bogdanova, K. Tomankova, K. Pizova, J. Malohlava, S. Binder, R. Bajgar, K. Langova, M. Kolar, J. Mosinger, H, Kolarova, *Microbio. Reser.,* 169, 163–170, **2014**.

37. Z. Yaghobi, Z. Rashidi Ranjbar and S. Gharbi, *Polyhed.,* 164, 176–184, **2019**.

38. K. R. Sangeetha Gowda, H. S. Bhojya Naik, B. Vinay Kumar, C. N. Sudhamani, H. V. Sudeep, T. R. Ravikumar Naik and G. Krishnamurthy, *Spectrochim Acta A.,* 105, 229–237, **2013**.

39. C. M. Cassidy, R. F. Donnelly, J. S. Elborn, N. D. Magee and M. M. Tunney, *J. Photochem. Photobiol. B*, 106, 95, **2012**.

Chapter-7

Synthesis, Characterization and Pharmacological Activity of Cu(II) and Co(II) Transition Metal Based Azo Dye Derivatives

7.1. Introduction.

Many researchers have been fascinated by the chemistry of aryl diazenato complexes of various transitional metals because of their striking structural features and applications in diverse areas, most notably in dyes and pigments [1]. Azo compounds are also used as a complexing agents and the combination of azo compounds and β-diketones are good Ligands. β-diketones as well as azo nitrogen are well known chelating agents, capable of forming stable complexes with transition metal ions [2-3]. β-diketones and their esters and anilides are found to be very good complexing agents especially for transition and inner transition metal ions [4]. Their complexing ability is enhanced by introduction of active groups like oximes, hydrazones, thiosemicarbazones etc [5]. The combination products of these two classes of chelating agents form new interesting compounds which act as very good bi or tridentate ligands [6].

Further, Abundant number of indole-containing natural and synthetic compounds ranging from lysergic acid to vincristine is being used for the treatment of various diseases. Thus, the arrangement of indole structure represents a highly significant heterocyclic system [7]. Especially, indoles that are substituted at the 2- or 3-position with a strong electron withdrawing group (i.e., nitro, phenylsulfonyl, cyano), are used in many fields. The pharmacodynamic compounds containing indole nucleus have been reported to possess a wide variety of biological properties, namely, anti-inflammatory [8,9], anticonvulsant [10], cardiovascular [11], antibacterial [12], CoX-2 inhibitor [13], and antiviral activities [14]. More specifically, several studies describe that indole-2-carbohydrazides and related compounds are endowed with antihistaminic [15], antidepressant [16] and MAO inhibitory activities [17]. The development of new transition metal containing indol in coordination with azo

nitrogen have been reported by several research groups [18]. Based on these findings and in continuation of our research work on coordination chemistry.

Therefore, from the overall observation we decide the synthesis of sulfadiazine based indol and β-diketones of two azo dyes and their coordination with the Cu(II) and Co(II) transition metal complexes. The present chapter describe the synthesis, spectral characterization, and biological studies of the synthesized hetercyclic metal complexes.

7.2. Experimental.

7.2.1. Methods and Material.

All chemicals and standard solutions were purchased from Sigma-Aldrich and used as received unless otherwise stated. The structure was confirmed by different analytical and spectroscopic techniques as described in **Chapter 2**.

7.2.2. Synthesis of azo dye (HL_6 and HL_7).

Azo ligand was synthesized by using diazotization process, briefly the mixture of sulfadiazine (0.01M) concentrated hydrochloric acid (5 mL) was stirred and cooled at 0-5 °C. The $NaNO_2$ in ice cold solution was added drop wise by maintain the temperature of 0-5 °C the reaction mixture was stirred for further 30 min. The coupling component (0.01M) in 10% KOH of 10 mL solution and cooled at below 5 °C in ice bath. This solution was then gradually added to the cooled diazonium salt solution and the resulting mixture was stirred at 0–5 °C for 1 hour. The coloured precipitate separates from the reaction mixture, The product was filtered washed with water and recrystallized from hot ethanol [19].

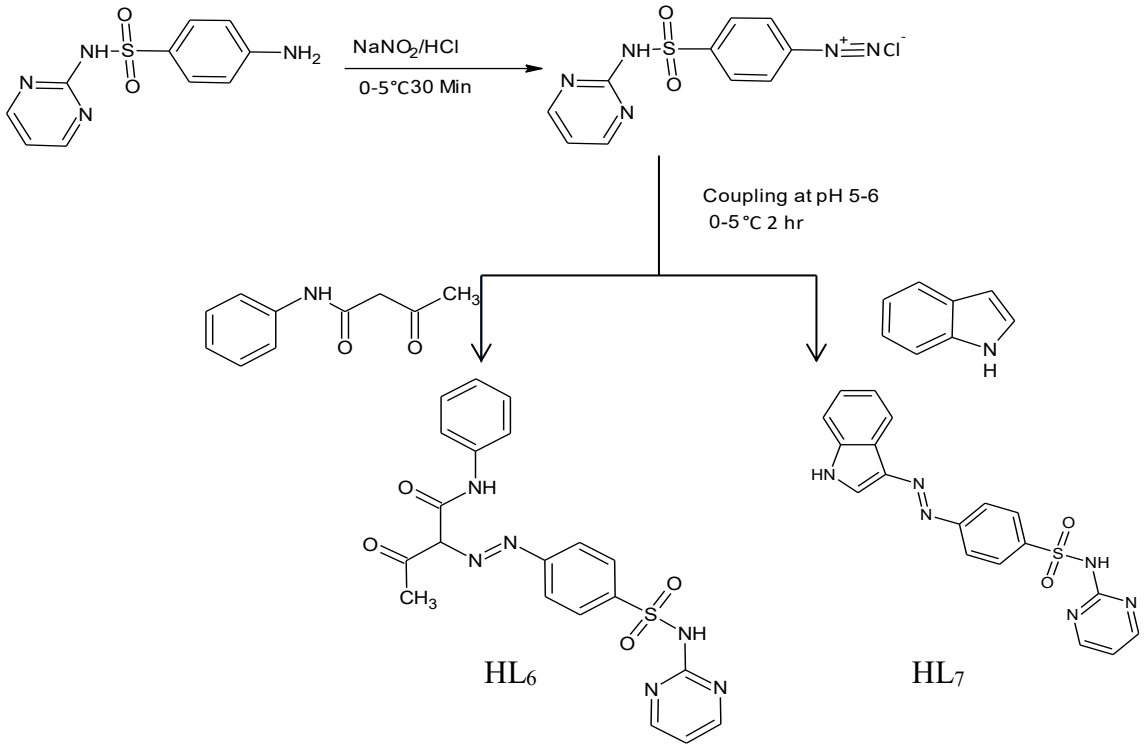

Scheme 7.1. Synthesis of azo dye ligands (HL_6 and HL_7)

7.2.3. Synthesis of Cu(II) and Co(II) metal complexes.

The Cu(II) and Co(II) metal complex was prepared by the reaction of azo dye ligands with appropriate metal hydrates in 1:1 M ratio in ethanol. The azo dye ligands (1 mM) was separately taken in 50 ml ethanol and heated on a magnetic stirrer at 60 °C for 10 min. The aqueous solution of metal hydrates (1 mM) was added dropwise to the flask with stirring. The mixture was reflexed at 60 °C for 2 hour. After completion of the reaction, colored precipitate of the respective complex separated from the reaction mixture which were filtered, washed with water, ethanol and dried at 100 °C [20]. The schematic representation was depicted in **Scheme 7.2**

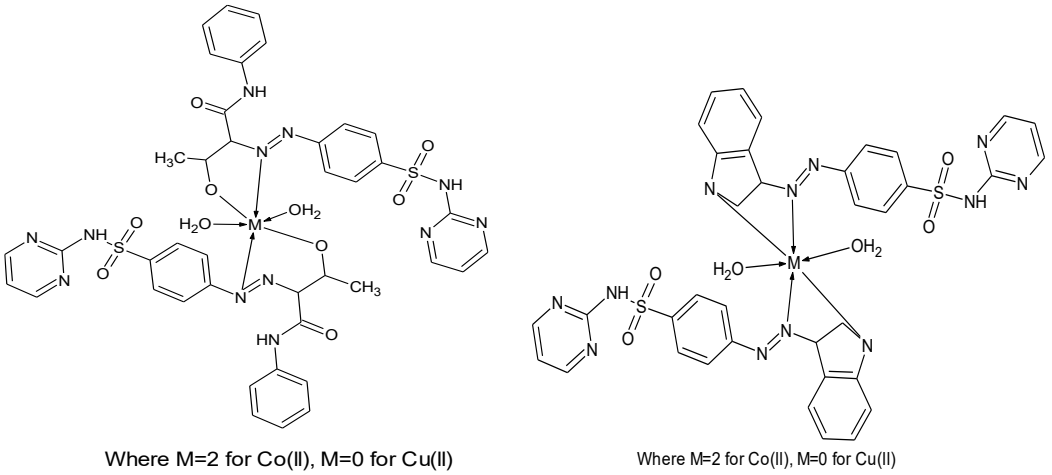

Scheme 7.2. The structure of synthesized metal complexes.

7.3. Result and Discussion.

The azo dye and its metal azo complexes have been synthesized by using different spacers. Metal azo complex and the azo ligands are stable in room temperature. The ligands are soluble in polar solvents whereas metal azo complexes are soluble in DMSO/DMF. The structure of the ligand was confirmed by using elemental analysis and the data was depicted inn **Table 7.1.** Complexes were further characterized and confirmed by various spectroscopic techniques.

Table 7.1. Elemental analysis and date of the synthesized metal complexes.

Sl No	Compound	Mol. Weight	Yield In%	MP In ^{0}C	Elemental Analyzer % Found (Calculated)					
					C	H	N	O	S	M
1	**HL_6**	438	80	250-252	54.76 (54.79)	4.10 (4.14)	19.12 (19.17)	14.00 (14.06)	7.34 (7.31)	-
2	Cu(II) complex of HL_6 (**7a**)	940	65	>300	50.90 (50.92)	4.00 (4.06)	17.80 (17.83)	13.50 (13.58)	6.84 (6.80)	6.70 (6.74)
3	Co(II) complex of HL_6 (**7b**)	900	62	>300	49.00 (49.33)	4.32 (4.35)	17.24 (17.26)	16.40 (16.43)	6.52 (6.58)	6.52 (6.58)
4	**HL_7**	378	85	278-280	56.62 (56.83)	4.26 (4.24)	22.00 (22.09)	8.40 (8.41)	8.42 (8.43)	-
5	Cu(II) complex of HL_7(**7c**)	818	58	>300	52.52 (52.58)	3.62 (3.68)	20.40 (20.44)	7.74 (7.78)	7.84 (7.80)	7.70 (7.73)
6	Co(II) complex of HL_7 (**7d**)	850	52	>300	50.60 (50.64)	4.00 (4.01)	19.60 (19.69)	11.20 (11.24)	7.51 (7.51)	6.90 (6.99)

7.3.1. ^{1}H-NMR Spectral studies.

NMR spectra were recorded using DMSO as solvent and TMS was used as an internal standard. Chemical shifts were reported in parts per million The ^{1}H-NMR spectra for both the ligands are showing the expected signals with splitting. The Spectrum of the ligand HL_6 showed signal at δ 11.69 ppm and singlet signal for NH Proton of the acetoacetanilinde moiety [21]. The NH proton of the sulfadiazine ring shows a singlet signal at 10.94 ppm [22]. The aromatic backbones in the range of 8.50-6.54 ppm with a multiplet [23]. The hydrogen atom attached to the carbon of the N=N- shows a signal at 5.98 ppm [24]. The methyl proton the acetacetanilide moiety shows a singlet at 2.507-2.491ppm. The NMR spectra of the azo ligands are shown in

Fig.7.1 and Fig 7.2. The spectrum of azo ligand HL_7 derived from indole, the single at 10.93 ppm was attributed to be -NH proton of the indole moiety [25]. The aromatic region shows a signal at 8.58 to 6.54 ppm. The -NH proton of the sulfadiazine ring shows a singlet at 3.30ppm [26].

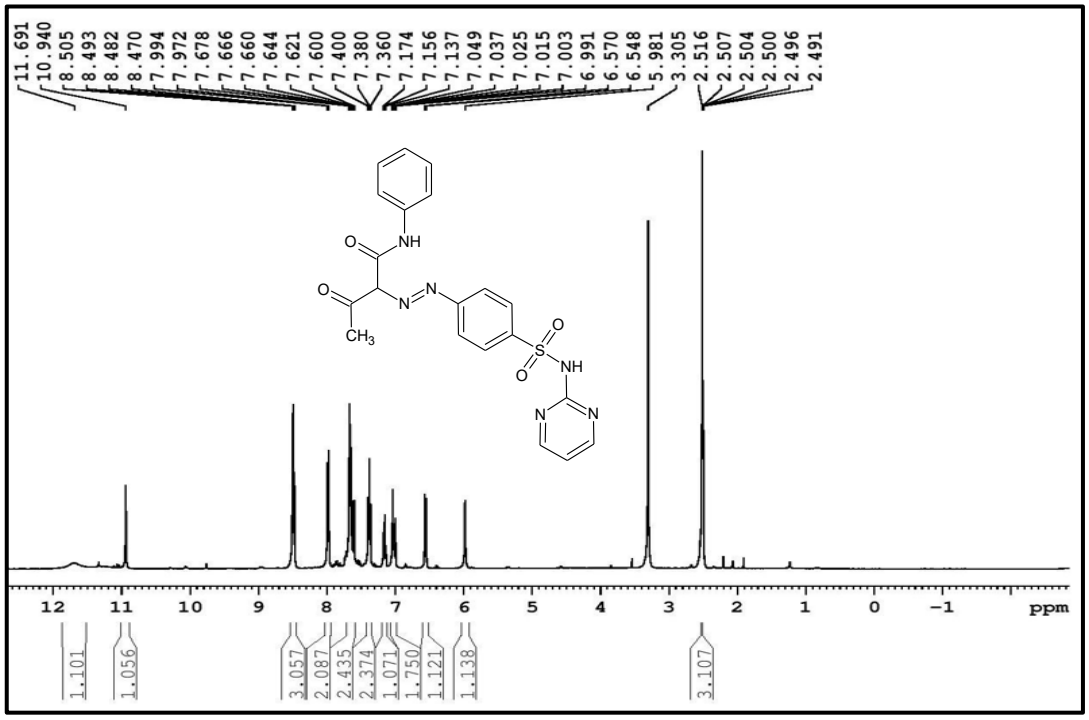

Fig.7.1. ^{1}H-NMR spectrum of azo dye ligand HL_6

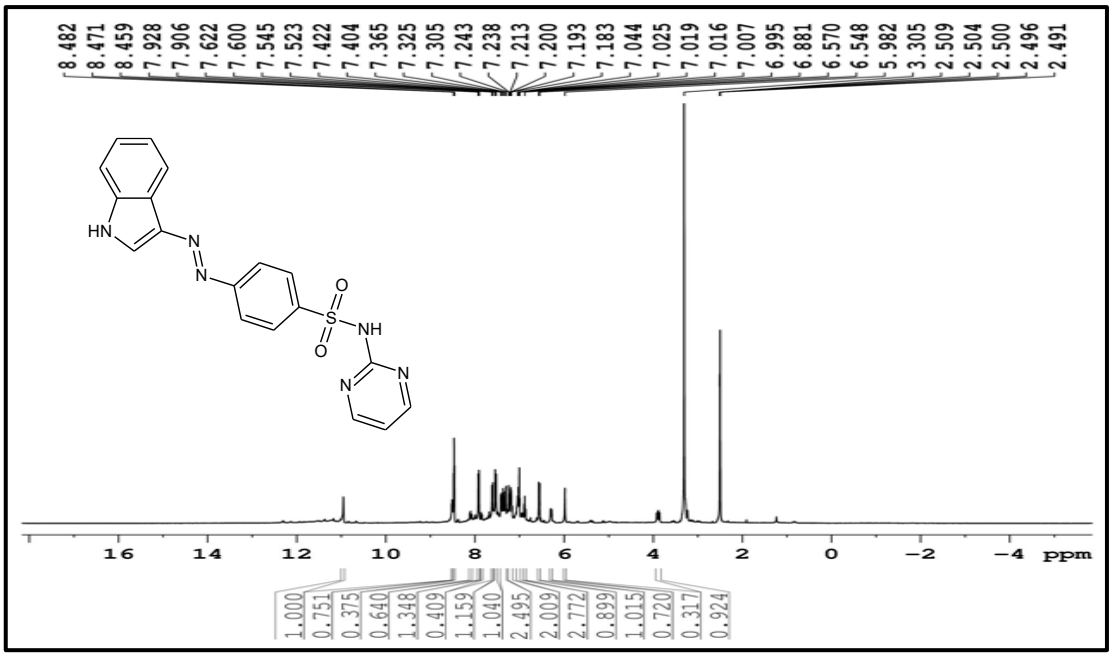

Fig.7.2. ^{1}H-NMR spectrum of azo dye ligand HL_7

7.3.2. UV-Visible Spectra.

The UV-Visible spectra for the free ligand as well as their metal complexes were recorded in DMSO solution. The electronic spectral results of ligand and its metal complexes are given in **Table 7.2** and the tentative electronic spectra are shown in **Fig. 7.3** and **Fig. 7.4.** The absorption spectrum of the free ligand HL_6 and HL_7 showed a single absorbtion peak at 412 nm and 362 nm this is because of transition involving electron migration along the entire conjugate system of the ligand. This band shows bathochromic shift in all the complexes. According to Molecular orbital theory the absorbtion of the metal complexes was depends on the central metal ion. In the spectra of complexes new bands in the range of 496-670 nm was assigned as charge transfer spectrum (LMCT), which were absent in ligand [27]. The Cu(II) complexes of HL_6 shows well-defined Bands at 381, 499 nm and Cu(II) complex of HL_7 shows at 373, 490 nm these bands are assigned to the transitions of $^2B_{2g} \rightarrow {}^2B_{1g}$ and $^2B_{2g} \rightarrow {}^2A_{1g}$ region reveal that the presence of square planar geometry of Cu(II) complex [28]. The Co(II) complex of HL_6 showed the absorption of 400 and 659 nm and For HL_7 the Co(II) complexes shows bands at 386, 502 nm these bands were assigned as $^4T_{1g}(F) \rightarrow {}^4T_{2g}(F)$ and $^4T_{1g}(F) \rightarrow {}^4A_{2g}(F)$, [29] this assignment was the result of octahedral geometry of the Co(II) complex.

Table 7.2. UV-Visible spectra of the Ligand HL_6 and HL_7 and their metal complexes.

Compound	λ_{max} (nm)	Transition	Geometry
HL_6	412	$\pi \rightarrow \pi^*$	--
7a	381,499	$^2B_{2g} \rightarrow {}^2B_{1g}$ $^2B_{2g} \rightarrow {}^2A_{1g}$	Square planar
7b	400, 659	$^4T_{1g}(F) \rightarrow {}^4T_{2g}(F)$ $^4T_{1g}(F) \rightarrow {}_4A_{2g}(F)$,	Octahedral
HL_7	362	$\pi \rightarrow \pi^*$	--
7c	373, 490	$^2B_{2g} \rightarrow {}^2B_{1g}$ $^2B_{2g} \rightarrow {}^2A_{1g}$	Square planar
7d	386, 502	$^4T_{1g}(F) \rightarrow {}^4T_{2g}(F)$ $^4T_{1g}(F) \rightarrow {}^4A_{2g}(F)$,	Octahedral

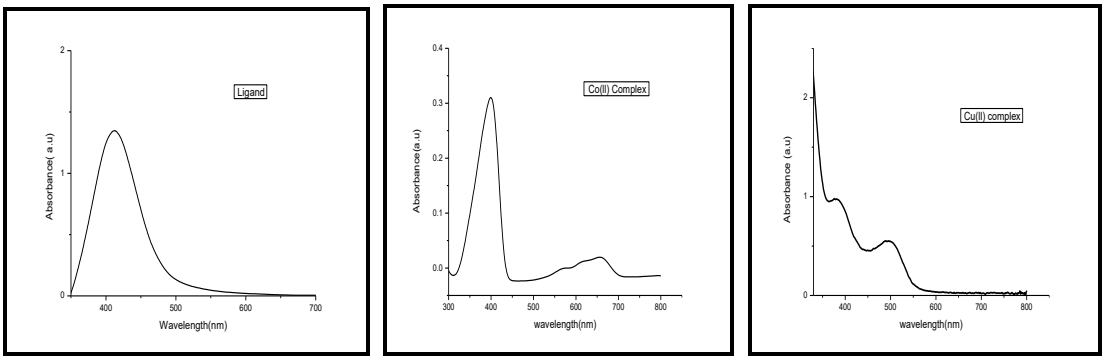

Fig.7.3. Uv-Visible spectra of HL_6 and their metal complexes.

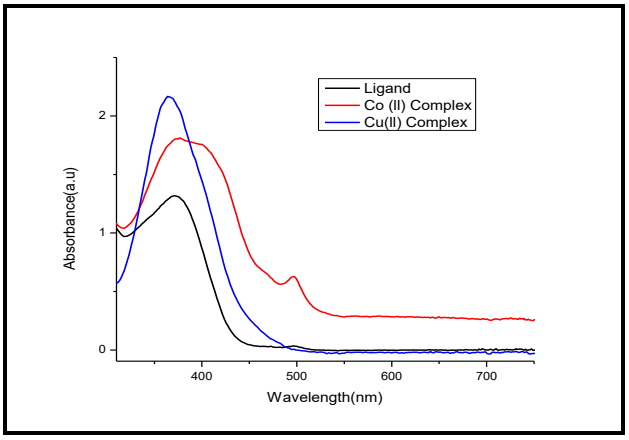

Fig.7.4. Uv-Visible spectra of HL_7 and their metal complexes.

7.3.3. FT-IR Spectra.

The infrared spectra of the metal azo complexes and the free ligands are compared in **Fig.7.5a-Fig.7.5f**. The IR spectra of the complexes and the azo ligands were studied to explain the coordination modes of the ligands and the effect of the metal center on the ligand. The assignment of the observed bands has been achieved on the basis of careful evaluation between the spectra of metal azo complexes with that of free ligands and the data were summarized in **Table 7.3.** In the IR spectrum free ligand (HL_6) shows a band at 3438 cm^{-1} due to the presence of –OH group and a medium intensity band at 3251 cm^{-1} corresponds to NH stretches [30]. In the free ligand spectrum the SO_2 asymmetric and symmetric mode is observed at 975 cm^{-1}. In all the complexes this bond shows a blue shift. This blue shift is because of the shortening of the S-N bond length relative to that of the uncoordinated ligand [31]. After compexation, the band of the pyrimidine ring in the range 1581-1591 cm^{-1} is unaffected this indicates that the N-atoms of the pyrimidine ring are not involved in complex formation [32]. Furthermore, the ν(–N–N-C–) absorption band at 1601 cm^{-1}, appearing in the spectra of free ligand, this band is absent in all the complexes. The appearance of new band around 1428-1430 due to –N=N– vibration. This supports in all complexes the azo-enol form of the ligand in the metal(II) complexes [33]. The appearance of this peak at relatively lower field may indicate the coordination via the azo -N=N- group. The broad band at 3424-2432 cm^{-1} and medium intense band at 1525-1509 cm^{-1} conforms the presence of both lattice and coordinated water molecule [34]. The appearance of new bands in the region 662-589 and 573-413 cm^{-1} assignable M-O and M- N, respectively [35], replicates the bonding of the metal ions to oxygen and nitrogen atoms.

The IR spectrum of the azo dye ligand HL_7 exhibits a broad peak at 3181 cm^{-1} due to the presence of -NH of the indole ring. This vibration was disappeared in all the metal complexes suggested that -NH of the indole ring involved in complex formation [36]. The free ligand shows a medium intensity band at 1557cm^{-1} which shifted to higher frequency by 10-30 cm^{-1} in all the metal chelates and shows bands at 1582 and 1585 cm^{-1} indicates the coordination of nitrogen atom of the azo group with the metal [37]. further the metal to ligand bonding was confirmed by the appearance of non-ligand bands in the region 744-751 cm^{-1} and 615-618 cm^{-1} due to ν_{M-N} (Indole NH) and ν_{M-N} (azo-N=N-) vibrations respectively [38].

Table 7.3. Important IR Frequencys of the azo dye ligands HL_6 and HL_7 and their metal complexes.

Compounds	ν(O-H)/H_2O	ν(N=N)	ν(M-N) (Indole NH)	ν(M-N) (azo-N=N-)	ν (M-O)
HL_6	3438	1437	--	--	---
7a	3436	1509	--	573	664
7b	3430	1525	--	414	589
HL_7	3438	1557	--	---	--
7c	3437	1582	744	618	--
7d	3425	1585	751	617	--

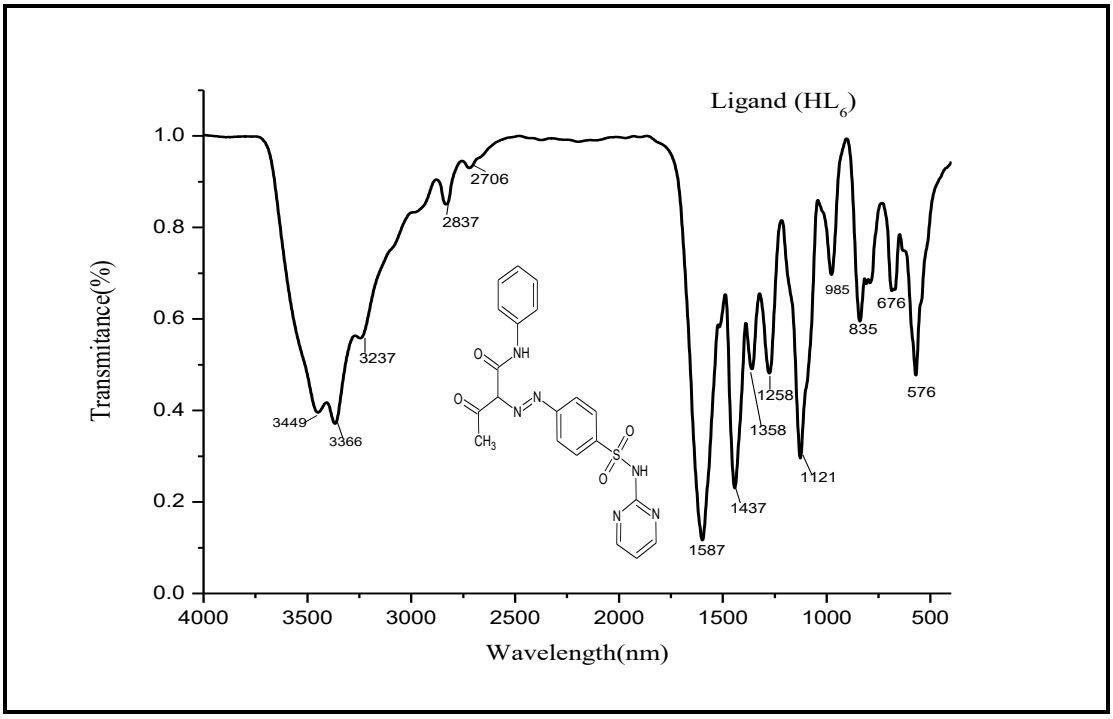

Fig.7.5a. FT-IR spectra of the azo dye HL_6 ligand.

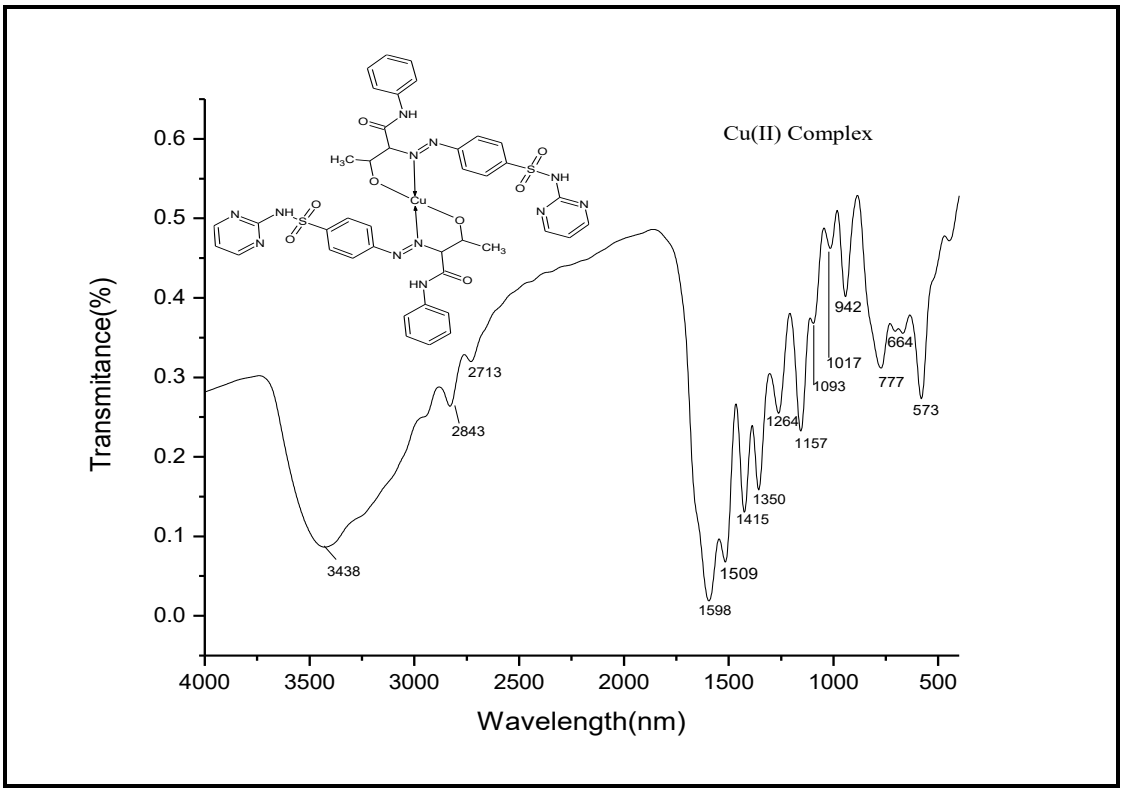

Fig.7.5b. FT-IR spectra of the Cu(II) complex of the azo dye HL_6.

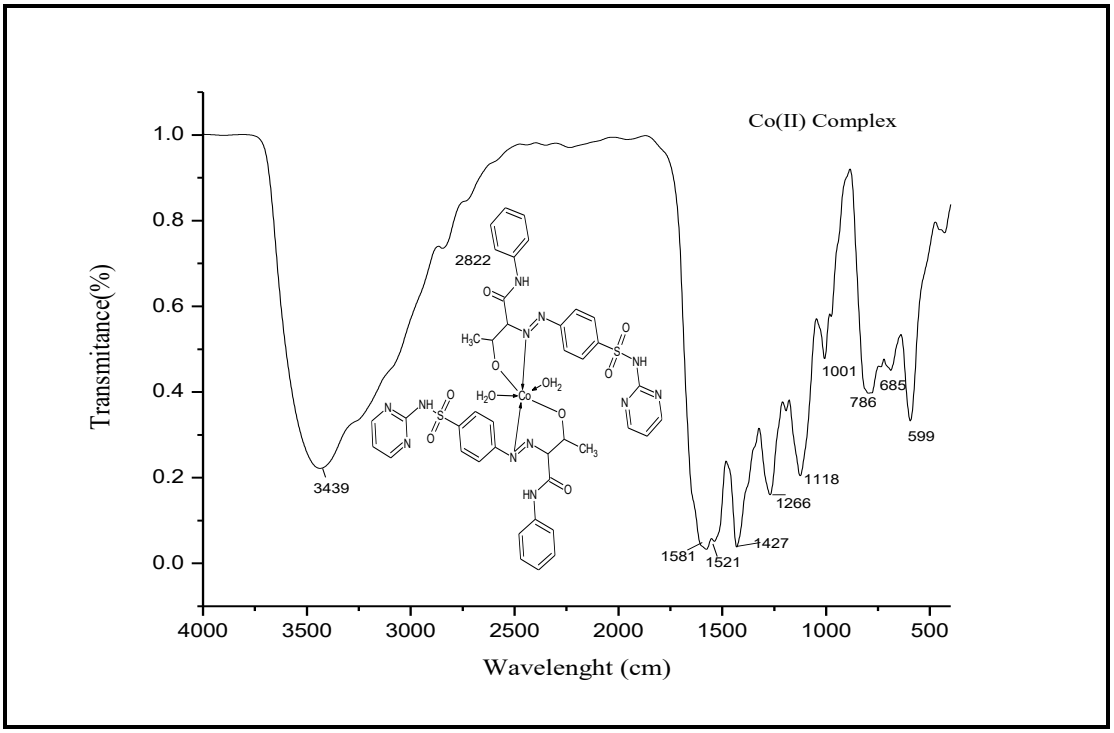

Fig.7.5c. FT-IR spectra of the Co(II) complex of the azo dye HL_6.

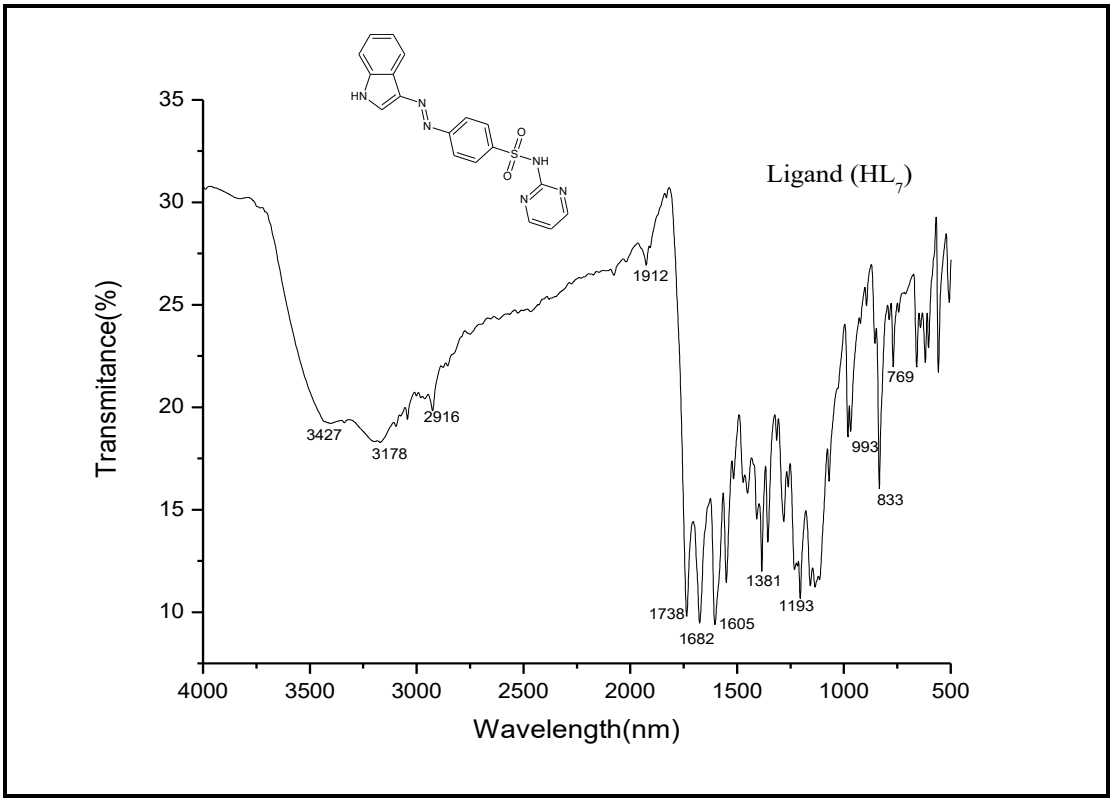

Fig.7.5d. FT-IR spectra of the azo dye HL_7 ligand.

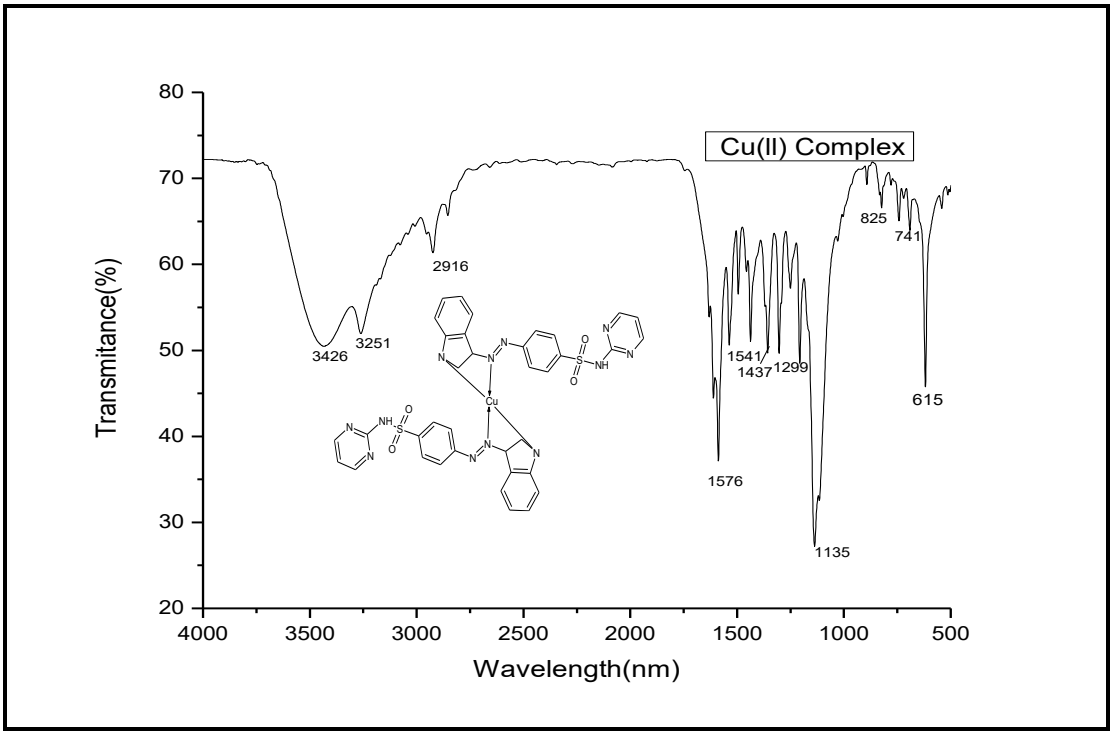

Fig.7.5e. FT-IR spectra of the Cu(II) complex of the azo dye HL_7 ligand.

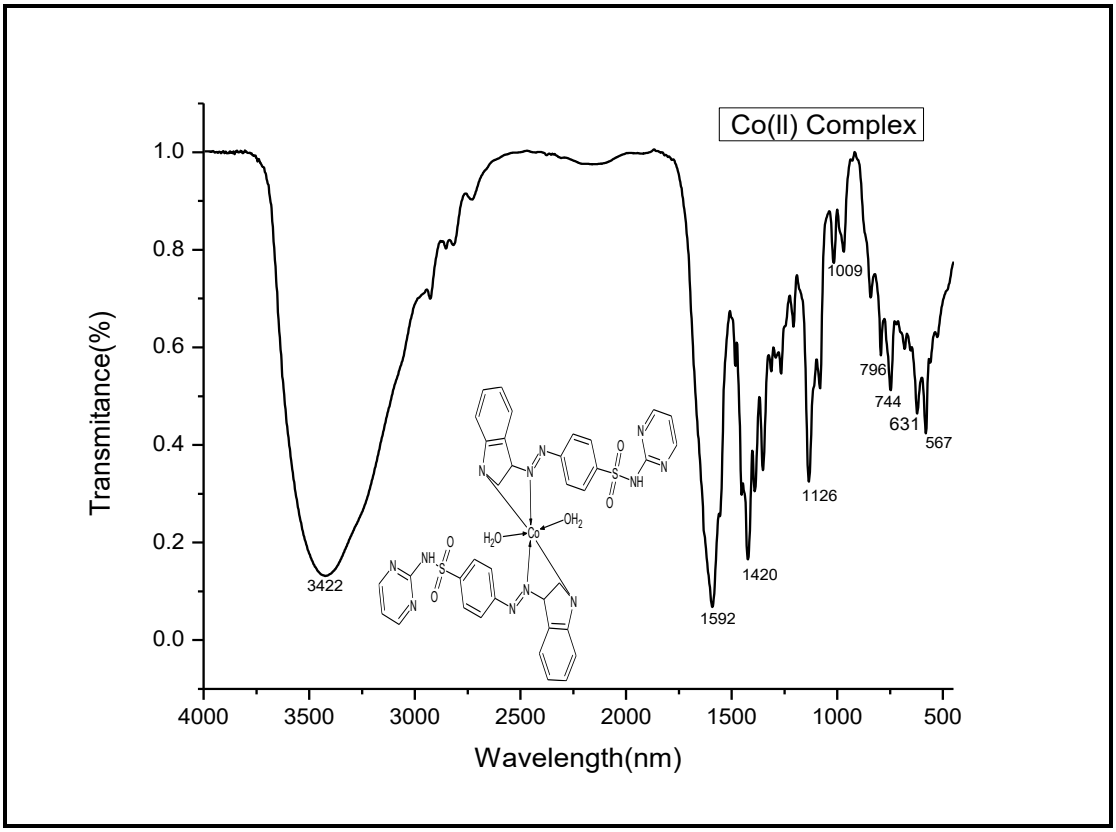

Fig.7.5f. FT-IR spectra of the Co(II) complex of the azo dye HL_7 ligand.

7.3.4. Mass spectra.

The mass spectrum of the heterocyclic ligands and the metal complexes showed molecular ion peak analogous to their molecular mass. The mass spectrum of the azo dye ligand HL_6 and HL_7 displayed a apparent molecular ion peak at m/z 438, and m/z 378. One and the other are similar to its molecular mass of the ligand and the spectra of all the synthesized heterocyclic ligand with their metal azo complexes are showed in **Fig.7.6a and Fig.7.6f.** The metal azo complex were also studied to know their molecular mass and the molecular ion peak of the synthesized complexes. From ligand HL_6, the m/z for Cu(II) complex were found to be 940, for Co(II) complexes shows a molecular ion peak at m/z 900, for ligand HL_7 the Cu(II) and Co(II) complexes will display a molecular ion peak at m/z 818 and 850 respectively, which are matches with the stoichiometric configuration of $[M(L)_2]$ type. Moreover, the experimental molecular ion peaks in all the spectra are in good agreement with the recommended molecular formula indicated from elemental analyses.

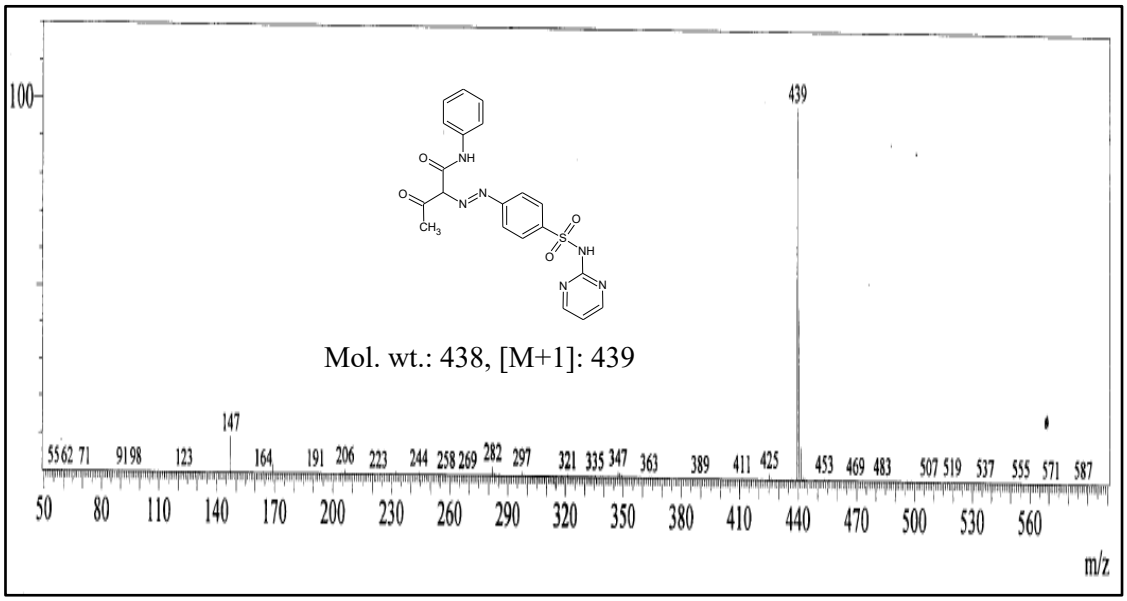

Fig.7.6a. Mass spectra of azo dye ligand (HL_6).

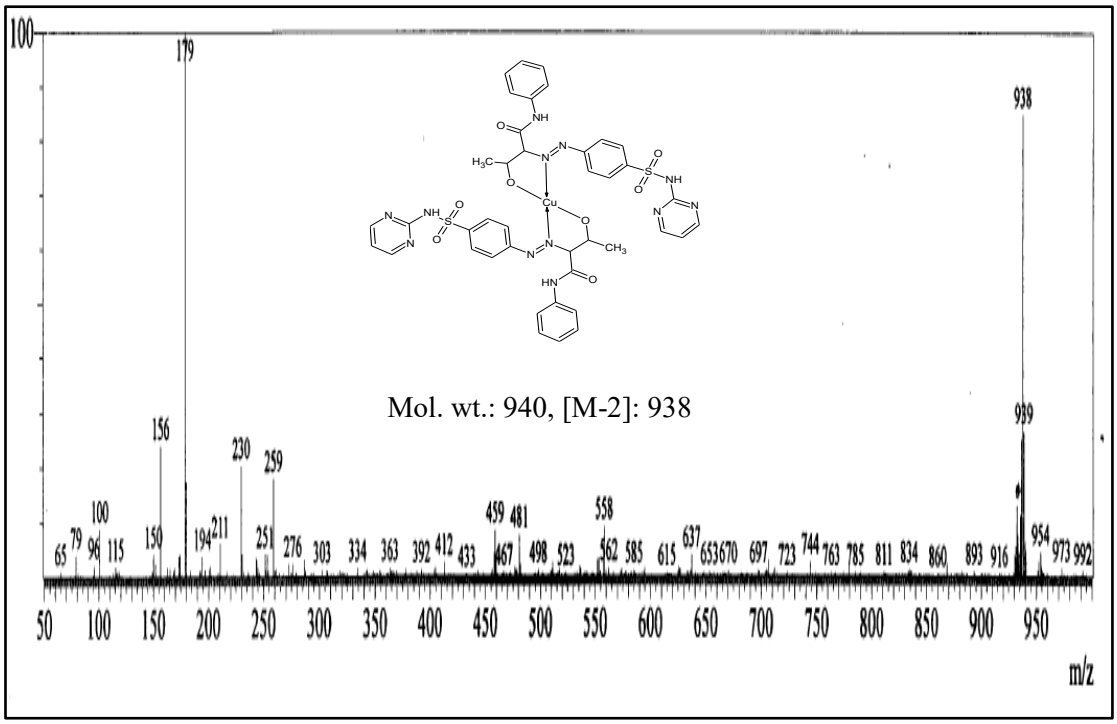

Fig.7.6b. Mass spectra of Cu(II) Complex of azo dye ligand (HL_6)

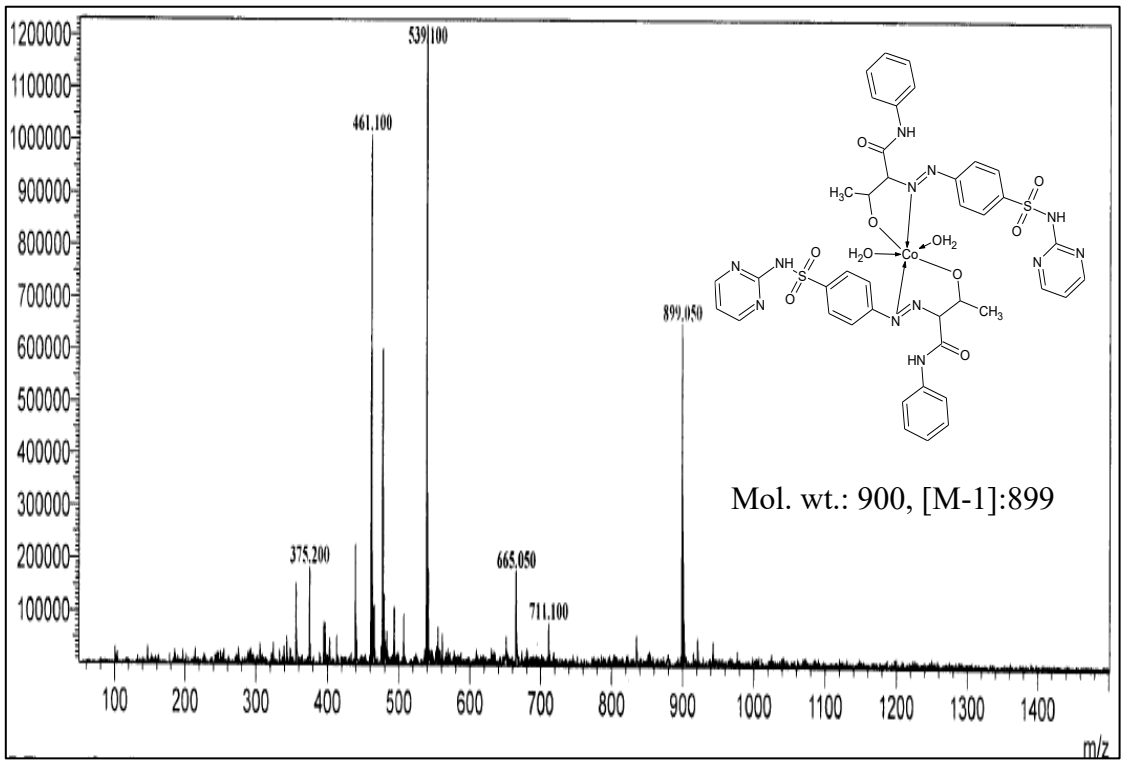

Fig.7.6c. Mass spectra of Co(II) Complex of azo dye ligand (HL_6).

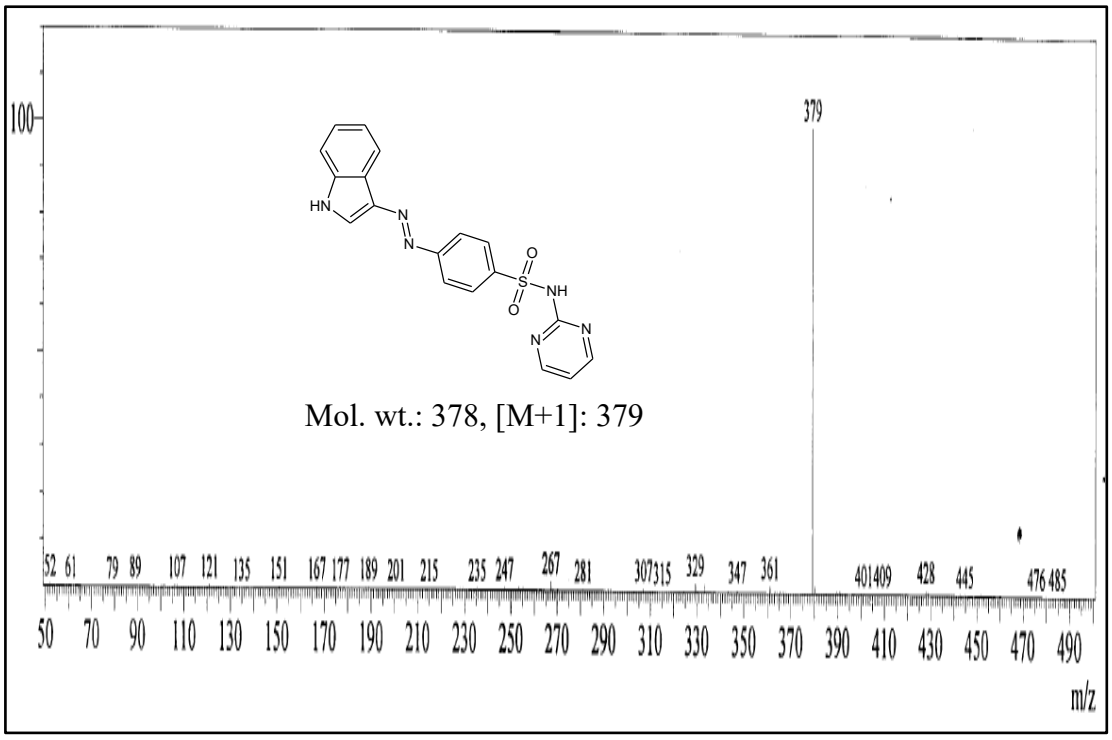

Fig.7.6d. Mass spectra of azo dye ligand (HL_7).

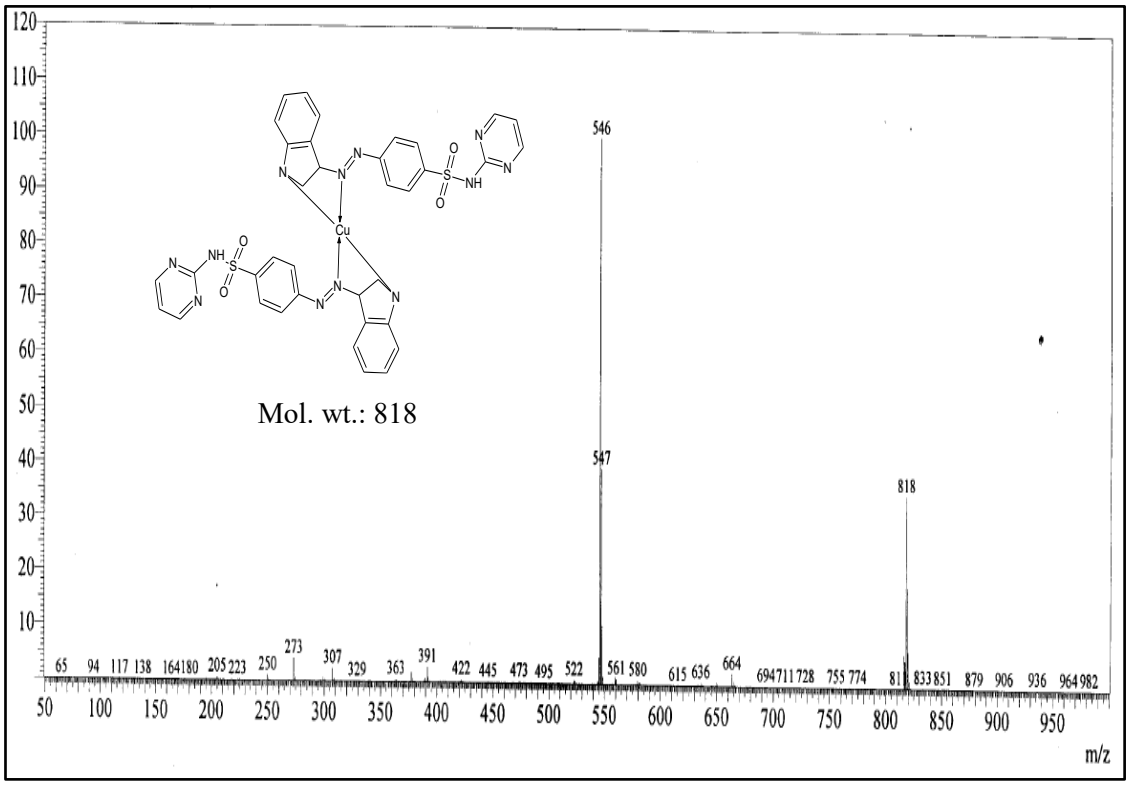

Fig.7.6e. Mass spectra of Cu(II) complex of azo dye ligand (HL_7).

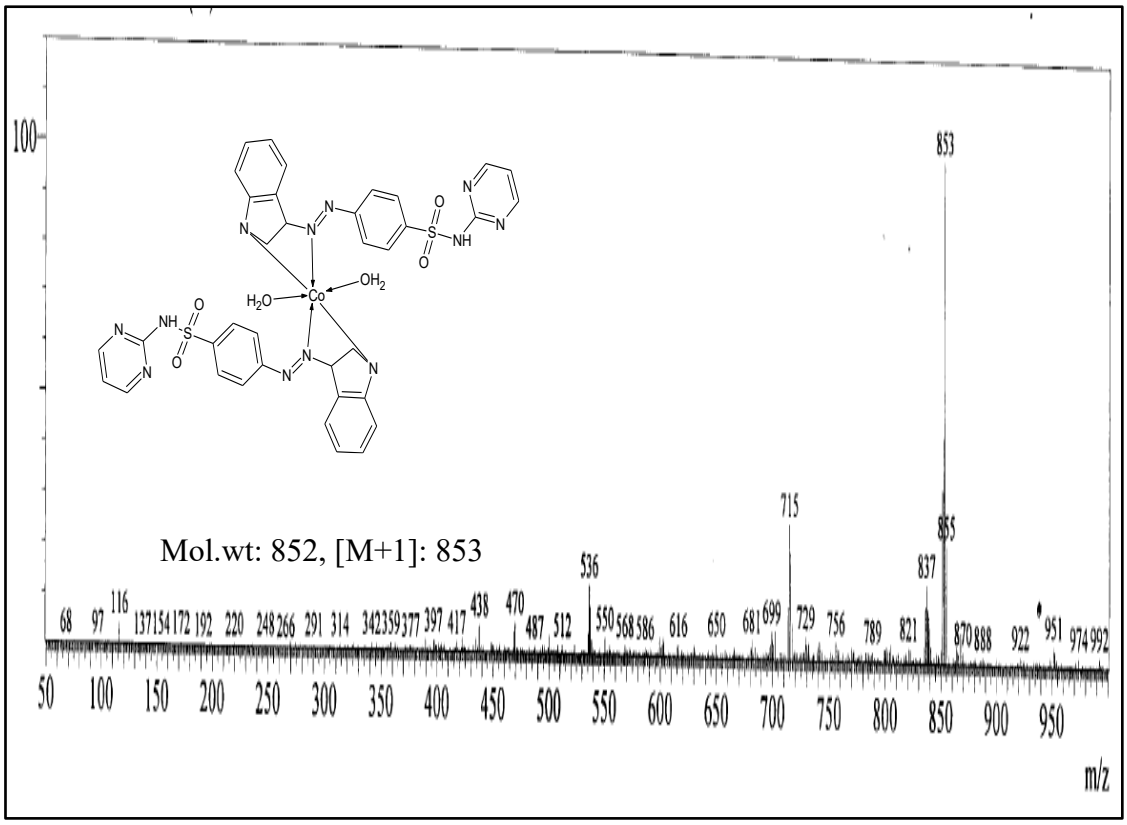

Fig.7.6f. Mass spectra of Co(II) complex of azo dye ligand (HL_7).

7.3.5. Thermogravimetric analysis.

The thermal properties of binuclear metal(II) azo complexes were explored by thermogravimetric analysis (TGA) at a temperature ranging from 24-800 °C in nitrogen atmosphere. The loss of mass of the metal complexes for the different steps was compared with theoretically calculated for the suggested formula based on the results of elemental analyses. At the end product the formation of metal oxide can be calculated and compared with that obtained from analytical determination. And also, the mass losses, relative residues, temperature ranges, and final decomposition products observed in each step of TGA curves for the solid complexes **Fig.7.7** presents the recorded TGA curves of four metal(II) azo complexes and important data are summarized in **Table 7.4.**

The Cu(II) complex of ligand HL_6 degrades in three stages, in the first step the loss lattice water molecule with some part of organic moiety of the coordination sphere at a temperature ranging from 34-270 °C. The calculated weight loss was found to be 12.67 % (Calculated 12.9 %). The loss of two moles of pyrimidine takes place in the second step at temperature 271-404 °C with a mass loss of 36.8 % (Calculated 36.8 %) at temperature 404-432 °C the loss of two moles of phenylamine with the mass loss of 62 % (Calculated 62.4 %). Further with the increase in temperature the degradation of complex to form a copper oxide. The percentage of overall degradation was found to be 97.4 %.

Four stages of degradation were found for Co(II) complex of ligand HL_6. In the first stage the loss of two moles of coordinated water molecule was takes place at a temperature range of 24-88 °C with the calculated mass loss were 3.69 % (Calculated 3.60 %). The loss of 2 moles of pyrimdine at a temperature ranging 88-285 °C with mass lose 20.2 % (Calculated 21.2 %) in the third stage loss of two moles sulfate with carboxylic group at a temperature 285-299 °C with the loss of 28 % (Calculated 28.2%). In the final step the loss of two moles of $C_{12}H_{13}N_2$ takes place with 63.47 % (Calculated 63.10 %) mass loss at temperature 300-496 °C. Further continuation in heating to form cobalt oxide.

The Cu(II) complex of ligand HL_7, the degradation takes place in three stages, in the first stage the loss of two moles of pyrimidine ring at a temperature ranging from 30-243 °C with loss of 23.2 % (Calculated 22.7 %). In the second stage the loss of organic moiety with molecular formula $C_{10}H_{16}$ mass loss percentage was found to be 53.6 % (Calculated 52.6 %) at a temperature range 244-400 °C. With The mass loss of 65.05 % (Calculated 65 %) was due to the loss of $C_{10}H_{14}O_4S_2$ at tempetature 401-

507 °C. The Heating was continued further until the formation of its metal oxide. The overall percentage degradation was found to be 87.92%.

The Co(II) complex of ligand HL_7 the degradation takes place in four stages in the first stage loss of water molecules takes place with the loss of 4.2 % (Calculated 4.5 %) at temperature ranging from 24-70 °C. The loss of two moles of pyrimidine was come about in stage two with mass loss was found to be 23.28 % (Calculated 23.2 %) at temperature 71-243 °C. The loss of 2 moles of SO_2 molecule at temperature 244-305 °C with the loss of 44.8 % (Calculated 45.1 %) was befall in stage 3.in the lost stage, the loss of reaming organic moiety attached to central metal i.e, $C_{14}H_{16}$ at temperature 306-351°C with loss of 52.42 % (Calculated 52.36 %). Further heating continues to form metal oxides.

Table 7.4. Decomposition statics of metal complexes (7a-7d).

Complexes	Stages	Decomposition Temp (^{0}c)	Probable Assignment	Loss Of Mass In (%) Found (Calc)	Residual Species
Cu(II) Complex(**7a**)	1st 2nd 3rd	34-270 271-404 404-432	2 Pyrimidine ring $C_2O_6S_2H_2$ 2 phenyl amine	12.67(12.9) 36.8(36.87) 62(62.4)	CuO
Co(II) Complex(**7b**)	1st 2nd 3rd 4th	24-88 88-285 286-299 300-496	$2H_2O$ 2 Pyrimidine ring $C_2O_6S_2H_2$ 2 $C_{12}H_{13}N_2$	3.69(3.60) 20.2(21.0) 28.3(28.8) 63.47(63.10)	CoO
Cu(II) Complex(**7c**)	1st 2nd 3rd	30-243 244-400 401-507	Pyrimidine ring $C_{10}H_{16}$ $C_{10}H_{14}O_4S_2$	23.2(22.7) 53.6(52.6) 65.05(65)	CuO
Co(II) Complex(**7d**)	1st 2nd 3rd 4th	24-70 71-243 244-305 306-351	$2H_2O$ Pyrimidine ring S_20_4 $C_{14}H_{16}$	4.2(4.5) 23.28(23.2) 44.8(45.1) 52.42(52.36)	CoO

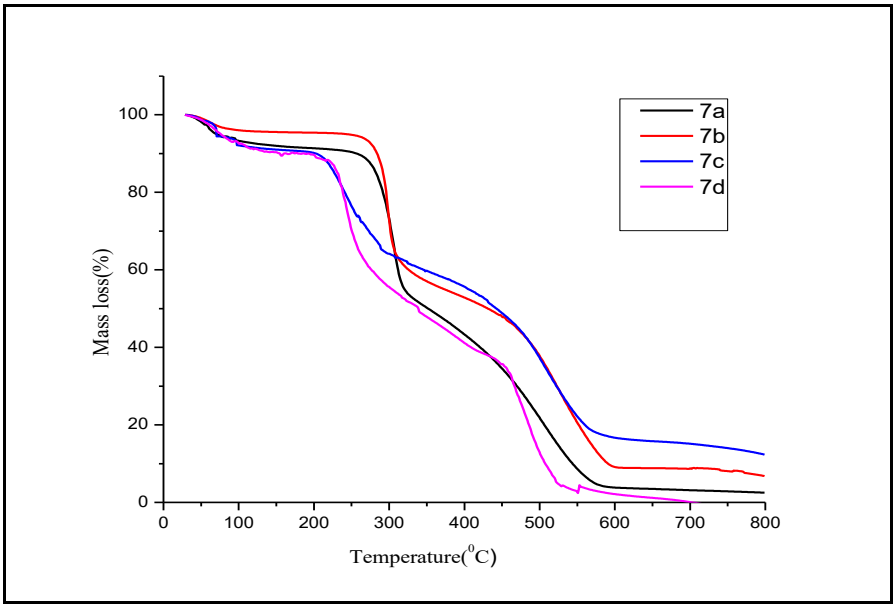

Fig.7.7. The TGA graph of the synthesized metal complexes.

7.3.6. XRD.

The metal azo complexes are partially soluble in common organic solvents and soluble only in some polar solvents like DMF and DMSO. Because of this, the crystals suitable for the single-crystal studies were not obtained. Consequently, in order to know the degree of crystallinity, we recorded the powder XRD pattern of the metal complexes in at room temperature. From the results Cu(II) complexes shows a certain amount of crystallinity whereas Co(II) are non-crystalline in nature.

The XRD patterns of the Cu(II) complex of the ligand HL_6 showed eight reflections in the range 8-44 (2θ), the reflection was due to the diffraction of the plane of the complex with X-ray radiation. By using Bragg's equation **$2d\sin\theta=n\lambda$** interplanar speacing was calculated [39]. At **Table 7.5a** and **Fig. 7.8.** Represents the inter planar spacing together with relative intensities for selected peaks. The unit cell parameters were evaluated for cubic symmetry and $h^2+k^2+l^2$ values are also determined. The calculated inter-planar parameters were found to be $a=b=c=$ 8.030 Å. The forbidden number 7 was observed in the calculated $h^2+k^2+l^2$ values was found to be 1, 1, 3, 5, 7, 12, 16 and 23, this shows that Cu(II) complex may belong to either hexagonal or tetragonal system

Similarly, the same calculations were also done for Cu(II) complex of Ligand HL_7 which displayed 10 reflections in the range 8-37° (2θ), respectively. By knowing the important peaks the inter-planar spacing was calculated and represented in **Table 7.5b**. The unit cell parameters together with the $h^2+k^2+l^2$ values were determined. The $h^2+k^2+l^2$ values were found to be 1, 1, 3, 4, 8, 9, 11, 13, 15 and 19. The presence of forbidden numbers like 15 confirms that the complex may belong to hexagonal or tetragonal systems. The calculated lattice parameter for Cu(II) complexes were

a=*b*=*c*= 8.6 Å. Further, due to the non-crystalline nature, the Co(II) complexes of both the ligand unit cell parameters were not obtained.

Table 7.5a. Powdered XRD data of Cu(II) Complex of HL_6 (7a)

Sl no	2Θ	Θ	sin Θ	Sin^2 Θ	$Sin^2Θ\times 1000$	$h^2+l^2+k^2$	h k l	D	A
1	8.866	4.433	0.07729	0.005974	5.9742	1(1)	100	9.9663	8.0303
2	9.626	4.813	0.08390	0.007039	7.0398	1.179(1)	100	9.1811	8.0325
3	15.114	7.557	0.1315	0.01729	17.2955	2.897(3)	111	5.867	8.0332
4	19.653	9.826	0.17065	0.02912	29.12	4.877(5)	210	4.5152	8.0314
5	22.69	11.3455	0.19672	0.03870	38.700	6.559(7)	--	3.916	8.0317
6	31.577	15.7885	0.2720	0.07403	74.0313	12.400(12)	222	2.831	8.0176
7	36.136	18.068	0.3101	0.09619	96.1902	16.100(16)	400	2.4840	8.0296
8	43.122	21.5613	0.3674	0.1350	135.0536	22.606(23)	----	2.0966	8.0307

Table 7.5b. Powdered XRD data of Cu(II) Complex of HL_7 (7c)

Sl no	2Θ	Θ	sin Θ	Sin^2 Θ	$Sin^2Θ\times 1000$	$h^2+l^2+k^2$	h k l	d	A
1	8.212	4.1063	0.07160	0.005161	5.1315	1(1)	100	10.758	8.660
2	10.091	5.0455	0.08793	0.007743	7.7438	1.051(1)	100	8.7603	8.691
3	13.045	6.5225	0.1135	0.01290	12.9014	2.514(3)	111	6.7867	8.664
4	17.478	8.739	0.1519	0.02308	23.08	4.498(4)	200	5.0710	8.663
5	23.451	11.722	0.2032	0.04129	41.2961	8.047(8)	220	3.7908	8.665
6	24.8866	12.4433	0.2154	0.0464	46.4166	9.047(9)	300	3.5761	8.666
7	27.7993	13.8995	0.4021	0.05770	57.7034	11.244(11)	311	3.2069	8.663
8	30.078	15.039	0.2594	0.06732	67.3280	13.120(13)	320	2.9695	8.665
9	31.577	15.7885	0.2720	0.074029	74.029	14.515(15)	--	2.8319	8.690
10	36.1364	18.0682	0.3101	0.09619	96.19	18.745(19)	331	2.4840	8.664

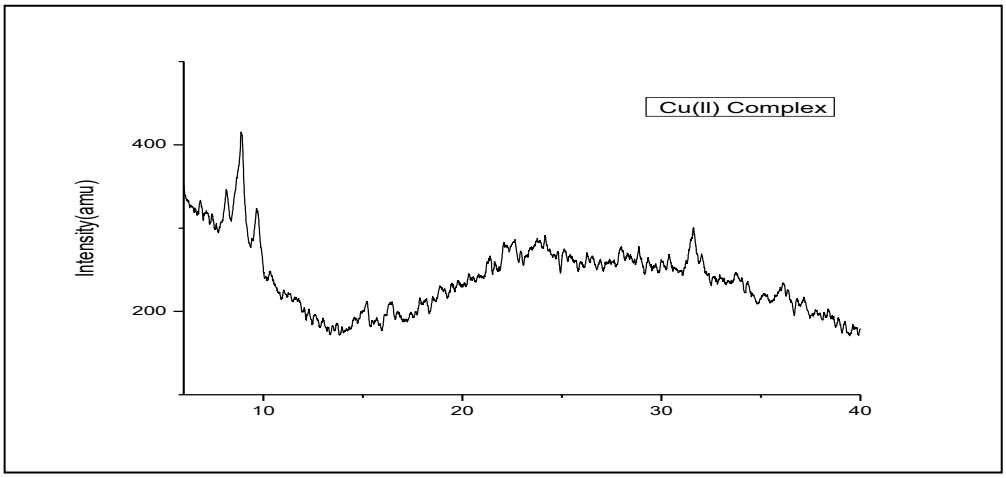

Fig. 7.8a. Powdered XRD data of Cu(II) Complex of HL_6 (7a)

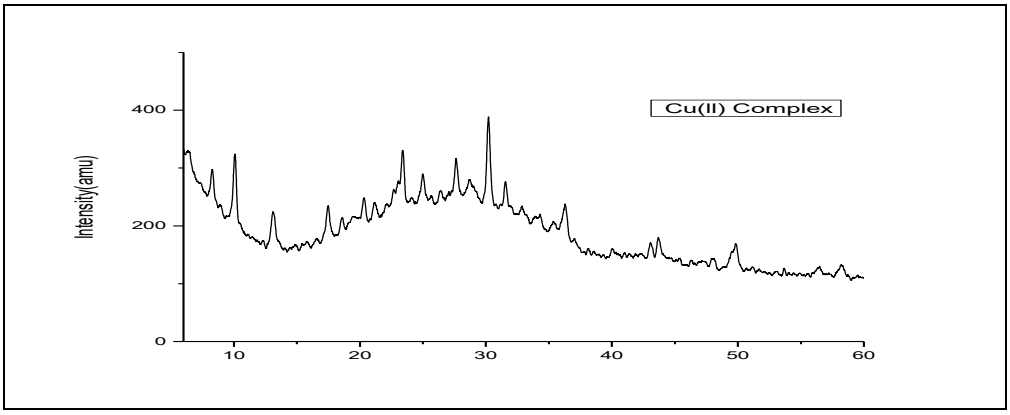

Fig. 7.8b. Powdered XRD data of Cu(II) Complex of HL_7(7c)

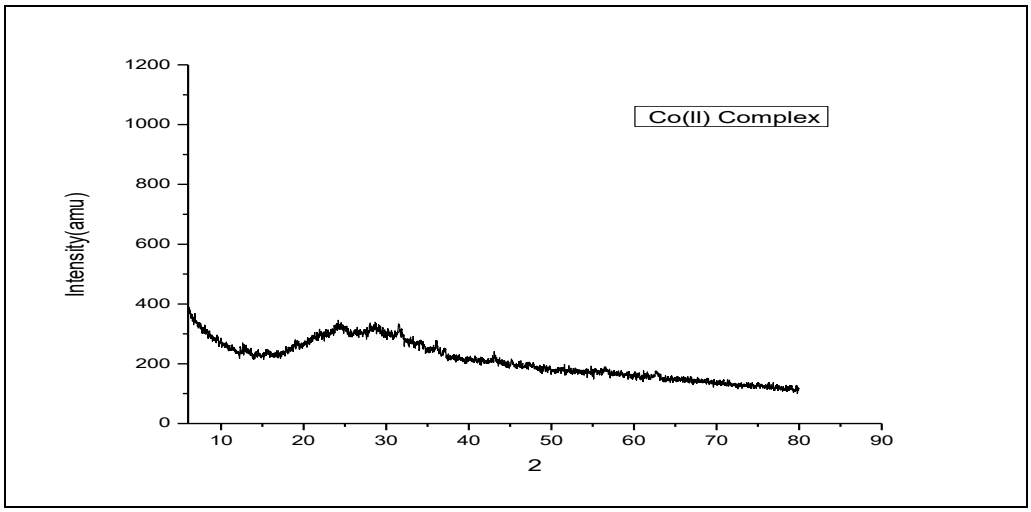

Fig. 7.8c. Powdered XRD data of Co(II) Complex of HL_6 (7b)

7.3.7. Biological activity.

7.3.7.1. Antibacterial activity.

In-vitro antibacterial activities of all the metal complexes were evaluated by Well diffusion method, and its experimental procedure was discussed in detail in **Section 5.3.8.1**. of **Chapter 5**. The bacterial strains are *E. coli, S. typhimurium* and *K. pneumonia* were used for the study. Amoxicillin were used as a standard drug compare with synthesized azo ligand and its metal complex.

The Results of the antibacterial activity are presented in **Table 7.6**. The metal complexes showed considerable antibacterial activity against the all the microorganisms when comparing its free ligand because this enhancement of antibacterial activity in complexes is based on Overtone's concept and chelating theory. The metal ion charge decrease the hydrophobic nature of the metal complexes increases which breaks down the permeability barrier of the cell and cause cell death [40]. The biological screening was concentration dependent manner.

Table 7.6. Antibacterial activity of HL_6 and HL_7 ligand and their metal complexes.

Compounds	*E. coli*		*S. typhimurium*		*K. pneumonia*	
	25 mg/mL	50 mg/mL	25 mg/mL	50 mg/mL	25 mg/mL	50 mg/mL
HL_6	1.3±0.4	1.7±0.6	1.5±0.5	1.8±0.5	1.2±0.5	1.5±0.7
7a	1.7±0.2	1.8±0.5	2.2±0.12	2.3±0.24	1.7±0.3	1.9±0.2
7b	1.5±0.22	1.9±0.12	1.7±0.21	2.1±0.6	1.7±0.23	2.0±0.24
HL_7	1.4±0.12	1.6±0.40	1.6±0.21	2.1±0.21	1.6±0.15	2.1±0.30
7c	1.6±0.23	1.8±0.4	1.5±0.2	1.9±0.32	1.5±0.21	2.1±0.32
7d	1.5±0.23	1.9±0.21	1.6±0.2	2.2±0.15	1.7±0.23	2.0±0.23
Streptomycin	1.8±0.25	2.5±0.21	2.0±0.31	2.5±0.34	2.0±0.24	2.4±0.26

7.3.7.2. Anti-tubercular Activity.

Mycobacterium tuberculosis is a pathogenic bacterium as resulting the infectious diseases of tuberculosis (TB) in human [41]. With the appearance of Multidrug-resistant and extensively drug resistant microbial strains of Mycobacterium tuberculosis, revolutions in TB drug discovery and developing strategies to bring novel drug with best performance is an essential investigation [42]. Taking this into account, there is a demanding need to develop new and more effective anti-tubercular agents. Thus the present work we studies the synthesized metal complexes for their antituberculosis activity against *M. tuberculosis* (H37RV strain) by microplate alamar blue assay (MABA) method using pyrazinamide as standard. This methodology is non-toxic, uses a thermally stable reagent and shows good connection with proportional and BACTEC radiometric method [43].

The brief procedure of this method involves, the sterilized 96-wells plate received 100 µl of the Middlebrook 7H9 broth. And the synthesized metal complexes (1a-2b) were added to the plate with serial dilution (100 to 0.2 µg/ml) in DMSO. Plates were covered and sealed with parafilm and incubated at 37°C for five days. After this time, 25µl of freshly prepared 1:1 mixture of Almar Blue reagent and 10% tween 80 was added to the plate and incubated for 24 hrs. Now the colour change was observed from pink to blue which indicated the inhibition of bacterial growth. A blue color in the well was interpreted as no bacterial growth, the results was recorded by MIC which defined as lowest drug concentration which prevented the color change from blue to pink. Further the strandard drug pyrazinamide with a standard MIC value 3.125 µg/ml.

Results and Discussion.

Tuberculosis is most common disease leading to cause death worldwide and it is infected by microorganism *mycobacterium tuberculosis.* Lots of work has been carried out to destroy the disease but many of drugs were failed to fight against bacterial because of unusual development of resistance against drugs by the bacteria, lack of selectivity and increased toxicity [44]. Therefore, from the above observation, we have studied the anti-mycobacterial efficiency of the synthesized metal complexes against *M. tuberculosis.* The results were represented in terms of MIC were presented in **Table 7.7.** From the **Fig.7.9** describes the conversion of the pink colour to blue colour. This indicates the suppression of the bacteria activity of the metal complexes. From the results it is indicated that all the compounds shows appreciable activity against *M. tuberculosis*. And the order of reactivity is as follows 7c>7a>7b>7d. 7c exhibits the highest activity with MIC value at 50 µg/ml compare to the other metal complexes. This could be due to heterocyclic rings present in the molecular structure of the metal complexes.

Table 7.7. The results of the Antitubercular activity against *M. tuberculosis* (MIC, mg/mL) of the compounds **(4a-4d)**

Synthesized Compounds	100 µg/mL	50 µg/mL	25 µg/mL	12.5 µg/mL	6.25 µg/mL	3.12 µg/mL	1.6 µg/mL	0.8 µg/mL
7a	S	S	S	S	S	S	S	R
7b	S	S	S	S	S	S	S	R
7c	S	S	S	S	S	S	R	R
7d	S	S	S	S	S	S	R	R

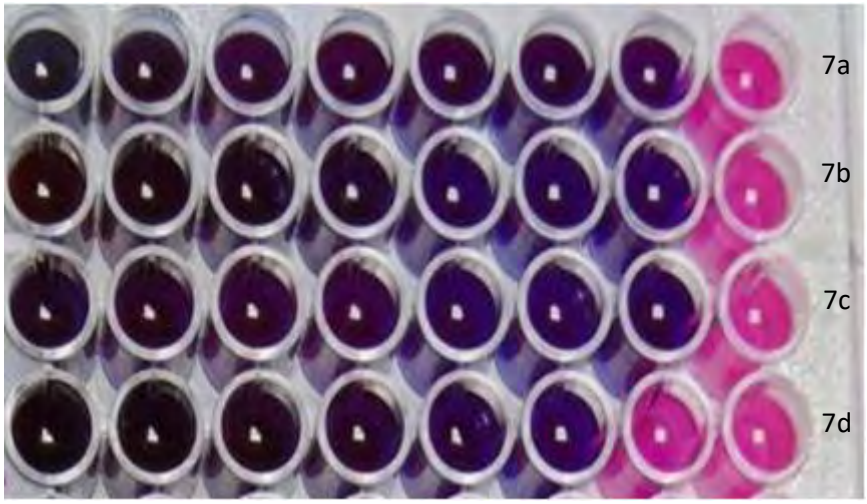

Fig. 7.9. Antitubercular activity of synthesized metal complexes against *M. tuberculosis*.

7.4. Conclusion.

The present work describes the synthesis of novel azo dye ligand of indol and aceto acetanilide derivatives and their Cu(II) and Co(II) metal complexes and they were systematically characterized by different physicochemical technique. Based on the physicochemical data, it was proposed that the azo dye ligand coordinates through the nitrogen of the azo dye ligand (-N=N-) and for the ligand HL_6 it coordinates through C=O and for the ligand HL_7 its coordinates through -NH Group. Further the biological studies like antibacterial and anti-tubuercular studies were carried out to explore the pharmacological activity of the metal complexes, from the results Cu(II) and Co(II) metal complexes derivatives of acetoactanilide moiety provides to be more efficient against the bacteria. Therefore, this work is a wide-ranging and more applicable to biomedical field.

7.5. Reference.

1. U. Misra, A. Hitkari, A. K. Saxena, S. Gurtu, and K. Shanker, *Euro. J. of Medi. Chem.*, 31, 7-8, 629–634, **1996**.
2. P. Rani, V. K. Srivastava, and A. Kumar, *Eur. J. of Medi. Chem.*, 39. 5,. 449–452, **2004**.
3. A. E. Gendy Adel, A. Abdou Naida, Z. Sarhan El-Taher, and A. El-Banna Hosney, *Alex. J. of Pharmac. Scie.*, 7, 99–103, **1993**.
4. N. Karali, A. Gursoy and F. Kandemirli, *Bioorg. Medi. Chem.*, 15, 17, 5888–5904, **2007**.
5. A. Dandia, V. Sehgal, and P. Singh, *Ind. J. Chem. Sec. B.*, 32, 1288–1291, **1993**.
6. Z. Chena, W.Yiqun, G. Donghong and G.Fuxi, *Spectrochem. Acta Part A.,* 68 918–926, **2007**.
7. A. E. Gendy Adel, A. Abdou Naida, Z. Sarhan E. Taher and E. Banna Hosney, *Alexa. J. of Pharm. Scie.*, 7, 99–103, **1993**.
8. N. Karali, A. Gursoy and F. Kandemirli, *Bioorg. Medi. Chem.*, 15, 17, 5888–5904, **2007**.
9. A. Dandia, V. Sehgal, and P. Singh, *Ind. J. Chem. Sec. B.*, 32, 1288–1291, **1993.**
10. A. S. Kalgutkar, B. C. Crews, S. Saleh, D. Prudhomme, and L. J. Marnett, *Bioorg. Medi. Chem.*, 13,. 24, 6810–6822, **2005.**
11. S. Olgen and D. Nebioglu, *Farmaco.*, 57. 8, 677–683, **2002**.
12. I. A. Leneva, N. I. Fadeeva, and I. T. Fedykina, *Proceedings of the 7th Inter. Confer. Anti. Res.*, 187, **1994**.
13. A.Y. Merwade, S. B. Rajur, and L. D. Basanagoudar, *Ind. J. Chem. Sec. B.*, 29, 12, 1113–1117, **1990**.
14. D. Deepa Parab and A. Y. Desai, *Sci. Res. Rep.,* 1(2), 105 - 107, **2011.**
15. A. L. Harris, X. Yang, A. Hegmans, L. Povirk, J. J. Ryan, L. Kelland, N. P. Farrell, *Inorg Chem.*, 44, 9598-9600, **2005**.
16. V. Nishal, D. Singh, R. K. Saini, V. Tanwar, S. Kadyan, R. Srivastava and P. S. Kadyan, *Cog. Chem.,* 1, 107, 92-91, **2015**.
17. Z. Chena, W. Yiqun, G. Donghong and G. Fuxi, *Spectrochim. Acta Part A,* 68, 918–926, **2007.**
18. G. M. Golzar Hossain, A. J. Amoroso, A. Banu and K. M. A. Malik, *Polyhed,* 26, 967–974, **2007**.

19. M. S. Refat, T. Sharshar, K. M. Elsabawy, A. A. Majid Adam, *J. Molec. Liq.,* **2016**.
20. N. M. Mallikarjuna, J. Keshavayya and B. N. Ravi, *J. Mol. stru.,* **2018.**
21. D. D. Parab and A. Y. Desai, *Sci. Res. Rep., 1(2),* 105 - 107, **2011.**
22. M. M. Uzzaman and S.N. Mohammad Nasir Uddin, *App.Sci.*, 2, 880, **2020.**
23. M. Shahid, M. Salim, M. Khalid, M. Nawaz Tahir, M. Usman Khan and A. Albert Carmo Braga, *J. Mol. stru., **2018**.*
24. M. S. Refat, T. Sharshar, K. M. Elsabawy, A. Majid and A. Adam, *J. Molec. Liq.,* **2016**.
25. M. R. Karekal, M. B. Hire Mathada, *Turk. J. Chem.*, 37, 775 -795, **2013.**
26. S. Ramesh, Y. Yamgar Nivid and S. Sudhir Sawant, *Inter. J. Adv. Res.,* 1, 9, **2013**.
27. L. A. Mohammed, A. J. Kadhim and N.H. Aubaid, *Acta Chim. Pharm. Indica.* 3(2), 111-118, **2013.**
28. P. S. Nejman, A.M.Z. Slawin, P. Kilian and J. Derek Woollins, *Cog.Chem.,* 2, 1, **2016**.
29. F. Ruyffelaere, V. Nardello, R. Schmidt, J.Marie Aubry, *J. Photoche.Photobio. A: Chem.,* 183, 98–105, **2006**.
30. S. Banerjee, M.S. Capper, G. J. Clarkson, H. Huang and P. J. Sadler, *Polyhed.,* 172, 157–166, **2019.**
31. M. C. Prabhakara, H. S. Bhojya Naik, V. Krishna and H. M. Kumaraswamy, *Nucle. Nucl. Nucle. Aci.,* 26,459–47, **2008.**
32. S. M. El Megharbel, A. S. Megahed and M. S. Refat, *J. Mole. Liq.*, 216, 608, **2016.**
33. A. Shaikh and J. S. Meshram, *Cog. Chem.*, 1, 1019809, **2015.**
34. B. G. Devika, B. H. Doreswamy, N. M. Mallikarjuna and H. C. Tandon, *J. Mole. Struct*, 1185, 69, **2019**.
35. D. S. Y. Gaelle, D. M. Yufanyi, R. Jagan and M. O. Agwara, *Cog. Chem.*, 2, 1253201, **2016**.
36. S. Mondala, S. M. Mandalb, T. K. Mondala and C. Sinhaa, *J. Mol. stru.,* **2016**.
37. C.W. Tang and S. A. Vanslyke, *Appl. Phys. Lett*. 51, 913, **1987.**
38. V. Bulovic, G. Gu, P. E. Burrows and S. R. Forest, *Nature*, 380, 29, **1996.**
39. Q. Wu, M. Esteghamatian, N.X. Hu, Z.D. Popovic, G. Enright, Y. Tao, M. D'Iorio and S. Wang, *Chem. Mater*. 12, 79, **2000**.

40. M. Dinakaran, P. Senthilkumar, P. Yogeeswari, A. China, V. Nagaraja and S. Dharmarajan, *Inte. J. Antimicrob. Agents.*, 31, 337, **2008**.

41. J. E. McGarrah, Y. J. Kim, M. Hisser and R. Eisenberg, *Inorg. Chem.*, 40, 4510, **2001**.

42. Y. Kunugi, K. R. Mann, L. Miller, C. L. Exstrom, *J. Amer. Chem. Soc.,*120, 589, **1998**.

43. L. Annamaria, M. Jialin, W. Baojie, W. Yuehong, G. F. Scott, P. K. Alan. *J Med Chem.*, 58, 2109, **2009**.

44. J. Sarva, I. Yasuyoshi, W. Baojie, G. F. Scott and P. K. Alan, *Chem. Med. Chem.*, 1, 593, **2006**.